Structural rearrangements and subunit interactions in P2X receptors

Dissertation
zur Erlangung des Doktorgrades
der Naturwissenschaften

vorgelegt beim Fachbereich Biochemie, Chemie, Pharmazie
der Johann Wolfgang Goethe – Universität
in Frankfurt am Main

von

Yogesh Bhargava
aus Jabalpur (Indien)

Frankfurt 2009
(D30)

Vom Fachbereich Biochemie, Chemie, Pharmazie der
Johann Wolfgang Goethe – Universität als Dissertation angenommen.

Deken: Prof. Dr. Dieter Steinhilber
1. Gutachter: Prof. Dr. Bernd Ludwig
2. Gutachter: Prof. Dr. Ernst Bamberg
Datum der Disputation: **20-Nov-2009**

Abstract iv
1. Introduction 1
1.1 Study of neurotransmitter gated ion channels 1
1.1.1 Ligand gated ion channels and their functions 1
1.1.2 Consequence of the ligand-receptor interactions 2
1.2 Historical perspective 4
1.2.1 Discovery of purinergic receptors 4
1.2.2 Classification and nomenclature of purinergic receptors 5
1.3 The P2X receptor family 7
1.3.1 Gene family 7
1.3.2 Protein family 7
1.4 P2X receptor channels 9
1.4.1 Molecular structure 9
1.4.1.1 Membrane topology 9
1.4.1.2 Amino-terminal tail 9
1.4.1.3 Extracellular loop 10
1.4.1.3.1 ATP binding pocket 10
1.4.1.3.2 Conserved amino-acids 11
1.4.1.4 The pore 12
1.4.1.5 Carboxy-terminal tail 13
1.4.2 Channel stoichiometry 13
1.5 Properties of P2X1 receptors 15
1.5.1 Ligand binding 15
1.5.1.1 Agonists 15
1.5.1.2 Antagonists 18
1.5.2 Desensitization and recovery 20
1.5.3 Internalization 21
1.6 Techniques to study ligand-receptor interactions 22
1.6.1 Photolabeling 22
1.6.1.1 Requirements of the photoprobe 23
1.6.1.2 Photolysable groups 23
1.6.1.3 Photoaffinity labeling with purine based analogs 25
1.6.2 Fluorescence labeling 25
1.6.2.1 Strategies of fluorescence labeling 25
1.6.2.2 Real time assessment of receptor function 27
1.6.3 Electrophysiology 29
1.6.3.1 Electrical characteristics of biological membranes 29
1.6.3.2 The voltage clamp technique 30
2. Materials and Methods 34
A) Molecular Biology materials 34
B) Chemicals 34
C) Electrophysiology materials 35
D) Animals and related stuff 37
2.1 Molecular biology 37
2.1.1 cDNA construct of P2X2/1 receptor chimera 37
2.1.2 cDNA constructs of cysteine mutants of P2X2 and chimera 38
2.1.3 cDNA constructs of cysteine mutants of P2X1 38
2.2 Bacterial culture and cDNA purification 39

2.2.1 Culture medium and transformation 39
2.2.2 Plasmid DNA purification 39
2.2.3 cRNA synthesis 39
2.3 Heterologous expression in *Xenopus laevis* oocytes 40
2.3.1 Frog maintenance 40
2.3.2 Surgical preparation 40
2.3.3 Oocyte preparation and heterologous expression 41
2.4 Functional measurement of receptors 42
2.4.1 Design of the photolabeling setup 42
2.4.2 Design of voltage clamp fluorometry setup 43
3. Results 47
3.1 Probing allosteric interactions between P2X receptor subunits using photolabeling 47
3.1.1 Photolabeling of wild type P2X1 receptors 48
3.1.1.1 Agonist unbinding is required for the recovery from desensitization 48
3.1.1.2 Time course of photolabeling at P2X1 receptors 49
3.1.2 Photolabeling of wild type P2X2 receptors 50
3.1.2.1 Efficacy and potency of BzATP and ATP on P2X2 receptors 50
3.1.2.2 Each subunit contributes to the gating process 51
3.1.3 Photolabeling of the P2X2/P2X1 receptor chimera 52
3.1.3.1 Efficacy and potency of various ligands on the chimera 53
3.1.3.2 Time course of covalent activation of the chimera 55
3.1.3.3 Effect of prolonged application of light and BzATP on the chimera 57
3.1.3.4 Photolabeling modulates response of the receptors 58
3.1.3.4.1 Modulation of full agonist response by photolabeling 58
3.1.3.4.2 Modulation of partial agonist response by photolabeling 60
3.1.3.5 Estimating the number of bound ligands required for the maximal response generated by TNP-ATP on the receptors 61
3.2 Probing allosteric interactions between P2X receptor subunits using fluorescent ligand 64
3.2.1 Potency and efficacy of ATP and Alexa-ATP on P2X1 receptors and the chimera 64
3.2.2 Optimization of conditions for studying ligand-receptor interactions 67
3.2.2.1 Optimization of light irradiation protocol 67
3.2.2.2 Membrane trafficking of receptors 70
3.2.3 Allosteric interactions between subunits regulate the dissociation of bound agonist 72
3.2.4 Allosteric model for ligand-receptor interactions 76
3.2.4.1 Negative cooperativity in P2X1 receptors 76
3.2.4.2 Steady-state binding of Alexa-ATP to P2X1 receptors 82
3.2.4.3 Correlation between occupancy level and functional state of the receptors 84
3.2.4.4 Dissecting the number of agonist molecules required to desensitize the P2X1 receptors 86
3.3 Probing structural rearrangements in P2X receptors using voltage clamp fluorometry 90
3.3.1 TMRM treatment does not affect the function of CRD-1 mutants 91
3.3.2 Agonist mediated changes in the fluorescence intensity 93
3.3.2.1 Different positions sense different structural rearrangements 93
3.3.2.2 Fluorescence shift correlates with receptor activation and desensitization 96
3.3.2.3 Structural rearrangements during recovery from desensitization 97

3.3.3 Antagonist mediated changes in the fluorescence intensity 99
4. Discussion 101
4.1 Probing allosteric interactions between P2X receptor subunits in the gating process using photolabeling 101
Concurrent photolabeling and functional measurements..... 101
Photolabeling of P2X receptors..... 103
Modulation of potency and efficacy of agonists after photolabeling 105
4.2 Probing allosteric interactions between P2X receptor subunits using fluorescent ligand..... 109
Optimization of conditions for studying ligand-receptor interactions..... 109
Allosteric interactions between subunits depends on occupancy level of receptors 111
Allosteric model for ligand-receptor interactions..... 115
4.3 Probing structural rearrangements in P2X receptors during ligand-receptor interactions..... 119
Functional expression of CRD-1 mutants..... 119
TMRM accessibility to CRD-1 mutants..... 120
Agonist and antagonist binding induces structural rearrangements in the CRD-1 region of P2X1 receptors..... 121
An insight into the scheme for ligand-receptor interactions in P2X1 receptors.... 124
5. Miscellaneous results 126
5.1 Introduction..... 126
5.2 Fluorescence resonance energy transfer (FRET) 127
5.3 Structural information about P2X receptors 128
5.4 FRET between TMRM and Alexa-ATP in C165S mutant of P2X1 receptors..... 131
Summary 136
Zusammenfassung 143
References 150
Acknowledgements 161
Curriculum Vitae..... 163

Abstract

P2X receptors represent the third superfamily of ligand gated ion channels with ATP as their natural ligand. Most of the mammalian P2X receptors are non-selective cation channels, which upon activation, mediate membrane depolarization and have physiological roles ranging from fast excitatory synaptic transmission, modulation of pain-sensation, LTP to apoptosis etc. In spite of them being an attractive drug target, their potential as a drug target is limited by the lack of basic understanding of the structure-function relationship of these receptors.

In my thesis, I have investigated the behavior of homomeric P2X receptor subunits with the help of photolabeling and fluorescence techniques coupled to electrophysiological measurements using *Xenopus laevis* oocytes heterologous expression system. Concurrent photolabeling by BzATP and current recordings from the same set of receptors in real time has revealed that the gating process in homomeric P2X receptors is contributed individually by each subunit in an additive manner.

Our study for the first time describes the agonist potency of Alexa-ATP (a fluorescent ATP analog) on P2X1 receptors. The use of Alexa-ATP in our experiments elucidated that receptor subunits are not independent but interacting with each other in a cooperative manner. The type of cooperativity, however, depended on the type and concentrations of allosteric/competing ligands. Based on our results, in my thesis we propose an allosteric model for ligand-receptor interactions in P2X receptors. When simulated, the model could replicate our experimental findings thus, further validating our model. Further, correlation between occupancy of P2X1 receptors (determined using binding curve for Alexa-ATP) with the steady-state desensitization suggests that binding of three agonist molecules per receptor are required to desensitize P2X1 receptors.

We further extended the approach of fluorescence with electrophysiological measurement to assign the role for different domains in P2X1 receptors with the help of environmental sensitive, cysteine reactive fluorophore (TMRM). Cysteine rich domain-1 of P2X1 receptors (C117-C165) was found to be involved in structural rearrangements after agonist and antagonist binding. In contrast to the present understanding, that the binding of an antagonist cannot induce desensitization in P2X1 receptors and the receptors need to open first before undergoing desensitization, we propose based on our results that a competitive antagonist can also induce desensitization in P2X1 receptors by bypassing the open state.

Abstract

We have attempted to answer few intriguing questions in the field of P2X receptor research and we think that our answers provide many avenues to the basic understanding of functioning of P2X receptors.

1. Introduction

1.1 Study of neurotransmitter gated ion channels

1.1.1 Ligand gated ion channels and their functions

Fast synaptic neurotransmission, both excitatory and inhibitory, is mediated by extracellularly activated ligand gated ion channels. These channels are oligomeric transmembrane proteins made of several subunits. Depending on the occupancy state of the receptor, these ion channels exist in at least two conformations i.e. open and closed. The equilibrium between various conformations is affected by the binding of ligands on these channels. Upon selective binding of an agonist in the extracellularly located ligand binding site, a series of conformational changes would open the central ion-selective pore, this process is called gating. In general, excitation from resting membrane potentials is associated with the opening of cation-influx channels (depolarization), while inhibition of neuronal firing is generally associated with increased chloride ion permeability (hyperpolarization) [1]. A number of different receptors are responsible for these actions. Fast synaptic transmission includes channels directly gated by the neurotransmitter including L-glutamate, acetylcholine, glycine, ATP, serotonin (5HT), GABA. Based on our current understanding about these receptors, there are three different superfamilies of extracellularly activated ligand gated ion channels [2]:

1. Cys-loop superfamily: The receptors of this superfamily are made of five homologous subunits, each with four transmembrane segments e.g. nicotinic receptors, 5HT3 receptors, serotonin activated anionic channels.
2. Ionotropic glutamate activated cationic channels superfamily (iGluR): The receptors of this superfamily are made of four homologus subunits, each with three transmembrane segments e.g. NMDA receptors, AMPA receptors, Kainate receptors etc.
3. Ionotropic ATP gated channels superfamily: The receptors of this superfamily are made of three homologous subunits, each with two transmembrane segments e.g. P2X receptors.

Fig. 1.1 shows the schematic representation of families of neurotransmitter gated ion channels.

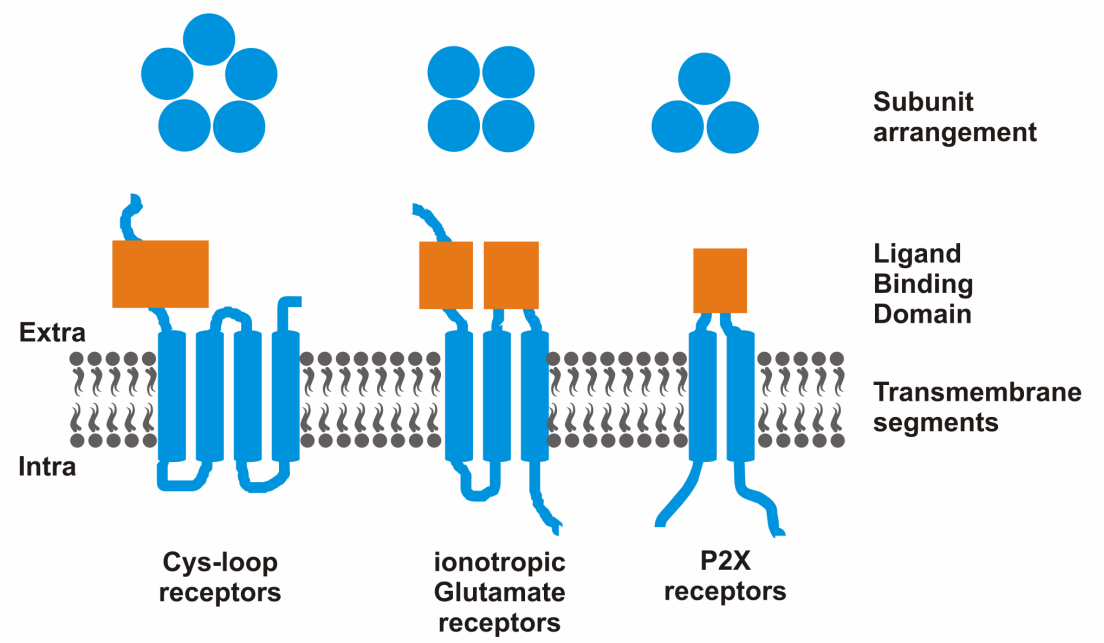

Fig. 1.1 Families of neurotransmitter gated ion channels: Cys-loop receptors have pentameric subunit arrangements, with each subunit having four transmembrane domains. Ionotropic glutamate gated ion channels have tetrameric subunit arrangements, with each subunit have three transmembrane domains. Ionotropic ATP gated ion channels have trimeric subunit arrangements, with each subunit have two transmembrane domains. The members of each superfamily have extracellular ligand binding site.

1.1.2 Consequence of the ligand-receptor interactions

Ligand gated ion channels offer a unique opportunity to study the effect of drugs/ligands as the ligand binding site and the machinery to generate a response are contained in a single macromolecule. According to the classical receptor theory [3], it is assumed that the effect of a drug is proportional to the fraction of receptors occupied by the drug and that maximal response occurs when all the receptors are occupied. In molecular terms, a physiologically relevant measure of response (channel activity) is the total fraction of time that the channel is open upon binding of agonist molecules (Po) i.e. an ion channel responds to an agonist by briefly permitting particular ions to flow along their concentration gradient from one side of the membrane to the other. Reflecting the fact that ion channels cannot be open more than 100% of the time, dose response curves constructed from plot of Po versus agonist

concentrations often results in S shape curves on log concentration axes (Fig. 1.2a). The concentration dependence or steepness of these functions can be expressed in terms of conventional Hill slope. The Hill coefficient gives a rough estimate of number of agonist molecules required to open the channel. In a kinetic scheme of the ligand-receptor interactions [4], association of agonist to the closed state of the receptor gives rise to the agonist-receptor complex. This complex could undergo conformational changes that result in the channel opening. Under this scheme, ***potency*** is a term used to describe the dependency of agonist's effect on its concentration, while ***affinity*** is the term used to describe the microscopic equilibrium (or rate) constants for the binding of agonist to the inactive closed state(s) of the receptor. An ***efficacy*** is the term used to describe microscopic equilibrium (or rate) constants, which describes all the transduction events that follow the initial agonist binding reaction [5]. At equilibrium, efficacy (ε) would be equal to the ratio of the two microscopic rate constants (β/α). Both these constants can be determined from the distribution of open and closed channel lifetimes i.e. α is simply the reciprocal of the average open channel lifetime, and β is the reciprocal of the average time when the channel is closed during the burst [6].

Therefore, based on the above concepts, a ***full agonist*** is a ligand whose binding would lead to an increase in the open probability of the ion channel (maximum open probability), whereas, a ***partial agonist*** is a ligand that would lead to the less open probability of the ion channel i.e. the relative opening and closing rates of the ligand-bound channel in which open state(s) are less frequent and the channel spends most of its time in closed state(s). In contrast, an ***antagonist*** would be a ligand, whose binding would not lead to opening of the ion channels. An antagonist can be competitive or non-competitive. ***Competitive*** antagonists compete for the agonist binding sites and their inhibition can be overcome by increasing the concentration of the agonist, ultimately achieving the same maximal effect. A ***non-competitive*** antagonist binds to different binding sites other than agonist binding sites and reduces the maximal response of an agonist. Its inhibitory effect cannot be overcome by increasing the concentration of agonist.

Therefore, the partial agonists that also compete for the same binding sites are often considered as competitive antagonists for the full agonists. Because, once there in the receptor binding sites, they not only producing weak response of their own but also prevent the access of full agonists to these sites. Agonists and antagonists could have same affinity for a receptor binding sites, but the former would have a high and the latter would have no efficacy. Fig. 1.2 shows the schematic representation of various terminologies used in this thesis.

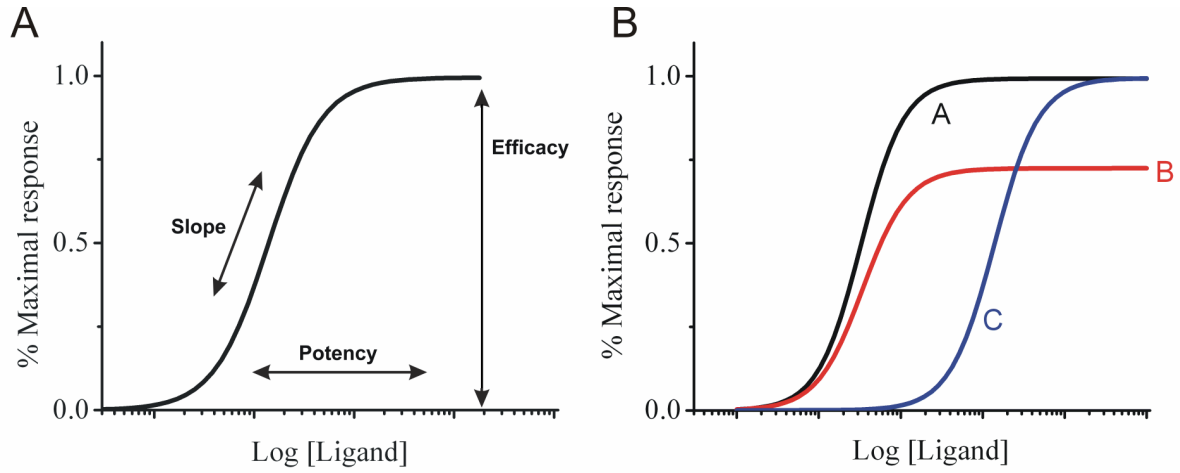

Fig. 1.2 Ligand-receptor interactions: (A) A sigmoidal dose-response curve results when the magnitude of effect observed is plotted versus the logarithm of ligand (agonist) concentration. Various important parameters are highlighted here. Potency is dependency of ligand's effect on its concentration. Efficacy is response produced by the ligand on the receptor. **(B)** Hypothetical dose-response curves. ***Interpretation of Curves A and C:*** Both agonists (A and C) have similar efficacy but differing in potency (A is more potent than C) or the dose-response curve of an agonist in the absence (curve A) and in the presence (curve C) of a competitive antagonist. ***Interpretation of Curves A and B:*** Both agonists (A and B) have similar potency but differing in efficacy (A is full agonist, and B is partial agonist) or the dose-response curve of an agonist in the absence (curve A) and in the presence (curve B) of non-competitive antagonist.

1.2 Historical perspective

1.2.1 Discovery of purinergic receptors

Early investigations into the effects of adenosine and ATP were made in a variety of tissues particularly in heart and vasculature. In a comprehensive report, Drury and Szent-Györgyi showed that adenosine and AMP extracted from heart muscles have pronounced biological effects including heart block, arterial dilation, lowering of blood pressure, and inhibition of intestinal contraction [7]. Further insight into different action of adenosine and ATP came from the studies of Gillespie [8]. His studies showed that ATP caused an increase in blood pressure in rabbits and cats which was rarely or never observed with AMP or adenosine. He also showed that ATP was more potent than AMP and adenosine in causing contraction of Guinea pig ileum and uterus. These studies, for the first time indicated the existence of different purine receptors in higher organisms.

Early lines of purine research elucidating the physiological roles of extracellular purines and pyrimidines came from the studies of their biological sources and the stimuli for their release.

Experiments by Holton [9] showed that ATP could be released from sensory nerves in the rabbit ear. Berne [10] showed that adenosine is released from the heart during hypoxia to play an important role in reactive hyperemia.

In early 1970s, Burnstock et al. [11,12] suggested that ATP or related nucleotides might be neurotransmitters, released by non-adrenergic or non-cholinergic neurons in the gut. The idea behind the concept of "purinergic transmission" was the existence of specific "purinergic receptors" present in the post-junctional cell membrane.

Since then, the active research in the field of purinergic signaling has established that numerous blood cells, immune and cardiovascular system are important source of purines that can be released under physiological and pathophysiological conditions, which may act on the purine receptors associated with these or neighboring cells [13-16]. Contrary to purine, not enough is known about the sources and release of pyrimidines which limits our understanding of the role played by the widely distributed receptors that are activated by pyrimidines.

1.2.2 Classification and nomenclature of purinergic receptors

Purines and pyrimidines mediate their effects by interacting with distinct cell-surface receptors. Burnstock (1978) [17] for the first time formally recognized "Purinergic" receptors and suggested a basis for classifying them. He proposed that purinergic receptors can be divided into two classes termed as "P1-purinoceptors" having adenosine as the principal natural ligand and "P2-purinoceptors" having ATP and ADP as principal natural ligands. This division was based on the criteria that ATP was acting directly on P2 receptors, whereas its ecto-enzymatic breakdown products were active on P1 receptors. Other important considerations behind this suggested classification were the relative potency of ATP, ADP, AMP and adenosine, selective antagonism of the effects of adenosine by methylxanthines, activation of adenylate cyclase by adenosine and stimulation of prostaglandin synthesis by ATP and ADP.

Again in 1985, Burnstock and Kennedy [18] proposed the first subdivision of P2 receptors into P2X and P2Y purinoceptors. This subdivision was based solely on the pharmacological action of αβ-MetATP on the visceral smooth muscle. It was then suggested that P2X receptors were involved in vasoconstriction and contraction of smooth muscles, whereas P2Y receptors were involved in mediating vasodilation and relaxation of smooth muscle upon αβ-MetATP application. Soon after the introduction of this subdivision, Gordon tentatively

proposed two more P2 purinoceptors: P2T (ADP selective and involved in platelet aggregation) and P2Z (which were activated by ATP^{4-} and are prominent in mast cells, macrophages and lymphocytes) [15]. With the growing interest and commercial availability of adenosine and ATP analogs, several further subclasses were proposed including P2U purinoceptors (where ATP and UTP were equipotent [19]), and P2D purinoceptors (selective for diadenosine polyphosphate [20]).

In the recommendations of International Union of Basic and Clinical Pharmacology (IUPHAR) subcommittee concerning the nomenclature of P2 purinoceptors [21] it was emphasized that the current purinoceptor sub-classification with so many alphabets being used was unsatisfactory because of randomly added new receptor subtypes. The committee supported a new system of classification proposed by Abbracchio and Burnstock [22]. In that proposal, it was suggested that P2 receptors should be placed in two major families: P2X (consisting of ligand gated cation channels) and P2Y (consisting of G-protein coupled receptors). Soon thereafter, Fredholm et al. [23] suggested "P1 receptors" and "P2 receptors" in order to replace "P1/P2-purinoceptor" terminology. This classification then brought ATP into line with most other neurotransmitters such as ACh, GABA, glutamate and 5HT where ligand-gated and G-protein mediated receptor sub-classification has already been established.

Recently, International Union of Pharmacology Committee on Receptor Nomenclature and Drug Classification (NC-IUPHAR 2008) has issued revised guidelines for ligand gated ion channels [24]. It was decided by the subcommittee chairs to drop the use of subscripts from all of the subunit names for P2X receptors. Therefore, in this thesis this guideline will be followed.

1.3 The P2X receptor family

1.3.1 Gene family

There are seven genes for P2X subunits. The chromosomal locations of human subtypes of P2X genes are listed below (HUGO denotes Human Genome):

Receptor subtype	HUGO gene name	Chromosomal location
P2X1	P2RX1	17p13.3
P2X2	P2RX2	12q24.33
P2X3	P2RX3	11q12
P2X4	P2RX4	12q24.32
P2X5	P2RX5	17p13.3
P2X6	P2RX6	22p11.21
P2X7	P2RX7	12q24

1.3.2 Protein family

Early pharmacological studies established a strong basis for discriminating various subtypes of P2X receptors, which later in mid 1990s, coupled with molecular cloning of these receptors from native excitable tissues has continuously broaden our understanding of P2X receptors. Till date seven P2X receptor proteins (P2X1 to P2X7) have been cloned [25] and expressed in *Xenopus* oocytes or in mammalian cells. Pharmacologically they all show distinct profiles. Due to the lack of considerable sequence homology with any known protein to date, and absence of motifs (e.g. Walker motif) their structure prediction is not possible. Among themselves they share less than 50% protein sequence homology. Based on the available data and analysis of hydrophobic pattern, it is predicted that P2X subunits have two transmembrane domains, with a large extracellular loop containing the putative ATP binding site (Fig. 1.3). This type of subunit topology has been seen with acid-sensing-ion-channels (ASIC) [26]. Thus, P2X receptors constitute one of the main receptor family that is distinct from Cys-loop and glutamate receptor families [27].

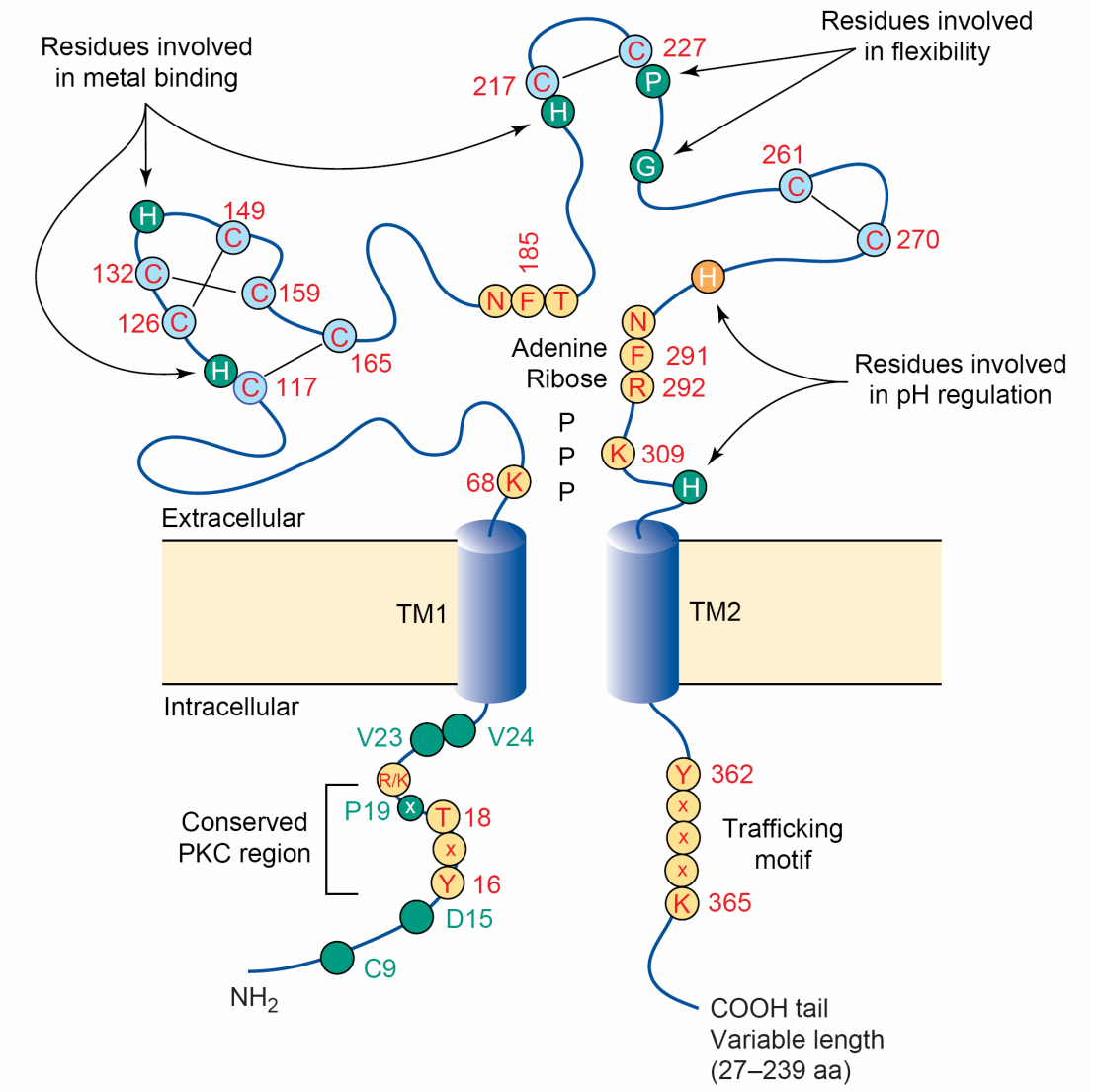

Fig. 1.3 Schematic representation of various domains of human P2X1: The putative topology of P2X receptors in general has both N and C terminals facing towards cytosolic side. There is a one large extracellular domain connecting the two putative transmembrane domains. The N terminal domain of P2X receptor has conserved PKC site. Many conserved amino acids are present in the extracellular region as shown in red. It has been suggested that positively charged residues (K, R) are involved in ATP binding. There is a characteristic pattern of cysteine bonds as judged by mutagenesis studies. The diagram shows human P2X1 numbering [28].

1.4 P2X receptor channels

1.4.1 Molecular structure

1.4.1.1 Membrane topology

The membrane topology of the P2X receptors has been addressed by various approaches. In the first approach, locations of glycosylation sites have been determined. The studies on P2X2 receptors indicated that asparagines (N182, N239 and N298) were localized to the extracellular domain (Fig. 1.3). Glycosylation had been observed at newly introduced asparagine sites on the P2X2 receptors in which these three natural asparagine sites had been removed. These studies provide direct support for the proposed topology of P2X receptors with a large extracellular domain between two membrane spanning regions [29,30]. Further evidence that N and C terminals reside on the same side of the membrane came from the studies in which two cDNAs have been joined in tandem [29,30]. Such constructs express fully functional channels. The cytosolic location of the amino and carboxy termini is also supported by the finding that an amino-terminal asparagine residue is not glycosylated at all. Finally, confocal immuno-fluorescence microscopy has been carried out on HEK293 cells transfected with P2X2 receptors carrying FLAG epitope at the N and C terminus. In either case the epitope was accessible to antibody only when the cells were permeabilized [30].

1.4.1.2 Amino-terminal tail

The amino-terminal tail of P2X receptors is short (20-30 residues) compared to carboxy-terminal tail (28-242 residues). P2X receptors are sensitive to changes in the intracellular environment [31] and can also be regulated by a phosphorylation mechanisms. All P2X subunits contain a conserved YxTxR/K motif in the intracellular N-terminus that incorporates a consensus protein kinase C site (T-X-K/R) (Fig. 1.3). Phosphorylation of serine, threonine or tyrosine residues is thought to control the receptor activity [32-34]. Apart from the conserved PKC site, other intracellular domains of P2X receptors can also interact with and regulate the properties of other ion channels.

1.4.1.3 Extracellular loop

1.4.1.3.1 ATP binding pocket

P2X receptors have a large extracellular ligand binding loop comprising ~280 amino acids. 93 of these amino acids are conserved in at least six P2X family members and could therefore be involved in ATP binding, because ATP gates P2X receptors when applied extracellularly. In addition, a purified extracellular loop obtained from P2X2 receptors binds ATP with low affinity [35]. ATP is generally complexed with magnesium, which suggests that negatively charged amino acids might coordinate ATP binding via magnesium. But, experiments in P2X1 [36] and P2X2 [37] suggested that 11 out of 12 point mutants designed to neutralize the conserved negative charges of receptors had a less than two fold effect on ATP potency thus indicating that these residues are not essential for mediating the actions of ATP. Aromatic amino acids are associated with recognition of adenine nucleotides in many ATP binding proteins [38]. Along the same lines, recent studies showed that conserved residues F185 and F291 regulate ATP potency at P2X1 receptors and suggested that they coordinate the binding of adenine ring or ATP (Fig. 1.3) [39]. Mutations of conserved adjacent residues to alanine (T184, N288, and R290) in P2X2 (R292 in P2X1) also affect the ATP potency indicating a NF(R/T) motif in the agonist binding site. This is similar to NWK motif in synapsin for which crystal structures have shown that aromatic tryptophan binds to the adenine ring of ATP [40].

Sequence homology between human P2X1 and rat P2X2 receptors suggests that conserved positively charged amino acids K68, R292, and K309 (P2X1 receptor numbering), are associated with the binding of phosphate chain of ATP [37,41]. Therefore, there were two possibilities that K68, K71, K309 etc (conserved positively charged residues), which has been shown to directly affect ATP potency (hence thought to contribute to the ATP binding domain), comes from the same subunit or contributed by adjacent subunits. Marquez-Klaka et al. [42] used disulfide cross-linking approach and non-reducing SDS-PAGE to answer this question. Their data demonstrated that K68C/F291C double mutant (both mutations in each subunit) resulted in the formation of trimer on the non-reducing SDS-PAGE, consistent with the formation of intersubunit disulfide bridges. In the functional studies on the P2X2/1 receptor chimera, it was found that ATP activated currents from these double mutants were small, indicating that formation of intersubunit disulfide bond either prevented ATP binding to the binding site or induced constraints to the gating. However, significant increase in current was observed after the extracellular application of reducing agent (DTT), indicating breakage of intersubunit disulfide bond. In the light of earlier mutagenesis evidences [39]

which suggests involvement of these positions to influence ATP potency, their observations support the hypothesis of intersubunit ATP binding sites.

Some attempts have been made in recent past to model the structure of P2X receptors especially the ATP binding domain. A structural similarity between first half of the extracellular domain (residues 170-330) of P2X receptors and class II aminoacyl-tRNA synthetase has been suggested [43] whose catalytic site is composed of seven stranded antiparallel β-pleated sheet [44]. But, in the absence of any template protein, homology modeling of P2X receptors remains a difficult task. The number of ATP molecules required to open the P2X receptors is also currently not known, however dose response curves of P2X receptors generally have a Hill coefficient of more than one, which suggests that at least more than one ATP binding is required to open the channel. It is also interesting to note that not all the nucleotides are active on P2X receptors e.g. adenosine, polyphosphates or other nucleotides such as GTP and UTP exhibit neither agonist nor antagonist action. In addition, heteromeric P2X receptors can have agonist sensitivity and time courses (activation and deactivation) that are distinct from that of their constituent subunits. These observations suggest that probably interactions between the subunits are also important in determining the properties of the channels.

1.4.1.3.2 Conserved amino-acids

P2X receptor subunits have a large extracellular domain. A striking feature of which is the presence of 10 conserved cysteine residues between P2X1-7. It was thought that these cysteines in an extracellular location contribute to the tertiary structure of the protein by disulfide bond formation. However, there is no direct evidence for this because of the fact that treatment with reducing agents has no effect on channel function [45,46]. The possible pattern of disulfide bond formation has been approached by systematic cysteine to alanine substitutions. Mutagenesis studies on human P2X1 by Ennion et al. [46] and on rat P2X2 by Clyne et al. [45] unraveled a specific pattern of disulfide bonds between these conserved cysteine residues (Fig. 1.3).

There are several other conserved glycine and proline residues that enable flexibility in the extracellular loop, raising the possibility that they are involved in conformational changes in P2X receptors upon agonist binding. Indeed channel function was abolished in P2X2 receptors with the mutations G247A [47] and P225A [48] indicating that the flexibility was

required in these regions. However further studies will be necessary to determine the role of other conserved proline and glycine residues in conformational changes.

The other striking feature which is common among all the subtypes of P2X receptors is the presence of consensus N-linked glycosylation (Asn-X-Ser/Thr) sites on the extracellular loop. The P2X1 subunit sequence has five such consensus sites, four of which are conserved among human, rat and mouse sequences (N153, N184, N284, and N300 with rP2X1 numbering) [49]. The P2X2 subunit has three such sites common among human, rat and mouse sequences (N182, N239, and N298 with rP2X2 numbering). All these sites were found to be glycosylated in oocytes [29] and in HEK293 cells [30]. Some of these glycosylation sites are essential for receptor trafficking to the plasma membrane [50]. The consequences of removal (by mutagenesis) or prevention (by tunicamycin) of glycosylation on trafficking and functionality of P2X2 receptors indicated that the receptors in which any two of the three sites were glycosylated traffic to the cell surface and were fully functional, while receptors in which only one site or no site is glycosylated are failed to traffic to the plasma membrane [29,30].

P2X receptors can be regulated allosterically by extracellular protons [51-53], divalent cations and various other ions [53-55]. However their effects are variable among receptor subtypes which is reflected by the lack of consensus among the contributing residues identified by mutagenesis.

1.4.1.4 The pore

P2X receptors gate upon agonist binding which enables the movement of monovalent cations and Ca^{+2} through the open channel [55]. Substituted cysteine accessibility mutagenesis has been extensively used to identify residues that line the pore walls of various channels. The pattern of accessibility to the modifying reagent is informative because the detection of an accessible residue in every 3-4 residues implies that the domain under investigation is α-helical. Based on such studies TM2 of P2X2 receptors seems to have an α-helical conformation in the closed state but not when the channels are open. The narrowest part of the channel pore is probably near a glycine residue at position 342 about halfway through TM2 [56,57]. On the basis of macroscopic current measurements on P2X2, P2X4 and P2X7, these channels can have at least two open states (I1 and I2) with distinct permeabilities. Permeability was shown to increase with sustained activation i.e. during longer ATP

applications the channels could allow larger cations such as N-methyl-D-glucamine ($NMDG^+$) and propidium analog YO-PRO-1 depending on subtypes. The pore of P2X7 receptors was found to dilate upon receptor activation on a time scale of seconds [58].

1.4.1.5 Carboxy-terminal tail

Different P2X subtypes show different length of C-terminal tail (28 to 242 amino acids). The P2X7 subunits have the longest C-terminal tail with additional hydrophobic domain (residues 510-530) that is sufficiently long to cross the plasma membrane. Orientation of C-terminal tail in P2X7 is currently unknown; however, membrane topology algorithms suggest an intracellular location. The presence of conserved YxxxK motif at the C-terminal tail is shown to be involved in efficient receptor trafficking to the plasma membrane [59]. Additionally C-terminal residues could also regulate the number of available channels at the cell surface by internalization of some P2X receptor isoforms [60-62]. Splice variants and mutants of C-terminal tail suggest that this region could also be involved in modifying the gating and pore properties (including pore dilation) [63,64]. Studies on co-expression of P2X2 receptors with excitatory nicotinic acetylcholine receptors [65], 5HT3 receptors [66] and inhibitory GABA receptors [67] of Cys-loop superfamily leads to inhibitory crosstalk between the channels. These studies highlighted the role of C-terminal domain of P2X receptors in the process of cross-inhibition. Sub cellular targeting studies on P2X2 receptors revealed that they were localized at the terminals but not in the cell body of hippocampal interneurons [68], thus indicating the possible interactions with other cellular proteins. Therefore, it seems likely that P2X receptors do not exist in isolation in the membrane but contribute to the organized regulatory signaling domains through these intracellular sites. Taken together, these studies highlighted the multiple role of C-terminal domain of P2X receptors.

1.4.2 Channel stoichiometry

Different techniques have been used to determine the channel stoichiometry of P2X receptors. Kim et al. [35] have purified His-tagged ectodomain of the rat P2X2 receptors (K53-K308) using bacterial expression system. After sulfitolysis and refolding, they specifically labeled the refolded protein domain with [α-^{32}P]ATP. Based on the molecular size of the labeled protein which was four times (132kDa, as estimated by equilibrium sedimentation centrifugation) the calculated size of ectodomain (29 kDa), they suggested that the P2X

receptors might assemble functionally as tetramers in the membrane. However later it was shown that multimerization of full-length P2X2 subunits into trimeric arrangement is determined by the second transmembrane domain, and not by the extracellular loop [69].

Since the last decade, a growing number of accumulated evidences have been indicating that P2X receptors functionally assemble as trimers into the membrane. At least 5 different approaches have been used to conclude the trimeric channel stoichiometry of P2X receptors.
In the first approach, Nicke et al. [49] used bifunctional cross-linking reagents and BN-PAGE methods to show the trimeric topology of P2X1 and P2X3 receptors. In that study, digitonin solubilized, His-tag purified receptors migrated entirely as non-covalently linked homo-trimers on BN-PAGE. Support to the trimeric topology also came when these receptors were cross-linked by chemical cross-linking agents on the intact oocytes (before purification) or during His-tag purification (on the Ni-NTA column) and analyzed by non-denaturing SDS-PAGE gel. It was found that P2X receptors were cross-linked to dimers and trimers.

Later, Jiang et al. [70] used functional characterization of single and double cysteine mutants of TM1 and TM2 regions of P2X2 and P2X3 receptors to determine the channel stoichiometry. From the pattern of current generated by these single or double mutants from the homo or heteromeric channels, it was deduced that TM1 of one subunit is adjacent to TM2 of the next subunit in homomeric P2X2 channels in a head-to-tail orientation. They also found that the coexpression of P2X2 double cysteine mutants with the wild type P2X3 subunits gave essentially normal P2X2/3 currents and these were unaffected by DTT. But, the coexpression of P2X3 double cysteine mutants with the wild type P2X2 subunits gave the oligomeric channel currents that were much smaller than control currents and these were augmented greatly by DTT. Thus, their results indicated trimeric arrangement of P2X2/3 heteromers with composition of one P2X2 and two P2X3 subunits.

In the third approach, based on selective cell surface radio-iodination and the use of glutaraldehyde-based *in situ* cross-linking of plasma membrane bound P2X receptors, Aschrafi et al. [71] showed that homomeric P2X2 and heteromeric P2X1/2 receptors share trimeric subunit organization on the plasma membrane. In their study, they found that the plasma membrane bound His-tagged homomeric P2X2 migrated as several defined oligomers on BN-PAGE. However these oligomers were dissociated into monomers, dimers and trimers when denatured with urea and (or) DTT. These results suggested that the functional homomeric P2X2 receptors arranged in oligomeric state on the plasma membrane. It was believed that these subunits were bound by weak interactions that could be lost during

receptor purification. Thus, in order to capture potentially existing loosely associated subunits, they cross-linked the functional receptors on the intact oocytes (prior to purification). When analyzed on reducing SDS-PAGE gels, these adducts were visible as three bands at ~65, ~130 and ~190kDa corresponding to monomer, dimer and trimer in homomeric P2X2 receptors. Similarly, when they expressed His-tagged P2X1 subunits with the non-tagged P2X2 subunits, they co-purified P2X2 subunits with His-tagged P2X1 under non-denaturing conditions, which migrated as one single protein complex on the BN-PAGE with a mass slightly larger and smaller than the P2X1 and P2X2 homotrimers respectively. Thus, together these results showed trimeric topology of homomeric P2X2 and heteromeric P2X1/2 receptors on the membrane.

Barrera et al. [72], used chemical crosslinking (Disuccinimidyl suberate, DSS) and direct imaging of individual receptors by atomic force microscopy (AFM) to demonstrate that P2X2 receptors are trimers. They studied the images of His-tagged P2X2 receptors cross linked with anti-hexa-His antibodies. For receptors with two bound antibodies, the mean angle between the antibodies was 123^{o}, indicating that the receptor was trimeric.

Similarly, Mio et al. [73] imaged glutaraldehyde cross linked FLAG-tagged P2X2 receptors using electron microscopy. The images demonstrated inverted three-sided pyramid with the dimensions of 215 Å in height and 200 Å in width. The threefold symmetrical top view demonstrated the first visual evidence that P2X2 receptors have trimeric topology.

1.5 Properties of P2X1 receptors

1.5.1 Ligand binding

1.5.1.1 Agonists

P2X receptors are well expressed and studied in heterologous systems like *Xenopus laevis* oocytes and HEK293 cells [74-76]. The homomeric P2X1 receptor is a cation-selective channel that shows little selectivity for sodium over potassium [77]. It has a low permeability to larger organic cations such as Tris (P_{Tris}/P_{Na} 0.18) or N-methyl-D-glucamine (P_{NMDG}/P_{Na} 0.04) at least when tested with brief agonist application. Extracellular calcium (up to 100mM) has little or no inhibitory effect on P2X1 receptor currents [77]. The single channel conductance of P2X1 channels is reported as ~18 pS [75,77].

Two defining characteristics of the homomeric P2X1 channels are its rapid desensitization kinetics and its sensitivity to activation by αβ-MetATP. These characteristics are also shared by homomeric P2X3 channels, and therefore cannot be used to uniquely define P2X1. It is reported that βγ-MetATP is equipotent as αβ-MetATP at P2X1 receptors, but it is approximately 30-50 fold less potent at P2X3 and more than 100 fold less potent on other P2X receptor subtypes [58,74,78-81]. Consequently, βγ-MetATP has been used as a selective agonist in some studies investigating P2X1 mediated smooth muscle contraction (e.g. urinary bladder, vas deferens, saphenous vein) [82-85]. ADP was originally reported to be an agonist of P2X1 with moderate potency (EC_{50} = 10-70μM) [74,86], however it has been shown that this activity was imparted by ATP impurities. Later, purified ADP at concentrations as high as 1mM failed to elicit currents in oocytes expressing human P2X1 [87].

P2X1 receptors are fast desensitizing receptors in which desensitization overlaps the channel activation. Due to this, sensitivities of various ligands cannot be studied in steady-state condition. Therefore, Rettinger et al. [88] used non-desensitizing P2X2/1 receptor chimera, which included the entire P2X1 ectodomain. It was found that different agonists activated the chimera with nanomolar potencies. Thus, it was suggested that the ectodomain of P2X1 has nanomolar sensitivity to ATP which is masked by desensitization in the wild type P2X1 receptors. Their results on the time course of deactivation of chimera was found to be inversely related to the agonist potency (e.g. For ATP: τ = 63s, EC_{50} = 3nM; while for αβ-MetATP: τ = 2.5s, EC_{50} = ~60nM). Thus, it was thought that the rate limiting step in the deactivation process was the rate of agonist unbinding. In the light of these results from chimera, it is expected for the wild type P2X1 receptors that the rate limiting step in the recovery of desensitization is the rate of agonist unbinding.

Diadenosine polyphosphates (APnA) are also known to bind P2X1 receptors with potencies similar to ATP. In case of rat P2X1 receptors, it was found that APnA activity increases with increasing number of phosphate moieties: AP_6A was a full agonist, whereas AP_5A and AP_4A were partial agonists, AP_3A had a weak effect and AP_2A had no effect at 30μM on hP2X1 [89]. The structures of some of the P2X agonists are shown in Fig. 1.4.

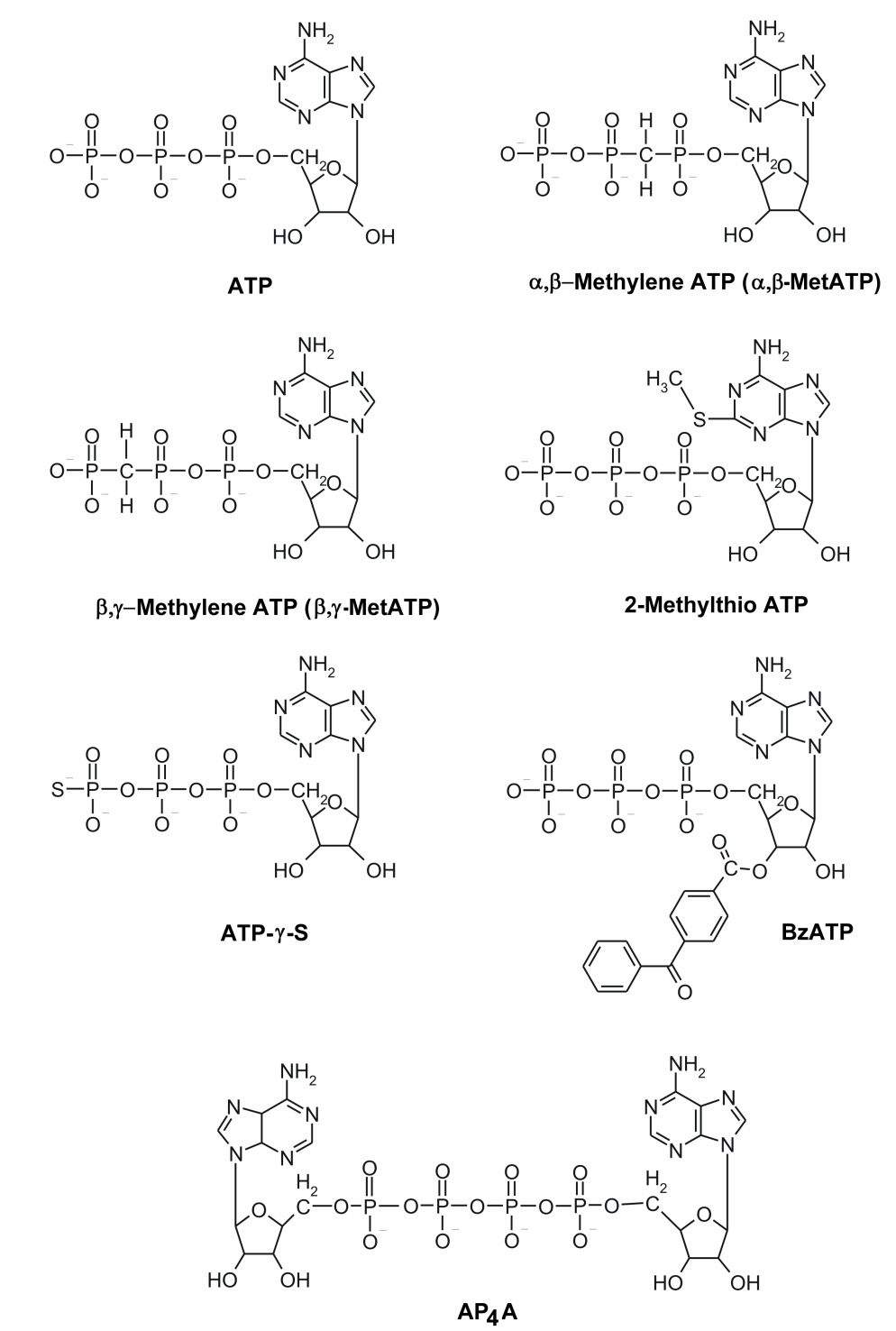

Fig. 1.4 Structure of various agonists of P2X receptors: Listed here are various agonists of P2X receptors. αβ-MetATP is a non-hydrolysable ATP analog used to differentiate between fast desensitizing P2X1 from non desensitizing P2X2. BzATP is a Benzophenone based ATP analog (BzATP) which could be used as a photoaffinity ligand.

1.5.1.2 Antagonists

Initially, Suramin and pyridoxal-phosphate-6-azophenyl-2', 4'-disulfonate (PPADS) were used as antagonists of P2X1 channels [75,90,91]. Subsequently several analogs of both suramin and PPADS were synthesized that had increased selectivity and potency against P2X1.

NF023 is a suramin analog that was first used to inhibit αβ-MetATP evoked vasoconstriction in pithed rats [92]. Later, NF023 was shown as a potent antagonist of P2X1 (IC_{50} = ~300nM) with selectivity over P2X2, P2X3 and P2X4 [93]. Even greater potency was achieved with the discovery of another suramin analog, NF279 which had an IC_{50} value of ~20nM and increased selectivity towards P2X1 over P2X2, P2X3 and P2X4 [94]. Further modification of NF279 compound yielded NF449. NF449 showed the IC_{50} value of 0.3nM on rP2X1 expressed in oocytes [95]. The mechanism of antagonism of NF279 was investigated on P2X2/1 receptor chimera which maintains the ectodomain of P2X1 receptors and represents the non desensitizing phenotype. In the presence of NF279, dose response curve for ATP was rightward shifted consistent with the competitive antagonism [88].

PPADS analogs with increased potency and selectivity have also emerged. The first PPADS analog identified with modest selectivity for rP2X1 over other P2X and P2Y receptors was MRS2220. It showed IC_{50} = 10μM for rP2X1 [96]. PPNDS, another analog of PPADS, inhibited αβ-MetATP induced isometric contraction of rat vas deferens and inward currents in rP2X1 expressing oocytes with IC_{50} value of ~10nM (vs ~200nM for PPADS) [97]. Thus, indicating that PPNDS is a potent P2X1 antagonist.

TNP-ATP is another potent antagonist of P2X1 receptors, which has an IC_{50} value of ~1-6nM [98,99]. Diinosine polyphosphates (IP_nI) (synthesized through deamination of AP_nA by the AMP-deaminase of *Aspergillus* sp.) are also potent P2X1 antagonists with nanomolar potencies [100]. Extracellular pH also regulates the agonist-induced currents in P2X1 receptors. Lowering the pH to 6.3 reduced the current, but increasing the pH to 8.5 has no effect on current responses [77,101]. The structures of main antagonists are shown in Fig. 1.5.

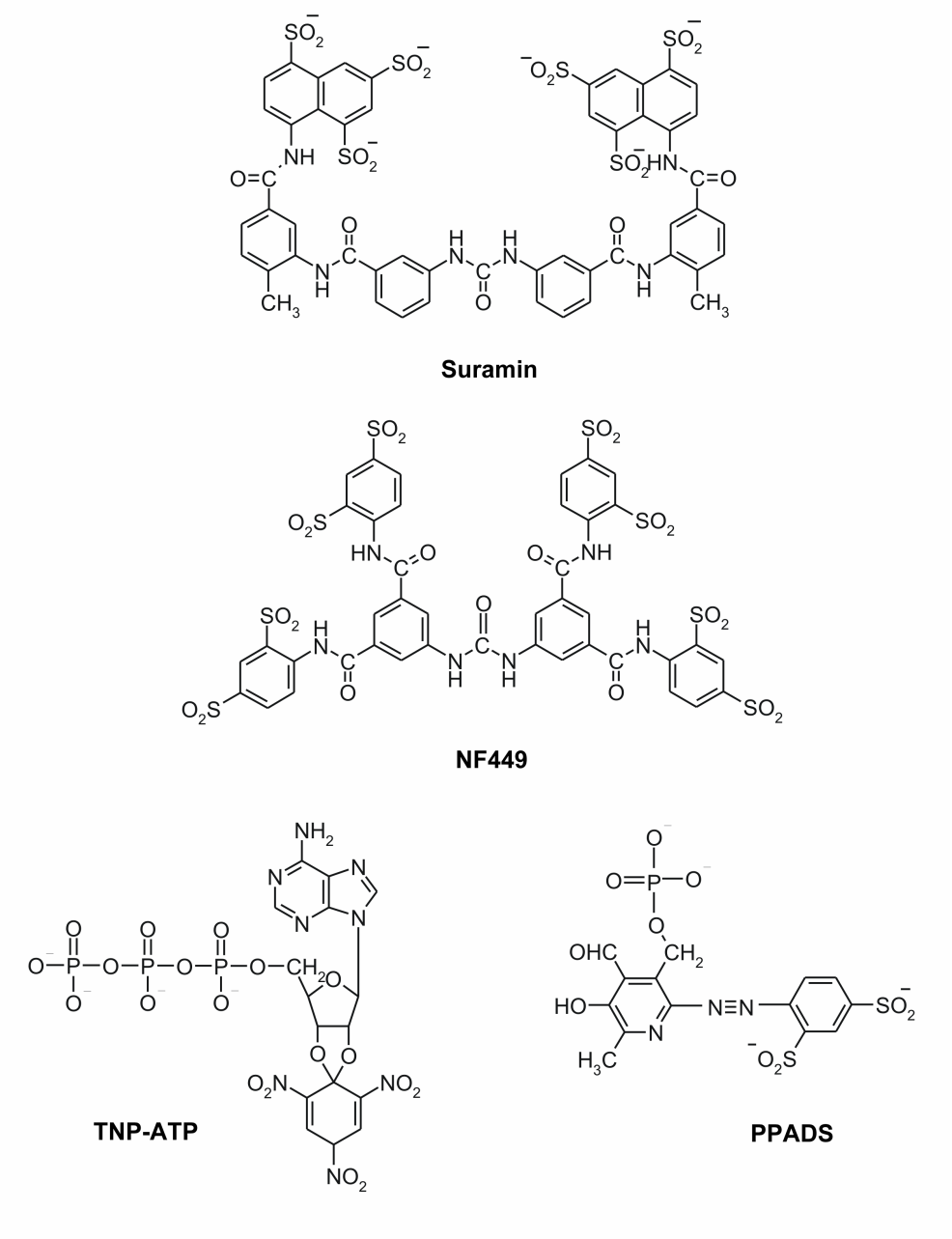

Fig. 1.5 Structure of various antagonists of P2X receptors: Listed here are various antagonists of P2X receptors. The general mode of action of these compounds is through competitive inhibition.

1.5.2 Desensitization and recovery

Desensitized state of a receptor represents an electrophysiologically silent state where even in the continuous presence of an agonist no response can be elicited. The desensitized state corresponds most likely to a ligand bound closed state of the receptor. The process of recovery from desensitization is believed to occur in two steps. The first step must involve agonist unbinding and the second step then involves recovery from the agonist free desensitized to the resting state where the channel can be activated again.

Human leukemia cells (HL60) and rat basophilic leukemia cells (RBL) express P2X1 receptor mRNA and protein, but inward currents in response to extracellular ATP can only be observed after treating the cells with apyrase [102]. This surprising observation suggested that ATP was being continuously released from the cells which could induce desensitization.

P2X1 and P2X3 receptors desensitize in the presence of ATP (EC_{50} or more) with time constants of 300ms and 50ms respectively [77]. The time course of recovery from desensitization is 10-20min [76,103]. Generally second and subsequent applications of ATP do not elicit currents equivalent to the first application. Experiments on non-desensitizing P2X2/1 receptor chimera indicated that desensitization require both TM regions of the P2X1 receptors. If either of the regions was replaced by the equivalent segment from P2X2 receptors, desensitization no longer occurred [76]. These results suggest that the closure of the channel during continued presence of the agonist requires concerted conformational changes involving both TM segments.

In studies on recombinant rat P2X1 receptors expressed in oocytes, Rettinger et al. [104] revealed some of the important findings about the desensitization and recovery of the receptors from desensitization. They found that in the presence of near saturating micromolar ATP concentrations (e.g. 30µM), P2X1 receptors quickly activate and the current declines to baseline in less than 1s, suggesting that P2X1 receptors undergo fast desensitization in the continuous presence of ATP. Even at an ATP concentration as low as 100nM, which elicits only 10% of the maximum current response, they found that receptors could be fully desensitized in few seconds. Under these non-steady-state conditions i.e. when virtually all activated P2X1 receptors were closed rapidly by desensitization and not by direct transition to the re-activable closed state, the EC_{50} value of receptor activation was found to be 0.7µM. In their search for the lowest ATP concentration to desensitize P2X1 receptors, they pre-equilibrated P2X1 receptors with different nanomolar ATP concentrations until steady-state binding was achieved. Functional response by near saturating ATP concentration (30µM)

from these equilibrated receptors gave 3nM as a $K_{1/2}$ value of steady-state desensitization, indicating that the desensitized state of P2X1 receptors has nanomolar affinity to agonists. Due to the high affinity of desensitized state to bound agonist, the bound agonist dissociates very slowly from the desensitized state, thus, suggesting that the rate limiting step in the recovery of P2X1 receptors from desensitization is the agonist unbinding step.

When they compared the mechanism of desensitization in P2X1 receptors and nicotinic receptors, they found that both show different mechanisms of desensitization. Nicotinic receptors already have high affinity desensitized state in equilibrium with the resting state, thus, the agonist can bind directly to the desensitized state before opening of the receptor. However, P2X1 receptors can be desensitized by nanomolar concentrations of agonists, but the area under the current traces elicited by different agonist concentrations (18-300nM) was found to be similar indicating that P2X1 receptors must open first before undergoing desensitization.

Further support to these observations came from their work on a P2X2/1 receptor chimera which indicates that the ectodomain of P2X1 receptors has nanomolar affinity for ATP and that an inverse relationship existed between EC_{50} value of agonist and the time course of deactivation of current [88]. These results suggest that unbinding of agonist is the prerequisite for channel deactivation. By eliminating the desensitization from the P2X1 receptors (i.e. use of chimera), the stationary currents become amenable to analysis that allows for a determination of the EC_{50} value under steady-state conditions. Thus, on chimera, the EC_{50} value of receptor activation was found to be 3nM. However, the additional processes which regulate the slow unbinding of agonists from the desensitized state of P2X1 receptors are currently unknown.

1.5.3 Internalization

Direct visualization of agonist mediated internalization of P2X1 receptors comes from the study of P2X1-coupled green fluorescent protein (GFP) chimeras. The work of Dutton et al. [105] showed that P2X1-GFP chimera undergoes internalization in HEK293 cells upon prolonged exposure (~40s) to ATP. The observed co-localization of an endosome marker with P2X1-GFP confirmed the role of endosomes in internalization of these chimeras. Similar results using P2X1-GFP chimera transfected and expressed in sympathetic neurons from superior cervical ganglion showed that upon exposure to αβ-MetATP, formation of clusters

occur under the plasma membrane [106]. The loss of GFP fluorescence upon receptor activation was possibly due to quenching of GFP fluorescence by the acidic environment of endosomes. Thus, pretreatment of transfected ganglia with 5μM monensin (which disrupts the pH gradient in endosomes) prior to the addition of αβ-MetATP resulted in retention of GFP fluorescence, demonstrated the role of endosomes in agonist mediated receptor internalization. Similar conclusion of agonist mediated receptor internalization was drawn by Ennion et al. in their studies on rat vas deferens which expressed biotinylated P2X1 receptors [107].

1.6 Techniques to study ligand-receptor interactions

1.6.1 Photolabeling

Photolabeling and crosslinking refers to a variety of methods developed in the past 30 years to probe the structural and functional properties of various biological targets [108]. Photoaffinity labeling is widely used in structure-function analysis of biological systems because this approach allows direct verification of spatial proximity of molecular components. The photolysable group can be attached to a known ligand at a position thought not to interfere with binding of ligand to the receptor and the resultant photoaffinity label can be tested for pharmacological activity in the dark. Thus, the lack of covalent binding of the ligand before photolysis gives this technique a great advantage of reversible binding to the receptors for its pharmacological characterization. Photolysis is usually achieved by the use of ultraviolet light. Mercury lamps, which mainly emit wavelengths at 254nm, 313nm and 366nm are often used for photolabeling, sometimes at a very high intensity to minimize exposure time. Wavelengths greater than 300nm generally cause less damage to the proteins [109]. For detection of the cross-linked product i.e. the macromolecule, and finally the sites of its modification, the probe must contain a reporter (radioactive, fluorescent, or immunoreactive) group, as this enables the detection of the specific amino acid residues of a protein which are in contact with the ligand. Sometimes the functional response from the receptor itself can be used as a reporter for covalent modification [110,111]. Thus, photoaffinity labeling of a macromolecule can provide valuable information about the location and architecture of the ligand binding site and functional state of the receptor [112-114].

1.6.1.1 Requirements of the photoprobe

The photoprobes used in photoaffinity labeling should have the following distinctive properties [112]:

1. Reasonable stability under ambient light.
2. Life time of photochemically generated excited state should be shorter than the dissociation of ligand-receptor complex, but long enough to spend sufficient time in the close proximity of target site for covalent linkage, so that the excited species should get cross-linked to the receptor before the dissociation of ligand-receptor complex.
3. An unambiguous photochemistry to provide a single and stable adduct.
4. Excited state should react indiscriminately with various chemical groups and should form a stable adduct so as to survive under various analytical conditions.
5. Activation wavelength of the photoprobes should be (preferably) longer than 300nm, thus reducing protein degradation and allowing studies on cell cultures or other living systems.
6. It should not induce significant disorders in the biosystem.

1.6.1.2 Photolysable groups

There are three photolysable groups commercially available viz. Azido, Diazo and Benzophenone. Highly reactive, photo-generated species which are suitable for use in photo-affinity labeling are the electron deficient Carbenes (produced by the loss of nitrogen during the photolysis of diazo) [115], Nitrenes (produced by the loss of nitrogen during the photolysis of azido) [116] or biradical triplet state (produced by the absorption of photon by Benzophenone) [112]. In case of Benzophenone based photo probes, the life time of the excited state (triplet state) containing two unpaired electrons is much longer than that of the singlet state. The triplet state readily relaxes to the ground state if it does not find a proton-donor with the required geometry. This relaxation process does not require a scavenger and this constitutes one of the major advantages of Benzophenone based photoprobe [112]. Other photoreactive groups are activated in a photodissociative mode, i.e. activation is irreversible. In contrast to Carbene and Nitrenes, Benzophenone photoprobes show reversible activation i.e. they may undergo excitation-relaxation cycles until a favorable geometry for covalent

modification is achieved. The probability of achieving an optimal geometry for covalent attachment can be further improved by using a flexible linker, although more rigid linkers should give superior data in topographic mapping of an active site. Therefore, Benzophenone photochemistry in biological systems can be most regio-selective when the flexibility is limited only to that extent which is necessary to achieve efficient H-abstraction. General mechanism of photolabeling by Benzophenone group is shown in Fig. 1.6.

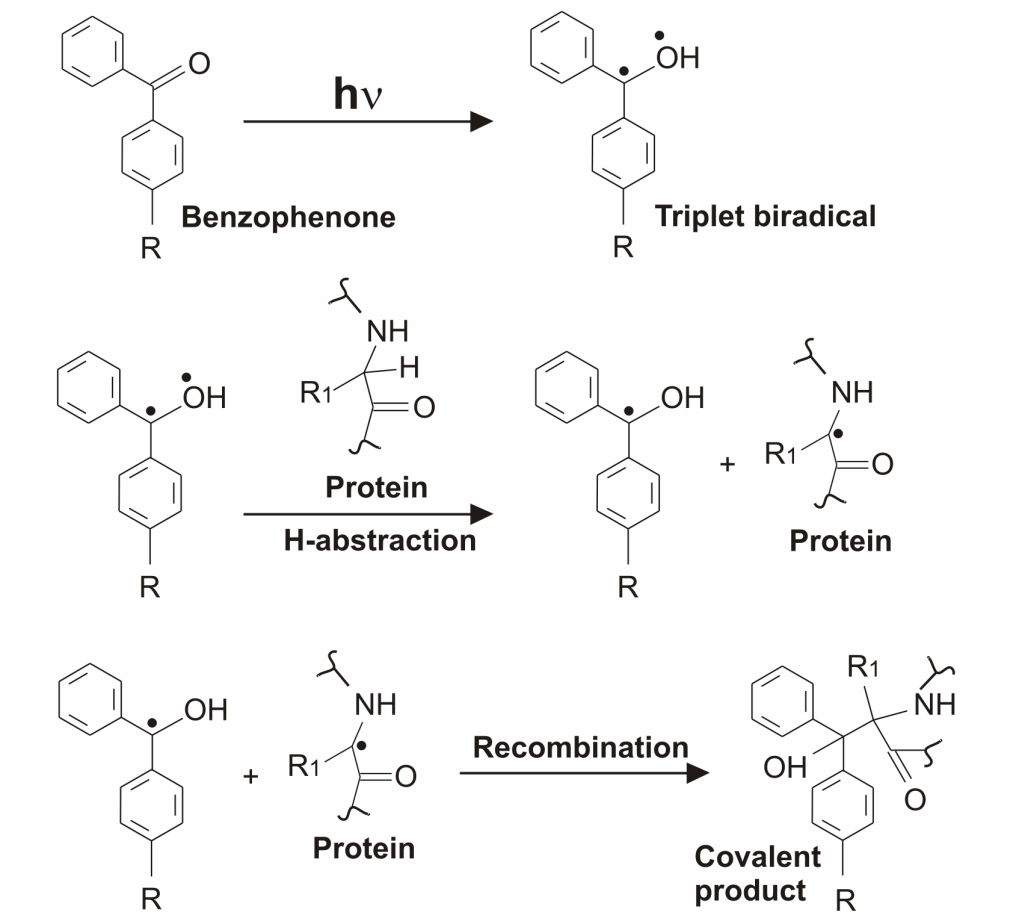

Fig. 1.6 Mechanism of photolabeling by Benzophenone: Diradicaloid triplet state forms after the Benzophenone absorbs light of wavelength 366nm. The electron deficient oxygen n-orbital is electrophilic and therefore interacts with weak C-H σ-bonds, resulting in hydrogen abstraction to complete the half filled n-orbital. The ketyl and alkyl radicals that are formed readily recombine to generate a new C-C bond producing benzpinacol-type compounds. The triplet state readily relaxes to the ground state if it does not find an H-donor with the required geometry. This relaxation process does not require scavenger and constitutes one of the major advantages of this photoprobe.

1.6.1.3 Photoaffinity labeling with purine based analogs

Purine photoaffinity analogs with nearly all the photolysable groups are now commercially available and have been successfully used in structure-function studies of various receptors and purinergic receptors [109,117,118]. The first purine based photoaffinity analog (carbene) was synthesized by Brunswick and Cooperman in 1971 [119]. A carbene based analog of cAMP was used to label the cAMP binding sites of phosphofructokinases [120]. It was also used to label cAMP binding sites in intact ghost from human erythrocytes [121]. Later, Haley and Hoffman [122] synthesized the azido based purine photoaffinity analog by substituting the C8 position with the simple nitrene precursor. But due to the inherent disadvantage of the requirement of a strong 280 nm wavelength to photolyze (which often damages the protein under investigation), only limited studies have been performed on intact cells. Now, benzophenone based ATP analog i.e. 3'(2')-O-(4-benzolybenzoly)-ATP (BzATP) is commercially available. Earlier, BzATP has been demonstrated to label purinoceptors [118,123-125]. In the current study, I have used BzATP as an agonist and photolabeling agent to label P2X receptors heterologously expressed in *X. laevis* oocytes.

1.6.2 Fluorescence labeling

Spectroscopic techniques such as X-ray diffraction, nuclear magnetic resonance spectroscopy, electron microscopy and scanning probe techniques allow measurements with resolution of an angstrom (Å). In general, these techniques require large quantities of purified protein and they are often performed under non-physiological conditions and are seldom suitable to observe the molecular rearrangements in real time. Recent developments have made fluorescence based techniques suitable for real time analysis of molecular interactions under physiological conditions such as in the live cells.

1.6.2.1 Strategies of fluorescence labeling

A prerequisite for the fluorescence techniques is that the molecules of interest must be strongly fluorescent and distinguishable from natural background fluorescence. The system (ligand/receptor) of interest is rarely fluorescent by itself; therefore, much effort has been devoted to the synthesis of fluorescent systems (ligand/receptor) that feature the pharmacological profile of the non-labeled probes [126].

Methods, to make the system of interest (ligand or receptor) a fluorescent one, can be based on three general ways (1) the use of receptor subunits fused to genetically engineered green fluorescent protein (GFP) or their mutants, (2) covalently attaching a fluorophore on the protein of interest and (3) the use of fluorescent analogs of natural ligands to study ligand-receptor interactions.

Method 1: In the recent years the green fluorescent protein from *Aequorea victoria* has been used as a unique tool to monitor and localize gene expression, proteins and molecular interactions in living cells [127]. The versatility of GFP as a biological marker is based on the fact that its intrinsic strong green fluorescence requires no co-factor; the fluorophore fluoresces after correct folding of the protein. By genetic engineering, GFP can be fused as a tag to the protein of interest often without altering its normal function. The obvious advantage of these proteins is that one can selectively label the protein of choice in-vivo. However, the molecular mass of these probes (~26 kD for GFP alone) might be problematic, owing to the interference with the expression and the folding of the labeled protein and with the non-specific interactions between different cellular components.

Method 2: One of the oldest and still most widely used strategies is to attach a fluorophore to a particular functional group in the target protein by spontaneous covalent reaction. Most amenable to such modification are amines and thiols. Depending on the structure of the target protein, chemical labeling can be selective to a single site or to multiple sites. Proteins that contain a single cysteine [128] or a single primary amino group (the N-terminal) [129] have been constructed by mutagenesis which allows selective, single-residue chemical labeling.

Method 3: The use of fluorescent analogs of natural ligands offers a great advantage that they can be applied directly to the receptors or systems of interest in a reversible fashion i.e. the binding of fluorescence ligands is not covalent [130]. A limitation to this method is that the chemical attachment of bulky fluorophore groups to natural ligands could affect binding properties of ligands. Nucleotide triphosphates are crucial mediators of life. ATP is not only used to drive unfavorable chemical reactions to fuel biological machines, and to regulate a number of processes via protein phosphorylation but it also acts as neurotransmitter by regulating purinoceptors. GTP in turn is used almost exclusively for the regulation of signal transduction and transport processes. Thus, considerable efforts have been made on modifying these nucleotides to improve their utility as fluorescent probes for investigations of nucleotide-binding proteins [131,132]. Many fluorescent ATP analogs are now commercially available [133]. The first fluorescent ribose-modified ATP was TNP-ATP [134]. TNP-ATP is

a known antagonist of P2X receptors. It has been used as a fluorescent ATP analog to study extracellular localization of P2X receptors on isolated cochlear hair cells [135] and in kinetic studies of P2X receptors [98]. To study various aspects of P2X receptors activation, a fluorescent ATP analog with agonist potency would be desirable, as there is no reported fluorescent ATP analog which has agonist potency on P2X receptors. In the current study, I have described the agonist property of Alexa-647 ATP and its use to study the desensitized state of P2X1 receptors.

1.6.2.2 Real time assessment of receptor function

Electrophysiology provides direct measurement of receptor function by the virtue of its ability to measure the response (ionic conduction in form of currents) generated by protein (channels/pumps) upon external stimuli. Since channels and pumps are the integral part of all excitable cells, their structure-function analysis under physiological conditions in real time has been a great interest for scientists since decades. In the recent years with the progress in site-specific fluorescence labeling and the cloning and expression of the various proteins (channels/pumps), it has been possible to monitor conformational changes at specific location at single amino acid level in a physiological environment with a technique known as Voltage-clamp-fluorometry (VCF) or Patch-clamp-fluorometry (PCF). The method was pioneered in the labs of Isacoff [136] and Bezanilla [128] where it was initially applied to voltage gated K^+ channels. Subsequently it was extended to a variety of other systems like hERG potassium channel [137], Na^+/glucose co-transporter [138], serotonin transporter [139], GABA receptor [140], GABA transporter (GAT1) [141], glutamate transporter [142], nicotininc acetylcholine receptor [143] and Na^+ pump [144].

The technique of VCF

The basic methodology of VCF includes the engineering a cysteine into an otherwise cysteine-free protein. The protein is then labeled with a cysteine reactive fluorophore (methanethiosulphonate or maleimide moiety). Many robust cysteine reactive fluorophores are now commercially available with Alexa, rhodamine or fluorescine derivatives. Thus, a readily accessible docking site (free cysteine residue) to the environmentally sensitive fluorophore allows the fluorophore to attach to these engineered sites. As the emission from the fluorophore is sensitive to the change in the local environment (the accessibility to

quenching molecules, or the changes in proximity of fluorophores upon conformational changes) the change in the fluorescence emission reflects the real time observation of conformational rearrangements in the channel proteins. Therefore, concurrent recording of fluorescence and current allows to investigate the correlation between changes in channel structure and changes in channel function. Fig. 1.7 shows the schematic representation of principle of VCF measurement.

Fig. 1.7 General mechanism of voltage clamp fluorometry: Free cysteines are generated by mutagenesis at the site of interest. Functionally expressed mutants are labeled with environmentally sensitive fluorescent dye, where accessible cysteines are covalently labeled by the fluorophore (e.g. tetramethylrhodamin-6-maleimide fluorophore, TMRM). Any local change in environment/surrounding of the fluorophore due to structural changes associated with the receptor function could be sensed by the environmentally sensitive fluorophore in real-time. Thus, concurrent measurement of current (receptor function) and fluorescence change (conformational change at that position) upon external stimulus (ligand/voltage etc) gives insight into the mechanism of receptor activation.

Important considerations in VCF experiments

Expression system: *Xenopus laevis* oocytes have been the preferred choice of expression system because they offer large surface area, easy handling, generate very little autofluorescence and provide high expression levels. However, VCF experiments using mammalian cells would be more desirable, but it imposes a lot of technical limitations i.e. their smaller surface area leads to reduced signal-to-noise and signal-to-background ratio.

Chamber: VCF experiments with ligand gated ion channels impose additional technical challenges, because they require a constant perfusion and fast solution changes. This requires a more rigid positioning of the oocyte to minimize the artifacts induced by the movement of oocytes caused by the solution exchange.

Light source: The choice of the fluorescent light source depends mainly on the spectral properties of the dye in use, but generally mercury, xenon and halogen lamps provide good results for a range of dyes.

Fluorophore: The fluorophore selection is largely a matter of trial and error. However, the use of variable linkers attached to the fluorophore could enhance the chance of fluorophore to reach the docking site. As the lifetime of the fluorophore's excited state is on the nanosecond scale, but the dynamics of ion channels occurs on the microsecond scale, VCF can provide real-time information on protein motions. As fluorophores molecules can attach to native membrane proteins or non-specifically incorporate into the membrane itself, the labeling procedure has to be optimized by varying dye concentrations (typically 5-50µM), labeling time (60s to 60 min) and temperature (4-25 ^{0}C).

Detection system: For most VCF applications, a standard epifluorescence microscope fitted with an appropriate filter set and a powerful objective will be sufficient. Photodiode, photomultiplier tubes (PMTs) or fast charge-coupled devices (CCDs) can be used for fluorescence detection. The combined use of spectrophotometers and CCD cameras could allow real-time monitoring of the spectral emission of the fluorophore in use. This can be useful because many organic fluorophores change their spectral properties depending on the hydrophobicity of their environment e.g. the emission peak of rhodamine derivates is blue-shifted when exposed to a more hydrophobic environment. Thus, the use of spectrophotometers could allow to differentiate between (de)quenching events caused by changes in the positions of nearby quenching groups and changes in the hydrophobicity of the microenvironment of the fluorophore [128,145].

1.6.3 Electrophysiology

1.6.3.1 Electrical characteristics of biological membranes

Electrophysiology deals with the investigation of the electrical properties of cell membranes. The lipid bilayer represents a resistor with a very low conductance between cytoplasm and the extracellular fluid, and consequently the membrane current generates a potential difference across the membrane in the range of several tens of millivolts which is governed by Ohm's law. According to Ohm's law the magnitude of a current (I) flowing between two points in a closed circuit is determined by the potential difference between those points and the resistance (or inverse of conductance, G) to current flow.

$$V = IR = \frac{I}{G} \qquad \text{Equation 1.1}$$

Therefore, if a biological cell follows ohm's law, the potential difference across the membrane would be zero in the absence of an externally applied current. However, biological cells often do not show a linear relationship between current and voltage (I-V relationship). Instead, most cells maintain a negative potential difference across their plasma membrane at the steady-state condition. This membrane potential at the resting state is called resting membrane potential (Vm) and results from the three factors (1) unequal distribution of ions at each side of the plasma membrane, (2) difference in the permeability to these ions, (3) the action of active and passive pumps that helps in maintaining the ion gradients. The membrane is "hyperpolarized" when Vm is more negative than the resting membrane potential and is "depolarized" when Vm is more positive than the resting membrane potential.

The resting membrane potential of a cell can be changed by the extracellular binding of a ligand, which leads to the opening of ion channels i.e. change in the membrane conductance. This results in a net flow of ions across the membrane until an equilibrium between chemical and electrical gradient is reached. The potential difference in this steady state is defined by Nernst potential (equation 1.2) [146].

$$\Delta E_N = -\frac{RT}{Z_a F} \ln \frac{[A_i]}{[A_o]} \qquad \text{Equation 1.2}$$

In the equation 2, R is the gas constant (8.314 V C K^{-1} mol^{-1}), T is the absolute temperature, Za is the charge of ion A, F is Faraday's constant (9.648 x 10^4 C mol^{-1}) and [Ao] and [Ai] are the concentrations of ion A outside and inside the cell, respectively.

1.6.3.2 The voltage clamp technique

The voltage clamp technique was developed by Keneth Cole in 1949 to establish the membrane potential of neurons for experimental purpose [147]. The principle of the technique is to inject a current which is equal in amplitude but opposite in sign to the current flowing across the cell. This results in no net current flow across the membrane, and the membrane potential remains constant. By passing current across the cell membrane, the membrane potential can be stepped rapidly to a predefined level (command voltage). Voltage clamp does not mimic a process found in nature, however it offers the following advantages (1) Clamping the voltage eliminates the capacitive current, except for a brief time following a step to a new voltage (2) The currents that flow are proportional only to the membrane conductance i.e. number of open channels, (3) if channel gating is determined by the transmembrane voltage

alone, voltage clamp offers control over the key variable that determines the opening and closing of ion channels [148].

Xenopus laevis oocytes are widely used as an expression system for the expression of membrane proteins to study the structure-function relationship by voltage clamp technique. One-electrode-voltage-clamp, however, cannot be successfully performed in oocytes because: (1) the membrane capacitance is around 200nF, (2) the input resistance is as low as 1kΩ during peak currents of expressed ion channels, (3) the use of glass electrodes that have ohmic resistance greater than 1MΩ could lead to an unacceptably long charging time of the oocytes capacitance. Slow current injection can also lead to the improper voltage clamp clamping when currents are activating and/or deactivating rapidly, resulting in a membrane potential that deviates from the command potential. Therefore a second electrode serving for the independent determination of the actual membrane potential is needed. This is achieved by the use of "two electrode voltage clamp" (TEVC) (Fig. 1.8).

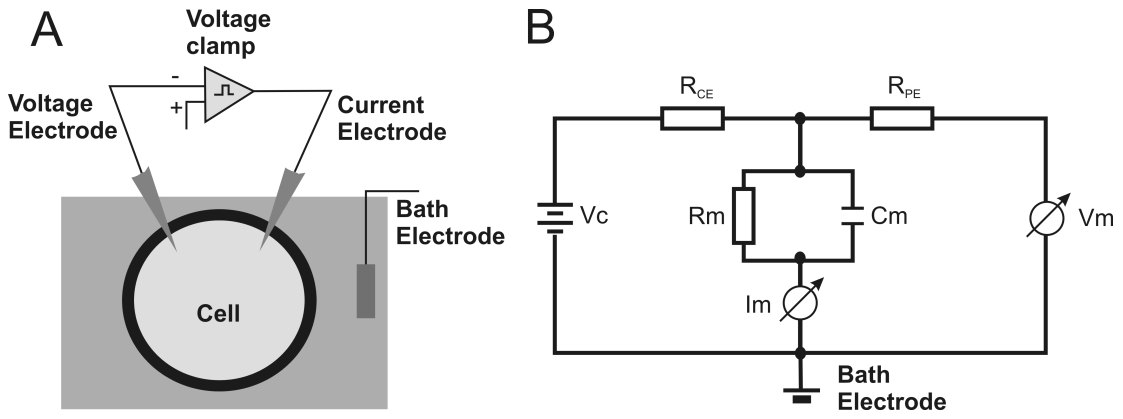

Fig. 1.8 Schematic representation of a two electrode voltage clamp: (A) Voltage clamp operates by a negative feedback mechanism. The membrane potential electrode measures the membrane voltage and sends output to the feedback amplifier which subtracts the membrane voltage from the command voltage. This signal is amplified and the output is sent into the cell through the current electrode. **(B)** Two electrode voltage clamp circuit with a current electrode (CE) and a potential electrode (PE).

The electrodes

The two intracellular electrodes in TEVC are pulled from glass capillaries with a tip diameter of ~10µm, which allows penetration of the cell membrane without much harm to the cell. The electrical contact between cytoplasm and the electronics is achieved by filling the capillaries with an electrolyte solution (3M KCl) and via Ag/AgCl connection. The charge carriers in the

wire are the electrons (e^-) and in the solution are chloride ions. The electrode reaction is governed by:

$$AgCl + e^- \Leftrightarrow Ag + Cl^-$$

3M KCl brings the resistances of pipettes to the mega-ohm range, and makes liquid-junction potentials occurring at the tip of the electrode nearly independent of changes in the outer solution due to the similar mobility of potassium and chloride ions. As a reference, an extracellular bath electrode also made of Ag/AgCl is used. A separation made by agar can be used to avoid direct contact between electrode solution and cytoplasm or bath.

The operational amplifiers

The voltage clamp, as described above, is a negative feedback system in which the value of the output of the system, is "fed back" to the input of the system, where it is compared to a command signal for the desired output. Any difference between the command potential and the output signal has to be re-adjusted in order to reduce the difference. Electronically this is done by devices called "operational amplifiers" (op-amp) (Fig. 1.9A and B), which automatically reduce the difference between command potential and the output signals and maintain the membrane potential exactly equal to the command potential [149]. The main characteristic of an op-amp is its ability to amplify the difference between its two inputs by a factor A (gain).

$$e_0 = A(e_+ - e_-) \qquad \text{with output voltage } e_0$$

When the negative input is connected to the output, the op-amp works as a voltage follower meaning that the output signal equals the signal at the negative input (Fig. 1.9B). These two op-amp variants can be used to complete the TEVC circuit as shown in Fig. 1.9C.

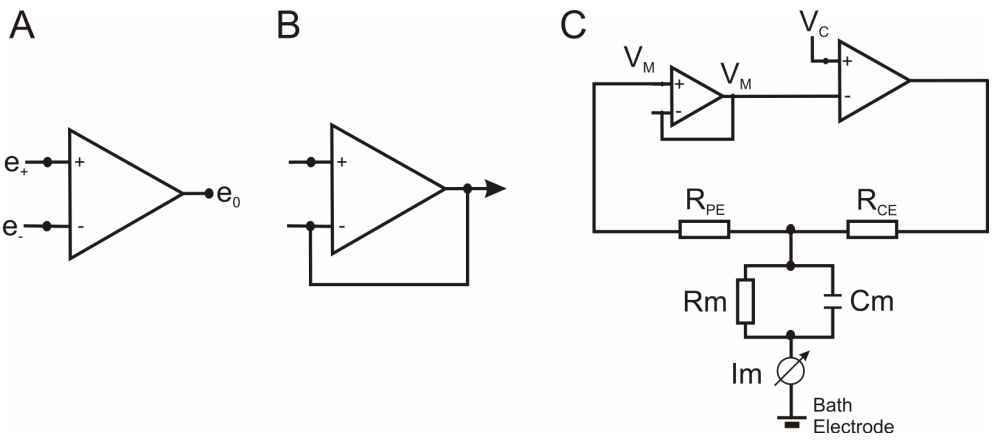

Fig. 1.9 Schematic drawing of an operational amplifier and two electrode voltage clamp circuits: (A) Operational amplifier (op-amp). **(B)** Voltage follower (op-amp with unity gain). **(C)** Two electrode voltage clamp circuit using op-amps and voltage follower for performing voltage clamp by feedback mechanism.

The voltage follower serves as a high resistance input in order to minimize the current flow through the voltage electrode. The second op-amp amplifier is used as a negative feedback amplifier with high gain. The current which flows from the feedback amplifier is identical to the membrane current and can be measured at the output of the op-amp. Two bath electrodes are commonly used to minimize the series resistance errors if large currents are to be measured.

2. Materials and Methods

A) Molecular Biology materials

Balance: Sartorius BL310 and Sartorius 2007 MP, Sartorius AG, Germany.

Centrifuges: Eppendorf centrifuge 5415R and 5417R, Eppendorf AG, Hamburg, Germany.

Centrifuge: Sigma 3-18K, Sigma, Osterode am Harz, Germany.

Concentrator: Eppendorf 5301, Eppendorf AG, Hamburg, Germany.

Refrigerators 4^0C and -32^0C: Kälte Klima Anlagen GmbH, Germany.

Gel documentation system: Biometra-UV solo, Biometra GmbH, Gottingen, Germany.

Gel electrophoresis: Powerpac 300, Bio-Rad Laboratories GmbH, Munich, Germany.

Glassware: Schott Duran, Germany.

Ice machine: Ziegra Eismaschinen, Isernhagen, Germany.

Incubator: Heraeus Instrument, Hanau, Germany.

Milli Q water: Millipore GmbH, Eschborn, Germany.

Oocyte incubator 18^0C: Heraeus Instrument, Hanau, Germany.

Petridish for oocytes: Nunclon Surface, Nunc, Denmark.

pH meter: Metrohm, Deutsche Metrohm GmbH and Co, Filderstadt, Germany.

Pipets: Pipetman, Gilson, France.

Shaker: Aerotron, Infors AG, Bottmingen, Switzerland.

Spectrometer: ND-1000 Nanodrop, NanoDrop Technologies, Wilmington, USA

Syringes: Omnifix, B Braun, Roth, Germany.

Thermo shaker: Schutron thromoshaker, MS Laborgeräte, Heidelberg, Germany.

Tips and tubes: Eppendorf AG, Hamburg, Germany.

Vortex mixer: Heidolph REAX-2000, Germany.

B) Chemicals

αβ-MetATP: Sigma-Aldrich Chemie GmbH, Munich, Germany.

Alexa-647 ATP: Molecular Probes, Invitrogen.

Alexa-C6 maleimide: Molecular Probes, Invitrogen.

Ampicillin: Sigma-Aldrich Chemie GmbH, Munich, Germany.

ATP: Sigma-Aldrich Chemie GmbH, Munich, Germany.

ATP-γS: Sigma-Aldrich Chemie GmbH, Munich, Germany.

ATTO-550 maleimide: ATTO-TEC GmbH, Seigen, Germany.

BzATP: Sigma-Aldrich Chemie GmbH, Munich, Germany.

$CaCl_2$: Merck Chemicals Ltd, Darmstadt Germany.

Collagenase: Sigma-Aldrich Chemie GmbH, Munich, Germany.

DMSO: Merck Chemicals Ltd, Darmstadt Germany.

DNA purification kit: Roche Diagonostics GmbH, Mannheim, Germany.

EDTA: Sigma-Aldrich Chemie GmbH, Munich, Germany.

Ethidium bromide: Sigma-Aldrich Chemie GmbH, Munich, Germany.

Gentamicin: Sigma-Aldrich Chemie GmbH, Munich, Germany.

H_2O_2: Sigma-Aldrich Chemie GmbH, Munich, Germany.

HEPES: Sigma-Aldrich Chemie GmbH, Munich, Germany.

KCl: Merck Chemicals Ltd, Darmstadt Germany.

$MgCl_2$: Sigma-Aldrich Chemie GmbH, Munich, Germany.

NaCl: Carl Roth GmbH, Karlsruhe, Germany.

Neomycin: Sigma-Aldrich Chemie GmbH, Munich, Germany.

Nuclease free water: Applied Biosystems/Ambion, Austin, USA.

PAO: Sigma-Aldrich Chemie GmbH, Munich, Germany.

Peptone: Carl Roth GmbH, Karlsruhe, Germany.

Plasmid purification kit: Qiagen GmbH, Hilden, Germany.

Propionic acid Maleimide (PAM): Sigma-Aldrich Chemie GmbH, Munich, Germany.

Restriction enzymes and buffers: New England Biolabs, MA, USA.

RNA synthesis kit: Applied Biosystems/Ambion, Austin, USA.

TNP-ATP: Sigma-Aldrich Chemie GmbH, Munich, Germany.

TMRM: Molecular Probes, Invitrogen.

Tricaine (for anesthesia): Sigma-Aldrich Chemie GmbH, Munich, Germany.

Tris: Carl Roth GmbH, Karlsruhe, Germany.

Yeast extract: Carl Roth GmbH, Karlsruhe, Germany.

C) Electrophysiology materials

Amplifier TEVC: TURBO TEC-03X, npi Electronics, Germany.

Computer for fluorescence: HP Compaq, Intel IV, Windows XP, Germany.

Computer for photolabeling: Madex, Intel IV, Windows 2000, Germany.

Computer for TEVC: Compaq Presario, AMD Athlon, Windows ME, Germany.

Custom made oocyte chamber: Workshop, Max Planck Institute for Biophysics, Germany.

Digidata: INT-20X, npi Electronics, Germany.

Drip tube system (solution perfusion): Intrafix Air, B Braun, Melsyngen, Germany.

Electrode holders: Science Products, Hofheim, Germany.

Epifluorescence (inverted) microscope: Axiovert 35M, Zeiss, Germany.

Fluorescence filter sets: Omega Optical, Brattleboro, USA.

Fluorescence microscope objective: 0.75 NA, FLUOR-20X, Zeiss, Germany.

Glass capillaries (injection): 3-000-203-G/X, Drummond Scientific Co., USA.

Glass capillaries (TEVC): GB150-8P, Science Products, Hofheim, Germany.

Injection binocular: Leica M26, Leica.

Injection needle puller: Model 700D, David Kopf Instrument, USA.

Lamps: Osram GmbH, Germany.

Nanoliter injector: World Precision Instruments, USA.

Magnetic foot: Drummond Scientific Company, USA.

Magnetic valves: ESF Electronics, Germany.

Manipulators: Drummond Scientific Company, USA.

Microfil syring needle: World Precision Instruments Inc, USA.

Optical bench and stuff: Linos photonics GmbH and Co. KG, Goettingen, Germany.

Patch clamp amplifier: EPC-5, HEKA Electronics, Germany.

Photodiode: PIN-022A photodiode, United Detector Technologies, USA.

Pipette puller (TEVC): PC-10, Narishige, Japan.

Pipette puller (TEVC): PE-1642, Philips, Belgium.

Power supply: Delta Electronika, Schulz Electronics GmbH, Baden, Germany.

Pump: KNF Neuberger GmbH, Germany

Quartz optic fiber (1mm ID): FOC GmbH, Stuttgart, Germany.

Shutter: D-122 UniBlitz, Optilas, USA.

Silver wire: Science Products, Hofheim, Germany.

Software (analysis): OriginLab, Northampton, MA, USA

Software (electrophysiology): Cell works/reader, npi Electronics, Germany.

Software (modeling): Gepasi 3.0, http://www.gepasi.org/

Solution manifold: ALA MLF-8, ALA Scientific Instruments Inc, USA.

D) Animals and related stuff

Animal fed: Local butcher shop, Frankfurt, Germany.

Surgical instruments: Finescience Tool GmbH, Heidelberg, Germany.

Water tanks for frog: Chemowerk GmbH, Weinstadt, Germany.

Xenopus laevis frogs: Nasco International, Fort Atkinson, WI, USA.

2.1 Molecular biology

2.1.1 cDNA construct of P2X2/1 receptor chimera

The complete cDNA construct of P2X2/1 receptor chimera (here onwards referred as chimera) was generously provided by Prof. Günther Schmalzing, Department of Molecular Pharmacology, University Hospital Aachen, Germany. The construction of chimera has been described previously [49,88]. Briefly, plasmid pNKS2-rP2X1 encoding rat P2X1 subunit (GeneBank/EBI accession number: X80477) and plasmid pNKS2-His6-rP2X2A encoding rat P2X2A subunit (GeneBank/EBI accession number: U14414) were used to construct chimera. The chimera was constructed in such a way that the first 47 N-terminal amino acids of the rP2X2 subunit were joined in-frame with Val48-Ser399 of the 399 amino acids of rP2X1 subunit. For this *SnaBI* sites were introduced by site-directed mutagenesis, cutting just before the corresponding Val48 codon in both plasmids. Then the N-terminal of Hexa-His-rP2X2A sequence was excised with *HindIII* and *SnaBI* and ligated in-frame between the *HindIII* site of the vector containing the inserted *SnaBI* cleavage site of pNKS2-rP2X1 plasmid to generate pNKS2-rP2X2/1 plasmid. The full sequence of chimera is downstream to SP6 promoter. Fig. 2.1 represents schematics of P2X2/1 receptor chimera.

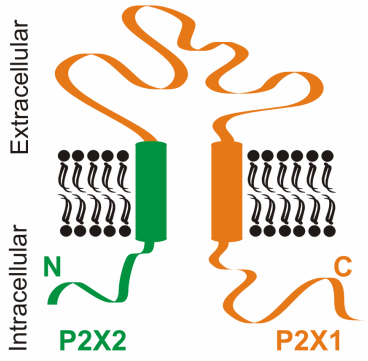

Fig. 2.1 Schematic representation of P2X2/1 receptor chimera: The chimera consisted of N-terminal and TM1 of P2X2, while full extra cellular loop, TM2 and C-terminal are from P2X1. As ATP binding pocket is

located in the extracellular loop and the chimera has extra cellular loop from P2X1, it maintains ligand binding properties of P2X1.

2.1.2 cDNA constructs of cysteine mutants of P2X2 and chimera

These clones were generated by Benjamin Marquez-Klaka at the Max Planck Institute for Brain Research, Germany. All the single substituted cysteine mutants were generated by PCR amplification of the primers containing corresponding mutation in the pNKS2-rP2X2 and pNKS2-rP2X2/1 plasmid for rP2X2 and chimera respectively.

- P2X2 2nd TM mutants: S326C, L327C, T330C, I331C, I332C.
- Chimera binding site mutants (P2X1 numbering without His-tag): K68C, K70C, F185C, K190C, F291C, R292C, K305C, K309C, I328C.
- Chimera 1st TM mutants (P2X1 numbering without His-tag): W46C, V47C, V48C, F49C, V50C.

2.1.3 cDNA constructs of cysteine mutants of P2X1

Two types of cysteine mutants were generated in the P2X1 receptors:
In the first type, cysteine mutants were generated by individually mutating the first six conserved cysteines in the extracellular loop to serine i.e. C117S, C126S, C132S, C149S, C159S, C165S. These clones were generously provided by Prof. Günther Schmalzing, Department of Molecular Pharmacology, University Hospital Aachen, Germany.

In the second type, individual amino acids from position 118 to 125 were mutated to cysteine residues i.e. A118C, E119C, N120C, P121C, E122C, G123C, G124C and I125C. These clones were generated by Benjamin Marquez-Klaka at the Max Planck Institute for Brain Research, Germany. All these clones (both types) were generated by PCR amplification of the primers containing corresponding mutations in the pNKS2-rP2X1 plasmid.

2.2 Bacterial culture and cDNA purification

2.2.1 Culture medium and transformation

Standard techniques were used for growing *E.coli* DH5α bacterial cells in LB (Luria Bertani) medium (10 g peptone, 5 g yeast extract, 10 g NaCl per 1 L distilled water). 15 g agar per litre was added to the respective medium for agar plates. Cultures were grown in a shaker incubator at 37°C. cDNA constructs were transformed into chemically competent *E.coli* DH5α cells in the presence of appropriate antibiotic as follows: 50µl aliquots of chemically ultra-competent *E.coli* DH5α cells were mixed with plasmid (~100 ng) and incubated on ice for 30 min. Then, cells were heat shocked for 90s at 42°C and immediately kept on ice for 3 min. After addition of 950µl LB medium the cells were incubated at 37°C for 1 hour. 100µl out of 1ml of the transformed cell suspension was streaked out on LB agar plates containing 100µg/ml Ampicillin and incubated overnight at 37°C.

2.2.2 Plasmid DNA purification

Single bacterial colonies were picked from agar plates with a sterile toothpick and incubated overnight in LB culture medium supplemented with 100µg/ml Ampicillin at 37°C with vigorous agitation (220 rpm). For large scale DNA preparation the Qiagen® plasmid midiprep kit was used according to manufacturer's instructions. Following purification, the cDNA concentration was determined by measuring absorbance at 260nm (A260) on the NanoDrop® ND-1000 spectrophotometer. All cDNAs were stored at -20°C for later use.

2.2.3 cRNA synthesis

Linearization of template DNA of corresponding mutants was performed with 3µg plasmid DNA in 50µl volume with appropriate enzyme (1hr, 10U) (wild type and all the mutants of P2X2: *XhoI*; chimera and its all mutants, wild type and all the mutants of P2X1: *EcoRI*). Linearized DNA was purified using the Roche High-Pure-PCR purification kit according to manufacturer's instructions and concentrated in speed-vac. Capped cRNAs were synthesized from linearized DNA templates with SP6 RNA polymerase using the Message Machine kit. Integrity of purified cRNAs was checked by gel electrophoresis using 1% agarose gel in TAE buffer. Concentration of purified cRNA was determined by measuring absorbance at 260nm

(A260) on the NanoDrop® ND-1000 spectrophotometer. All cRNAs were stored at -20°C for later use.

2.3 Heterologous expression in *Xenopus laevis* oocytes

2.3.1 Frog maintenance

10-15 frogs were placed in a large tank of capacity ~200 liters filled ~2/3 with fresh water free from chlorine. To avoid frog escape, each tank was covered with a grid in a wooden frame. For their well-being, each tank was bare bottom and contained few hiding sites (open ends cylinders of baked clay). Individual arrangements were made in each tank for continuous fresh water circulation. Temperature of water was maintained in the range of 16-19^{0}C. 12/12h light/dark cycle was maintained by the use of one tungsten lamp. Beef heart pellets were used to feed the frogs twice a week. Tanks were regularly cleaned from any food debris in order to reduce microbial growth.

2.3.2 Surgical preparation

A small fish net was used to capture a healthy female from the tank and transfer it to a small box with a lid containing ~500ml of general anesthetic. 0.2% solution (pH 7) of tricaine methanesulfonate (MS-222) in tap water was used as general anesthetic. Anesthesia was applied by transferring the frog into the anesthesia solution for 10-15min. The anaesthetized frog was then rinsed with distilled water to remove excess of MS-222. The frog was placed on an ice box with dorsal side facing down. The ventral surface of frog was covered with clean wet paper towels in order to protect the skin from drying. A small trans-section cut was made with a sterile scissor in one of the two lower quadrants of the abdomen by lifting the skin with sterile tweezers. Ovarian lobes were pulled out with the help of tweezers. A cut was made through the ovarian lobes in order to detach them from the frog's body. Ovarian lobes were then placed in calcium supplemented Oocyte Ringer solution until further use. The wall of the coelom (surgical cut in the abdomen) was closed using two to three simple interrupted sterile synthetic sutures which included the skin, serosa and muscles. After the surgical procedure, the frog was placed in a small recovery tank for post surgical monitoring. Complete recovery usually occurs within 2-4 hours.

2.3.3 Oocyte preparation and heterologous expression

Extracted ovary lobes (as described above) were subjected to collagenase (2mg/ml) treatment (2-3 hrs or overnight) in calcium supplemented Oocyte Ringer's solution (CaSORI) in order to isolate the oocytes. After collagenase treatment oocytes were washed several times with calcium-free ORI. Defolliculated oocytes of stage V or VI were manually selected and injected with 50nl of cRNA. To get optimal expression for each clone, different amounts of cRNA was injected e.g. 25ng/cell for wild type P2X1 and cysteine mutants of P2X1; 5ng/cell for chimera; 2.5ng/cell for binding site cysteine mutants of chimera and TM2 mutants of P2X2; 0.5ng/cell for wild type P2X2. Injected cells were incubated in calcium supplemented Oocyte Ringer solution (CaSORI) containing 0.05mg/ml gentamicin at 18°C for 1-3 days depending on the clones.

Table 2.1: Oocyte buffer compositions:

Magnesium Oocyte Ringer's solution (MgORI):

Chemical	**mM**
NaCl	90
KCl	1
$MgCl_2$	2
HEPES	5
pH 7.5 by NaOH	

Calcium supplemented Oocyte Ringer's solution (CaSORI):

Chemical	**mM**
NaCl	110
KCl	5
$CaCl_2$	2
$MgCl_2$	1
HEPES	5
pH 7.5 by NaOH	

2.4 Functional measurement of receptors

Current responses to various ligands were measured 1-3 days after cRNA injection into *X. laevis* oocytes by the two-electrode-voltage-clamp (TEVC) technique. The amount of cRNA to be injected and expression time in functional experiments was determined individually for each construct to avoid current amplitudes that were greater than 50µA or smaller than 500nA. As P2X receptors are permeable to calcium ions, calcium salts were omitted from the solutions to avoid calcium activated Cl^- currents. Therefore, all measurements were performed in MgORI. Two electrode voltage clamp was performed in a ~50µl recording chamber perfused at a flow rate of ~10ml/min [104] or by using a custom made chamber as described by Chang et al. [140]. Solutions were switched by software controlled magnetic valves. Two intracellular glass microelectrodes with resistances of < 1MΩ were used to clamp the oocytes at -60mV. Currents were recorded with the TEC-03X amplifier, low pass filtered at 100Hz and sampled at >200Hz (INT-20X AD/DA converter) using Cell-Works software. All measurements were performed at room temperature (20-22°C). Data are presented as mean ± SE for the indicated number of experiments (*n*). EC_{50} values were calculated from a nonlinear fit of the Hill equation using Origin software. All graphs were plotted in Origin 7.5 software.

2.4.1 Design of the photolabeling setup

For concurrent photolabeling and current measurement from the same set of receptors, a custom made oocyte chamber was used which consisted of two partitions connected by a ~0.6mm hole between them (Fig. 2.2). The oocyte was placed in the upper compartment so that a portion of the oocyte via the 0.6mm hole faced the lower compartment. The upper compartment allowed the access for intracellular electrodes, while in the lower compartment solutions were perfused by gravity flow. A quartz optic fiber transmitted high intensity UV light (λ_{max} = 366nm with energy = 10mJ at 410nm) from a 100W HBO lamp to the bottom of the chamber in such a way that the portion of the oocyte that was exposed to agonist was also entirely within the area of the fiber optic tip. This enabled efficient ligand perfusion and photolabeling of the same population of receptors.

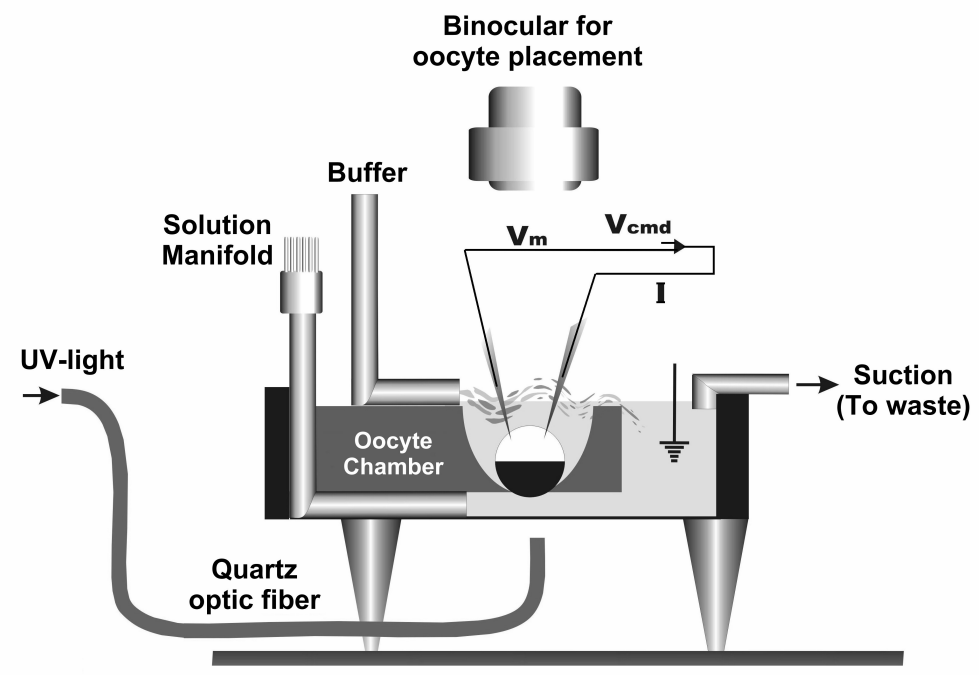

Fig. 2.2 Photolabeling setup: Custom made oocyte chamber for concurrent photolabeling and current measurement from the same population of receptors in real time. UV light was transmitted from HBO lamp to the chamber by quartz optic fiber. Ligands were applied by solution manifold. Oocyte was placed in the chamber in such a way that the same population of receptors facing ligand also faces light.

The custom made oocyte chamber offered two fold advantages. It offered electrode impalement in the upper chamber for electrophysiological measurements, while the flow of solution in the lower compartment helped the oocyte to form a seal around the 0.6mm hole due to venturi effect, thus minimizing solution exchange between the upper and lower partitions and stabilized the oocytes.

2.4.2 Design of voltage clamp fluorometry setup

For concurrent fluorescence and current measurement from the same population of receptors, previously described custom made oocyte chamber was assembled on an inverted epifluorescence microscope equipped with a FLUOR-20X objective (NA=0.75) as shown in Fig. 2.3.

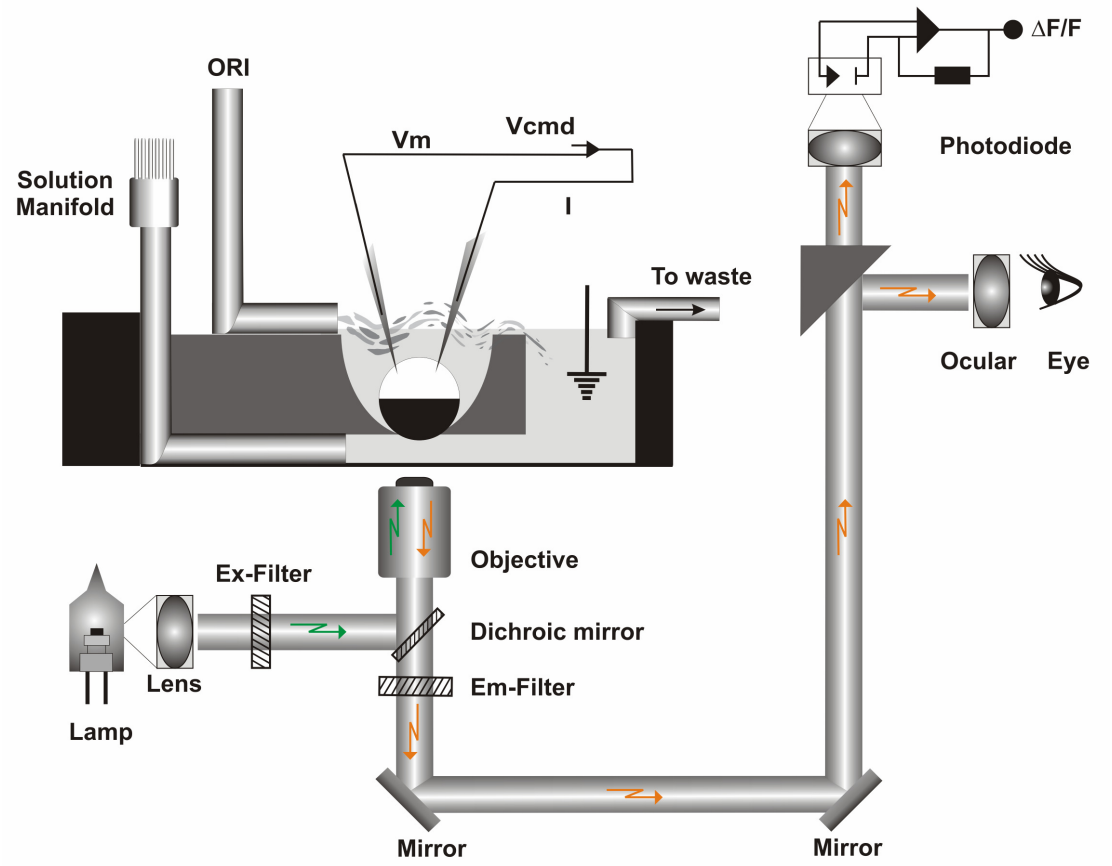

Fig. 2.3 Voltage clamp fluorometry setup: Experimental setup for real time fluorescence and current measurement from the same population of receptors expressed in an oocyte. Excitation light was applied to the oocyte after filtering by excitation filter. Fluorescence emission from oocyte was again filtered by dichroic mirror and emission filter. Filtered fluorescence light was detected by photo diode placed near eye piece.

Electrophysiological measurements were performed as described in section 2.4. The fluorescence emission was stimulated by the light from a 100W/12V Halogen (XENOPHOT) lamp placed in HAL 100 lamp housing of the microscope and whose intensity was regulated with the external amplifier. In order to control the time of irradiation a TTL controlled shutter was used. Light was then filtered by a filter set (Table 2.2). The fluorescence emission was measured through a PIN-022A photodiode mounted on the eye port of the microscope. The signal from the photodiode was amplified by an EPC-5 patch clamp amplifier and filtered at 0.3 kHz. The fluorescence and current signals were simultaneously acquired through the Cell Works software. Fluorescence spectra and filter sets used for the corresponding fluorophores is shown in Fig. 2.4.

Table 2.2: Omega optical filters used for different fluorescent dyes:

Dye/Experiments	Excitation	Dichroic mirror	Emission	Filter set
TMRM	XF1074	XF2017	XF3085	XF101-2
Alexa-Fluor 647 ATP (as Alexa-ATP)	XF1069	XF2035	XF3076	XF110-2
FRET (between TMRM and Alexa-ATP)	XF1074	XF2017	XF3302	---

Table 2.3: Fluorescence properties of dyes:

Dye	λabsorption (nm)	λemission (nm)	Extinction coefficient $(M\ cm)^{-1}$	Quantum yield (%)	Life time (ns) (water)
TMRM	555	580	110,000	45	1.62
ATTO 550 maleimide	554	576	120,000	80	3.2
Alexa-ATP	650	665	239,000	33	1.0

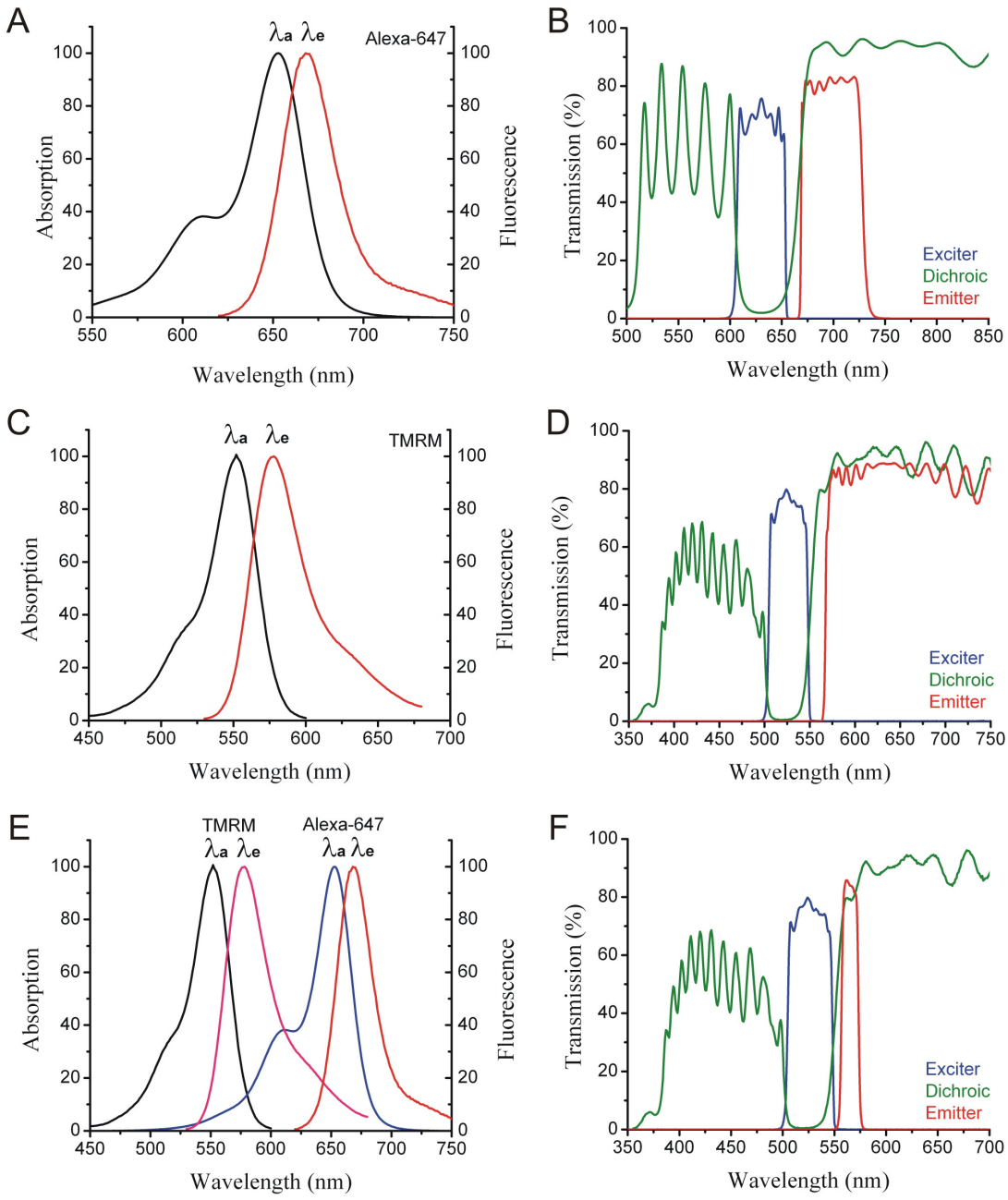

Fig. 2.4 Spectral properties and filter-sets used for different fluorophores: Absorption (black trace) and fluorescence (red trace) spectra of **(A)** Alexa-ATP, **(C)** TMRM. Properties of corresponding filter sets (Exciter, Dichroic and Emitter filters) are shown in **(B)** Alexa-ATP, **(D)** TMRM. **(E)** Spectral properties of TMRM and Alexa-ATP allow their use as a FRET pair. **(F)** For the FRET measurement between Alexa-ATP and TMRM, where the decrease in TMRM fluorescence was used as criteria, only the Emitter filter in the TMRM filter set was changed.

3. Results

3.1 Probing allosteric interactions between P2X receptor subunits using photolabeling

In pentameric nicotinic acetylcholine receptors (nAChRs), the acetylcholine binding site is formed by the extracellular N-terminal domain and has been localized at the interface of neighboring nAChR subunits [150]. The agonist binding site in tetrameric iGluRs is formed by two segments (extracellular N-terminus and the loop between TM3 and TM4) of a single subunit which are separated by two transmembrane domains and a re-entry loop [151,152]. P2X receptors, on the other hand represent the third family of ligand gated ion channels. They show trimeric subunit topology and form non-selective cation channels that open in response to extracellular ATP binding [49,75]. Recently it was shown that the ATP binding site in P2X receptors is formed by the loops from neighboring P2X subunits [42]. However, the mechanism of P2X receptors activation upon ATP binding at the interface of subunits is still unclear. P2X receptors activation is thought to involve a series of allosteric ligand binding steps, albeit the contribution of each ligand binding step to the gating of P2X receptors remains unknown.

Therefore, in my thesis, I have focused on studying the contribution of each receptor subunit in the process of gating. This cannot be studied in isolation as the ligand binding and unbinding from the receptor occurs continuously. To address this and related questions, I used photolabeling technique, where I used 2'-& 3'-O-(4-benzoylbenzoyl)-ATP (BzATP, a photoaffinity ATP analog) for concurrent activation and photolabeling of homomeric rat P2X receptors (P2X1, P2X2) and P2X2/1 receptor chimera (henceforth referred as chimera)). Using this approach, I could overcome the limitation of ligand unbinding events which facilitated us to control the occupancy level of binding sites. This also allowed us to study the contribution of the remaining unoccupied binding sites to the gating process without the ambiguities that arise from continuous binding and unbinding of ligands to the channel subunits. Change in the efficacy of the partial and full agonists on P2X receptors upon progressive photolabeling by BzATP was determined as the parameter for contribution of each subunit towards gating.

3.1.1 Photolabeling of wild type P2X1 receptors

3.1.1.1 Agonist unbinding is required for the recovery from desensitization

P2X1 receptors desensitize during prolonged application of agonists. It is believed that the desensitized state is a ligand bound state and the recovery from desensitization involves agonist unbinding steps. In order to demonstrate this, 1µM BzATP (a photoaffinity ATP analog) was used as an agonist for concurrent photolabeling and to activate and to completely desensitize wild type P2X1 receptors using voltage-clamp photolabeling setup (Fig. 2.2). Photoaffinity ligands have characteristic properties that they show reversible binding to the receptors in the absence of UV-light, but get covalently cross-linked in the presence of UV-light. The first application of BzATP (Bz1) in the absence of light for 20s evoked a large peak current response. Further applications of BzATP (20s) to the same set of receptors at 5 min intervals yielded constant peak responses. For covalent labeling, BzATP was applied for 40s in the presence of UV-light (Fig. 3.1B). As a control, BzATP was also applied for 40s in the absence of light (Fig. 3.1A).

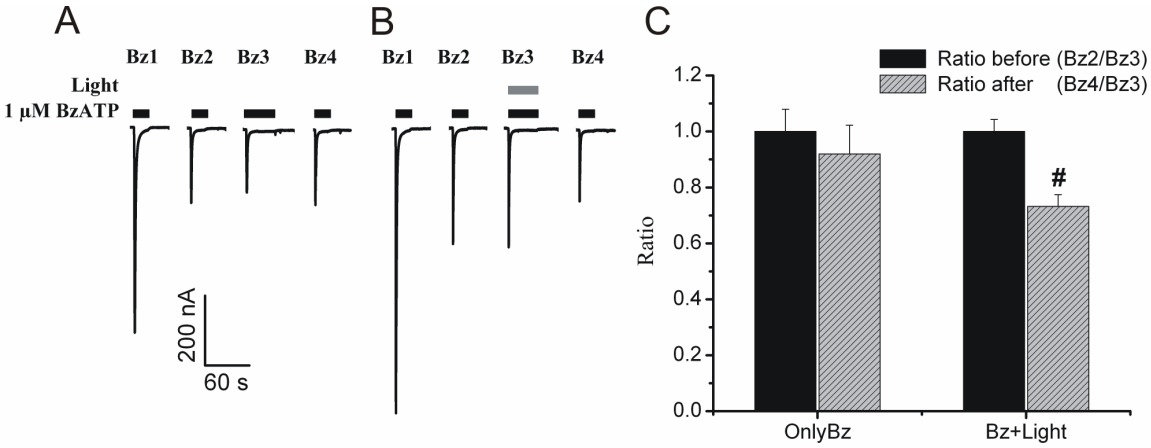

Fig. 3.1 Effect of prolonged BzATP application in the presence and absence of light on the P2X1 recovery from desensitization: (A) In the absence of photolabeling, prolonged application of BzATP showed similar recovery from desensitization as shown by similar peak current responses after treatment of BzATP (20s and 40s). **(B)** In the presence of light, covalent attachment of BzATP significantly decreased the subsequent peak current response (Bz4) i.e. reduced recovery from desensitization. **(C)** Ratio of peak current response generated by 2^{nd} (Bz2) to 3^{rd} (Bz3) application of BzATP was compared with the ratio of 4^{th} (Bz4) to 3^{rd} (Bz3) response. Data are plotted as mean ± SE of 4-5 cells for each treatment. # $P < 0.01$ (t-test)

Fig. 3.1 shows that the prolonged application of BzATP without light had no effect on the constant peak current responses, indicating that similar number of receptors recovered from

desensitization. However, subsequent peak current responses significantly decreased when BzATP was applied along with the light, indicating that less number of receptors recovered from desensitization due to the covalent attachment of BzATP to P2X1 receptors. Covalent attachment of BzATP limits the agonist unbinding which is reflected in the form of decreased current response after the light treatment. Thus, the present experiment demonstrates that the agonist unbinding is required for the recovery of P2X1 receptors from desensitization.

3.1.1.2 Time course of photolabeling at P2X1 receptors

After photolabeling, current responses generated by subsequent BzATP application to the same set of P2X1 receptors were found to decrease due to the permanent desensitization of the receptors caused by the covalent attachment of BzATP. To determine the time-course of covalent modification of P2X1 receptors, 1µM BzATP was applied four times to the P2X1 receptors designated as Bz1 to Bz4. Between each application, ligand free buffer was applied for 5 min. The first application of BzATP (Bz1) (20s) elicited the large peak current; whereas subsequent responses were constant till Bz3 application. For photolabeling, different duration of BzATP + UV-light was applied during third application (Bz3) (Fig. 3.2A). The effect of different durations of BzATP + UV-light i.e. photolabeling, was determined by the BzATP induced response after UV-light treatment (Bz4) (Fig 3.2A).

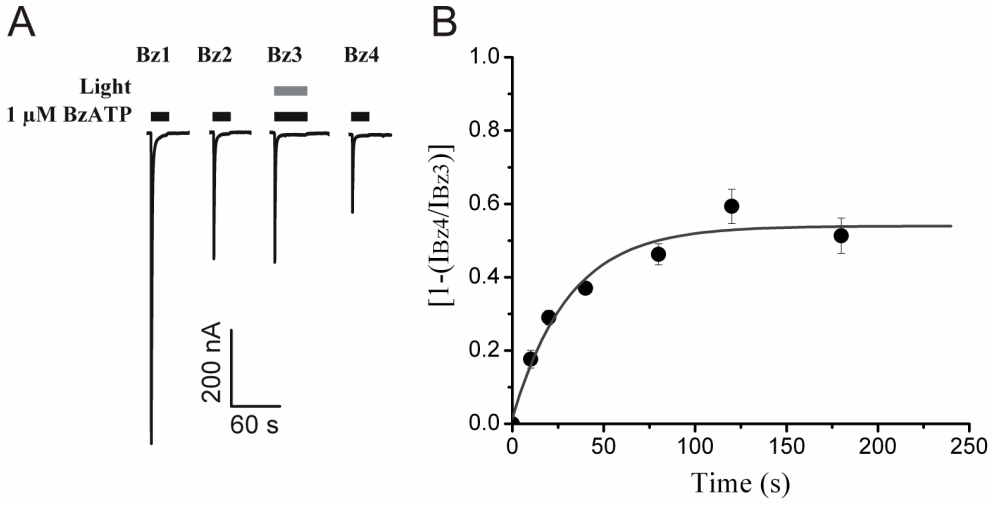

Fig. 3.2 Time course of photolabeling of wild type P2X1 receptors: (A) Representative current traces of P2X1 receptors during BzATP induced responses. Different applications of BzATP are denoted as Bz1, 2, 3 etc. Between each BzATP application, ligand free buffer was applied for 5 min. During the third application (Bz3), receptors were exposed to both BzATP + UV-light for different period of time for photolabeling. In the representative current trace (Bz3), BzATP + UV-light were applied for 40s. The level of photolabeling was determined by generating Bz4 response after photolabeling. As a control, BzATP was applied for 40s without

light (Fig. 3.1A), which indicated that prolonged application of BzATP (Bz3) had no effect on subsequent responses (Bz4). **(B)** Ratio between the current responses generated at Bz4 to Bz3 is plotted against progressive photolabeling for different periods of time. The time course of photolabeling was fitted with mono exponential equation with a time constant of (τ) 31 ± 7s. Each data point represents mean ± SE of 3-4 cells.

A maximum of about 50% steady state level was reached with a time constant of 31 ± 7s. 100% desensitization was not observed even after extended period of time (~200s), possibly due to constant receptor trafficking/ turnover on the membrane or lateral diffusion of receptors outside the field of light application (outside the hole).

3.1.2 Photolabeling of wild type P2X2 receptors

3.1.2.1 Efficacy and potency of BzATP and ATP on P2X2 receptors

Photolabeling leads to persistent desensitization of P2X1 receptors. Thus, contribution of each subunit towards gating could not be studied in P2X1 receptors. Due to this limitation further experiments were performed on P2X2 receptors which represent the non-desensitizing phenotype. Therefore, the efficacy and potency of BzATP was determined on P2X2 receptors and compared with ATP (full agonist). Fig. 3.3 shows the comparison between complete dose response curves for BzATP and ATP. Saturating concentrations of BzATP (300µM) were found to elicit ~20% of the current responses elicited by saturating concentrations of ATP (300µM), thus indicating that BzATP is a partial agonist on P2X2 receptors. Table 3.1 shows EC_{50} values and Hill coefficients for ATP and BzATP on the P2X2 receptors.

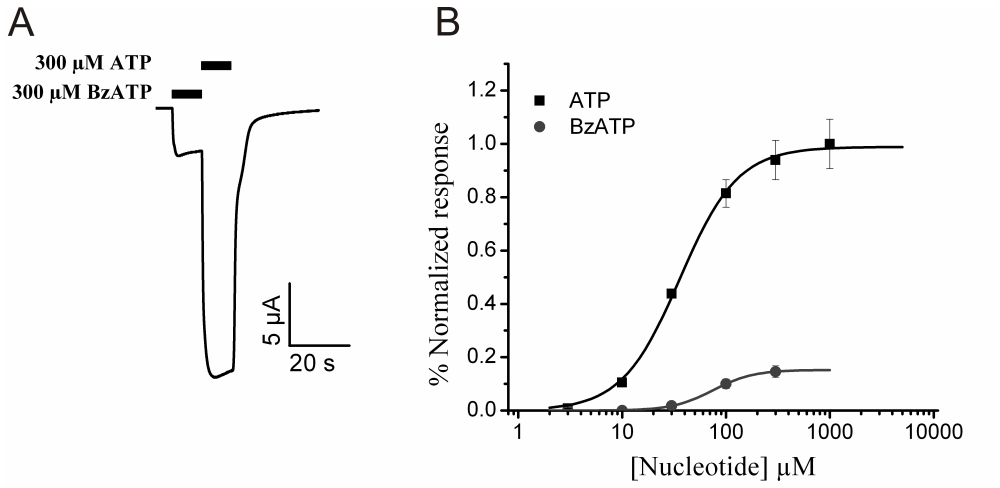

Fig. 3.3 Efficacy and potency of BzATP and ATP on wild type P2X2 receptors: (A) Representative current trace of saturating concentration of BzATP (300µM) and saturating concentration of ATP (300µM) on the same

oocyte expressing wild type P2X2 receptors. **(B)** Comparison of dose response curves for ATP and BzATP on the P2X2 receptors. All dose response curves were normalized to the response generated by saturating concentration of ATP (300µM). Data are presented as mean ± SE of 5 cells for each ligand concentration.

Table 3.1: EC_{50} values and Hill coefficients for ATP and BzATP on the P2X2 receptors

Ligand*	**EC_{50} (µM)**	**Hill coefficient**
ATP *(5)*	36 ± 2	1.5 ± 0.1
BzATP *(5)*	75 ± 2	2.2 ± 0.1

* Number of cells for each ligand concentration is indicated in parentheses.

3.1.2.2 Each subunit contributes to the gating process

P2X receptors gate upon agonist binding. Due to the continuous ligand binding and unbinding, a defined contribution of each subunit towards gating is difficult to study. Therefore, BzATP was used as a photoaffinity analog of ATP to lock the non-desensitizing P2X2 receptors in partially liganded state and the contribution of remaining unoccupied subunits towards gating was studied.

In the experiment, 30µM BzATP was used for photolabeling. At this concentration, it is expected that BzATP would cross-link P2X2 receptors in a partially liganded state. To generate maximum response from the P2X2 receptors, saturating concentration of ATP (300µM) was used. Fig 3.4 shows that the ratio of current generated by 30µM BzATP to 300µM ATP changes only when BzATP gets covalently attached to one or two subunits of P2X2 receptors in the presence of UV-light, whereas in the absence of UV-light, the ratio remained unchanged. BzATP being a partial agonist also acts as a competitive antagonist. Prolonged BzATP application in the presence of light lead to the photolabeling of the receptors and one or two binding sites were permanently occupied. These sites were not available for further action of ATP (full agonist) and therefore, ATP could not evoke a maximal response from the receptors locked with partial agonist in a partially liganded state. Thus, these results indicate that each subunit contributes to the process of gating i.e. response of a full agonist (gating) was affected if one or two subunits of P2X2 receptors were cross-linked by BzATP (partial agonist).

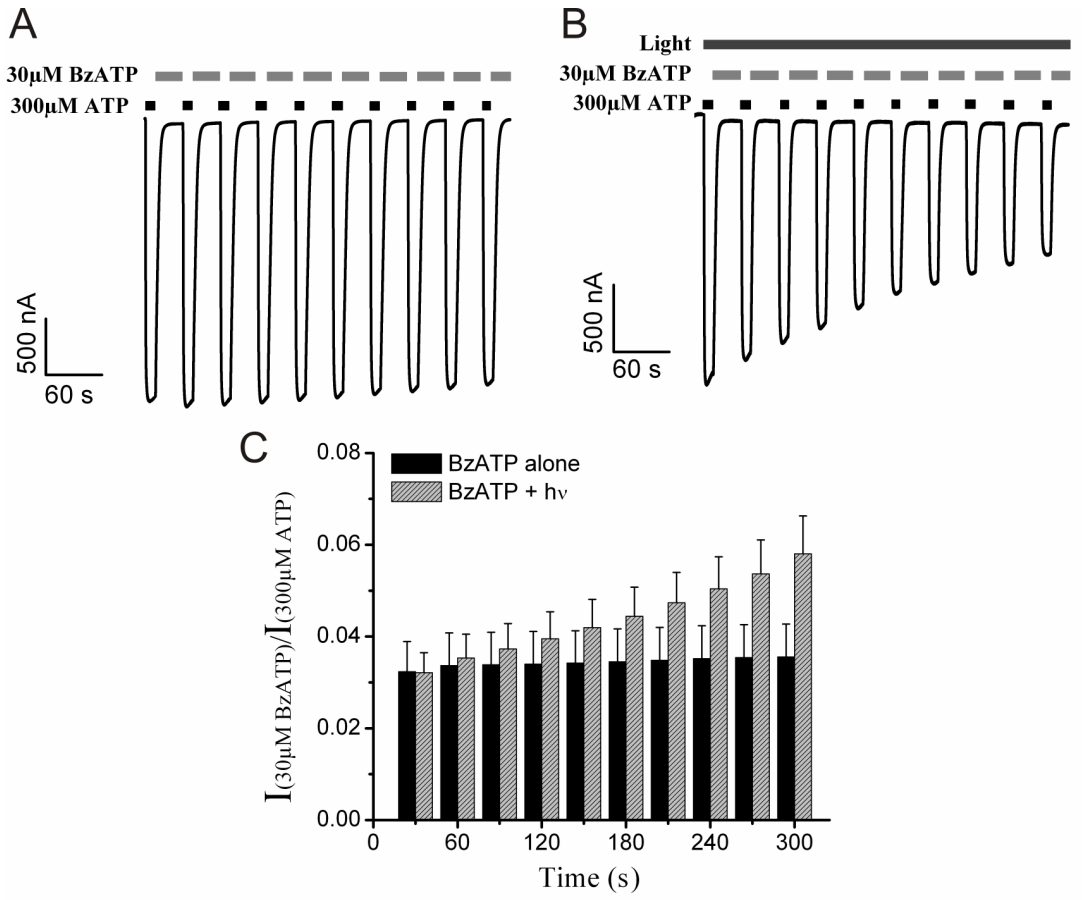

Fig. 3.4 Effect of photolabeling by partial agonist on the maximal response of P2X2 receptors: Representative current traces of 30µM BzATP and 300µM ATP applied to P2X2 receptors in **(A)** Absence of light, **(B)** Presence of UV-light. Progressive photolabeling by BzATP to the P2X2 receptors lead to progressive decrease in ATP induced current responses. **(C)** Corresponding ratio of current responses generated by 30µM BzATP to 300µM ATP is plotted against time during prolonged BzATP application in the absence and presence of UV-light. The ratio of current responses progressively changed when one or two BzATP gets covalently attached to P2X2 receptors. The ratio remained unchanged when there is no photolabeling (in the absence of UV-light). Data are presented as mean ± SE of 7 cells (BzATP alone) and 12 cells (BzATP + light).

3.1.3 Photolabeling of the P2X2/P2X1 receptor chimera

It was observed that covalent labeling by BzATP on P2X1 and P2X2 receptors lead to selective modification of the functional receptors. On P2X1 receptors, covalent labeling of BzATP lead to persistent desensitization, making them unavailable for functional studies. On P2X2 receptors, BzATP is a partial agonist and its covalent attachment lead to significant reduction in the maximal response of a full agonist on the receptors. Due to the non-availability of functional receptors which maintain their full activity after photolabeling, it

was difficult to continue on these wild type receptors. Therefore, a receptor was required which not only maintains the non-desensitizing phenotype but also retains the functional activity after covalent attachment of BzATP. To this end, the use of a receptor chimera was tested. The chimera was made from a portion of P2X2 (N-terminal and TM1 domain) and a portion of P2X1 (full extracellular loop, TM2 and complete C-terminal domain). This chimera offered several advantages over wild type counterparts. It has a non-desensitizing phenotype similar to the P2X2 receptors and shows nanomolar potency for various ligands as it maintains the ligand binding domain of P2X1 receptors. For differences in the potency of ATP on P2X1 receptors and the chimera see a detailed description in the introduction section 1.5.2.

3.1.3.1 Efficacy and potency of various ligands on the chimera

When the dose response curve for BzATP on the chimera was compared with dose response curves for other agonists (ATP and αβ-MetATP), it was found that saturating concentration (1μM) of BzATP, αβ-MetATP and ATP elicited the same current amplitude, indicating that BzATP and αβ-MetATP are full agonists of the chimera (Fig. 3.5A and C).

Thus, BzATP could be used as a photoaffinity analog of ATP maintaining the full agonist efficacy on the chimera. On the other hand, αβ-MetATP which shows a ~10-fold faster deactivation time course after washout as compared to ATP could be used to generate complete dose response curves before and after photolabeling on the same oocyte. TNP-ATP is a known potent antagonist of P2X1 and P2X3 receptors with an IC_{50} value of 6nM for P2X1 receptors [99]. When 300nM TNP-ATP was applied to the chimera, a weak inward current (~2% of the response generated by 1μM ATP) was observed (Fig. 3.5B), indicating that TNP-ATP acted as a very partial agonist on the chimera. Thus, the effect of progressive photolabeling by BzATP (full agonist) on the efficacy and potency of αβ-MetATP (full agonist) and TNP-ATP (partial agonist) could be use to study the contribution of each subunit of the receptors to the process of gating. Dose response curves for various ligands on the chimera indicated that ATP maintains the highest potency on chimera followed by BzATP and αβ-MetATP (Fig. 3.5D). Table 3.2 shows EC_{50} values and Hill coefficients of these ligands on the chimera.

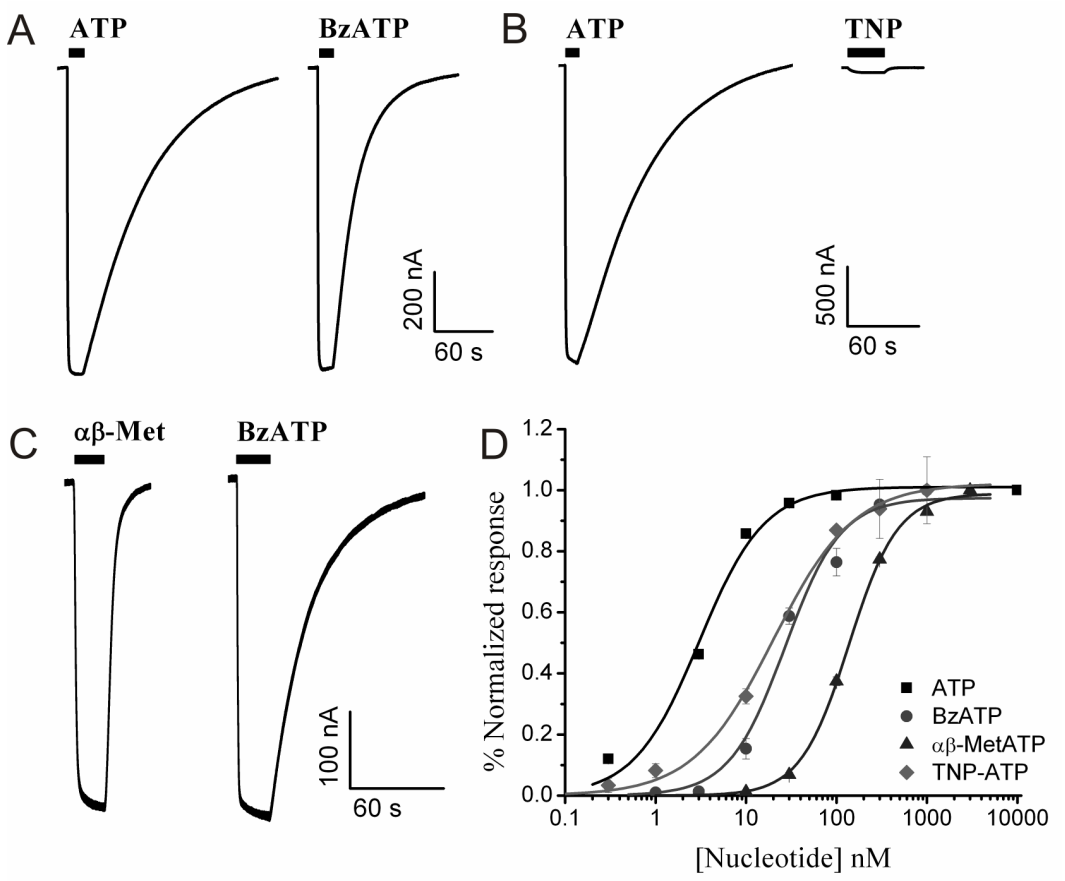

Figure 3.5: Efficacy and potency of various ligands on the chimera: Representative current traces obtained by the application of various ligands on the same oocyte **(A)** 1µM ATP and BzATP, **(B)** 1µM ATP and 100nM TNP-ATP, **(C)** 1µM αβ-MetATP and BzATP. **(D)** Dose response curves for various ligands on the chimera. All responses were normalized to the response generated by the saturating concentration of the respective ligands. Data are represented as mean ± SE for 4-34 cells for each concentration.

Table 3.2: EC_{50} values and Hill coefficients for various ligands on the chimera

Ligand*	**EC_{50} (nM)**	**Hill coefficient**	**Relative Efficacy**
ATP *(7)*	3 ± 0.4	1.2 ± 0.2	1
BzATP *(9)*	27 ± 4	1.4 ± 0.2	~1
αβ-MetATP *(21-34)*	137 ± 6	1.6 ± 0.1	~1
TNP-ATP *(4-7)*	20 ± 3	0.9 ± 0.1	~0.01

* Number of cells for each ligand concentration is indicated in parentheses.

3.1.3.2 Time course of covalent activation of the chimera

To determine the time course of photolabeling, covalent activation of the chimera was determined from the level of persistent current induced by cross-linking of BzATP in the binding sites of the chimera. Fig. 3.6A shows the representative current trace for the photolabeling procedure and determination of persistent current after photolabeling by Neomycin block on the same cell. Fig. 3.6B shows the ratio between persistent current (I_p) and the total current from the chimera after photolabeling (I_{max}) is plotted against different lengths of light irradiation.

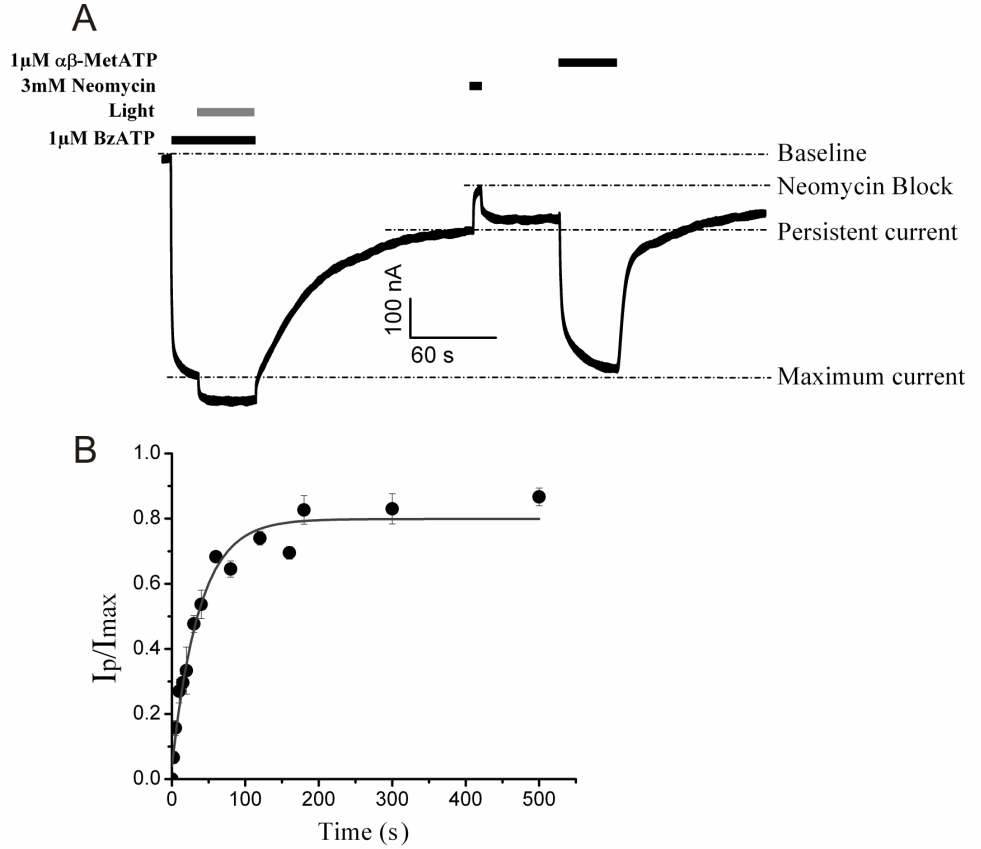

Fig. 3.6 Covalent activation of the chimera by BzATP: (A) Representative current trace on the chimera generated after BzATP activation. UV-light application leads to the photolabeling which is shown by persistent current. After photolabeling, the level of persistent current could be specifically blocked by the application of Neomycin. Block generated by Neomycin is completely reversible. After photolabeling, the remaining closed receptors could be activated by the application of full agonist e.g. αβ-MetATP. **(B)** Time course of BzATP photolabeling. Ratio between persistent current (I_p) and the total current from the chimera after photolabeling (I_{max}) is plotted against different lengths of light irradiation The curve was fitted by a mono exponential equation with time constant (τ) = 37 ± 5s. Data are presented as mean ± SE of 3-11 cells for each time point.

In these experiments, saturating concentration of BzATP (1µM) was first used to maximally activate the chimera (I_{Bz}) in the absence of UV-light. It is expected that during the full activation (I_{max}), all receptors are in fully liganded state i.e. all the binding sites are occupied. UV-light was applied only when the channels were fully activated i.e. in the continuous presence of 1µM BzATP. Light + ligand were applied for different periods of time. After photolabeling, the oocyte was washed extensively with the nucleotide free buffer for at least 3-5 times the time required for complete deactivation of the chimera in the absence of light (i.e. without photolabeling). Neomycin which is described as an open channel blocker of P2X receptors [153], also showed a partial block of currents through open channels on the chimera when applied externally (unpublished results, Eva Bongartz). Therefore, after the extensive washout, 3mM Neomycin was then applied externally to generate block of current through permanently open channels i.e. receptors in which all the binding sites were cross-linked by BzATP. As the Neomycin block was partial, specific block by Neomycin was determined on each oocyte before photolabeling by first activating the receptors with 1µM BzATP in the dark, and at the steady-state current level 3mM Neomycin was applied for a short duration (5s). Open channel block by Neomycin is expressed as a ratio between current blocked by Neomycin and the maximum current generated by 1µM BzATP before photolabeling (equation 3.1). It was found that the mean ratio of block generated by 3mM Neomycin was 0.49 ± 0.01 (n = 34) on different oocytes.

$$Ratio\ of\ Neomyin\ \ block = \frac{I_{Neo}}{I_{Bz}\ (before\ photolabeling)} \qquad \text{Equation 3.1}$$

After the photolabeling, the level of persistent current (I_p) was determined on each oocyte using equation 3.2.

$$Ip = \frac{I_{Neo}\ (After\ photolabeling)}{Ratio\ of\ Neomyin\ \ block\ before\ photolabeling} \qquad \text{Equation 3.2}$$

The level of covalent activation of the chimera was expressed as the ratio between persistent current (I_p) and the total current from the receptors (I_{max}) after photolabeling (whereas, I_{max} = I_p + current that can be activated by applying saturating concentrations of agonists (e.g. αβ-MetATP) concentration on individual oocytes after photolabeling) (equation 3.3).

$$Covalent\ activation = \frac{Ip}{Imax} \qquad \text{Equation 3.3}$$

It is apparent that upon progressive photolabeling, more molecules of BzATP would covalently bind to the channels and drive them towards permanently open state. This would

increase the ratio of Ip/Imax towards unity. However, possibly due to the constant receptor trafficking on the membrane or lateral diffusion of receptors outside the field of light application (outside the hole), complete covalent activation of all receptors was not observed.

3.1.3.3 Effect of prolonged application of light and BzATP on the chimera

In the time course determination, the chimera was also exposed to prolonged BzATP + UV-light, therefore, as a control experiment individual effect of UV-light and BzATP on the chimera was determined for an extended period of time (180s) (Fig. 3.7).

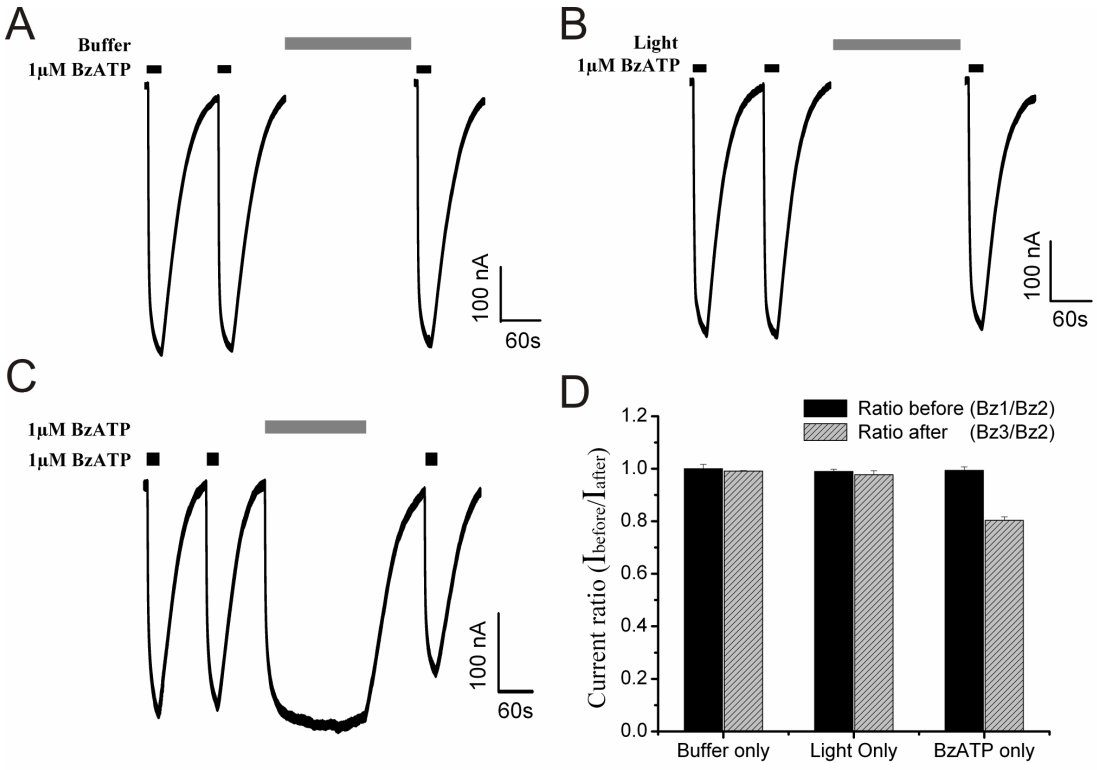

Fig. 3.7 Effect of various parameters on the response generated on the chimera during such treatments: Representative current traces of BzATP induced currents on the chimera, when 180s treatment of **(A)** Ligand free buffer (MgORI), **(B)** UV-light, **(C)** BzATP, was given between second (Bz2) and third (Bz3) BzATP applications. **(D)** Ratio of current amplitudes generated by first BzATP (Bz1) to second BzATP application (Bz2) i.e. before treatment, is compared with the ratio of current amplitudes generated by third BzATP (Bz3) to second BzATP application i.e. after treatment. Data are represented as mean ± SE of 3-4 cells for each treatment group.

In these experiments, full activation of chimera was performed on the same oocyte three times by 1µM BzATP designated as Bz1, Bz2 and Bz3. Treatment of UV-light or BzATP was given between second (Bz2) and third response (Bz3) for 180s (Fig. 3.7B and C). In the control experiment, ligand free buffer (MgORI) was applied for 180s in the absence of light between second (Bz2) and third (Bz3) application (Fig. 3.7A). Ratio of responses generated before (Bz2/Bz1) and after treatment (Bz3/Bz2) was compared with the control experiment i.e. when ligand free buffer was used (Fig. 3.7D). It was found that prolonged application of BzATP alone in the absence of light lead to ~20% decrease in the current response. From the time course of photolabeling of chimera it is also evident that due to the constant receptor trafficking on the membrane, results obtained for more than 120s were not different than obtained at 120s. Therefore, experiments involving prolonged 1µM BzATP (more than 120s) application were not performed in future. Prolonged application of light to the chimera in the absence of any ligand did not affect the current response generated before and after the treatment, indicating that light alone has no effect on receptor functionality.

3.1.3.4 Photolabeling modulates response of the receptors

The conclusion that gating is a process contributed by each subunit of a receptor came from the result that the response of the full agonist (ATP) was decreased when one or two P2X2 receptor subunits were cross-linked by the partial agonist (BzATP). To further support this conclusion, the effect of photolabeling on the gating response of the chimera by full and partial agonist was studied when the receptors were cross-linked by a full agonist. BzATP, a full agonist on the chimera was used as a photoaffinity analog of ATP. Dose response curves for αβ-MetATP (another full agonist on the chimera) and TNP-ATP (partial agonist on the chimera) were made on the same oocyte before and after different levels of covalent activation. The occupancy state of the chimera was controlled by application of UV-light + BzATP for different lengths of time.

3.1.3.4.1 Modulation of full agonist response by photolabeling

Photolabeling on the chimera was used to determine the change in potency of αβ-MetATP. To this end, first the dose response curve for αβ-MetATP was determined on the chimera before photolabeling. The same cell was then photolabeled by 1µM BzATP for 2, 20 or 40s and the dose response curve for αβ-MetATP was then again determined (Fig. 3.8 and Table 3.3).

After photolabeling, when one or two subunits of the receptor would be permanently occupied by BzATP (full agonist), sub-saturating concentrations of another full agonist (αβ-MetATP) is expected to become more effective because the probability that these channels will be fully liganded at any given αβ-MetATP concentration would be higher. These changes are evident in our case that the progressive photolabeling by a full agonist (BzATP) increased the potency of another full agonist (αβ-MetATP) i.e. EC_{50} values and Hill coefficients reduced progressively upon photolabeling. Thus, these results support our earlier conclusion that the process of gating is contributed by each subunit of the P2X receptors.

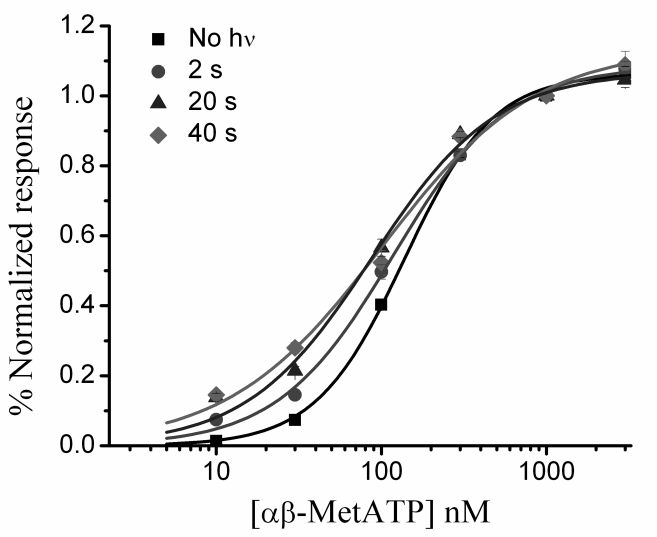

Fig. 3.8 Modulation of αβ-MetATP response by progressive photolabeling on the chimera: Dose response curves for αβ-MetATP on the chimera were determined before and after different levels of covalent activation. The curves get leftward shifted upon progressive photolabeling. Data are presented as mean ± SE of 5-34 cells for each concentration.

Table 3.3: EC_{50} values and Hill coefficient for αβ-MetATP on the chimera

Time of photolabeling*	**% Covalent activation**	**EC_{50} (nM)**	**Hill coefficient**
0s *(21-34)*	0	137 ± 6	1.6 ± 0.1
2s *(5-12)*	2 ± 0.3	118 ± 8	1.2 ± 0.1
20s *(5)*	33 ± 7	87 ± 12	1.1 ± 0.1
40s *(8-10)*	54 ± 4	101 ± 18	0.9 ± 0.1

* Number of cells for each length of light irradiation is indicated in parentheses.

3.1.3.4.2 Modulation of partial agonist response by photolabeling

Similarly, the dose response curves for TNP-ATP (partial agonist on the chimera) were determined before and after photolabeling for 2 or 40s on the oocytes expressing the chimera (Fig. 3.9). It was found that 1μM TNP-ATP generated ~2% of the maximum full agonist response without photolabeling. The response increased to ~6% after 2s of photolabeling, which further increased to ~12% when the time of photolabeling was increased to 40s. However, photolabeling had no effect on the apparent affinity (EC_{50} value) for TNP-ATP (Table 3.4). Thus, it is evident that if one or more binding sites of the receptor were preoccupied with full agonist, gating process of the receptor becomes more effective for a partial agonist. Together these results further support the conclusion that the process of gating is contributed by each subunit of the P2X receptors.

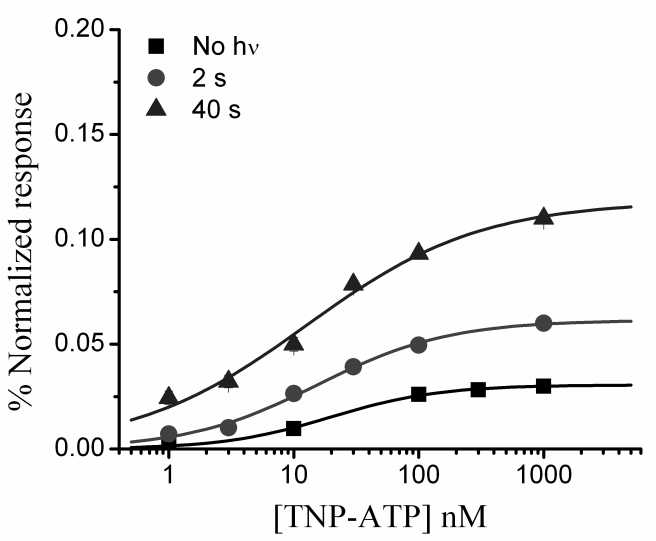

Fig. 3.9 Modulation of TNP-ATP response by progressive photolabeling on the chimera: Dose response curves for TNP-ATP on the chimera were determined before and after different levels of covalent activation. The curves showed an increase in the maximal response by TNP-ATP on the receptor upon progressive photolabeling. All dose response curves were normalized to the response generated by 1μM BzATP before photolabeling. Data are presented as mean ± SE of 3-11 cells for each ligand concentration.

Table 3.4: EC_{50} values and Hill coefficients for TNP-ATP on the chimera

Time of photolabeling*	**EC_{50} value (nM)**	**Hill coefficient**
0s *(4-7)*	13 ± 3	1.1 ± 0.2
2s *(3-8)*	16 ± 2	0.8 ± 0.1
40s *(5-11)*	13 ± 4	0.6 ± 0.1

* Number of cells for each length of light irradiation is indicated in parentheses.

3.1.3.5 Estimating the number of bound ligands required for the maximal response generated by TNP-ATP on the receptors

As the process of gating is contributed by each subunit of the receptors, the number of covalently attached BzATP molecules per receptor can be used to estimate the number of BzATP required for the maximal response generated by TNP-ATP i.e. to increase the efficacy of TNP-ATP to maximum. Thus, the change in ratio of current generated by saturating concentration (300nM) of partial agonist (TNP-ATP) ($I_{sat.TNP}$) to the saturating concentration (1µM) of full agonist (BzATP) ($I_{sat.BzATP}$) was determined at each level of covalent activation. Fig. 3.10 shows the current traces and the plot of an increase in ratio of ($I_{sat.TNP}$) to ($I_{sat.BzATP}$) during progressive photolabeling.

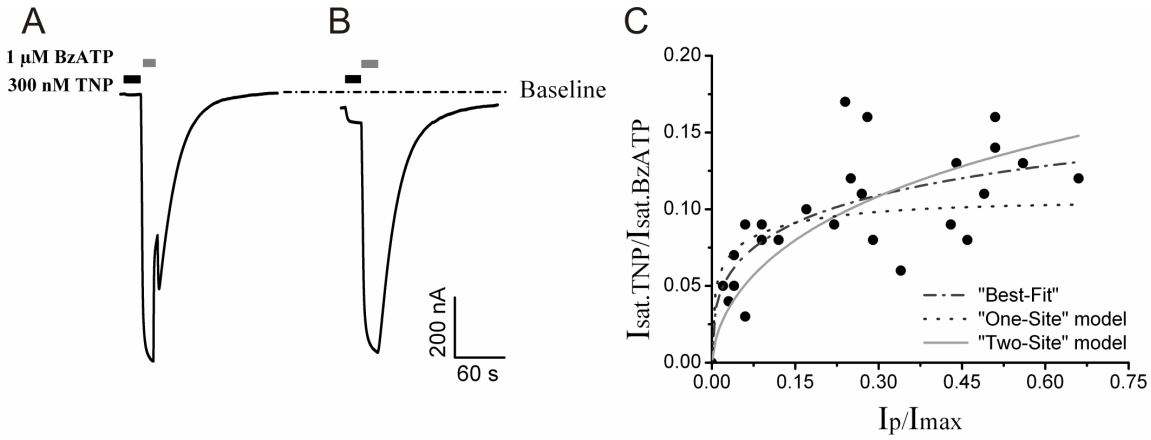

Fig. 3.10 Effect of progressive photolabeling on the ratio of response generated by saturating concentration of TNP-ATP and BzATP on the chimera: Representative current traces of BzATP and TNP-ATP on the chimera **(A)** Before, **(B)** After photolabeling. Before photolabeling TNP-ATP elicited negligible current compared to BzATP. After photolabeling (for 10s) TNP-ATP elicited significant current from the same population of receptors when compared to BzATP. **(C)** Progressive photolabeling increased the ratio of responses generated by saturating concentration of TNP-ATP to the saturating concentration of BzATP. Change in the ratio was fitted with "One-site" or "Two-site" model equation 3.4 or "Best-fit" (with all the free parameters) as described in results.

Table 3.5: Summary of fitting results of "One-site", "Two-site" model and "Best fit"

Model	Bf(1)	Cf(2)
One-site	0.1 ± 0.02	0.1 ± 0.01
Two-site	0	0.17 ± 0.01
Best fit	0.06 ± 0.02	0.14 ± 0.01

To fit the progressive change in the gating response of the receptor by TNP-ATP during different levels of covalent activation, the following equation was used:

$$\frac{I_{sat.TNP}}{I_{sat.BzATP}} = Af(0) + Bf(1) + Cf(2) \qquad \text{Equation 3.4}$$

The gating response of the receptor for TNP-ATP at any given time is contributed by the statistical distribution of total population of functionally activable receptor under consideration at that point of time (i.e. current generated by TNP-ATP from 0, 1, 2 BzATP bound receptors). In the equation 3.4, A, B and C are the currents induced by saturating TNP-ATP concentration through the statistical distribution of receptors (f(x)) with 0, 1 and 2 bound BzATP respectively.

It is apparent that without photolabeling, TNP-ATP produced negligible response (Fig. 3.10A), thus the contribution of Af(0) population can be neglected from the equation 3.4. The gating response of the receptor for TNP-ATP increased only when the binding sites contained one or two covalently attached BzATP (Fig. 3.10B). Thus, we considered two theoretical possibilities:

1) TNP-ATP produced significant response after at least one binding site is labeled by BzATP and the TNP-ATP induced current from the population of receptors with two labeled BzATP will not be different from the current generated by one bound BzATP. Hence, the response generated by Bf(1) population will be equal to the response generated by Cf(2) population. Therefore, Bf(1) = Cf(2) in equation 3.4. This is termed as "One-site model".

2) TNP-ATP produced significant response only after at least two binding sites are labeled by BzATP and the TNP-ATP induced current from the population of receptors with one bound BzATP will not be different from the current generated by 0 bound BzATP. Hence, response from Af(0) population will be equal to the response generated by Bf(1) population. Therefore, Af(0) = Bf(1) = 0. This is termed as "Two-site model".

As photolabeling was performed at the saturating concentration of BzATP (1µM), we expected all the binding sites to be occupied at all time irrespective of the individual binding site affinity. In order to calculate the fractional distribution of 0, 1, 2 and 3 BzATP bound population of receptors, we used binomial equation (equation 3.5). To this end, we considered

that at saturating concentration of BzATP (1μM) for the chimera, covalent crosslinking occurs randomly and not with efficiency based on binding sites' affinity.

$$f(x) = \frac{n!\left(p^x q^{n-x}\right)}{\left[(n-x)!\,x!\right]} \qquad \text{Equation 3.5}$$

Where n is the total number of ligand binding sites per receptor, p is the probability that a particular site is labeled; q is the probability that a particular site is not labeled (1-p), and x is the number of bound BzATP molecules.

As chimera is a trimeric receptor, therefore we assumed three binding sites per receptor i.e. n equals to 3. To calculate the probability (p) that a particular site is labeled, we assumed that three ligands per receptor are required to open the channel significantly i.e. below three bound ligands, the channel is essentially closed and will not contribute to any current response. Under these circumstances equation 3.5 would give:

$$f(3) = p^3 \quad or \quad p = f(3)^{1/3} = \left(\frac{Ip}{\mathrm{Im}\,ax}\right)^{1/3} \qquad \text{Equation 3.6}$$

The level of covalent activation (I_p/I_{max}) (according to our assumption that three ligands are required to open the channel) was determined from the time course of photolabeling e.g. at 40s, ~47% of covalent activation was observed (Fig. 3.6C).

Thus, with the help of equation 3.6, p was calculated for each level of covalent activation. After determining p, fractional distribution of receptors *f*(x) with 0, 1 and 2 bound BzATP can be calculated from equation 3.5. For example, at fractional covalent activation (I_p/I_{max}) of 0.47 (Fig. 3.6C), the probability (p) that a given site is labeled is 0.77, and statistical distribution of channels (*f*(x)) containing 0, 1, and 2 bound ligands is 0.012, 0.12 and 0.40 respectively. In this way, at each level of covalent activation, fractional distribution of 0, 1, and 2 BzATP bound population was calculated and used in equation 3.4 to fit the increasing trend of gating response for TNP-ATP with respect to BzATP on the chimera.

Thus, these fitting results suggest that out of one-site and two-site model, change in the efficacy of TNP-ATP upon progressive photolabeling was well described by two-site model, thus indicating that two BzATP are required to increase the efficacy of TNP-ATP to a significant level.

3.2 Probing allosteric interactions between P2X receptor subunits using fluorescent ligand

Upon activation, many ligand gated ion channels enter a desensitized state in which the neurotransmitter remains bound but the ion channel is closed. Over the last few decades, research has focused on the mechanisms involved in the desensitization of ligand gated ion channels [154]. In nAChRs, subunit composition governs the rate of desensitization, whereas the recovery from desensitization is an agonist specific phenomenon [154-156]. High resolution structural data for iGluRs suggest that perturbations that destabilize the intradimer interface enhance desensitization [157], whereas the rate limiting steps in the recovery from desensitization are reassembly of the two dimer interfaces [158]. In case of P2XRs, kinetic studies suggest that P2X1 receptors need to open before undergoing desensitization and the rate limiting step in the recovery from desensitization is the dissociation of bound agonist molecules [104]. However, after agonist binding, the allosteric interactions between subunits, which result in desensitization and regulate the dissociation of bound agonist, remains poorly understood till date. Therefore, in my thesis, I have studied the nature of contribution of each receptor subunit in the process of desensitization and the recovery from desensitization.

To address these questions on wild type P2X1 receptors, I used Alexa-ATP (a fluorescent ATP analog) for concurrent activation (represents the functional state) and fluorescence measurement (represents the occupancy state) from the same set of receptors. In the functional studies, occupancy state of the receptor was correlated with the level of desensitization. Change in the rate of dissociation of bound agonist in the presence of a competing ligand was used as a parameter for the contribution of each subunit in the process of recovery from desensitization.

3.2.1 Potency and efficacy of ATP and Alexa-ATP on P2X1 receptors and the chimera

The desensitized state of P2X1 receptors is a ligand bound closed state, which limits functional characterization of the desensitized state by current measurement. Therefore, to get an insight into the desensitized state, the level of fluorescence of the bound fluorescent agonist could be used as a parameter for the occupancy level of the receptors in the desensitized state. Because P2X1 receptors undergo desensitization only after activation

[104], a fluorescent ligand was required which could activate and thus desensitize the P2X1 receptors. Currently no fluorescent ATP analog is known which can act as an agonist on P2X1 receptors. Alexa-ATP is a commercially available fluorescent ATP analog. Therefore, to determine the efficacy and potency of Alexa-ATP, current responses were generated by Alexa-ATP on P2X1 receptors and the chimera.

In order to compare the efficacy of 1µM Alexa-ATP with respect to 1µM ATP, following protocol was used. First, 30µM ATP was used to completely activate and desensitize P2X1 receptors. After washing for 1 min in ligand free buffer, peak response was elicited by 1µM ATP, followed by 1µM Alexa-ATP and again by 1µM ATP. Each ligand application was separated by a 1 min washing step. 1µM Alexa-ATP produced only ~50% of the peak response as compared to 1µM ATP on the same cell (Fig. 3.11A, B).

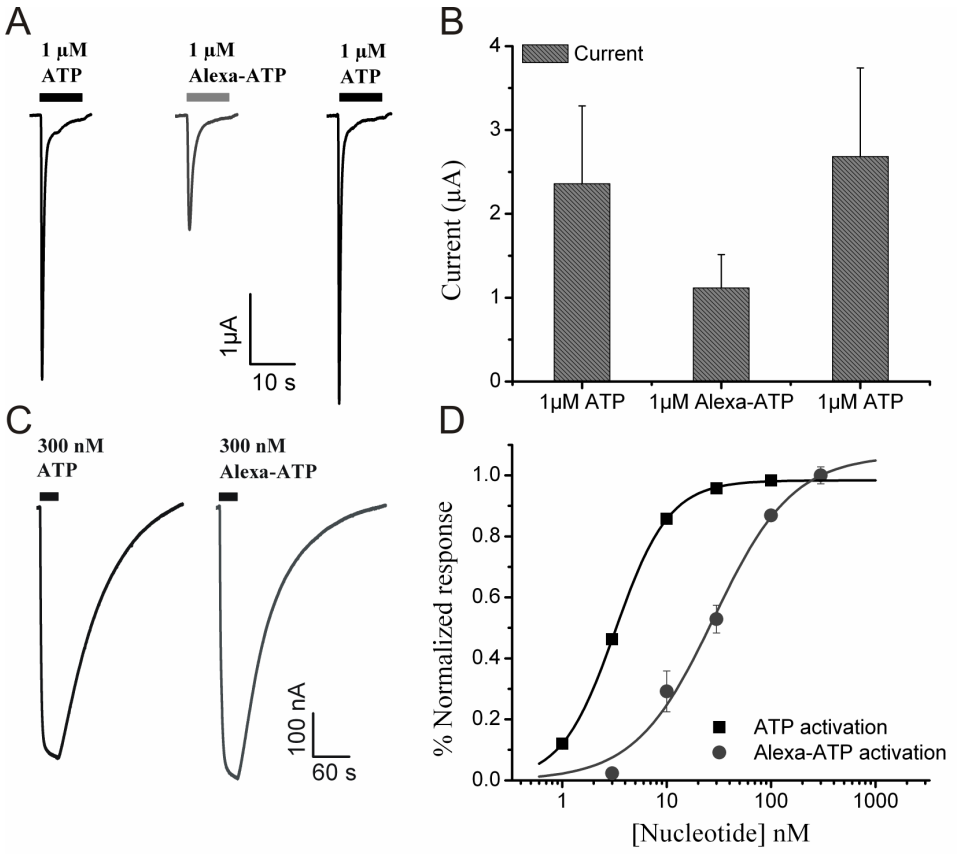

Fig. 3.11 Potency and efficacy of Alexa-ATP on P2X1 receptors and the chimera: (A) Representative current traces generated by 1µM ATP followed by 1µM Alexa-ATP and again followed by 1µM ATP on the same oocyte expressing P2X1 receptors. Each agonist application was separated by a 1 min ligand free washing step. **(B)** Mean current generated on P2X1 receptors during ATP and Alexa-ATP applications. Data are presented as mean ± SE of 3 cells for each agonist application. **(C)** Representative current traces generated by 300nM ATP

and Alexa-ATP on the same oocyte expressing the chimera. **(D)** Comparison of dose-response curve for ATP and Alexa-ATP on the chimera. Data are presented as mean ± SE of 5-8 cells for each concentration.

Table 3.6: EC_{50} values and Hill coefficients of ATP and Alexa-ATP on the chimera

Ligand *	**EC_{50} (nM)**	**Hill coefficient**
ATP *(8)*	3 ± 0.1	1.6 ± 0.1
Alexa-ATP *(5)*	28 ± 7	1.2 ± 0.2

* Number of cells for each ligand concentration is given in parentheses.

On P2X1 receptors, the EC_{50} value of receptor activation by ATP is ~1µM, which is determined under non-steady state conditions (a detailed description is given in the introduction section 1.5.2); therefore, complete dose response curve of P2X1 activation by Alexa-ATP was not determined due to the high cost of Alexa-ATP. However, an estimate of EC_{50} value of Alexa-ATP was determined using the Hill equation (equation 3.7).

$$\frac{I}{\mathrm{Im}ax} = \frac{1}{1 + \left(\frac{EC50}{[A]}\right)^{n}} \qquad \text{Equation 3.7}$$

In this calculation, it is considered that the EC_{50} value for ATP is ~1µM at the P2X1 receptors i.e. 1µM ATP would produce 50% of the peak current response [99]. In equation 3.7, I denotes the current produced by 1µM Alexa-ATP with respect to 1µM ATP, I_{max} denotes the maximum current produced by ATP at highest concentration, [A] denotes 1µM Alexa-ATP concentration, EC_{50} denotes the half maximal concentrations of Alexa-ATP, n denotes the Hill coefficient of ATP. Using this equation, EC_{50} value for Alexa-ATP on P2X1 receptors is estimated to be ~2µM.

Complete dose response curve of Alexa-ATP could be determined on the chimera, due to its nanomolar sensitivity for various ligands (Fig. 3.11D) [88]. For differences in the potency of ATP on P2X1 receptors and chimera see a detailed description in the introduction section 1.5.2. Dose response curve for Alexa-ATP on the chimera was found to be rightward shifted as compared to ATP, which indicates that Alexa-ATP is less potent compared to ATP. Corresponding values for Hill coefficient and EC_{50} of ATP and Alexa-ATP on the chimera are listed in Table 3.6. However, saturating concentration of ATP (300nM) and Alexa-ATP

(300nM) elicited the same maximum amplitude of current on the same cell, thus indicating that both agonists have a similar efficacy on the chimera (Fig. 3.11C).

3.2.2 Optimization of conditions for studying ligand-receptor interactions

3.2.2.1 Optimization of light irradiation protocol

Time course of dissociation of bound radio-ligand in the presence of high concentrations of non-labeled competing ligands has been used as a parameter for cooperative interactions in the hB2 (human bradykinin) receptors [159]. Similarly, we have exploited the fluorescence properties of Alexa-ATP to study the subunit interactions in P2X1 receptors where dissociation of bound Alexa-ATP from the desensitized state of P2X1 receptors was measured. I used the voltage-clamp fluorometry setup for concurrent current and fluorescence measurements from the same set of receptors (Fig. 2.3). The receptor current served as a parameter for the functional state of P2X1 receptors and the level of fluorescence was used as a parameter for the occupancy state of the binding sites.

In continuous presence of light, photobleaching is a common problem associated with the fluorescent probes. As the bound agonist dissociates slowly from desensitized P2X1 receptors and the fluorescence of Alexa-ATP is susceptible to photobleaching, a protocol was optimized to minimize photobleaching. This was achieved by exposing the receptors to light for different periods of time during the dissociation of bound Alexa-ATP from the desensitized state of P2X1 receptors (Fig. 3.12, Table 3.7). 300nM Alexa-ATP was used to elicit current responses and to induce complete desensitization in P2X1 receptors. For the first 15s, washout of Alexa-ATP was done in the absence of light in order to wash non-specifically bound Alexa-ATP. The time course of decay of bound Alexa-ATP fluorescence was monitored in real time under voltage clamp condition in the continuous presence of ligand free buffer (MgORI buffer). After 15s from the onset of washout, dissociation of bound Alexa-ATP was monitored either in the continuous presence of light, or light was applied for 2s every 10 to 40s intervals (Fig. 3.12C). With decreasing frequency of light exposure during the measurement, a reduction in photobleaching is expected. As expected, faster time course (faster time constant of decay) of Alexa-ATP dissociation was observed from protocols in which light was applied continuously as compared to the protocol where light was applied less frequently. However, 30s and 40s light irradiation protocols gave similar results (Fig. 3.12C). Therefore, all the future experiments were performed with 30s light irradiation

protocol. In order to further minimize the photobleaching component (if any), light was irradiated for 1s every 30s interval in all subsequent experiments.

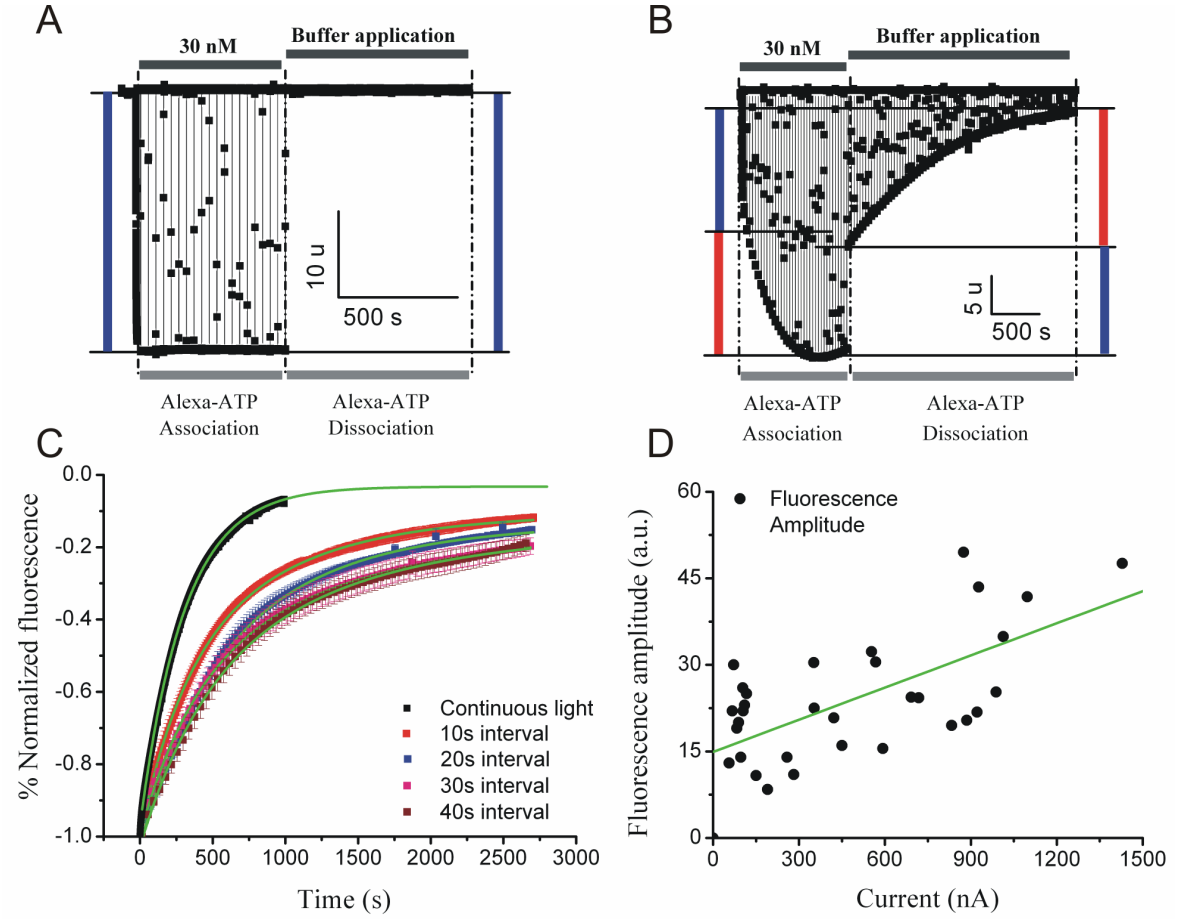

Fig. 3.12 Association and dissociation of Alexa-ATP and light irradiation protocol: Representative fluorescence traces for association and dissociation of 30nM Alexa-ATP on the **(A)** control oocyte (No RNA injected), **(B)** P2X1 expressing oocyte. Blue and red bars indicate the non-specific (background) and P2X1 specific Alexa-ATP fluorescence respectively. In both cases, the dissociation of bound Alexa-ATP was performed in the presence of ligand free buffer (MgORI). In the control cells, the washout of non-specific fluorescence was completed within 15s from the onset of washout. **(C)** Time course of decay of Alexa-ATP fluorescence from P2X1 receptors under different light irradiation protocols. During the optimization of measuring conditions for Alexa-ATP dissociation, light was applied for 2s every 10 to 40s. All traces were individually normalized to the level of fluorescence obtained after 15s from the onset of Alexa-ATP dissociation in each measurement. All fluorescence responses were monitored in real time under voltage clamp conditions. Data are presented as mean ± SE of 3-8 cells for each protocol. **(D)** The correlation between fluorescence amplitude and the Alexa-ATP activated current in 32 individual oocytes expressing P2X1 receptors. The peak current was determined at 300nM Alexa-ATP and the specific fluorescence amplitudes were determined by subtracting the level of fluorescence after 15s of washout in MgORI buffer (fluorescence amplitude A1) to the level of fluorescence left at the end of extended washout (after 2500s) in MgORI buffer (fluorescence amplitude

A2). The solid line represents linear regression to the data points with an intercept of 15 ± 2 and slope of 0.02 ± 0.003.

Table 3.7: Kinetics of decay of Alexa-ATP fluorescence during various intervals of light application

Light protocol (s)*	**Time constant (τ_{fast}) (s)**	**Time constant (τ_{slow}) (s)**	**Fluorescence Amplitude (A1, 15s)**	**Fluorescence Amplitude (A2, 2500s)**	**Current (I) (µA)**
Continuous light *(3)*	304 ± 0.02	-	41 ± 15	-	0.9 ± 0.1
2/10 *(3)*	303 ± 4	861 ± 12	24 ± 2	3 ± 0.4	0.8 ± 0.04
2/20 *(3)*	437 ± 11	970 ± 38	39 ± 10	5 ± 1.3	1.8 ± 0.5
2/30 *(8)*	377 ± 9	1427 ± 43	31 ± 7	6 ± 2	0.6 ± 0.1
2/40 *(6)*	439 ± 11	1297 ± 101	36 ± 3	6 ± 1	0.7 ± 0.1

* Number of cells for each irradiation time is given in parentheses.

Using voltage-clamp fluorometry setup I have measured concurrent receptor activation (represents the functional state) and the level of fluorescence (represents occupancy state) on the same population of receptors. To see if there exists a correlation between the observed fluorescence and current from the receptors, 300nM Alexa-ATP was applied to P2X1 receptors to activate and fully desensitize them. After washing the non-specific fluorescence for 15s, level of Alexa-ATP fluorescence bound to P2X1 receptors was determined by irradiating individual oocyte for 1s every 30s. A direct correlation was found between fluorescence amplitude and the current response i.e. increase in the number of receptors (current) showed correspondingly increase the number of bound Alexa-ATP molecules (fluorescence amplitude) (Fig. 3.12D).

Interestingly, a trace amount of residual fluorescence was always found to be associated with the receptors even at the end of extensive washout which decayed on a very slow time scale (Fig. 3.12C), resulting in a bi-exponential time course of decay of Alexa-ATP fluorescence. In the past, the slow component of biphasic fluorescence quenching in EGF receptor was attributed to receptor internalization [160], whereas, presence of similar biphasic kinetics during fluorescent ligand dissociation in torpedo nAChR receptors was attributed to non-

equivalent agonist binding sites [161]. However, considering all the binding sites in homomeric P2X1 receptors are the same, we speculated that the residual fluorescence at the end of extensive washout and the bi-exponential decay of Alexa-ATP fluorescence possibly originated from the internalization of Alexa-ATP bound P2X1 receptors and their slow recycling to the surface. We have tested the hypothesis in the following section.

3.2.2.2 Membrane trafficking of receptors

P2X1 receptors undergo constant receptor trafficking and agonist mediated internalization [105-107], which changes receptor density on the cell surface. Therefore, to probe the possibility that the residual fluorescence in Alexa-ATP dissociation experiments might have originated from the internalization of Alexa-ATP bound P2X1 receptors and their slow recycling to the surface, the time course of decay of Alexa-ATP fluorescence was monitored from phenyl arsine oxide (PAO) treated oocytes expressing P2X1 receptors. PAO has been shown to inhibit receptor trafficking in oocytes [162]. Oocytes expressing P2X1 receptors were treated with 100µM PAO at 18^0C for 1hr. PAO treated cells showed complete decay of Alexa-ATP fluorescence with a mono-exponential time course (Fig. 3.13A) (Table 3.8).

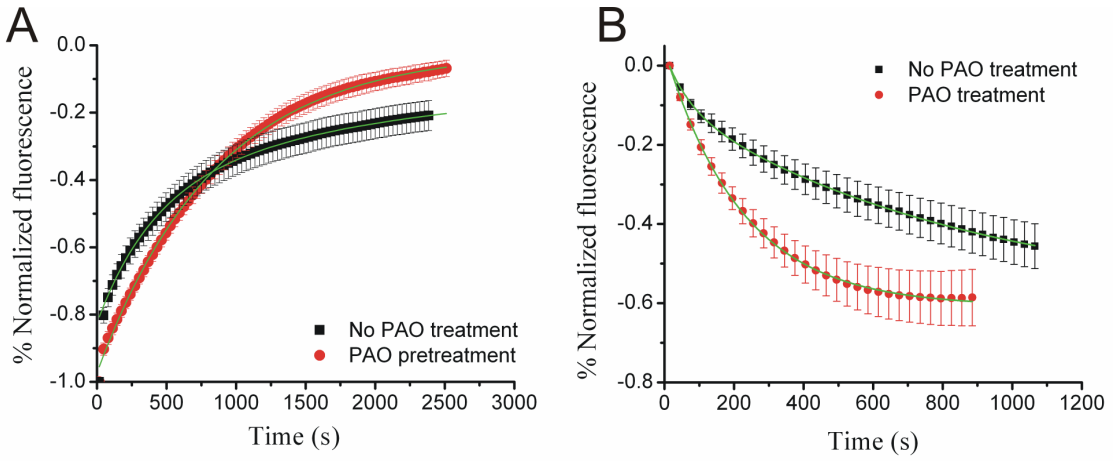

Fig. 3.13 Effect of PAO on P2X1 receptors trafficking: Time course of Alexa-ATP fluorescence from PAO treated and untreated cells expressing P2X1 receptors during **(A)** Dissociation (when receptors were activated with 300nM Alexa-ATP) measured in the presence of ligand free buffer, **(B)** Association (100nM Alexa-ATP). All traces were individually normalized to the level of fluorescence obtained after 15s from the onset of Alexa-ATP association or dissociation in each measurement. All fluorescence responses were monitored in real time under voltage clamp condition. Data are presented as mean ± SE of 5-6 cells for each treatment.

Table 3.8: Comparison of time constants of Alexa-ATP fluorescence between PAO treated and untreated oocytes

Experiment	Alexa-ATP	Treatment*	τ_{fast} (s)	τ_{slow} (s)
Dissociation	**300nM**	**No PAO treatment** *(6)*	394 ± 20	1910 ± 364
		PAO treatment *(5)*	850 ± 7	-
Association	**100nM**	**No PAO treatment** *(5)*	69 ± 6	848 ± 48
		PAO treatment *(5)*	223 ± 3	

* Number of cells for each measurement is given in parentheses.

These results suggest that the fast time constant in the time course of decay of Alexa-ATP fluorescence from the non-PAO treated oocytes is contributed by two components i.e. dissociation of bound Alexa-ATP from the surface receptors and agonist mediated internalization of P2X1 receptors. Whereas, the slow constant is possibly contributed by the slow trafficking of Alexa-ATP bound internalized P2X1 receptors back to the surface. The results from PAO treated oocytes suggest that PAO treatment blocked the agonist mediated receptor internalization, thus not only abolishing the residual fluorescence but also resulting in a time course of decay of Alexa-ATP fluorescence which could be described by mono-exponential function.

In Alexa-ATP association experiments, a continuous increase in Alexa-ATP fluorescence was observed on the P2X1 receptors from the non-PAO treated oocytes, even after prolonged application of 100nM Alexa-ATP (Fig. 3.13B). This resulted in the bi-exponential time course of increase in Alexa-ATP associated fluorescence (Table 3.8). We thought that the receptor trafficking on the membrane was possibly responsible for changing the receptor density (number of binding sites) on the cell surface. Therefore, the effect of PAO was also assessed on the steady-state fluorescence of Alexa-ATP upon binding to P2X1 receptors. PAO treated cells not only showed saturation in Alexa-ATP fluorescence upon binding to P2X1 receptors, but also resulted in the time course which could be described by mono-exponential function (Fig. 3.13B) (Table 3.8). Thus, these results indicate that PAO not only blocks the receptor internalization (as seen by the lack of residual fluorescence in Alexa-ATP dissociation experiments, Fig 3.13A) but also blocks receptor trafficking to the membrane (as seen by steady-state binding in Alexa-ATP fluorescence during the association experiments, Fig 3.13B). Therefore, all further experiments were performed with PAO treated cells.

3.2.3 Allosteric interactions between subunits regulate the dissociation of bound agonist

The desensitized state of P2X1 receptors has a high affinity to the bound agonist and the recovery from desensitization is thought to involve dissociation of bound agonist from the desensitized state [104]. Presence of allosteric sites on P2X receptors have been shown to modulate the affinity of agonist binding sites e.g. potentiation of ATP induced current on P2X2 receptors by zinc ions [53]. Therefore, we hypothesized that allosteric interactions between subunits may contribute to the change in the affinity of agonist binding site which in turn would control the dissociation of bound agonist from the desensitized state of P2X1 receptors. In order to probe this hypothesis, 300nM Alexa-ATP was used to activate and fully desensitize P2X1 receptors. The time course of dissociation of bound Alexa-ATP was then monitored in the presence of various allosteric/competing ligands (Fig. 3.14).

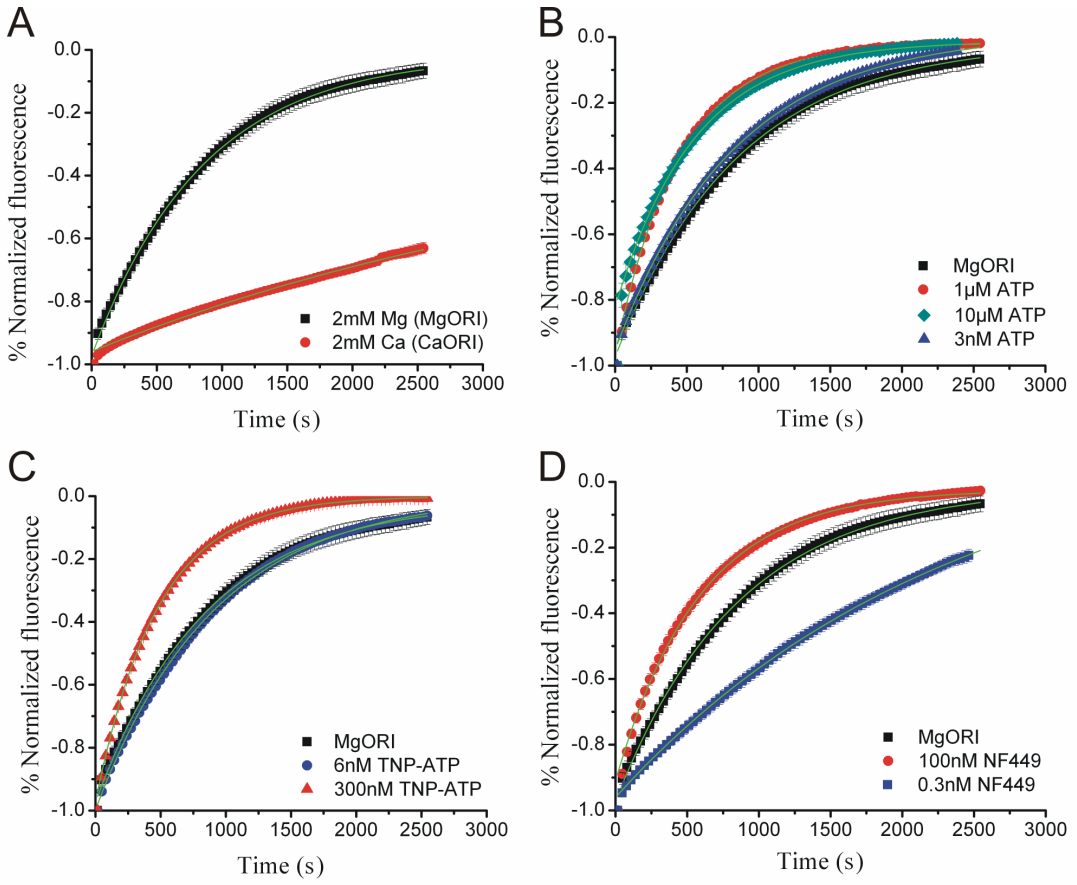

Fig. 3.14 Kinetics of the decay of Alexa-ATP fluorescence from P2X1 receptors in presence of various ligands: (A) MgORI buffer and CaORI buffer. **(B)** MgORI buffer, 10μM, 1μM (EC_{50}) and 3nM ATP. **(C)** MgORI buffer, 300nM (IC_{max}) and 6nM (IC_{50}) TNP-ATP. **(D)** MgORI buffer, 100nM (IC_{max}) and 0.3nM (IC_{50}) NF449. Data are represented as mean ± SE of 3-11 cells for each concentration.

Table 3.9: Effect of various cations, agonist and antagonists on the dissociation of bound Alexa-ATP from P2X1 receptors

Properties	Ligand	Concentration*	τ (s)	k (10^{-3} s^{-1})
Cation	Mg^{+2}	2mM *(5)*	874 ± 74	1.17 ± 0.10
	Ca^{+2}	2mM *(5)*	> 8000	-
Agonist	ATP	10μM *(3)*	554 ± 35	1.81 ± 0.10
		1μM (EC_{50}) *(7)*	452 ± 21	2.24 ± 0.11
		3nM *(11)*	832 ± 36	1.22 ± 0.05
Antagonist	TNP-ATP	300nM (IC_{max}) *(5)*	474 ± 8	2.11 ± 0.03
		6nM (IC_{50}) *(7)*	918 ± 46	1.10 ± 0.05
	NF449	100nM (IC_{max}) *(7)*	587 ± 32	1.73 ± 0.10
		0.3nM (IC_{50}) *(9)*	> 4000	-

* Number of cells for each ligand concentration is given in parentheses.

If the allosteric/competing ligands would accelerate the dissociation of bound Alexa-ATP from the desensitized state of P2X1 receptors it would indicate negative cooperative interactions between subunits, whereas a reduction in the dissociation rate would indicate positive cooperative interactions between subunits. All the time courses of Alexa-ATP dissociation were fitted with a mono-exponential function (Table 3.9).

ATP was used as an agonist because it would compete for the agonist binding site. Different concentrations of ATP (3nM, 1μM and 10μM) were used to monitor the time course of decay of bound Alexa-ATP fluorescence. It is expected that at 3nM ATP receptors are partially liganded and at 1μM or 10 μM ATP concentrations all binding sites would be occupied. Therefore, the effect of occupancy state of the P2X1 receptors at these concentrations was assessed on the dissociation rate of bound Alexa-ATP.

The dissociation of Alexa-ATP was also monitored in presence of P2X1 antagonists. Two antagonists, TNP-ATP and NF449 were used. TNP-ATP is structurally similar to ATP, whereas NF449 is different (Fig. 1.5), but both were shown to be competitive antagonists with nanomolar potency on P2X1 receptors [95,99,163]. The dissociation of Alexa-ATP was monitored at IC_{50} and IC_{max} concentrations of these antagonists. All these competing ligands were prepared in MgORI buffer.

As a divalent cation, the effect of calcium ions was monitored on the dissociation rate of Alexa-ATP; because calcium ions have been shown to modulate P2X receptors activities e.g. enhance the recovery from desensitization in P2X3 receptors [164].

The time course of decay of Alexa-ATP in the presence of Mg^{+2} ions (as MgORI) was taken as control and all the time courses of decay of Alexa-ATP in the presence of allosteric/competing ligands were compared with the time course of decay in the presence of MgORI buffer. The decay of Alexa-ATP fluorescence in MgORI buffer could be described by a mono-exponential function with a time constant of ~870s. Replacement of magnesium ions by calcium ions in the dissociation buffer dramatically decreased the decay of Alexa-ATP fluorescence (Fig. 3.14A). This observation contradicts earlier observations on desensitizing P2X receptors that the presence of calcium ions in the buffer has either no effect on the rate of recovery of P2X1 receptors from desensitization [101] or enhanced effect on the rate of recovery of P2X3 receptors from desensitization [103,164].

Presence of EC_{50} or higher concentrations of ATP in the dissociation buffer accelerated the decay of Alexa-ATP fluorescence. However, 3nM ATP concentration, which is sufficient to desensitize ~50% of P2X1 receptors [104], showed similar time course of decay of Alexa-ATP fluorescence as observed in MgORI buffer, probably due to slow rate of binding of ATP to the P2X1 receptors at this concentration [104]. Thus, due to lack of substantial binding of ATP at 3nM concentration, dissociation of bound Alexa-ATP occurred without the influence of ATP; hence, the time course of fluorescence decay was similar to the decay monitored in MgORI buffer (control conditions).

Antagonists like TNP-ATP or NF449, used at IC_{max} concentration in the dissociation buffer, accelerated the decay of Alexa-ATP fluorescence. However, at IC_{50} concentration both antagonists showed different effect. Similar time course of decay of Alexa-ATP fluorescence was observed in the presence of TNP-ATP at IC_{50} concentration as observed in MgORI buffer, whereas, NF449 at IC_{50} concentration slowed the decay of Alexa-ATP fluorescence.

These results indicate that ATP, TNP-ATP and NF449 at high concentrations (EC_{50} or more and IC_{max}), accelerated the dissociation of bound Alexa-ATP, therefore, indicating negative cooperative interactions between subunits. Divalent calcium ions (2mM) and NF449 at IC_{50} concentration significantly slowed down the dissociation of bound Alexa-ATP; thus, indicating positive cooperative interactions.

The positive cooperative interactions between subunits induced by calcium ions and NF449 (at IC_{50} concentration) would mean that in the presence of these ligands the affinity of desensitized P2X1 receptors for the bound ligand would increase, therefore, less Alexa-ATP would dissociates from the binding sites. Due to the fact that agonist will remain bound to the binding sites, less receptors would recover from the desensitization. These results were also confirmed functionally on P2X1 receptors (Fig. 3.15).

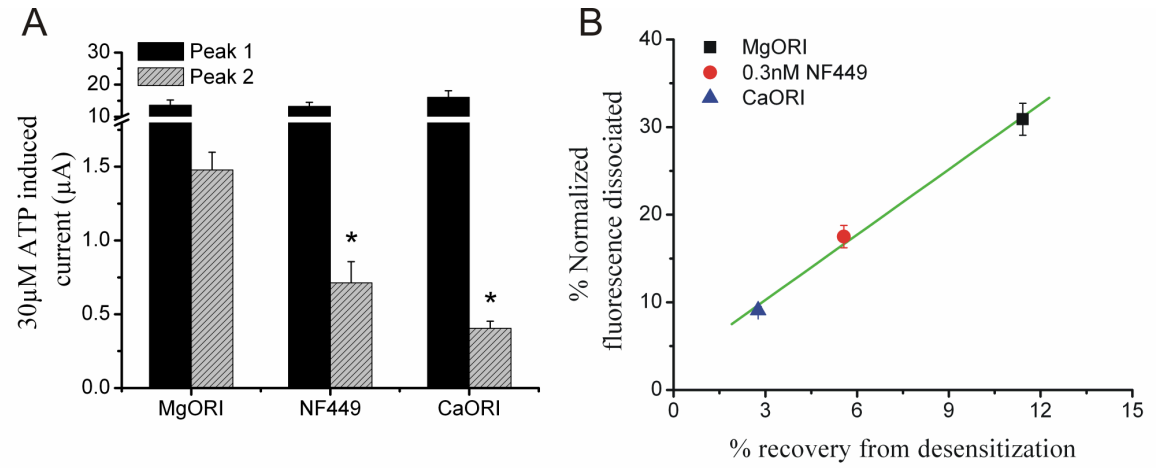

Fig. 3.15 Effect of calcium ions and 0.3nM NF449 on the functional recovery of P2X1 receptors from desensitization: (A) First application of 30µM ATP elicited peak currents (peak 1) from P2X1 receptors. Receptors were allowed to recover from desensitization for 5 min in the continuous presence of either 2mM Mg^{+2}, 2mM Ca^{+2} ions or 0.3nM NF449. Second application of 30µM ATP elicited peak currents (peak 2) from the receptors recovered from desensitization. Peak 2 of MgORI was compared with the peak 2 of NF449 and CaORI treated oocytes using one-way ANOVA followed by bonferroni's post test for paired comparison. NF449 and CaORI treatment significantly reduced the peak 2 response ($p < 0.01$) as compared to MgORI treated oocytes. Peak 1 of MgORI, NF449 and CaORI were not significantly different from each other. Asterisk sign (*) indicates level of significance ($p < 0.01$). **(B)** Percent recovery of P2X1 receptors from desensitization when the recovery was done either in 2mM Mg^{+2}, 2mM Ca^{+2} ions or 0.3nM NF449 (Fig. 3.15A) is plotted against the percent decay of Alexa-ATP fluorescence after 5 min when the dissociation was monitored in 2mM Mg^{+2}, 2mM Ca^{+2} ions or 0.3nM NF449 (Fig. 3.14). Data are presented as mean ± SE of 5-9 cells per treatment. The solid line represents linear regression to the data points with an intercept of 2.8 ± 1.3 and slope of 2.5 ± 0.17.

30µM ATP was used to elicit peak current (peak 1) and to completely desensitize P2X1 receptors. Desensitized receptors were allowed to recover for 5 min in the presence of MgORI buffer, CaORI buffer or 0.3nM NF449. 30µM ATP was again used to elicit current (peak 2) on the same oocyte to determine the percentage recovery of P2X1 receptors from desensitization. If these ligands would have no effect on the affinity of desensitized state of

P2X1 receptors, receptors would show similar percentage of recovery from desensitization. The recovery of P2X1 receptors from desensitization was found to be significantly reduced ($p < 0.01$) in presence of Ca^{+2} ions and 0.3nM NF449 as compared to Mg^{+2} ions (Fig. 3.15A). Thus, these functional results compliment our fluorescence data that in the presence of calcium ions and 0.3nM NF449, positive cooperative interactions between subunits take place. These positive cooperative interactions contribute to the increase in affinity of the bound agonist molecules in the desensitized state of P2X1 receptors, which resulted in the reduced dissociation of bound agonist, thus reducing the recovery from desensitization. This is also evident in Fig. 3.15B, where an inverse relation between levels of Alexa-ATP fluorescence was found with the percentage of receptors recovered from desensitization i.e. higher the amount of Alexa-ATP specific fluorescence associated with the receptors, less receptor recovered from desensitization. The effect of 0.3nM NF449 on the decreased decay of Alexa-ATP fluorescence has been discussed in detail in the discussion section 4.2.

3.2.4 Allosteric model for ligand-receptor interactions

3.2.4.1 Negative cooperativity in P2X1 receptors

Alexa-ATP dissociation in the presence of different ligands indicated positive and negative cooperative interactions between subunits (section 3.2.3). In order to understand the mechanism of negative cooperative contributions between receptor subunits in the process of dissociation of bound Alexa-ATP, we propose a simple allosteric model (Fig. 3.16).

In this model we propose that binding of three agonist molecules (Alexa-ATP) to the closed state of the receptor is required to open and thus desensitize the receptor (Scheme-I). In Scheme-II, the dissociation of bound agonist molecules from the desensitized state in the presence of ligand free buffer would result in non-liganded closed state of the receptor (Fig. 3.16). In Scheme-II, if the dissociation of bound agonist molecules would occur in the presence of competing ligands, then the receptor would be fully liganded at all the times. Based on our earlier results (Fig. 3.14), we hypothesize that negative cooperativity exists only in the fully liganded state of the receptor (three ligand bound state) and under the influence of negative cooperativity the dissociation of the first of the three bound ligands would be faster.

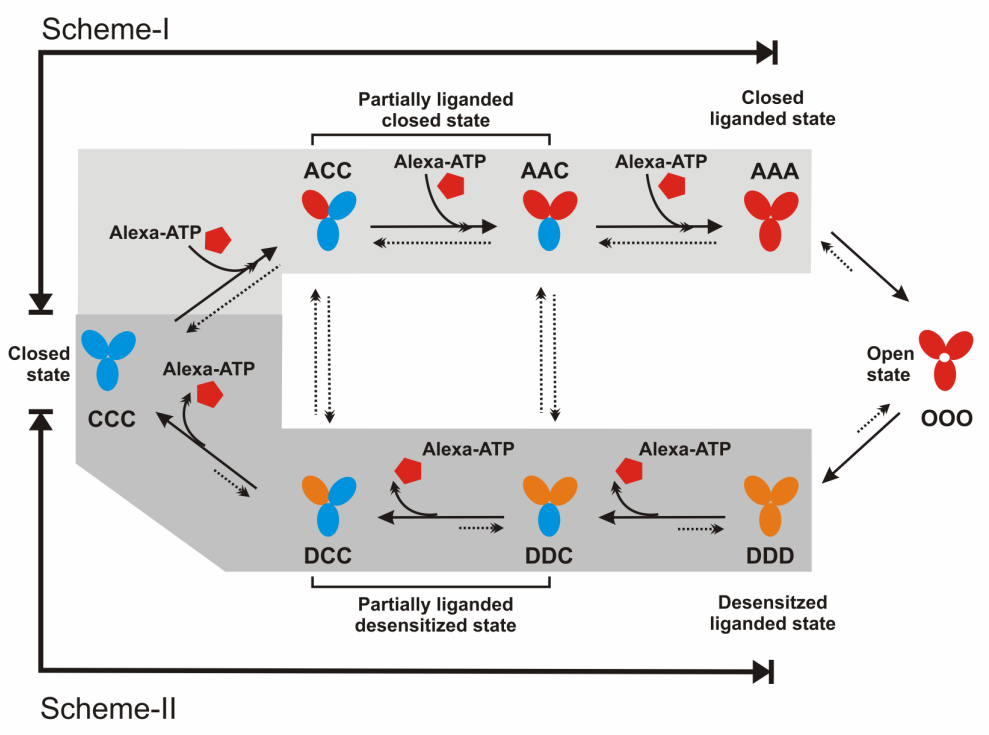

Fig. 3.16 Allosteric model for ligand-receptor interactions in the P2X1 receptors: We propose that binding of three agonist molecules (Alexa-ATP) per receptor to the closed state leads to receptor opening followed by desensitization (Scheme-I). The desensitized state is then a ligand bound closed state. Scheme-II depicts the dissociation of bound Alexa-ATP from the desensitized state of P2X1 receptors in the presence of a ligand free buffer. From the fully liganded desensitized state, negative cooperative interactions between subunits induce a decrease in the affinity of binding sites, which facilitates the dissociation of bound agonist from the desensitized state (Scheme-II). Under the influence of negative cooperativity, dissociation of bound agonist molecules will occur with a faster rate. Various states of the P2X1 receptor subunits are depicted by single letter codes; C stands for non-liganded state, A stands for agonist bound state, O stands for agonist bound open state and D stands for agonist bound desensitized state. Solid and dotted arrows indicate high and low probability of the reaction respectively.

In order to understand the negative cooperativity and to validate our hypothesis we simulated the Scheme-II of our proposed model for the conditions similar to that of in the presence and absence of competing ligands using Gepasi 3.0 software [104]. Gepasi is a Microsoft Windows based program intended for the simulation of kinetics (steady-state and time-course behavior) of systems of chemical reactions. For simulation, dissociation of bound Alexa-ATP from each binding site was taken into account. Fig 3.17 shows the schematic of dissociation of bound Alexa-ATP in the absence of competing ligands from the statistically distributed P2X1 receptors population based on Scheme-II. The dissociation of Alexa-ATP starts from

the fully liganded P2X1 receptors depicted as XXX (three Alexa-ATP molecules bound state) until all the bound Alexa-ATP would dissociate to produce non-liganded closed receptors depicted as CCC. However, in the presence of competing ligands (e.g. ATP), the probability of finding fully liganded receptors at any given time would be high, so each C in Fig. 3.17 would be replaced by L (competing ligand bound receptors) (not shown in the figure).

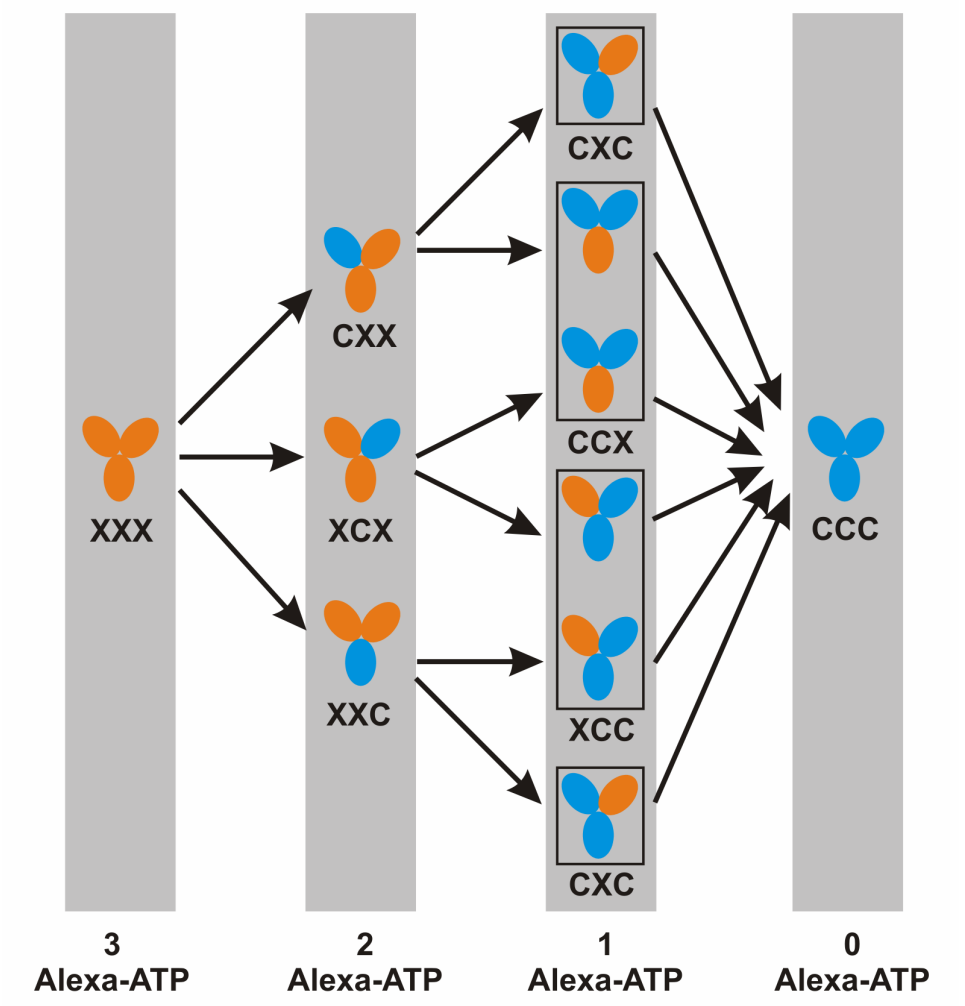

Fig. 3.17 Statistical distribution of P2X1 receptors population under Scheme-II in the presence of MgORI buffer: Dissociation of bound Alexa-ATP will occur from fully liganded P2X1 receptors. The dissociation of any molecule of Alexa-ATP would occur with equal probability which would produce a statistical distribution of P2X1 receptors population. Each subunit is depicted by a single letter code i.e. C stands for non-liganded and X stands for Alexa-ATP bound subunit.

Fluorescence signal from the receptors is contributed by each Alexa-ATP molecule (depicted as X in Fig. 3.17) i.e. receptors with three bound Alexa-ATP would produce two times more fluorescence signal as compared to receptors with only one bound Alexa-ATP. Accordingly,

the dissociation of each Alexa-ATP from the receptors would lead to a corresponding decrease in the fluorescence; therefore, the time course of dissociation of bound Alexa-ATP from the fully liganded receptors would be given by the mean distribution of population of receptors with 3, 2 and 1 bound Alexa-ATP molecules at any given time. From Fig. 3.17, the Alexa-ATP fluorescence is represented by following equation:

$$F = \frac{3([XXX]) + 2([CXX] + [XCX] + [XXC]) + [CXC] + [CCX] + [XCC]}{3}$$ Equation 3.8

First, we simulated Scheme-II for the conditions as that of in the presence of competing ligands i.e. when receptors would be fully liganded at all the times and dissociation of all the bound Alexa-ATP would occur with same rate under the influence of negative cooperativity. The simulation rate constants were manually adjusted in order to exactly match τ of dissociation of Alexa-ATP in presence of 1 μM ATP. In the simulation, the rate constant, which exactly reproduced the experimentally determined τ of dissociation of Alexa-ATP in the presence of ATP, was found to be 2.22 x 10^{-3} s^{-1}. The rate of backward reaction was taken as 1 x 10^{-9} s^{-1} ~ 0, to account for the high concentration of ATP leading to virtually immediate replacement of the dissociated Alexa-ATP by ATP. For simulation in the absence of competing ligands, the dissociation rate constant of first Alexa-ATP was taken as 2.22 x 10^{-3} s^{-1} (because it occurs from the fully liganded receptors) and the rates of remaining two bound Alexa-ATP were found to be 0.9 x 10^{-3} s^{-1}. Using these rate constants, the decay of fluorescence under control conditions (in MgORI) could be reproduced (Fig. 3.18 and Table 3.10)

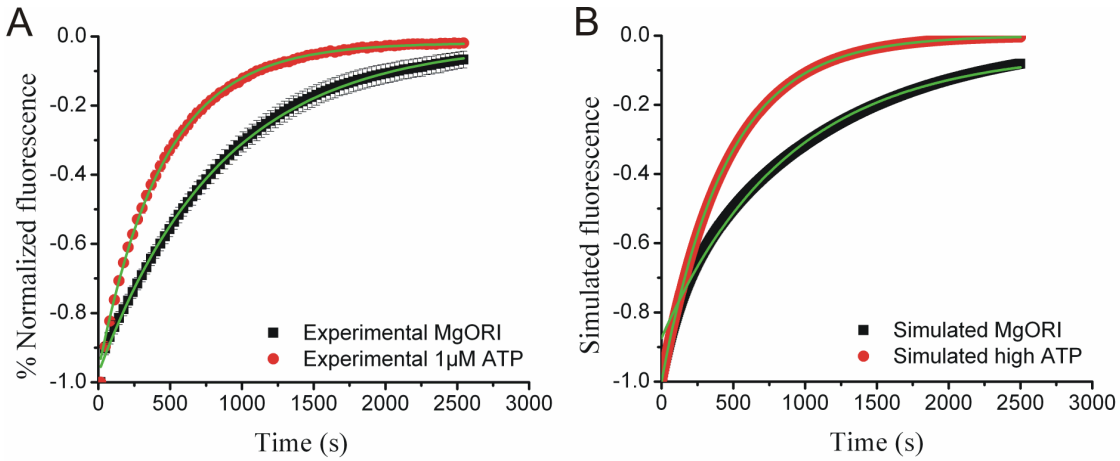

Fig. 3.18 Experimental and simulated decay of Alexa-ATP fluorescence: Comparison of the time course of decay of Alexa-ATP fluorescence in the presence and absence of a competing ligand **(A)** Experimentally determined, data taken from Fig. 3.14. **(B)** Simulated Scheme-II. Thin green lines represent the mono-exponential fits for both conditions (in the presence and absence of competing ligand).

Table 3.10: Comparison of time courses of Alexa-ATP dissociation between experimental and simulated data on P2X1 receptors

Conditions*	τ-Experimental (s)	τ-Simulated (s)	k_{-1} (10^{-3} s^{-1})	k_{-2} (10^{-3} s^{-1})	k_{-3} (10^{-3} s^{-1})
MgORI buffer *(5)*	874 ± 74	874	2.22	0.9	0.9
1 µM ATP *(7)*	452 ± 21	451	2.22	2.22	2.22

* Number of cells for each experimental determination is given in parentheses. Here k_{-1}, k_{-2} and k_{-3} denotes the simulated dissociation rate of first, second and third bound Alexa-ATP from the fully liganded desensitized state of P2X1 receptors respectively.

Thus, simulation of Scheme-II could reproduce the experimental findings with the manually derived rate constants (Table 3.10) and fits the dissociation of bound Alexa-ATP from desensitized state of P2X1 receptors in presence and absence of a competing ligand with a mono-exponential function (Fig. 3.18). Our simulated results validated our hypothesis that under the influence of negative cooperativity, i.e. in presence of high concentrations of ATP, the dissociation of all the bound Alexa-ATP would be fast and occur with equal rate. These results further suggest that the dissociation of the remaining two Alexa-ATP molecules from the partially liganded state would occur without the influence of negative cooperativity which would be slow and also occur with equal rate (Table 3.10). Thus we refined the Scheme-II of our proposed model. Fig. 3.19 shows the refined Scheme-II of our model with rate constants when the dissociation of Alexa-ATP would occur from the fully liganded desensitized state in the presence and absence of competing ligands.

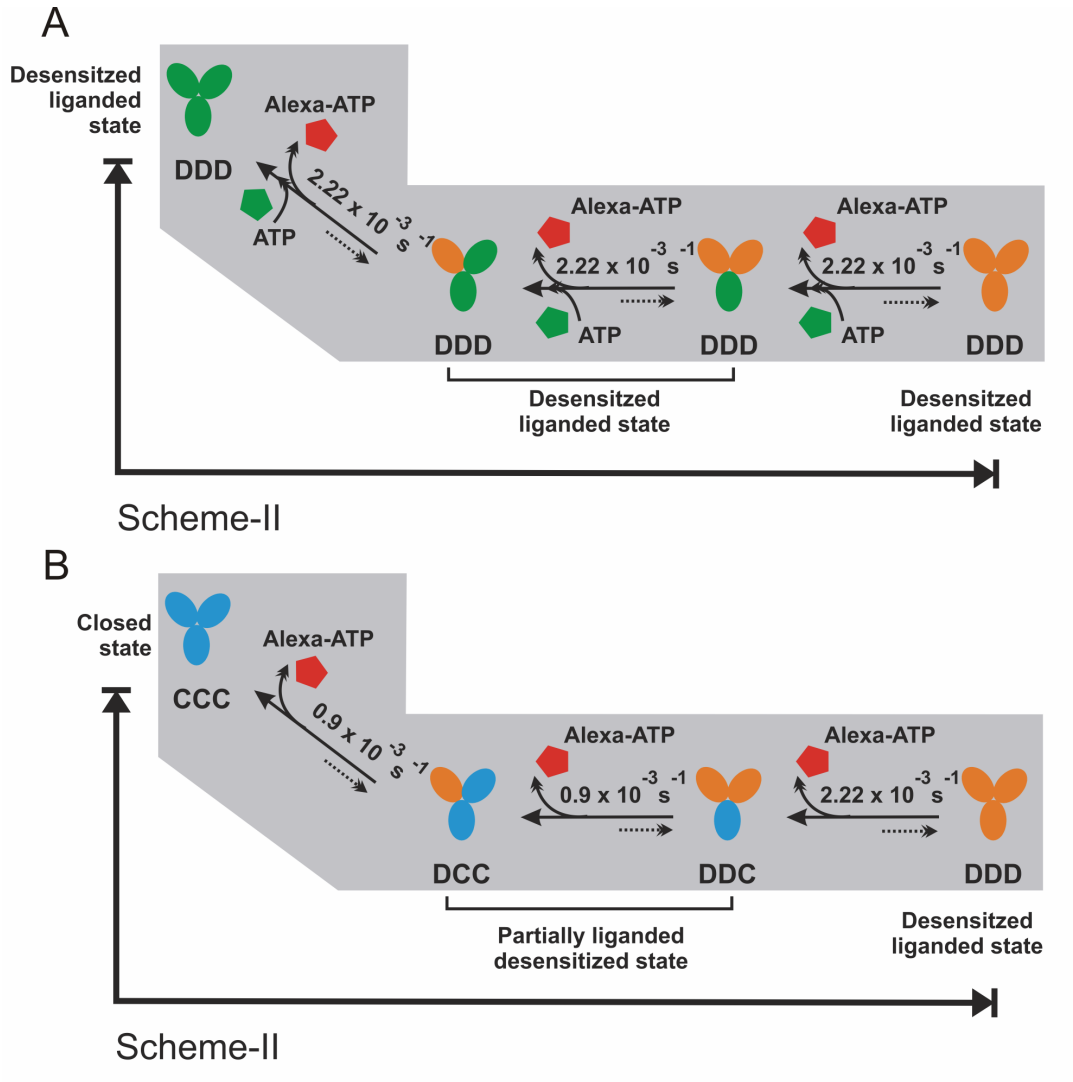

Fig. 3.19 Scheme-II with rate constants for each step: Dissociation of bound Alexa-ATP is shown from the fully liganded desensitized state of the receptors when the dissociation occurs in the **(A)** presence of competing ligand, **(B)** absence of competing ligand. In both these conditions, first Alexa-ATP molecule would dissociate under the influence of negative cooperativity with fast rate constant, leaving behind partially liganded desensitized receptors. In the absence of competing ligands, both subsequent Alexa-ATP molecules would dissociate without the influence of negative cooperativity and therefore with a slower time course giving rise to bi-exponential time course of Alexa-ATP dissociation. On the other hand, if the dissociation of bound Alexa-ATP would occur in the presence of a competing ligand (e.g. ATP), the receptor would remain fully liganded at all times and due to negative cooperative interactions between subunits (fully liganded desensitized state), dissociation of every Alexa-ATP molecule would occur with a fast rate constant, thus, suggesting mono-exponential decay of Alexa-ATP fluorescence. From the fully liganded, mixed occupancy state of P2X1 receptors (Alexa-ATP and ATP bound receptors); the probability of dissociation of ATP or Alexa-ATP would be the same. But, if ATP would dissociate, a new molecule of ATP would immediately bind to the receptor because

of the high concentration of ATP available to the receptors. However, if dissociation of Alexa-ATP would occur instead of ATP, it will be visible as a corresponding decrease in the level of fluorescence from the receptors.

According to our simulated results, Scheme-II predicts a biphasic decay of Alexa-ATP fluorescence in the absence of a competing ligand and mono-exponential decay in the presence of a competing ligand. Surprisingly, both experimental and simulated time course of Alexa-ATP dissociation could be described by a mono-exponential function. The explanation for this apparent mono-exponential behavior is that 1) the two time-constants differ only by a factor of two and 2) it was not possible to resolve the first tens of seconds in the experimentally determined fluorescence decay.

3.2.4.2 Steady-state binding of Alexa-ATP to P2X1 receptors

In the earlier section we showed that the occupancy levels (full and partial) in the desensitized state of the receptor could regulate the dissociation of bound Alexa-ATP (i.e. fast dissociation from fully liganded desensitized receptors and slow dissociation from partially liganded desensitized receptors in the Scheme-II). In order to determine if the occupancy levels (partial) in the non-desensitized state (Scheme-I) could also regulate the dissociation of bound Alexa-ATP, the following approach was used.

First, to correlate the particular concentration of Alexa-ATP to the occupancy level of P2X1 receptors, binding curve of Alexa-ATP was prepared on the P2X1 receptors. Next, the level of fluorescence at different concentrations of Alexa-ATP in the binding curve was correlated with the occupancy level of the receptors using binomial equation, i.e. fractional population of receptors with 0, 1, 2, and 3 Alexa-ATP bound receptors at each Alexa-ATP concentrations was determined. Then, the occupancy level was correlated with the functional state of the receptors using steady-state desensitization curve. Finally, to elucidate if the occupancy level (partial occupancy) of receptors in the non-desensitized state (Scheme-I) could also regulate the dissociation of bound Alexa-ATP, the dissociation of Alexa-ATP from the P2X1 receptors pre-equilibrated with different Alexa-ATP concentrations was monitored in the presence of MgORI buffer. We then compared this with the dissociation of Alexa-ATP in the presence of MgORI buffer from the fully occupied desensitized P2X1 receptors (Scheme-II).

In order to generate the steady-state binding curve, different nanomolar concentrations of Alexa-ATP were directly applied to PAO treated P2X1 expressing oocytes followed by a

reference Alexa-ATP concentration. All concentrations (including reference) were applied until steady-state binding (steady-state level of fluorescence) was achieved. As a control experiment, nanomolar concentrations of Alexa-ATP along with the reference concentration were also applied to the non-injected control cells (Fig. 3.20).

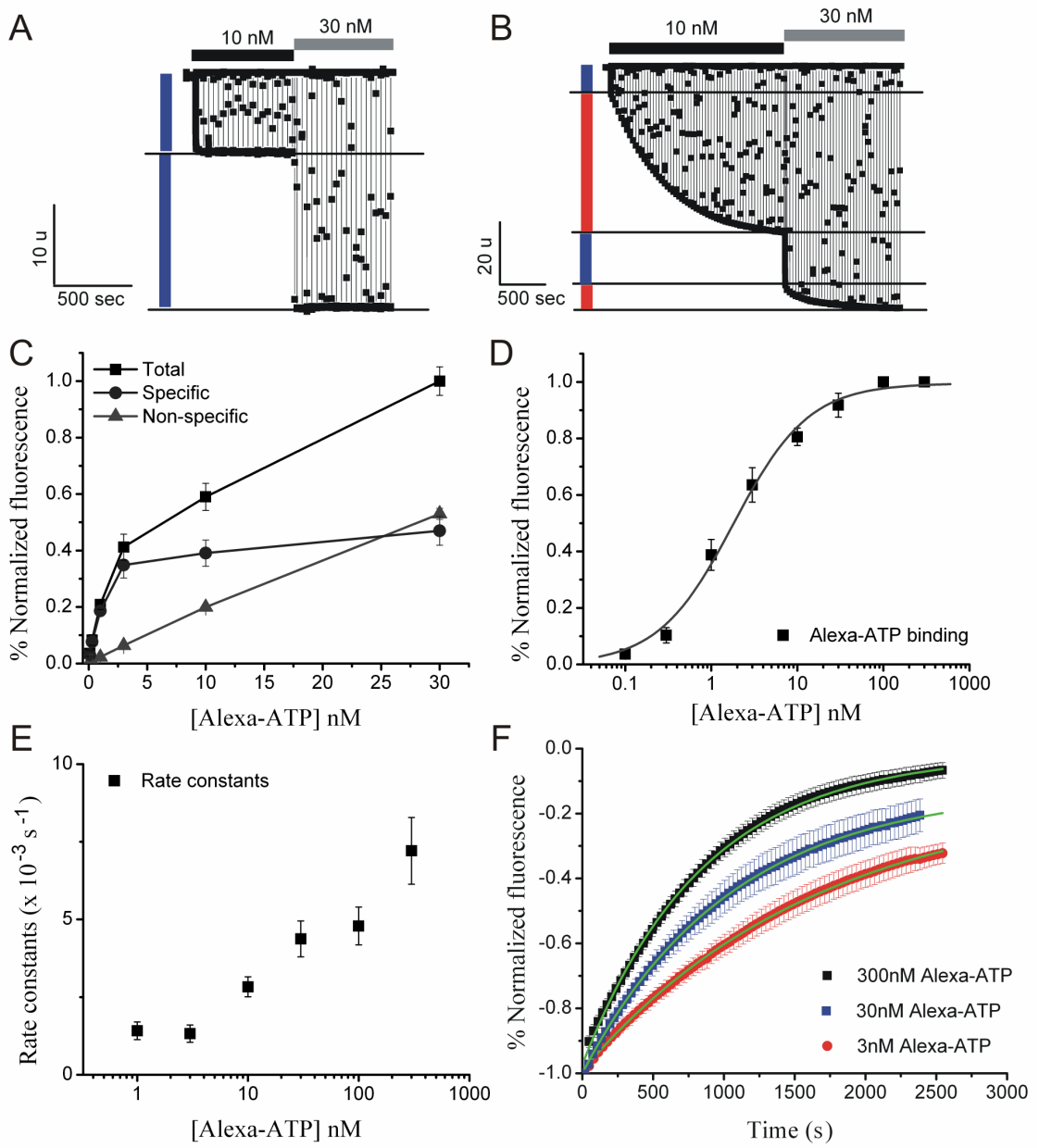

Fig. 3.20 Steady-state binding and dissociation of Alexa-ATP on the P2X1 receptors: Representative fluorescence traces in presence of 10nM and 30nM Alexa-ATP to **(A)** a non-injected cell and **(B)** to a P2X1 receptors expressing cell. Blue and red bars represent background and P2X1 specific Alexa-ATP fluorescence respectively. **(C)** P2X1 specific Alexa-ATP fluorescence was determined by subtracting the non-specific fluorescence from the total Alexa-ATP fluorescence after steady-state binding. Data are presented as mean ± SE of 3-9 cells for each concentration. **(D)** Binding curve for Alexa-ATP at P2X1 receptors. Data are presented as

mean ± SE of 3-9 cells for each concentration. **(E)** Rate constants of Alexa-ATP association to P2X1 receptors are plotted against different Alexa-ATP concentrations. Data are presented as mean ± SE of 5-11 cells for each concentration. **(F)** Time course of decay of Alexa-ATP fluorescence in the presence of MgORI buffer from the P2X1 receptors when the binding sites were pre-equilibrated with either 3nM, 30nM or 300nM Alexa-ATP. Data are presented as mean ± SE of 3-5 cells. All traces were fitted with mono-exponential functions and normalized to the level of fluorescence obtained after 15s from the onset of Alexa-ATP dissociation in each measurement. All fluorescence intensities were monitored in real time under voltage clamp conditions.

Table 3.11 Kinetics of dissociation of Alexa-ATP from variable occupancy state

[Alexa-ATP] nM*	**τ (s)**	**k (10^{-3} s^{-1})**	**Fluorescent amplitude (A)**
300 *(5)*	874 ± 74	1.1	27 ± 0.1
30 *(3)*	1045 ± 4	0.9	15 ± 0.1
3 *(4)*	1680 ± 17	0.6	15 ± 0.1

* Number of cells for each ligand concentration is given in parentheses.

The kinetics of association of Alexa-ATP to P2X1 receptors were monitored in real time under voltage clamp conditions. Specific binding, i.e. fluorescence of Alexa-ATP associated with P2X1 receptors, was determined for each concentration by subtracting the non-specific fluorescence from the total fluorescence (Fig. 3.20C). Fig. 3.20D shows the binding curve of Alexa-ATP on P2X1 receptors. The binding curve for Alexa-ATP binding was fitted with the Hill equation. The half maximal binding constant (BC_{50}) was found to be 1.8 ± 0.2 nM with a Hill coefficient of 0.9 ± 0.1. Fig. 3.20D suggests that at 3nM, 30nM and 300nM Alexa-ATP concentrations, the probability of receptor labeling is ~60%, ~90% and 100%, respectively. In addition, the dissociation of bound Alexa-ATP was monitored in the presence of MgORI buffer after equilibrating the binding sites with 3nM, 30nM and 300nM Alexa-ATP. As compared to the desensitized state, Alexa-ATP dissociated with different rates from the P2X1 receptors pre-equilibrated with different Alexa-ATP concentrations (Fig. 3.20F) (Table 3.11), suggesting that the non-desensitized, partial occupancy state of the receptors also regulate the dissociation of Alexa-ATP.

3.2.4.3 Correlation between occupancy level and functional state of the receptors

In order to correlate the average occupancy level (steady-state distribution between 0, 1 and 2 Alexa-ATP bound receptors) with the functional state (desensitized and non-desensitized

receptors), steady-state desensitization was determined after equilibrating them with different nanomolar Alexa-ATP concentrations. To this end, P2X1 expressing oocytes were incubated in Petri dishes with different concentrations of Alexa-ATP for different times (until steady-state binding was reached) at room temperature. Then, each oocyte was voltage-clamped and 30µM ATP was immediately applied to elicit the residual peak current response (P_E1) (experimentally determined peak-1) by activating all the P2X1 receptors still present in the non-desensitized closed state. After allowing the completely desensitized receptors to recover for 1 min in ligand free conditions under voltage clamp, 30µM ATP was again applied on the same oocyte to generate current response (P_E2) (experimentally determined peak-2) from those receptors which recovered from complete desensitization induced by the first ATP application. As a control experiment, P2X1 expressing oocytes were incubated in ligand free buffer for 1 hr at room temperature and P_E1 and P_E2 responses were generated by applying 30µM ATP. These experiments showed that 5.1 ± 1.2 percent of the P2X1 receptors recovered from desensitization after 1 min (n = 22) in ligand free buffer. Now, the first response which would have been elicited without Alexa-ATP pre-incubation was also calculated for each oocyte from the individual peak-2 (P_E2) response and termed "calculated peak response (P_C). The normalized mean current responses (P_E1/ P_C1) generated by 30µM ATP on P2X1 receptors pre-equilibrated with different Alexa-ATP concentrations is plotted in Fig. 3.21 (blue curve) and fitted with Hill equation.

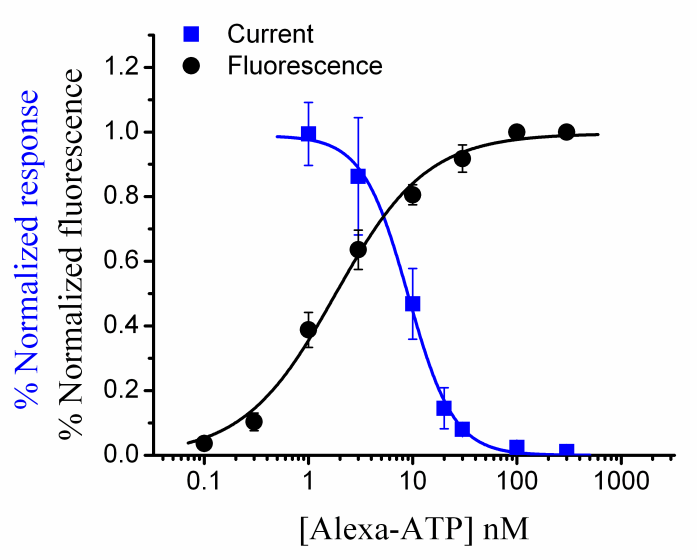

Fig. 3.21 Correlation between average occupancy level and steady-state desensitization: The black curve represents the binding curve for Alexa-ATP (taken from Fig 3.20 D). The blue trace represents the Alexa-ATP concentration dependence of steady-state desensitization. All traces were fitted with the Hill equation. The half maximal binding (BC_{50}) (black trace) was seen at 1.8 ± 0.2 nM Alexa-ATP with a Hill coefficient of 0.9 ± 0.1 (n

= 3-9 cells). The half maximal desensitization (DC_{50}) (blue trace) was seen at 9 ± 0.5 nM Alexa-ATP with a Hill coefficient of 1.9 ± 0.1 (n = 5-33 cells).

The half maximal desensitization (DC_{50}) was found to occur at 9 ± 0.5 nM Alexa-ATP with a Hill coefficient of 1.9 ± 0.1. The black curve in Fig. 3.21 is taken from Fig. 3.20D and represents the average occupancy level of P2X1 receptors i.e. Alexa-ATP fluorescence at different Alexa-ATP concentrations. The half maximal binding (BC_{50}) was found to occur at 1.8 ± 0.2 nM Alexa-ATP with a Hill coefficient of 0.9 ± 0.1. The inference from these results is that although 50% of binding sites are occupied at 1.8nM, a 5-fold higher Alexa-ATP concentration is needed for 50% steady-state desensitization. Therefore, at 1.8 nM Alexa-ATP almost no desensitization can be detected, indicating that the binding of more than two ATP molecules per receptor is required for desensitization.

3.2.4.4 Dissecting the number of agonist molecules required to desensitize the P2X1 receptors

Functional dose response curve for ATP on the P2X1 receptors pre-equilibrated with different Alexa-ATP concentrations suggests that ATP would only produce functional responses from the non-desensitized P2X1 receptors. Therefore, in order to dissect the fractional distribution of partially liganded receptors with 0, 1 and 2 Alexa-ATP bound from the fully liganded receptors with 3 Alexa-ATP bound, binomial equation (equation 3.5) was used.

$$f(x) = \frac{n!\left(p^x q^{n-x}\right)}{\left[(n-x)!\,x!\right]} \qquad \text{Equation 3.5}$$

Where n is the total number of ligand binding sites per receptor, p is the probability that a receptor is labeled; q is the probability that a receptor is not labeled (1-p), and x is the number of bound Alexa-ATP molecules.

It is important to note that P2X1 receptor subunits are interacting in a cooperative manner. In order to determine the fractional population of 0, 1, 2, and 3 Alexa-ATP bound receptors using binomial equation, we need to consider that the ligand binding in P2X1 receptors is a random process. The presence of cooperativity can be neglected for the calculation purposes because the binding rate between the first two ligands and the last ligand is not much different (i.e. only by factor of two).

As P2X1 receptors are thought to be formed by the trimeric assembly of homologous subunits, therefore we assumed three binding sites per receptor. The probability of Alexa-ATP binding (steady-state fluorescence level) of the receptors was taken from the binding curve (Fig. 3.20D) i.e. at 1nM, 3nM, 30nM and 300nM Alexa-ATP the probability that the receptor is labeled is 38%, 63%, 91% and 100% respectively. Thus, with the binomial distribution, fractional population (*f(x)*) of 0, 1, 2 and 3 Alexa-ATP bound receptors at different nanomolar concentrations of Alexa-ATP was calculated (Table 3.12).

Table 3.12: Calculated distribution of fractional population of 0, 1, 2 and 3 Alexa-ATP bound P2X1 receptors

Alexa-ATP (nM)	**P**	***f(0)***	***f(1)***	***f(2)***	***f(3)***
0.1	3.67 ± 1.2	0.8939	0.1022	0.0039	4.9431E-5
0.3	10.33 ± 2.73	0.721	0.2492	0.0287	0.0011
1	38.78 ± 5.44	0.2294	0.436	0.2762	0.0583
3	63.57 ± 6.1	0.0483	0.2531	0.4417	0.2569
10	80.56 ± 3.1	0.0073	0.0913	0.3785	0.5228
30	91.78 ± 4.23	5.5541E-4	0.0186	0.2077	0.7731
100	100	1E-12	2.9997E-8	2.9994E-4	0.9997
300	100	1E-12	2.9997E-8	2.9994E-4	0.9997

*P stands for probability that receptor is labeled, *f(0), f(1), f(2)* and *f(3)* stands for fractional population of receptors with 0, 1, 2 and 3 Alexa-ATP bound receptors respectively.

After determining the fractional distribution of 0, 1, 2 and 3 Alexa-ATP bound receptors at each Alexa-ATP concentration, we tested three hypotheses:

1) Binding of three agonist molecules per receptor is required to desensitize P2X1 receptors: Three-site model. *(Therefore, ATP would produce functional response from the 0, 1 and 2 Alexa-ATP bound receptors i.e. fractional population of closed receptors under Scheme-I = f(0) + f(1) + f(2)).*

2) Binding of two agonist molecules per receptor is required to desensitize P2X1 receptors: Two-site model. *(Therefore, ATP would produce functional response from the 0 and 1 Alexa-ATP bound receptors i.e. fractional population of closed receptors under Scheme-I = f(0) + f(1)).*

3) Binding of one agonist molecule per receptor is required to desensitize P2X1 receptors: One-site model. *(Therefore, ATP would produce functional response from the 0 Alexa-ATP bound receptors i.e. fractional population of closed receptors under Scheme-I = f(0)).*

Fractional distribution of population of closed receptors for all these models (One, Two or Three-site model) is plotted in Fig. 3.22 and compared with the steady-state desensitization curve determined on P2X1 receptors pre-equilibrated with different Alexa-ATP concentrations.

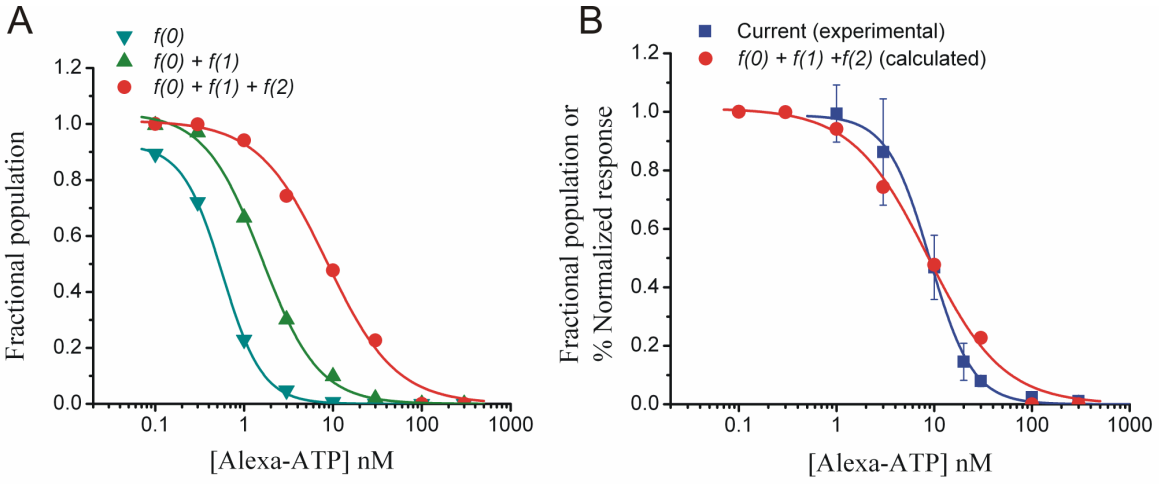

Fig. 3.22 Fractional distribution of closed-state of the receptors for One, Two or Three-site model: (A) Using binomial equation, fractional distribution (*f(x)*) of 0, 1, 2 and 3 Alexa-ATP bound receptors was calculated. According to these three models (One, Two or Three-site model), different closed-states were assumed and plotted against different Alexa-ATP concentrations. After fitting each distribution of population of closed-states with Hill equation, the half maximal distribution of population for One, Two and Three-site model was found to occur at Alexa-ATP concentration of 0.6 ± 0.01, 1.6 ± 0.1 and 8.6 ± 0.09 nM with Hill coefficient of 1.9 ± 0.05, 1.3 ± 0.01 and 1.1 ± 0.1 respectively. **(B)** Comparison of experimentally determined steady-state desensitization curve with the Three-site model which describes that binding of three agonist molecules is required to desensitize the receptors. Near superimposition of closed-states formed by population of 0, 1 and 2 bound Alexa-ATP (Three-site model) with the experimentally determined steady-state desensitization curve support our first hypothesis that binding of three agonist molecules are required to desensitize the receptors. The

half maximal distribution of population of closed-states for Three-site model was found to be 8.6 ± 0.8 nM Alexa-ATP is comparable to the DC_{50} value of 9.0 ± 0.5 nM Alexa-ATP for steady-state desensitization curve.

After fitting both curves (distribution of closed-states under Three-site model and steady-state desensitization curve) by Hill equation we found a direct relationship between these two curves as the half maximal distribution of population of receptors for Three-site model was found to be 8.6 ± 0.9 nM Alexa-ATP concentration and the half maximal desensitization (DC_{50}) for steady-state desensitization was found to be 9.0 ± 0.5 nM Alexa-ATP concentration. Near superimposition of both curves support our conclusion that binding of three agonist molecules are required to desensitize the P2X1 receptors and receptors with less than three agonist molecules are essentially in non-desensitized, closed state. Therefore, it is evident that the dissociation of bound Alexa-ATP in Fig. 3.20F at 3nM concentration most probably occurred from partially liganded closed state (Scheme-I), whereas, the dissociation of bound Alexa-ATP at 30nM or 300nM concentrations occurred primarily from partially/fully liganded desensitized state (Scheme-II).

Hence, these results suggest that not only the full occupancy of the receptors (desensitized) (Scheme-II) but also the partial occupancy of the receptors (non-desensitized) (Scheme-I) could regulate the allosteric interactions between subunits which in turn controls the dissociation of bound agonist from the binding sites of the receptors.

3.3 Probing structural rearrangements in P2X receptors using voltage clamp fluorometry

Among the three superfamilies of ligand gated ion channels (i.e. Cys-loop, iGluR and P2XR) high resolution structural details are only available for ligand binding domains of Cys loop family members (e.g. AChR [150]) and iGluR [152]. There is no high resolution structural information available for P2X receptors and therefore, most of the structural understanding of P2X receptors came from site directed mutagenesis and biochemical analysis [28]. Although, crystal structures provide valuable "snapshots" of the protein under investigation, it fails to provide information about the various conformations of the protein during transition from closed to open and desensitized states. Consequently, the precise mechanism by which binding of one or more ligand molecules is translated into structural rearrangements that trigger channel opening is still not well understood for these ligand gated ion channels. There are two methods of choice to study ligand receptor interactions i.e. ligand binding assay and electrophysiology. However, the former method alone cannot resolve receptor function and the latter method cannot resolve events that are electrophysiologically silent i.e. desensitized states.

Voltage clamp fluorometry (VCF) offers certain advantages over these techniques, by simultaneously monitoring receptor function (through changes in elicited current) and structural rearrangements in or around the domains of interest (through site specific changes in the fluorescence intensity of the attached fluorophore) in real time. Thus, this technique can serve as a real time correlate of the channel structure and function. VCF has been widely used to investigate structural rearrangements in the ligand binding domain of Cys-loop receptors [140,143,145,165]. It was found that agonists and antagonists can induce distinct conformational changes in the Cys-loop receptors.

It is hypothesized that, in P2X receptors ATP binding at the interface between neighboring subunits initiates structural rearrangements which propagate to the channel gate through conformational waves. Therefore, to understand the mechanism of activation and desensitization of P2X1 receptors, it would be interesting to investigate these molecular motions induced by ligand receptor interactions. To this end, several mutants in the cysteine-rich-domain 1 (CRD-1) were generated by site directed mutagenesis in which individual amino acids from position 118 to 125 were mutated to cysteine residues. Accessibility of the engineered cysteine residues was determined by covalently attaching an environment

sensitive cysteine reactive fluorophore e.g. tetramethylrhodamin-6-maleimide fluorophore, TMRM. Any change in the local environment of the attached fluorophore during receptor activation or desensitization was monitored as a change in its fluorescence intensity using VCF.

3.3.1 TMRM treatment does not affect the function of CRD-1 mutants

The extracellular loop of P2X receptors contains ten conserved cysteine residues arranged in two cysteine-rich-domains (CRDs). The region from C117-C165 contains six disulfide bonded cysteine residues called CRD-1, while region from C217-C270 has four disulfide bonded cysteine residues called CRD-2 (P2X1 numbering) (Fig. 1.1). In the present study, residues from position 118 to 125 were individually mutated to cysteine residue (i.e. A118C, E119C, N120C, P121C, E122C, G123C, G124C and I125C), thus creating one free cysteine in the CRD-1 region. These clones were generated by Benjamin Marquez-Klaka at the Max Planck Institute for Brain Research, Germany.

The environmental sensitive fluorophore (TMRM) was used to label oocytes expressing these cysteine mutants. TMRM quantum yield increases when it lies in a hydrophobic milieu as compared to a hydrophilic one. Accordingly, change in the fluorescence intensity can be used to obtain information about the structural rearrangements that affect the surroundings of the residue to which TMRM is bound. TMRM treatment to the oocytes expressing single cysteine mutants was done by incubating the oocytes in CaSORI buffer containing 3µM TMRM for 15 min on ice in the dark. The labeling was brought about by the ability of the maleimide moiety in TMRM to form a spontaneous covalent bond with free cysteines. The excess dye was removed by extensive washing of the oocytes in dye free CaSORI buffer. The labeled oocytes were then stored in the dark at room temperature until the beginning of measurements. Change in the fluorescence intensity coupled to structural rearrangements during receptor activation and desensitization was determined under voltage clamp conditions in real time through the use of a photo diode (Fig. 2.3). Fig. 3.23 shows functional expression and specific TMRM labeling of CRD-1 cysteine mutants of P2X1 receptors.

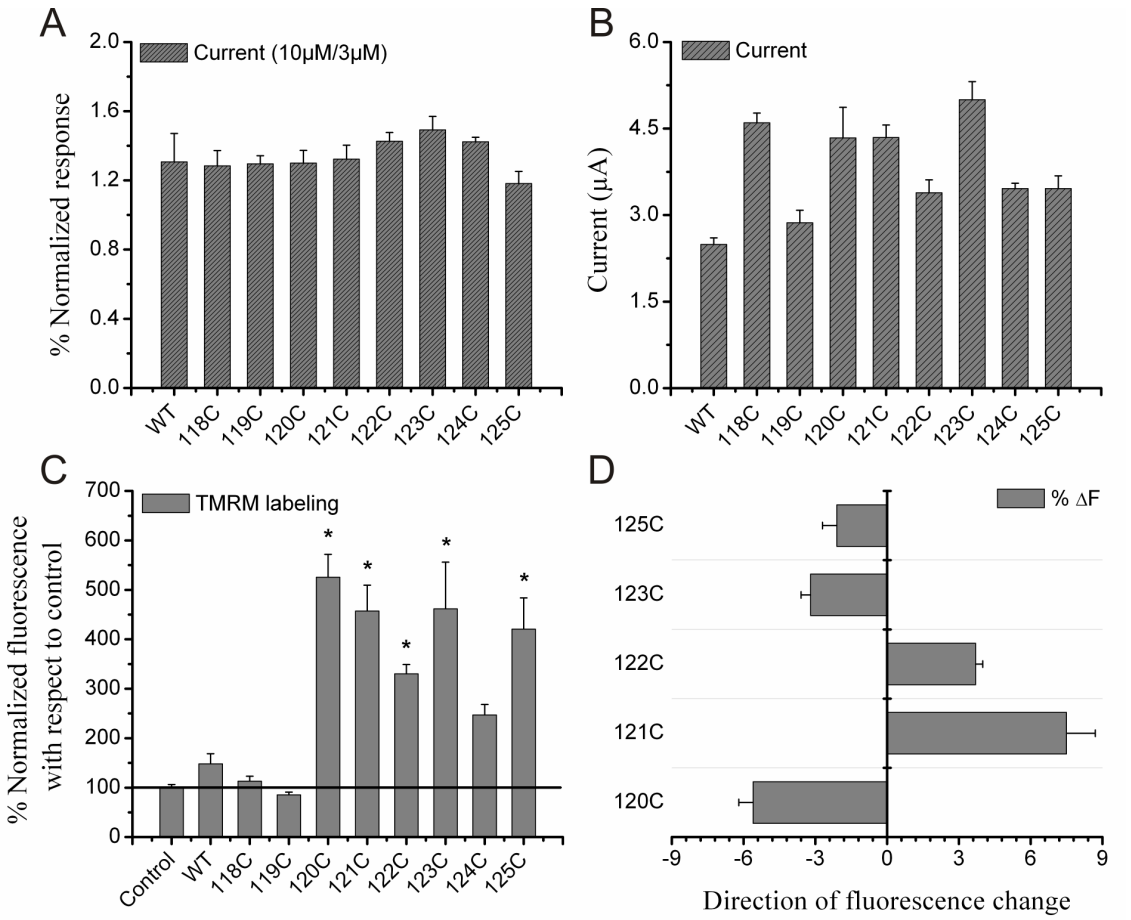

Fig. 3.23 Functional expression and specific TMRM labeling of cysteine mutants of P2X1 receptors: (A) Normalized current response generated by 10μM ATP and 3μM ATP on the individual oocyte expressing wild type (WT) or CRD-1 mutants. All currents were generated on oocytes not treated with TMRM. Average peak current generated by 10μM ATP on these receptors (WT or CRD-1 mutants) was >1μA, suggesting that all receptors were fully functional. Data are presented as mean ± SE of 3-9 cells for each group. **(B)** 10μM ATP evoked currents recorded from oocytes individually injected with wild-type (WT) or CRD-1 cysteine mutants. All currents were generated after TMRM treatment. Average peak current generated by 10μM ATP on these receptors (WT or CRD-1 mutants) was >1μA, suggesting that all receptors were fully functional after TMRM treatment. Data are presented as mean ± SE of 3-15 cells for each group. **(C)** Fluorescence intensity after TMRM treatment to control cells (No RNA injected), wild-type (WT) and CRD-1 cysteine mutants. The level of fluorescence was normalized with respect to the level of fluorescence obtained on the control oocytes treated with TMRM. Data are presented as mean ± SE of 5-25 cells for each group. Fluorescence intensity of TMRM treated control cells was compared with TMRM treated WT or CRD-1 mutants using one-way ANOVA followed by bonferroni's post test for paired comparison. Asterisk sign (*) indicates level of significance ($p < 0.01$). **(D)** Direction of change in the fluorescence (ΔF %) associated with five mutants that showed significant TMRM labeling. Data are presented as mean ± SE of 5-15 cells for each mutant.

All CRD-1 mutants were fully functional without TMRM treatment when tested using 10µM ATP (showed >1µA peak currents). They showed similar ratio of peak currents generated by 10µM/3µM ATP when compared to wild type receptors, suggesting that they maintained similar EC_{50} value as that of wild type receptors (Fig. 3.23A). The effect of TMRM treatment on these mutants was also compared with the TMRM treated wild type receptors (Fig. 3.23B). Peak current response from wild type and mutant receptors upon 10µM ATP application indicates that TMRM treatment has no effect on the functionality of these receptors as all these receptors (WT or mutants) produced similar peak response. These experiments indicated that not only cysteine mutation at these places can be tolerated by P2X1 receptors without compromising the receptor's function but also that TMRM treatment has no effect.

These experiments were performed on the VCF setup; therefore, concurrent recording of fluorescence and current signals could be performed from the same population of receptors. Thus, to test whether these endogenously or engineered cysteines are accessible to TMRM labeling, fluorescence signals from WT and these cysteine mutants treated with TMRM was also quantified by photodiode measurements (Fig. 3.23C). Fluorescence intensity from the control oocytes (no RNA injected) after TMRM treatment indicates non-specific binding of TMRM. Similarly, oocytes expressing wild-type P2X1 receptors were not significantly labeled by TMRM as compared to the control oocytes, indicating that the naturally occurring conserved cysteine residues in CRD-1 and CRD-2 regions in the wild type receptors are not accessible to TMRM labeling, most probably because they form pair-wise disulfide bonds. However, all except A118C, E119C and G124C cysteine mutants of CRD-1 region showed significant TMRM fluorescence ($p < 0.01$) when compared to the control cells, indicating that the engineered cysteine residue is accessible to TMRM binding at these positions. Fig. 3.23D shows corresponding percent change in the fluorescence (ΔF %) upon 10µM ATP application on the mutants who showed significant TMRM labeling.

3.3.2 Agonist mediated changes in the fluorescence intensity

3.3.2.1 Different positions sense different structural rearrangements

The fluorescence intensity of TMRM strictly depends upon the local environment of the attached fluorophore i.e. TMRM quantum yield increases when it lies in a hydrophobic milieu as compared to a hydrophilic one. In this way, change in the fluorescence intensity can be used to obtain information about the agonist mediated structural rearrangements during

receptor's activation and desensitization that affect the surroundings of the residue to which TMRM is bound. Fig. 3.23C shows that out of the eight cysteine mutants, six mutants showed more than 200% TMRM specific fluorescence as compared to control cells, indicating that TMRM was accessible to these positions. When concurrent measurement of the current and fluorescence intensity in TMRM labeled CRD-1 mutants was done, change in the fluorescence intensity (ΔF) was found in all mutants except G124C when activated by 10μM ATP (Fig. 3.23D and 3.24).

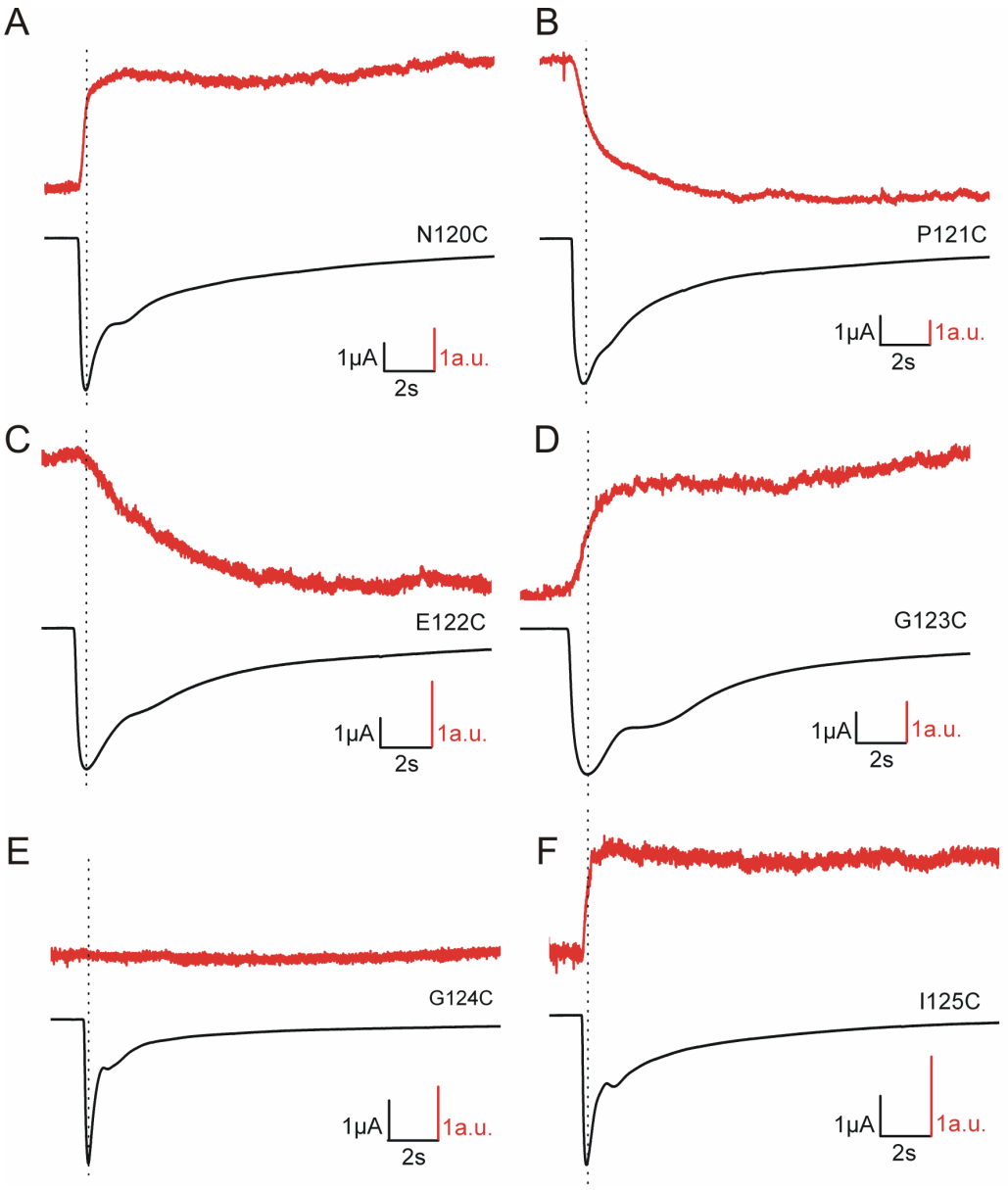

Fig. 3.24 Concurrent measurement of the current and fluorescence on CRD-1 mutants: Representative traces of the change in the fluorescence and current in various CRD-1 mutants when activated by 10μM ATP. The dotted line indicates the position of peak current and corresponding fluorescence value on these mutants.

Mutant N120C, G123C and I125C showed decrease in the fluorescence intensity upon agonist application. Mutant P121C and E122C showed increase in the fluorescence intensity upon agonist application, whereas mutant G124C was labeled by TMRM but showed no change in the fluorescence intensity on agonist application. All mutants were fully functional after TMRM labeling as judged by the current responses.

Table 3.13: Agonist mediated change in the fluorescence intensity of CRD-1 mutants

Mutants	Agonist	ΔF (%)	Direction	Imax (μA)	N (# cells)
N120C	10μM ATP	5.6 ± 0.6	Decrease	4.3 ± 0.5	8
P121C	10μM ATP	7.5 ± 1.2	Increase	4.3 ± 0.2	9
E122C	10μM ATP	3.7 ± 0.3	Increase	3.3 ± 0.2	15
G123C	10μM ATP	3.2 ± 0.4	Decrease	5 ± 0.3	6
G124C	10μM ATP	Not detected	-	3.4 ± 0.1	5
I125C	10μM ATP	2.1 ± 0.6	Decrease	3.4 ± 0.2	5

* ΔF denotes percentage change in the fluorescence; Imax is the maximum peak current.

Interestingly, mutant N120C, G123C and I125C showed decrease in the fluorescence suggesting exposure of these residues to more hydrophilic environment, while the other two mutants (P121C and E122C) showed an increase in the fluorescence upon activation by agonists suggesting an increase in the hydrophobic environment around these residues. Table 3.13 compares change in the fluorescence intensity and current measured by the application of 10μM ATP in various CRD-1 mutants. Comparison of corresponding changes in the fluorescence and peak current responses in these five mutants revealed some interesting observations. In N120C and I125C mutants the change in the fluorescence was nearly complete, for G123C the change was almost 80% complete when the peak current was reached. In the mutant P121C, the change in fluorescence was nearly 50% when the peak current was reached. Whereas, in the mutant E122C, the change in fluorescence started to occur only after the peak current was reached. Mutant G124C showed no change in the fluorescence but showed TMRM labeling.

3.3.2.2 Fluorescence shift correlates with receptor activation and desensitization

From the above results, it appears that these cysteine mutants are sensing progression of a conformational wave which originated after agonist binding. Therefore, to correlate change in the fluorescence (ΔF) at these positions with receptor activation or desensitization, time constants were determined by fitting the activation or desensitization component of the current waveform. These time constants were then compared with the time constants derived from fitting the change in the corresponding fluorescence waveform (Fig. 3.25). Mono-exponential function was used to fit both waveforms. Table 3.14 lists the kinetic properties of receptor activation, desensitization and change in the fluorescence for these CRD-1 mutants. Fig. 3.25 shows that for mutants N120C, G123C and I125C, the time constant of change in the fluorescence is kinetically correlated with the activation of receptors, whereas, in mutants P121C and E122C the time constant of change in the fluorescence is kinetically correlated with the desensitization of receptors. Thus, these results indicate that the positions N120C, G123C and I125C sense activation of the receptors after agonist binding and the positions P121C and E122C sense desensitization of the receptors.

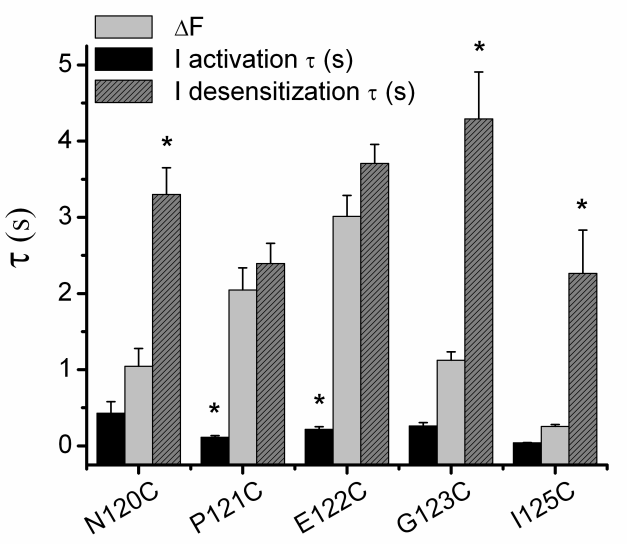

Fig. 3.25 Onset of ΔF correlates kinetically with the activation or desensitization: ATP induced change in the fluorescence (ΔF) of the attached TMRM and the onset of receptor activation and desensitization were fitted with a mono-exponential function. The time constants were determined after activating these mutants with 10μM and 30μM ATP. The τ (mean time constant) of ΔF was compared with the activation and desensitization of these five cysteine mutants using one-way ANOVA followed by bonferroni's post test for paired comparison. In mutants N120C, G123C and I125C, ΔF is kinetically correlated with receptor activation because τ of receptor desensitization is significantly different ($p < 0.01$) from τ of ΔF in these mutants. Whereas, in mutants P121C

and E122C, ΔF is kinetically correlated with the receptor desensitization, because τ of receptor activation is significantly different ($p < 0.01$) from τ of ΔF in these mutants. Asterisk sign (*) indicates level of significance ($p < 0.01$) when τ of receptor activation or desensitization is compared with τ of ΔF in the particular mutant. Data are presented as mean ± SE of n experiments. Number of cells for each mutant is listed in Table 3.14.

Table 3.14: Kinetic properties of CRD-1 mutants when activated by ATP

Mutants	Direction of ΔF	Activation τ (s)	Desensitization τ (s)	ΔF τ (s)	Number (# cells)
N120C	Decrease	0.4 ± 0.1	3.3 ± 0.3	1 ± 0.2	11
P121C	Increase	0.1 ± 0.02	2.3 ± 0.2	2 ± 0.2	12
E122C	Increase	0.2 ± 0.03	3.7 ± 0.2	3 ± 0.2	18
G123C	Decrease	0.2 ± 0.04	4.2 ± 0.6	1 ± 0.1	6
I125C	Decrease	0.04 ± 0.01	2.2 ± 0.5	0.2 ± 0.02	4

*ΔF denotes change in fluorescence; τ is the time constant of onset of receptor activation/ desensitization/ fluorescence change.

3.3.2.3 Structural rearrangements during recovery from desensitization

The rate of recovery from desensitization in three mutants (N120C, P121C and E122C) was also monitored. In these experiments, ATP-γS instead of ATP was used as an agonist to elicit peak current response from the receptors, because it has been shown earlier that the dissociation of ATP-γS from P2X1 receptors occurs on a faster time scale as compared to ATP [88].

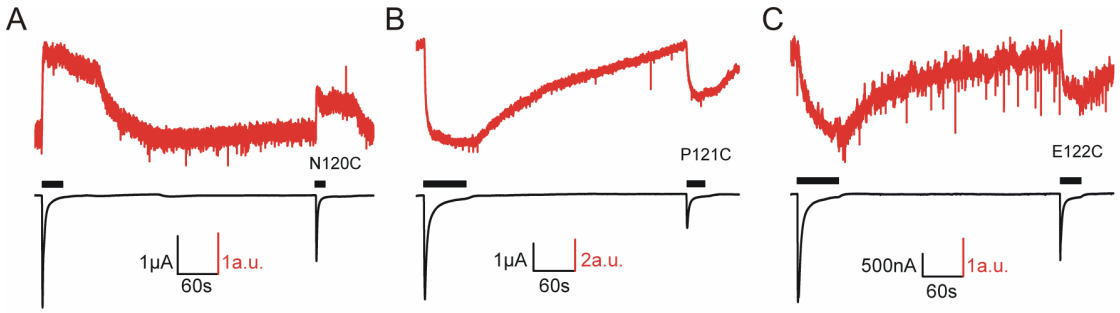

Fig. 3.26 Structural rearrangement in CRD-1 mutants during recovery from desensitization: Representative traces of current and corresponding change in the fluorescence in **(A)** N120C, **(B)** P121C and **(C)** E122C. 10μM ATP-γS was used to elicit peak current responses from these mutants. After the first application of agonist, receptors were washed for 5 min in the ligand free buffer in order to recover them from desensitization.

Current responses were again elicited on the same set of receptors that recovered from desensitization. The black bars above the current traces indicate the time of agonist application. Traces were not corrected for photobleaching. Baseline in these individual traces was manually corrected by subtracting a straight line.

Table 3.15: Recovery of mutants from desensitization in the presence of MgORI when activated by 10µM ATP-γS

Ligand	Mutants *(# cell)**	Peak-1 (µA)	ΔF1 (%)	Peak-2 (µA)	ΔF2 (%)	% Current recovery	% Fluorescence recovery
MgORI	**120** *(3)*	3 ± 0.1	4 ± 0.7	2 ± 0.2	3 ± 0.1	61	68
	121 *(3)*	3 ± 0.3	14 ± 3	1 ± 0.1	8 ± 2.2	36	57
	122 *(3)*	2 ± 0.1	5 ± 0.7	1 ± 0.1	3 ± 0.6	56	69

*Number of cells for each mutant is indicated in parenthesis.

Note: Peak-1 and Peak-2 are the peak currents produced by first and second application of 10µM ATP-γS. ΔF1 % and ΔF2 % are the corresponding percent change in the fluorescence during first and second application of 10µM ATP-γS on these mutants. % Current and % Fluorescence recovery indicates the corresponding recovery of signals (current and fluorescence) during second application of 10µM ATP-γS when compared to the first application.

In these experiments, first application of 10µM ATP-γS elicited peak current response (peak-1) from TMRM treated mutants. After continuous washing for 5 min in the presence of ligand free buffer (MgORI buffer), 10µM ATP-γS was again applied on the same population of receptors in order to elicit second peak current response (peak-2) from the receptors which recovered from desensitization (Fig. 3.26). Percent change in the fluorescence (ΔF %) and peak current responses during first and second application of 10µM ATP-γS is shown in Table 3.15. It was found that significant fraction of receptors recovered from desensitization (in terms of both current and ΔF %) when activated by 10µM ATP-γS. These results indicate that receptors recover from desensitization on a faster time scale when activated by ATP-γS due to the fast dissociation of the bound ATP-γS from the binding sites. The percent recovery of current signals after desensitization is also correlated with the percent recovery of the fluorescence signal (Table 3.15), suggesting that the recovery from desensitization not only involves dissociation of bound agonist from the desensitized receptors, but also involves reversal of structural rearrangements back to the closed state.

3.3.3 Antagonist mediated changes in the fluorescence intensity

NF compounds (NF279, NF449) are known competitive antagonists of P2X1 receptors [94]. They are structurally different as compared to ATP (Fig. 1.5). Therefore, it was interesting to determine if binding of structurally different ligands could also lead to structural rearrangements. 100nM NF449 (IC_{max}) alone was tested on TMRM labeled three mutants (N120C, P121C and E122C).

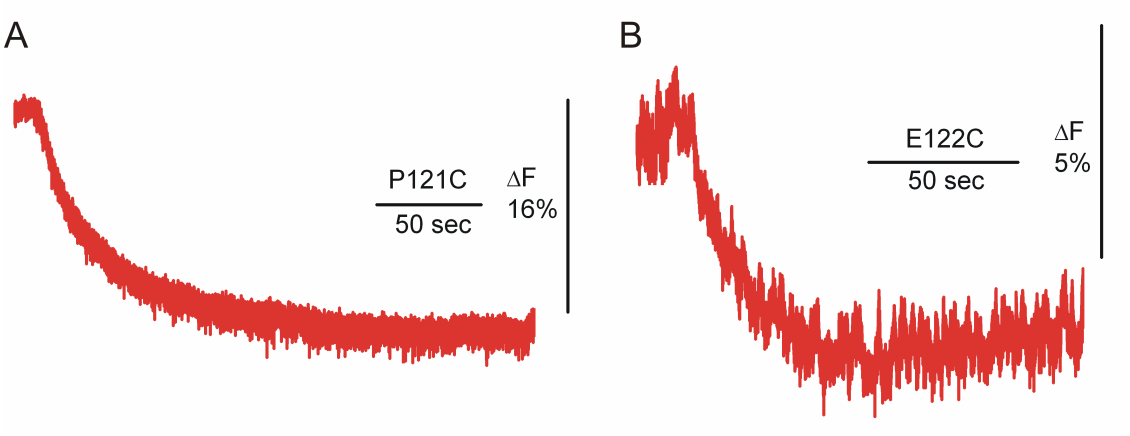

Fig. 3.27 Fluorescence change induced by 100nM NF449: Representative traces of change in the fluorescence in **(A)** P121C **(B)** E122C. An increase in the fluorescence was seen in both mutants.

Table 3.16: Antagonist mediated change in the fluorescence intensity of CRD-1 mutants

Mutants	Antagonist	ΔF (%)	τ_F (s)	Direction	N (# cell)
N120C	100nM NF449	Not detected	-	-	4
P121C	100nM NF449	11.3 ± 2.4	29.2 ± 3.1	Increase	3
E122C	100nM NF449	5.2 ± 0.7	30.4 ± 11.4	Increase	3

*ΔF denotes change in the fluorescence; τ_F is the time constant of onset of the fluorescence change.

No current was observed (as expected), but binding of NF449 induced an increase in the fluorescence in two mutants (P121C and E122C) (Fig. 3.27). Fluorescence change in mutant N120C was not detected. The relative change in the fluorescence caused by NF449 at IC_{max} concentration was comparable to the change caused by 10μM ATP (at concentrations greater than EC_{50} on these mutants) (Table 3.13 and 3.16).

Taken together, these results suggest that the CRD-1 region of P2X1 receptors is highly dynamic and is a part of the conformation wave which originates after ligand binding. Certain positions in the CRD-1 region could even differentiate between types of ligand bound in the binding site (e.g. position N120C showed a decrease in the fluorescence upon ATP binding but showed no change in the fluorescence upon NF449 binding).

4. Discussion

4.1 Probing allosteric interactions between P2X receptor subunits in the gating process using photolabeling

P2X receptors are thought to be formed by the trimeric assembly of homologous subunits [49,72], resulting either in homomeric or heteromeric channels [70,71]. Agonist binding at the interface between adjacent subunits is thought to initiate conformational waves which propagate to the receptor's gate through an unknown allosteric mechanism. An important step towards understanding the allosteric mechanism of receptor activation is to determine the number of subunits and the nature of their contribution in the gating process. Due to continuous ligand binding and unbinding steps, defined contribution of each subunit towards gating is difficult to study. Therefore, in my thesis, I sought to answer above and related questions using homomeric P2X receptors with the help of a photolabeling technique.

I used photolabeling to overcome the limitation of ligand unbinding events, where one or more ligands were covalently attached to the binding sites of P2X receptors, so that the contribution of remaining binding sites to the gating process can be studied. As gating of P2X receptors is a complex process, it has been necessary in the present study to make some simplifying assumptions to analyze these results which are discussed later in this section. However, even under the limitations of these assumptions, the present work unequivocally favors the interpretation that the gating process in P2X receptors is an additive outcome which is contributed by each subunit of the receptor individually.

Concurrent photolabeling and functional measurements

Photoaffinity ligands provide tools for real time functional modification of the system under investigation. To date many photoaffinity analogs of purines with nearly all the photolysable groups have been synthesized and many are now commercially available. Benzophenone and azido based photoaffinity analogs of ATP have been used earlier in the structure-function studies of purinergic receptors [117,118]. Benzophenone based probes offer several distinct advantages over azido based probes. They are stable under ambient light conditions and can be activated with wavelengths greater than 300 nm thus reducing protein degradation and allow studies on cell cultures or other living systems. Even the relaxation process does not

require a scavenger [112]. BzATP (3'(2')-O-(4-benzolybenzoly)-ATP) a benzophenone based photoaffinity analog of ATP is commercially available and shown to have agonist activity on various P2X receptor subtypes [99]. Therefore, I used BzATP to cross-link it to the binding site of P2X receptors (P2X1, P2X2 and chimera) that were expressed heterologously in *Xenopus laevis* oocytes.

The combination of photolabeling to cross-link photoaffinity agonists in the binding site of receptors along with functional measurements with the help of patch clamp has been used at CNG channels [111,166] and nAChRs [167]. In this study, I used two-electrode voltage clamp to measure functional responses from oocytes expressing P2X receptors. Therefore, for concurrent photolabeling and functional measurements from the same set of P2X receptors, a custom made oocyte chamber was used (Fig. 2.2). This chamber not only provided a rigid positioning of oocytes to minimize the artifacts induced by the movement of oocytes caused by the solution exchange but also allowed continuous and fast solution exchange. It allowed electrode impalement in the upper compartment for electrophysiological measurements, while the flow of solution in the lower compartment helped the oocyte to form a seal around the 0.6mm hole due to venturi effect, thus minimizing solution exchange between the upper and lower partition. This type of chamber has been used earlier to study concurrent receptor activation and fluorescence changes to monitor the structural rearrangements in GABA receptors heterologously expressed in *Xenopus laevis* oocytes [140]. The only limitation with this chamber (also reported by Chang et al. [140]) was the diffusion of ligand around the 0.6mm hole (seal) especially during prolonged ligand application. As this portion of the oocyte was outside the field of UV-light application, no photolabeling would occur on the receptors in this portion; however, an extended washout was used to completely deactivate the receptors (if any) in this portion of the oocyte especially during protocols in which agonist was applied for more than 60s. Therefore the diffusion of ligand around this hole is not likely to affect our interpretations of the experiments with this chamber.

BzATP is found to be an effective agonist on the chimera, but a partial agonist on P2X2 receptors. Efficacy of BzATP on P2X1 receptors is not determined in this study, although it has been previously published that BzATP is a partial agonist on P2X1 receptors [99].

Photolabeling of P2X receptors

Saturation of binding sites by the agonist (BzATP) in the absence of UV-light lead to the activation and desensitization of P2X1 receptors. However, covalent cross-linking of BzATP in the presence of UV-light resulted in locking of the receptor in an agonist bound desensitized state which was evident from the apparently reduced recovery of receptors from the desensitized state as compared to without photolabeling (Fig. 3.1). Recent functional [104] and covalent cross-linking studies [118] on P2X1 receptors also suggested that the recovery of P2X1 receptors from desensitization possibly involves dissociation of the bound agonist. Our results are in agreement with these studies, that the agonist unbinding is a pre-requisite for the recovery of P2X1 receptors from desensitization. P2X1 receptors could not be further used to study the contribution of each subunit towards gating due to the limitation of recovery of receptors from the persistent desensitization after photolabeling. Therefore, P2X2 receptors were explored for these functional studies as they represent the non-desensitizing phenotype of P2X receptors.

BzATP is found to be a partial agonist on the P2X2 receptors when compared to ATP (Fig. 3.3). ATP produced a maximal response from P2X2 receptors when all the binding sites were available (not cross-linked), but its response decreased gradually upon photolabeling with BzATP. Progressive photolabeling with BzATP lead to an increase in the number of binding sites cross-linked with a partial agonist i.e. knocked out (not available for the maximal contribution by ATP) (Fig. 3.4). Recently, in a study based on the coexpression of P2X1 mutants (T18A with K68A or wild type receptors), Ennion et al. [33] found that the response from the homo-trimeric T18A mutants was too low to be detected. But the hetero-trimers between T18A mutants and wild type P2X1 (in which one or two subunits of wild type P2X1 present) showed a significantly higher response. There was a corresponding increase in the receptor's activity as the number of wild type P2X1 receptor subunits increased in the hetero-trimers, indicating an additive functional effect. In a similar study, Stoop et al. [168] studied the MTSET block of concatenated P2X2 receptors in which one or more subunits carried the T336C mutation. Mutation of an amino acid to cysteine residue renders the subunit susceptible to block by MTSET. Introduction of mutant subunits in a concatemeric construct lead to a progressive increase in the channel block by MTSET as long as the mutant subunit remains in the position in the construct where it can line the wall of the pore. Their results showed that a maximum of three subunits constituted the structural basis for the P2X2 gate which contributes equally to the formation of the receptor's gate. Together with these studies,

our data lead to the conclusion that the gating process in P2X receptors is an additive outcome to which each receptor subunit contributes individually i.e. the contribution of a subunit bound by a partial agonist would be less as compared to the subunit bound by a full agonist and the overall gating would be determined by the additive outcome of all receptor subunits occupied by the type of ligand. Therefore, when one or two subunits in the functional P2X receptors were knocked out (either by cross-linking a partial agonist or by incorporating a non-functional subunit e.g. T18A) the maximal response from the receptor was decreased.

To further dissect the contribution of unoccupied binding sites towards the gating process on the partially liganded receptors, the challenge was to first determine the number of covalently attached BzATP molecules per receptor. On P2X2 receptors, the use of BzATP as a cross-linking agent lead to the selective knock-out of functional receptors i.e. maximal response of the receptors after covalent cross-linking was significantly reduced. Due to this limitation, number of covalently attached BzATP molecules per receptor could not be determined. Thus, a receptor was required which not only maintains the non-desensitizing phenotype but also retains the functional activity after the covalent attachment of BzATP. To this end, the use of a P2X2/P2X1 receptor chimera was tested.

The chimera consisted of a portion of P2X2 (N-terminal and TM1 domain) and a portion of P2X1 receptors (full extracellular loop, TM2 and C-terminal domain). The chimera represents a valid model of P2X1 receptors because it preserves the ligand binding domain of the P2X1 receptors [88]. In contrary to P2X1 receptors which have an EC_{50} value close to 1µM for receptor activation, the chimera has nanomolar potency for various agonists [88]. It is assumed that the µM potency of agonists on P2X1 receptors accounts to non steady-state measurements because virtually all activated P2X1 receptors close rapidly by desensitization and not by direct transition to the re-activable closed state. Whereas, by elimination of desensitization (the use of chimera), stationary currents become amenable to analysis that allows for a determination of an EC_{50} value under steady-state conditions [88,104].

On the chimera, BzATP is a full agonist when compared to ATP (Fig. 3.5). Covalent cross-linking of BzATP in the binding sites leads to persistent activation of the chimera. Due to the fact that once BzATP is cross-linked it cannot be dissociated from the binding sites, therefore, we speculate that persistent current originated from the fully liganded receptors in which all the binding sites were covalently attached by BzATP. Dose response curves for ATP on the P2X receptors in sensory neurons have a Hill coefficient close to three suggesting that three agonist molecules are needed to bind to the receptor to produce efficient channel activation

[169]. Therefore, it was assumed that binding of three agonist molecules per receptor is required for the gating of the receptor and the persistent current after photolabeling on the chimera resulted from the receptors in which three BzATP were cross-linked in the binding sites. To specifically determine the level of persistent current through the permanently open chimera channels, Neomycin was applied externally as an open channel blocker. Neomycin (an aminoglycoside) has been shown to induce concentration and voltage dependent block in a variety of Ryanodine [170] and P2X receptors [153]. Also, on the chimera, external application of 3mM Neomycin showed a partial block of cationic current through open channels (unpublished results, Eva Bongartz).

The time course of photolabeling (until all the binding sites in a given pool of receptors were cross-linked by BzATP) was also determined. The progressive photolabeling of P2X1 receptors resulted in persistent desensitization (Fig. 3.2), on P2X2 receptors it resulted in selective knocking out of receptors (Fig. 3.4) and on the chimera it resulted in permanently active channels (Fig. 3.6). Our results are in agreement with similar studies done on P2X receptors demonstrating that P2X1 receptors undergo persistent desensitization after covalent cross-linking of agonists in the binding sites [118] and that incorporation of one or more non-functional subunits leads to the decrease in the maximal response of the P2X receptors [33,168]. After prolonged photolabeling, both P2X1 and the chimera showed different levels of apparent steady state photolabeling (~50% in P2X1 and ~80% in chimera) (Fig. 3.2 and 3.6). As P2X receptors undergo constant receptor trafficking and agonist mediated internalization [105], such processes could be responsible for the incomplete steady state levels of photolabeling even after prolonged times.

Modulation of potency and efficacy of agonists after photolabeling

Modulation of agonist generated responses from the photolabeled chimera receptors was determined on the same oocyte by comparing the dose response curves for agonists (partial and full agonist) before and after photolabeling. Upon washout of ATP or BzATP, the chimera deactivates slowly with a time constant (τ) of 63 ± 2s or 23.8 ± 0.5s, respectively [88]. Due to the slow dissociation of these agonists from the chimera, αβ-MetATP (another full agonist of chimera) was used, as the chimera deactivates after αβ-MetATP washout with a faster time constant (τ) of 2.5 ± 0.3s [88]. Thus, the use of αβ-MetATP permitted us to

generate complete dose response curves before and after photolabeling on the same oocyte expressing the chimera.

Progressive photolabeling lead to a leftward shift in the dose response curve with progressive decrease in the EC_{50} value and Hill coefficient for αβ-MetATP when compared to the dose-response curve prior to photolabeling (Fig. 3.8 and Table 3.3). A leftward shift in the dose-response curve would indicate an increase in the potency of the agonist. Similarly, Karpen et al. [110] found that the potency of a full agonist (cGMP) increased after photolabeling the rod channels with another full agonist. Hill coefficients gives lower estimate of number of ligands required to open the receptors. Agonist dose-response curves of P2X receptors often have Hill coefficient of more than one for different agonists [88,171], which seems to be reasonable since the channels are composed of three subunits [49]. Before photolabeling, when all the binding sites were available for αβ-MetATP to bind and produce functional response, the dose-response curve for αβ-MetATP at the chimera has a Hill coefficient of 1.6. During progressive photolabeling, the number of covalently attached BzATP molecules per receptor would increase by correspondingly decreasing the number of free binding sites until the receptor would need binding of a single agonist molecule to be opened. Under these conditions, properties of such a receptor would be similar to a receptor with only one agonist binding site. The agonist dose-response curve of a receptor with a single agonist binding site would have a Hill coefficient of one. Accordingly, we have observed a decrease in Hill coefficient of αβ-MetATP from 1.6 to ~1 during progressive photolabeling.

These results also support our earlier interpretation that the process of gating in P2X receptors is an additive outcome to which each subunit of the receptor contributes individually. The contribution of each subunit liganded by full agonists (BzATP and/or αβ-MetATP) would be maximal. Therefore, when one or two subunits of the receptor were permanently occupied by a full agonist (e.g. BzATP), sub-saturating concentrations of another full agonist (e.g. αβ-MetATP) became more potent because the probability that these channels will be fully liganded at any given αβ-MetATP concentration would be higher (Fig. 3.8). This also explains the leftward shift in the dose response curves for αβ-MetATP after photolabeling compared to without photolabeling.

Recently Cao et al. [172] demonstrated that the T339S mutant of P2X2 receptors shows constitutive receptor activation in the absence of ATP. Its increased sensitivity towards gating unraveled that not only the P2X2 partial agonist αβ-MetATP, but also the competitive antagonist TNP-ATP could favorably shift the gating equilibrium towards open state.

Similarly in the current study, nanomolar sensitivity of chimera for various ligands not only unraveled the partial agonist properties of TNP-ATP but also permitted us to measure the change in the efficacy of TNP-ATP upon progressive photolabeling (Fig. 3.5 and 3.9). Photolabeling of BzATP did not change the apparent affinity of TNP-ATP as judged by the comparison of dose response curves for TNP-ATP generated before and after photolabeling (Fig. 3.9). However, the ratio between the response generated by saturating concentrations of TNP-ATP and BzATP increased progressively upon photolabeling. The progressive increase in the ratio would indicate an increase in the functional response by TNP-ATP upon progressive photolabeling.

Historically, it is believed that partial agonists have low affinity for the open state and therefore stabilize the closed state of the receptors [4]. However, the absence of change in the apparent affinity of TNP-ATP during various levels of receptor activation ruled out the role of different affinities to explain the change in the efficacy of TNP-ATP after photolabeling. Single channel measurements of nicotinic receptors by Lape et al. [173] demonstrated a remarkable similarity in full and partial agonist affinity for open and closed conformations. They argued that partial agonism originated from the reduced ability of a ligand to shift the equilibrium from resting to flip state rather than the reduced ability to open the receptor. Our results are in agreement with Lape et al. [173] that before photolabeling full occupancy by TNP-ATP alone imparted less energy to the receptors, which resulted in the negligible response compared to the full agonist. Apparently, the energy barrier for channel opening was reduced when one or two ligand-binding sites were covalently labeled by BzATP molecules (full agonist), thereby increasing the efficacy of TNP-ATP. Thus, the increase in efficacy of TNP-ATP, when at least one or two binding sites of the chimera were covalently cross-linked by BzATP, unequivocally accounts for the allosteric interactions between subunits.

In order to estimate minimum number of covalently attached BzATP required to increase the TNP-ATP efficacy, we first determined the statistical distribution of receptors with different numbers of cross-linked BzATP molecules using binomial distribution. In order to fit the progressive increase in the ratio of response generated by the saturating concentration of TNP-ATP to the saturating concentration of BzATP some assumptions were made. We first assumed that the binding of three ligands is required to open P2X receptors and those receptors with only one or two labeled binding sites are essentially closed. However, in the absence of single channel data the existence of sub-conducting states at sub-maximal binding-site occupancy are difficult to rule out, although, evidence from sensory neurons indicates a

requirement of three agonist molecules for efficient channel activation [169] and single channel studies by Ding et al. [171] also suggested that the sub-conductance level of partially liganded P2X2 receptors is virtually negligible. We considered that at the saturating concentration of BzATP (1μM) for the chimera, covalent cross-linking occurs randomly and not with efficiency based on the binding sites' affinity. Moreover, it is expected that at 1μM BzATP concentration, all the binding sites should be occupied at all time irrespective of the individual binding site affinity. Based on these assumptions we explored two theoretical possibilities, in which the maximal response generated by TNP-ATP from the chimera occurred either from the population of receptors in which at least one BzATP (One-site model) or two BzATP (Two-site model) molecules were cross-linked. Under the limitations of these assumptions, our fitting results indicate that TNP-ATP would generate maximum response from P2X receptors in which two BzATP were cross-linked. Thus, we can conclude that in P2X receptors the contribution from each subunit to the gating process is an additive one in which each subunit contributes equally.

4.2 Probing allosteric interactions between P2X receptor subunits using fluorescent ligand

Agonist binding to the closed state of P2X1 receptors initiates allosteric interactions between subunits which result in opening of receptors followed by desensitization. Upon washout, receptors recover from desensitization on a slow time scale. Kinetic studies on recovery from desensitization proposed that dissociation of the bound agonist is a prerequisite for the process of recovery from desensitization [104]. We, therefore, hypothesized that allosteric interactions between subunits in desensitized state contribute to the change in the affinity of the binding sites of receptors which facilitates dissociation of the bound agonist molecules. To investigate this possibility, I have studied the nature of interactions between subunits contributing to the process of dissociation of bound agonist from the desensitized state of P2X1 receptors.

To this end, occupancy state of P2X1 receptors at different agonist concentrations was determined because allosteric interactions between subunits initiate only after agonist binding. Desensitized P2X1 receptors represent a ligand bound closed state and channels would not evoke an electrophysiological functional response, therefore, I used Alexa-ATP (a fluorescent analog of ATP) to equilibrate the binding sites of P2X1 receptors. At high concentrations, binding of Alexa-ATP activated and fully desensitized P2X1 receptors. Level of fluorescence from Alexa-ATP bound P2X1 receptors was used as a parameter for occupancy state of these receptors. In this study we also propose a simple allosteric model for subunit interactions which describes P2X1 receptors activation, desensitization and recovery from desensitization. Our proposed model is compatible with our experimentally determined and computationally simulated results and favors our interpretation that negative allosteric interactions between subunits in the fully liganded desensitized state contributes to the decrease in the affinity of binding sites, which facilitates dissociation of the bound agonist. Based on these evidences, our interpretation suggests that binding of three agonist molecules per receptor are required to desensitize P2X1 receptors.

Optimization of conditions for studying ligand-receptor interactions

Many fluorescent ATP analogs are now commercially available [133], but little is known about their pharmacological properties on P2X receptors. TNP-ATP, a fluorescent ATP

analog, is characterized as a potent antagonist of P2X receptors [163] and has been used to map the extra-cellular ATP binding sites in inner and outer hair cells isolated from guinea pig organ of corti [135]. However, none of the fluorescent ATP analogs were analyzed for agonist potency on P2X receptors. To the best of our knowledge, our study for the first time describes the agonist efficacy of Alexa-ATP (a fluorescent ATP analog) on P2X1 receptors and the chimera (Fig. 3.11). Complete dose response curve of Alexa-ATP could not be generated on P2X1 receptors owing to the high cost of Alexa-ATP. However, it was found that 1μM Alexa-ATP has less potency on P2X1 receptors as compared to 1μM ATP (Fig. 3.11A). Using the Hill equation, we estimated an EC_{50} value of ~2μM for Alexa-ATP on P2X1 receptors. Nanomolar sensitivity of the chimera for various agonists offered us an advantage to generate complete dose response curve for Alexa-ATP. Although, on the chimera, Alexa-ATP showed the similar efficacy as of ATP, the dose response curve of Alexa-ATP was rightward shifted, indicating that Alexa-ATP has a reduced potency on the chimera (Fig. 3.11C, D).

Although, 300nM Alexa-ATP does not generate maximum response, it could fully desensitize P2X1 receptors. Therefore, the level of fluorescence from the bound Alexa-ATP in the desensitized state of P2X1 receptors could be used as a parameter for the occupancy state of the receptors. Of note, being a fluorescent probe, Alexa-ATP is susceptible to photobleaching. Because of this limitation, the dissociation of bound Alexa-ATP from the P2X1 receptors could not be monitored in continuous light. So, we optimized a light irradiation protocol which allowed us to do fluorescence studies (association and dissociation of Alexa-ATP) with minimal photobleaching. We found that the time course of decay of Alexa-ATP fluorescence, when light was irradiated for 2s every 30s gave optimum result which was not different than light irradiated for every 40s. However, even under these conditions when the exposure of light to Alexa-ATP was severely reduced and after extensive washout, complete decay of Alexa-ATP fluorescence was not observed from the P2X1 receptors (Fig. 3.12C, 3.13A). Likewise, in ligand association experiments, when Alexa-ATP was allowed to equilibrate the binding sites of P2X1 receptors, steady-state binding was not observed (Fig. 3.13B).

P2X1 receptors are known to undergo agonist mediated receptor internalization [107] and therefore, we speculated that the origin of the bi-exponential time course of Alexa-ATP fluorescence during association and dissociation experiments on the P2X1 receptors might be due to the trafficking of receptors on the membrane (internalization and recycling of internalized receptors back to the membrane). We therefore hypothesized that the fast time

constant in the time course of decay of Alexa-ATP fluorescence on the non-PAO treated oocytes is possibly contributed by two processes: dissociation of bound Alexa-ATP from the surface receptors and agonist mediated internalization of P2X1 receptors. Whereas, the slow time constant possibly was contributed by the slow trafficking of Alexa-ATP bound P2X1 receptors back to the membrane. Similarly, the fast and slow time constants in the time course of association of Alexa-ATP fluorescence on the non-PAO treated oocytes is thought to be contributed by the agonist mediated internalization of P2X1 receptors and slow recycling/trafficking of P2X1 receptors to the membrane. Due to this, the density of P2X1 receptors (number of binding sites) constantly changes on the membrane which resulted in the lack of saturation during Alexa-ATP binding.

To test these possibilities, phenyl arsine oxide (PAO) was used which is reported to inhibit internalization of surface receptors expressed in oocytes [162] and receptor mediated endocytosis of protein nexin [174], EGF [175] and insulin [176]. When the association and dissociation kinetics of Alexa-ATP was performed on PAO treated oocytes expressing P2X1 receptors, not only complete decay of Alexa-ATP fluorescence (dissociation experiments) was seen but also steady-state binding of Alexa-ATP fluorescence (association experiments) was achieved (Fig. 3.13A, B). Taken together, these results confirmed that P2X1 receptors also undergo constant receptor trafficking and agonist mediated receptor internalization under our experimental conditions. Although, precise mechanism of PAO mediated block of P2X1 receptors internalization is unknown, earlier studies point towards the involvement of vicinal sulfhydryl groups in the inhibitory action of PAO on receptor mediated endocytosis [177]. The trivalent arsenicals form stable ring like structures with molecules having appropriately spaced vicinal sulfhydryl groups (such as those in lipoic acid) present on the surface of oocyte membrane. The equilibrium of such reactions strongly favor the complex formation, thus imparting rigidity to the membrane, which is thought to inhibit receptor trafficking.

Allosteric interactions between subunits depends on occupancy level of receptors

Ligand competition studies on muscarinic receptors [178], P2X7 and P2X4 receptors [179,180] have shown that allosteric regulators could affect the rate of dissociation of bound radioligand from these receptors. Therefore, it is quite possible that in the desensitized state of P2X1 receptors, subunit interactions could contribute to the process of ligand dissociation which is a prerequisite of receptor's recovery from desensitization. In the present study, to

investigate the nature of subunit interactions in the desensitized state of P2X1 receptors, dissociation of bound Alexa-ATP from the desensitized state of P2X1 receptors was monitored in the presence of various allosteric/competing ligands (divalent cations, agonist and antagonists).

P2X receptors can be allosterically regulated by extracellular protons [52], divalent cations and various other ions [54,55]. Therefore we have also tested the dissociation of bound Alexa-ATP from desensitized P2X1 receptors in the presence of various cations, agonists and antagonists. Dissociation of bound Alexa-ATP in 2mM Mg^{+2} (as MgORI buffer) was used as a control experiment. The dissociation of bound Alexa-ATP in MgORI buffer could be described with a mono-exponential function (Fig. 3.14A), indicating that dissociation occurred from a single population of desensitized receptors. In contrast to Mg^{+2} ions, presence of 2mM Ca^{+2} (as CaORI buffer), significantly decreased the decay of Alexa-ATP fluorescence from the desensitized P2X1 receptors, which is an indicator of positive cooperative interactions between subunits. It is important to note that extracellular Ca^{+2} ions have been shown to produce different effects on desensitizing P2X receptors. Cook et al. [164] showed that extracellular Ca^{+2} ions could enhance the recovery of P2X3 receptors from the desensitized state, while Evans et al. [77] and Haines et al. [101] found no effect of extracellular Ca^{+2} ions on the recovery of P2X1 receptors from desensitization. However, Michel et al. [181] found that P2X1 receptors possess high affinity for αβ-MetATP (an agonist of P2X1 receptors) in the presence of 4mM Ca^{+2} ions compared to the absence of Ca^{+2} ions, further emphasizing an unknown regulatory role of Ca^{+2} ions. Therefore, the precise effect of Ca^{+2} ions on the desensitized state of P2X1 receptors is at present debatable, although our experiments indicate positive cooperative interactions between subunits in the presence of Ca^{+2} ions.

Thus, it is plausible that presence of extracellular Ca^{+2} ions increases the affinity of desensitized state of P2X1 receptors for the bound ligand (in this case Alexa-ATP), which is measured as decreased dissociation of bound Alexa-ATP from the desensitized state. If this is true, then the presence of extracellular Ca^{+2} ions should also reduce the recovery of P2X1 receptors from desensitization. Our functional experiments on the P2X1 receptors confirmed that the presence of extracellular Ca^{+2} ions indeed significantly reduced the recovery of P2X1 receptors from desensitization as compared to the control experiments (i.e. in the presence of MgORI buffer) (Fig. 3.15). Thus, these functional results complement our fluorescence data that in the presence of extracellular Ca^{+2} ions, positive cooperative interactions between

subunits contribute to the increase in the affinity of desensitized P2X1 receptors to the bound agonist, which results in the reduced dissociation of bound agonist, thus, reducing the recovery of receptors from desensitization.

On the other hand, increase in the dissociation of labeled compound by excess of unlabeled compound from orthosteric or allosteric binding sites has been used as an indicator of negative cooperative interactions between subunits of the receptors (negative cooperativity model) e.g. insulin from insulin receptors [182], thyroid hormone from thyrotropin receptors [183], EGF receptor system [184] and P2X7 [179]. The dependence of dissociation of the labeled compound was also correlated to the structure of competing ligand and competition of ligands for individual attachment points on the binding sites of the receptor (multipoint attachment model) e.g. (+)-cis-Diltiazem from L-type Ca^{+2} channels [185]. When we monitored the dissociation of bound Alexa-ATP in the presence of high concentrations of ATP (EC_{50} or more), TNP-ATP or NF449 (IC_{max}), accelerated dissociation of bound Alexa-ATP was observed (Fig. 3.14B-D). The dissociation of Alexa-ATP from P2X1 receptors was found to be independent of the structure of the competing ligands, at least when these ligands were present in high concentrations, thus, suggesting negative cooperative interactions between subunits.

However, 3nM ATP which is sufficient to desensitize ~50% of P2X1 receptors [104] and 6nM TNP-ATP (concentration at which ~50% inhibition of P2X1 current occurs), showed similar time course of decay of Alexa-ATP fluorescence as observed in MgORI buffer (Fig. 3.14B-C). It has been shown earlier that the rate of entry of P2X1 receptors to the desensitized state at 3nM ATP concentration was slow (τ = 6.5 min) [104], probably due to the slow rate of binding of ATP to the P2X1 receptors. Therefore, we think that due to lack of substantial binding of competing ligands (ATP and TNP-ATP) at these nanomolar concentrations in our experimental conditions, dissociation of bound Alexa-ATP occurred without the influence of these competing ligands, hence, the time course of fluorescence decay was similar to the decay monitored in MgORI buffer (control conditions).

Interestingly, the dissociation of Alexa-ATP at IC_{50} concentration of NF449 was also found to be decreased (similar to Ca^{+2} ions) (Fig. 3.14D), suggesting that in the presence of 0.3nM NF449, affinity of the binding sites of P2X1 receptors also increases which is reflected in the form of decreased dissociation of bound Alexa-ATP from the desensitized P2X1 receptors. Decreased dissociation of Alexa-ATP also suggests positive cooperative interactions between subunits. When the effect of 0.3nM NF449 (IC_{50} concentration) was functionally analyzed, it

was found that NF449 being a competitive antagonist for P2X1 receptors resulted in 50% inhibition of ATP generated functional responses. This contradicts our fluorescence data that being a competitive antagonist, it would compete for the agonist binding site. Therefore, in the presence of 0.3nM NF449 we should either observe an increase in the dissociation of bound Alexa-ATP from the desensitized P2X1 receptors due to negative cooperative interactions between subunits (i.e. when both Alexa-ATP and NF449 would occupy the agonist binding sites), or we should observe similar time course of decay of Alexa-ATP as that of in MgORI buffer due to slow rate of binding of NF449 to the binding sites at 0.3nM concentration. Instead, we have observed decreased decay of Alexa-ATP fluorescence in the presence of 0.3nM NF449. To this end, we speculate that the dissociation of Alexa-ATP indeed started from the fully liganded receptors (three bound Alexa-ATP). When the dissociation of bound Alexa-ATP was monitored in the presence of 0.3nM NF449, dissociation of one of the three bound Alexa-ATP would occur due to negative cooperativity even before the binding of NF449 (as it is expected that at 0.3nM concentration binding of NF449 would be slow). Due to its huge structure, binding of NF449 to the partially liganded (one or two Alexa-ATP bound receptors) P2X1 receptors could induce constrains on the dissociation of remaining Alexa-ATP from the receptors, thus, reducing the rate of dissociation of bound Alexa-ATP. The reduced response of ATP in the functional experiments, in which P2X1 receptors were washed in presence of 0.3nM NF449, suggest an example of mode of action of a classical competitive antagonist i.e. at 0.3nM concentration, 50% of the binding sites of P2X1 would be occupied by NF449, thus, reducing the ATP generated responses to 50% (Fig. 3.15A). Based on above speculations, we suggest that the effect of 0.3nM NF449 on the dissociation of bound Alexa-ATP is due to its steric hindrance on the dissociation of bound Alexa-ATP rather than due to positive cooperative interactions between subunits or due to change in the affinity of the binding sites of the P2X1 receptors.

Together, these results indicate that at high concentrations of competing ligands (when the probability of finding fully liganded receptors would be high), negative cooperative interactions between subunits occurs. However, in the presence of allosteric/competing ligands (calcium ions or NF449 at IC_{50} concentration), decreased dissociation of Alexa-ATP occurs, possibly suggesting positive cooperative interactions between subunits in the presence calcium ions and the possible role of steric hindrance caused by NF449 on the slow dissociation of bound Alexa-ATP. Thus, based on our experiments we conclude that presence

of allosteric/competing ligands regulates the dissociation of bound ligands through allosteric interactions between subunits.

Allosteric model for ligand-receptor interactions

Several models have been proposed in the literature to understand the activation and desensitization mechanism of P2X receptors. Bean [169] proposed a linear model with independent subunits to understand the channel activation, based on the kinetics seen in the bullfrog sensory neurons. However this model cannot be used to interpret our results as it does not account for the accelerated dissociation of bound Alexa-ATP in our experiments.

Ding et al. [171] proposed a kinetic model based on single channel analysis on P2X2 receptors. Although their model took subunit interactions during receptor activation into consideration, their model also cannot be used to describe the desensitized state of P2X1 receptors, since it was developed for the non-desensitizing P2X2 receptors.

Recently, Rettinger et al. [104], proposed a simple kinetic model for P2X1 receptors activation and recovery from desensitization based on functional studies. Their model is, however, silent on the behavior of subunit interactions. Therefore, we extended the model proposed by Rettinger et al. [104] and incorporated kinetic steps to adequately explain the negative cooperative interactions between subunits (Fig. 3.16, 3.19). In this model, we hypothesized that binding of three agonist molecules to the closed state of receptor would be required to open and desensitize P2X1 receptors, since the channels are composed of three subunits [49]. Dissociation of bound agonist molecules from the fully liganded desensitized state of the receptors in the presence of ligand free buffer would bring the receptors back in non-liganded closed state. Our model also predicts the possibility of partially liganded states of the receptors in Scheme-I and II (Fig. 3.16). Partially liganded receptors in Scheme-I would be non-desensitized and in the Scheme-II would be desensitized (Fig. 3.16). In this model, we further hypothesized that the negative cooperativity will exist only in the fully liganded state of the receptors (three ligand bound state) and under the influence of negative cooperativity (i.e. in presence of high concentrations of ligand) the dissociation of all the bound ligands would be fast and occur with same rate.

Based on this model, we expect that the dissociation of all the bound Alexa-ATP molecules would occur under the influence of negative cooperativity in the presence of high concentration of competing ligands (τ = ~500s) (Table 3.9), as receptors would be fully

liganded at any given point of time. Due to this, the time course of decay of Alexa-ATP fluorescence is expected to be fast and mono-exponential, as the dissociation of each ligand would occur with same rate. Whereas, in the absence of a competing ligand (i.e. in the presence of MgORI buffer), dissociation of the first Alexa-ATP would be fast (as it would occur from a fully liganded state) but remaining two bound Alexa-ATP molecules would dissociate slowly (as it would occur without the influence of negative cooperativity), and thus is expected to be biphasic in nature (Table 3.9). Interestingly, the dissociation of bound Alexa-ATP in both the conditions (presence and absence of competing ligands) could be described by mono-exponential function in our experiments (Fig. 3.14). Nevertheless, when the dissociation of bound Alexa-ATP from the fully liganded desensitized state (Scheme-II in Fig. 3.16) was simulated on Gepasi 3.0 software [186,187] for both these conditions (presence and absence of a competing ligand) using manually adjusted rate constants under the framework of our hypotheses, the simulated dissociation could also be described by mono-exponential function (Fig. 3.18, Table 3.10). Therefore, we think that as the binding rate between the first two ligands and the last ligand is not much different (i.e. only factor of two) and also because of the experimental limitations (i.e. due to the time required to wash non-specifically bound Alexa-ATP and Alexa-ATP from the solution, it is difficult to resolve first tens of seconds), both simulated and experimentally determined time course of dissociation of bound Alexa-ATP from the P2X1 receptors could be described by mono-exponential function.

It is also interesting to note that our proposed model predicts the possibility of partially liganded closed states of the receptors both in Scheme-I and II. The only difference between partially liganded states in Scheme-I and II is that these states in Scheme-I could be further activated by application of high concentrations of ATP, therefore, they represent partially liganded non-desensitized closed states, whereas, the states in Scheme-II would not produce current response upon application of high concentrations of ATP, therefore, they represent partially liganded desensitized closed states. However, in terms of occupancy level, both Scheme-I and II states can be partially liganded (i.e. one or two liganded states). We then asked if partially liganded non-desensitized states (Scheme-I) could also influence the dissociation of bound Alexa-ATP. To this end, occupancy states of Alexa-ATP at different nanomolar concentrations were determined using binding curve and were then correlated with the functional states of the receptors. After this correlation, the dissociation of Alexa-ATP

from the partially liganded receptors (at low nanomolar Alexa-ATP concentrations) was determined in the presence of MgORI buffer.

At low nanomolar concentrations, it is expected that receptors would be partially liganded. Direct binding of Alexa-ATP to P2X1 receptors lead to an increase in the fluorescence until steady-state level is reached (Fig. 3.20). Half maximal binding (BC_{50}) of Alexa-ATP (i.e. 50% occupancy of binding sites) was found to be at ~2nM. However, the level of desensitization in P2X1 receptors at ~2nM of Alexa-ATP (i.e. 50% occupancy of binding sites) remains speculative. In a similar study, Rettinger et al. [104] found that 50% of P2X1 receptors desensitize at 3nM ATP concentration, although occupancy at 3nM ATP was not determined in their study.

Therefore, we tested three possibilities: binding of three agonist molecules per receptor is required to desensitize P2X1 receptors (Three-site model), binding of two agonist molecules per receptor is required to desensitize P2X1 receptors (Two-site model) or binding of one agonist molecule per receptor is required to desensitize P2X1 receptors (One-site model). It has been shown earlier in the single channel studies on P2X2 receptors that the channels do not open for a significant fraction of time in partially liganded states [171], therefore, for our different models we assumed that the fractional population of receptors in partially liganded states would primarily be expected to be in non-desensitized states (i.e. for each model in partially liganded states, there is one molecule less than that required to desensitize the receptor in that model). If we assume that the binding of Alexa-ATP to P2X1 receptors is a random event with only two outcomes i.e. either the receptor is labeled or not labeled, then the statistical distribution of population of receptors at the steady-state binding of Alexa-ATP would be given by their binomial distribution. However, it is important to note that P2X1 receptor subunits are interacting in a cooperative manner, but as the binding rate between the first two ligands and the last ligand is not much different (i.e. only a factor of two), the influence of cooperativity can be neglected for ligand binding events in order to use the binomial equation. Fractional distribution of population with 0, 1, 2 and 3 Alexa-ATP bound receptors was then calculated from binomial distribution for each Alexa-ATP concentration from the binding curve (Fig. 3.20D). Taken into consideration that P2X1 receptors need to open before they undergo desensitization [104], the fractional population of closed receptors based on these three proposed models (One, Two or Three-site model) were plotted against different Alexa-ATP concentrations and compared with the functional response generated by 30μM ATP on the P2X1 receptors pre-equilibrated with different Alexa-ATP concentrations

(Fig. 3.22). After fitting all the curves with Hill equation, we found that the half maximal distribution of closed-states for Three-site model was seen at 8.6 ± 0.9 nM Alexa-ATP concentration and half maximal desensitization (DC_{50}) for steady-state desensitization curve was found to be 9.0 ± 0.5 nM Alexa-ATP concentration. This comparison between fractional population of closed-states (based on our models) and steady-state desensitization curve for ATP indicates that the Three-site model describes best the behavior of the functional desensitization curve. Therefore we suggests that at BC_{50} Alexa-ATP concentration (1.8nM) (Fig. 3.21, black trace), majority of receptors would be in partially liganded non-desensitized state (Scheme-I), whereas at DC_{50} Alexa-ATP concentration (9nM) (Fig. 3.21, blue trace), majority of receptors would be in partially liganded desensitized state (Scheme-II). When the dissociation of Alexa-ATP from the P2X1 receptors pre-equilibrated with 3nM, 30nM and 300nM Alexa-ATP was monitored in the presence of MgORI buffer (Fig. 3.20F), different rates of dissociation of Alexa-ATP was observed indicating that not only the full occupancy of the receptors (negative cooperativity) but also the partial occupancy of functional state of the receptors regulates the allosteric interactions between subunits and therefore can influence the dissociation of the bound agonist.

To conclude, the use of Alexa-ATP, a fluorescent analog of ATP allowed us to distinguish between various functional states of P2X1 receptors. We successfully demonstrated the existence of negative cooperative contributions between P2X1 receptor subunits which controls the dissociation of bound agonist molecules. Our proposed model is highly compatible with our experimental results and can possibly be used to describe similar events even in some related ligand gated receptors. Based on these evidences, we estimated that binding of three agonist molecules per receptor is required to desensitize the P2X1 receptors.

4.3 Probing structural rearrangements in P2X receptors during ligand-receptor interactions

Various mutagenesis and chemical labeling studies have been performed on P2X receptors to probe the domains involved in ligand binding. These studies have so far been confined to identify the key residues which form the part of ligand binding pockets [37,41,42,188], transmembrane domains [189,190] and the channel pore [57]. However, the events that lead to channel opening after ATP binding remain unanswered.

To enhance our understanding of the molecular mechanisms involved in P2X1 receptors activation and desensitization, I used engineered cysteine mutants of CRD-1 region of the P2X1 receptors. The accessibility of free cysteine was determined by an environmental sensitive cysteine reactive fluorophore, TMRM. We monitored changes in the TMRM fluorescence intensity in the TMRM accessible mutants with concurrent measurement of current using voltage clamp fluorometry (VCF). Changes in the fluorescence intensity at different positions were found to be kinetically correlated with receptor activation or desensitization. We speculate that the CRD-1 region of P2X1 receptors is highly dynamic and is an active part of the conformational wave which originates after ligand binding.

Functional expression of CRD-1 mutants

P2X receptors contain ten conserved cysteine residues (designated as C1 to C10) in the extracellular region arranged in two "cysteine-rich-domains" (CRDs). Earlier studies have suggested a unique pattern of disulfide bridges in these regions, in which, C1 pairs with C6, C2 pairs with C4, C3 pairs with C5 in CRD-1 region and C7 pairs with C8, C9 pairs with C10 in CRD-2 region [45,46]. Although, P2X receptors show no sequence homology to any known protein, they share an apparent structural homology with acid sensing ion channels (ASICs). Recently, high resolution structure of ASIC1 was solved [26], which revealed that the "thumb" domain which lies at the interface between subunits shows extensive interactions with the "palm" domain of the neighboring subunit. The "thumb" domain of ASIC1 which is a part of CRD-1 region of ASICs is structurally comparable to the CRD-1 region of P2X receptors. This led us to speculate that the CRD-1 region of P2X1 receptors might also lie at the interface between subunits and is therefore likely to be involved in subunit-subunit interactions. To this end, eight amino acids from A118 to I125 were individually mutated to

cysteine residue in P2X1 receptors in order to generate a free cysteine residue in the CRD-1 region. Earlier findings have shown that the construction of a free cysteine residue in the CRD-1 region by individual deletion of these six endogenously occurring cysteine residues has no effect on receptor trafficking, EC_{50} value and mean current produced by mutated receptors as compared to the wild type receptors [46]. Similarly, we found that all the engineered cysteine mutants (A118C to I125C) were functionally expressed on the oocyte cell membrane (Fig. 3.23). Also, they (WT and CRD-1 mutants) showed similar ratio of peak currents generated by 10μM/3μM ATP, suggesting that they maintained similar EC_{50} value of receptor activation (Fig. 3.23A). Surprisingly, these results suggest that changes in the conserved CRD-1 region can be tolerated without compromising the receptor function.

TMRM accessibility to CRD-1 mutants

Substituted-cysteine accessibility method (SCAM) is a powerful technique that uses the specificity of sulfhydryl chemistry [191]. Cysteine residues contain sulfhydryl groups that react with a variety of sulfhydryl-specific reagents. By using site directed mutagenesis, individual amino acids in the protein can be mutated to a cysteine residue. The sulfhydryl group of the cysteine residue in a membrane protein (e.g. ion channel) could be in one of the three environments: the water accessible surface, the lipid-accessible surface or in the protein interior. In aqueous media sulfhydryl reagents react with ionized sulfhydryl groups billion times faster than with un-ionized –SH groups [192]. On the other hand, if a sulfhydryl group is in the lipid-accessible surface or in the protein interior, it will not be reactive, because ionization of –SH is suppressed due to the low dielectric constant of the environment [193]. TMRM is a cysteine reactive fluorophore and its fluorescence intensity depends on its local environment. Its fluorescence increases when there is an increase in the hydrophobicity in its close vicinity. The maleimide moiety in the TMRM spontaneously forms a covalent bond with a free cysteine; therefore it can be used to specifically label any accessible engineered or endogenous cysteine residue(s) in the protein of interest. Any change in the fluorescence of the attached TMRM will be associated with the local change in the environment around that residue. Due to this advantage, TMRM has been successfully used in the past to sense the conformational changes associated with the structural rearrangements in various ion channels [140,143,145,165] and ion pumps [144]. For CRD-1 mutants we found that TMRM was only accessible to six positions from N120C to I125C. The other two engineered cysteine residues (A118C and E119C) showed no TMRM labeling (Fig. 3.23C) which suggests that residues

A118 and E119 are probably deeply embedded in the structure of P2X1 and are therefore not available for spontaneous TMRM labeling.

Agonist and antagonist binding induces structural rearrangements in the CRD-1 region of P2X1 receptors

Concurrent measurement of current and change in the fluorescence intensity of the attached fluorophore to the engineered cysteine residues in nicotinic acetylcholine [143] and glycine receptors [145] showed that two different agonists could induce distinct protein movements during activation. It is an interesting observation as it suggests that although the end result of agonist binding to the receptor is activation of the receptor, but activation can be achieved by different transitions in the receptor itself. Thus, VCF could give an unprecedented resolution to study ligand-receptor interactions in real time which is otherwise not possible using conventional electrophysiology or fluorescence methods alone. It has been shown that similar to Cys-loop receptors, the agonist binding site in P2X receptors is formed at the interface between subunits [42]. It is therefore likely that allosteric interactions between subunits, originated after binding of agonist, are translated to the pore region of the receptors which finally leads to the process of gating. However, competitive antagonists like NF279, NF449 [94], also compete for the same binding site as that of an agonist, but the allosteric interactions between subunits originated after binding of an antagonist are not translated into the process of gating. Therefore, to detect agonist and antagonist mediated transitions in P2X1 receptors, we used VCF. Of note, the expression level of the cysteine mutants has been suggested as a limiting factor in observing any change in the fluorescence in VCF [165]. We have also observed that a high level of expression (>2μA) of these CRD-1 mutants was needed to observe any change in the intensity of TMRM fluorescence during structural rearrangements in the receptor. Therefore all our data is recorded from the cells expressing >2μA of current which avoided any ambiguities arising from lower expression.

In our allosteric model of ligand-receptor interactions (Fig. 3.16), we proposed that binding of three agonist molecules leads to opening and then desensitization of P2X1 receptors. When change in the fluorescence intensity of the attached TMRM was monitored after binding of ATP to the receptors, we detected some of the several transitions induced by agonist in five mutants (N120C, P121C, E122C, G123 and I125C) of the P2X1 receptors (Fig. 3.23D). Interestingly, during these conformational rearrangements, three mutants (N120C, G123C and

I125C) showed decrease in the TMRM intensity, while, the other two mutants (P121C and E122C) showed an increase in the fluorescence (Fig. 3.23D and 3.24). These results suggest that there are some structural rearrangements occurring in the receptors after agonist binding, where, different residues move independently and therefore are exposed to different environments leading to an increase or decrease in the intensity of TMRM attached to them. However, it is not possible to comment on different conditions responsible for such changes in TMRM fluorescence i.e. if change in the fluorescence intensity is occurring due to the physical movement of the particular residue of interest in different environments or if change in fluorescence is due to the movement of some quenching groups (portion of protein) towards or away from the fluorophores.

Nevertheless, the kinetics of fluorescence change could be used to extract valuable information about different states of the receptor e.g. kinetics of change in the fluorescence correlated with the desensitization phase in acetylcholine receptors [143], kinetics of change in the fluorescence correlated with the displacement of gating charges in shaker K^+ channel [128]. Similarly, we correlated the kinetics of change in the TMRM fluorescence (ΔF) during activation and desensitization in these mutant receptors with different states of the receptor (Fig. 3.24 and Fig. 3.25). In mutants N120C, G123C and I125C the fluorescence change was nearly complete when the peak current was reached and therefore was strongly correlated with the activation of receptors, whereas, in the mutants P121C and E122C the fluorescence change was still incomplete or not started when the peak current was reached and accordingly was strongly correlated with the onset of desensitization.

During the recovery from desensitization when receptors were activated with 10μM ATP-γS, significant fractions of receptors were recovered from desensitization after 5 min washout in the presence of ligand free buffer (Fig. 3.26). Due to a constant drift in the fluorescence baseline probably due to photobleaching, it is difficult to kinetically analyze the recovery of fluorescence signals. However, the percent recovery of current signals after desensitization is correlated with the percent recovery of the fluorescence signal (Table 3.15), suggesting that the recovery from desensitization not only involves dissociation of bound agonist from the desensitized receptors, but also involves reversal of structural rearrangements back to the closed state. In the Cys-loop receptors, Chang et al. have demonstrated agonist mediated changes in the fluorescence of attached fluorophore in loop A, C and E, where they concluded that the movements in these loops are likely to represent the closure of the agonist binding pocket upon agonist binding [140]. The CRD-1 region of P2X receptors also forms a loop like

structure, therefore, it is likely that the CRD-1 region is a part of the conformational wave which initiates on activation of receptors and continues until closing of the agonist binding pocket. The movements in the CRD-1 mutants are therefore likely to represent this conformational wave.

Chang et al. [140] further revealed interesting observations that even competitive antagonists could alone induce distinct conformational changes in the loops A and E. Thus, suggesting that competitive antagonists do not merely occupy the ligand binding site, but also induce discrete conformations by "actively" stabilizing the closed state of the channel. In the P2X1 receptors, suramin analogs (NF279, NF449) have been shown to have competitive antagonist properties [94], indicating that if NF449 occupies the binding pocket, ATP cannot bind to the receptors. In the present study, when the effect of NF449 was tested on three mutants (N120C, P121C and E122C), an increase in the fluorescence was observed in P121C and E122C similar to that induced by agonist binding (Fig. 3.27). It is quite surprising that binding of agonists and antagonists produced a similar change in the fluorescence in P121C and E122C mutants. However, the kinetics of increase in fluorescence induced by NF449 was nearly an order of magnitude slower as compared to increase in the fluorescence intensity induced by ATP in these mutants (Table 3.14 and 3.16). Possibly the huge structure of NF449 as compared to ATP (Fig. 1.4 and 1.5) is responsible for the observed slow changes in the fluorescence induced by NF449 as it might induce constraints in the movement of the CRD-1 loop around the binding site.

These results provide a stronger clue in P2X1 receptors that both agonist and antagonists could induce structural rearrangements. Although, our finding is unique for P2X superfamily, Chang et al. have also reported similar findings in Cys-loop receptors i.e. on loop C of GABA receptors [140], where loop C which is thought to be a key element in triggering channel activation responds with similar changes for both agonists and antagonists. The reason for apparent lack of discrimination between agonists and antagonist by these mutants in P2X1 receptors is currently unknown. However, it is interesting to note that NF449 showed no detectable change in the fluorescence on N120C mutant, where ATP showed a significant change in the fluorescence at this position, suggesting that N120 position is possibly a part of agonist specific conformational change.

An insight into the scheme for ligand-receptor interactions in P2X1 receptors

It is known for P2X receptors that the rate of recovery from desensitization depends on the agonist used to induce the desensitization [194], and dissociation of bound agonist is the limiting factor in the process of recovery from desensitization [88]. Based on such observations, we have proposed a simple allosteric model of ligand-receptor interactions of P2X1 receptors (Fig. 3.16), that binding of three agonist molecules to the resting state would transform the receptors to the open and then to the desensitized states. Desensitized receptors transform more slowly to the resting state by dissociating the bound agonist after hundreds of seconds. As binding of antagonists does not induce functional response from the receptors, it is difficult to study antagonist-receptor interactions. Therefore, it is currently unknown if the binding of an antagonist would also induce a desensitized state in the P2X1 receptors by bypassing the open state.

To understand the molecular mechanisms of ligand-receptor interactions at the resolution of amino acid level, we monitored ligand induced changes in the fluorescence intensity of TMRM attached to various mutants of CRD-1 region. It was found that N120C mutant showed change in the fluorescence only upon agonist binding and not upon antagonist binding (Fig. 3.24) (Table 3.13 and 3.16). On the other hand P121C and E122C mutants showed similar change in fluorescence upon both agonists and antagonists binding (Fig. 3.24 and 3.27). Moreover, kinetic analysis of change in the fluorescence and current waveform (after agonist binding) of these mutants suggests that change in the fluorescence of N120C could be correlated with the onset of receptor activation and change in the fluorescence in P121C and E122C mutants could be correlated with the onset of desensitization. In P2X1 receptors, desensitization can only be induced after activation of receptors [104], suggesting that the desensitized state of P2X1 receptors is an agonist bound closed state. Therefore, if mutants P121C and E122C sense the desensitization phase of P2X1 receptors after agonist binding and if the antagonist (NF449) also induced similar changes in these positions, then it is possible that binding of an antagonist could also induces desensitization in P2X1 receptors. Thus, we speculate that ATP (agonist) would induce desensitization in P2X1 receptors after opening the receptors, whereas, NF449 (antagonist) would induce desensitization by bypassing the open state. However, the rate of recovery from the desensitized state will be governed by the rate of dissociation of bound ligand either agonist or antagonist from the desensitized closed state.

To conclude, our findings demonstrate for the first time that in P2X receptors, binding of both agonist and antagonist could induce structural rearrangements in the CRD-1 region. Different positions could sense different structural rearrangements. Antagonists could also induce desensitization in P2X1 receptors without opening them. We strongly believe that these results would serve as a milestone in the P2X research to understand its structure-function relationship.

5. Miscellaneous results

5.1 Introduction

In 1935, Dr. Aleksander Jablonski proposed an illustration of the electronic states of a molecule and the transitions between them. The states are arranged vertically by energy and grouped horizontally by spin multiplicity (2S+1, i.e. spin multiplicity denotes the number of possible quantum states of a system with principal quantum number S). At room temperature, fluorescent molecules are predominantly present in the lowest vibrational level of the electronic ground state S_0 (Fig. 5.1).

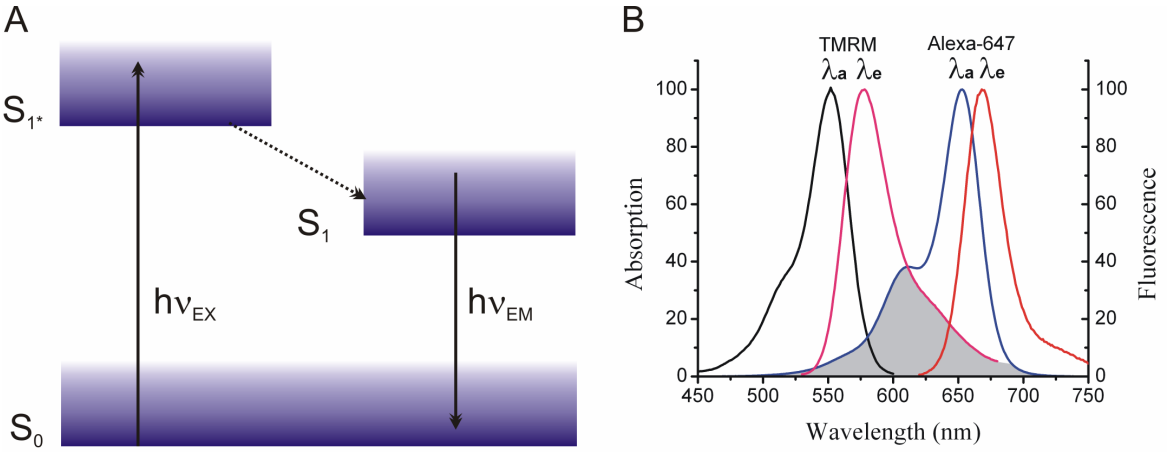

Fig. 5.1 Excitation and emission of a fluorophore: (A) Jablonski diagram, showing ground state of fluorophore as S_0. Upon absorbing a photon with energy ($h\nu_{EX}$), fluorophore reaches excited state (S_{1*}). After dissipating part of the energy, the molecule reaches to singlet state (S_1) (ground state of the excited state). From S_1 state, molecule would emit photons of lower energy ($h\nu_{EM}$) and reach to ground state (S_0). **(B)** Spectral properties of TMRM and Alexa-647 fluorophores. The gray area in the spectral diagram represents the overlap within the emission spectra of TMRM and absorption spectra of Alexa-647. It means, if two different fluorophores (TMRM and Alexa-647) are in "close-proximity" (1-10nm) then the first fluorophore (TMRM) would non-radiatively transfer energy from S_1 state to the other fluorophore (Alexa-647), leading to the excitation of other fluorophore (Alexa-647). Finally the other fluorophore would emit photons of lower energy ($h\nu_{EM}$). This non-radiative transfer of energy from one fluorophore to other is termed as FRET.

A molecule can absorb a photon of energy ($h\nu_{EX}$) supplied by an external source such as a lamp or a laser, thus creating an excited electronic singlet state (S_{1*}). The absorption of a photon is achieved within about 10^{-15}s. The excited state exists for a finite time (10^{-12}s). During this time, the fluorophore undergoes conformational changes and is also subjected to a

multitude of possible interactions with its molecular environment. These processes have two important consequences. First, the energy of S_{1*} is partially dissipated, yielding a relaxed singlet excited state (S_1) from which the fluorescence emission originates. Second, not all the molecules excited initially by absorption return to ground state (S_0) by fluorescence emission. Other processes such as collisional quenching, fluorescence resonance energy transfer (FRET) and inter-system crossing may also depopulate S_1 [195]. From the relaxed excited state (S_1), the molecule finally returns to ground state (S_0) by emitting photon of energy $h\nu_{EM}$. Due to energy dissipation during excited state lifetime, the energy of this photon is lower and therefore of longer wavelength than excitation photon ($h\nu_{EX}$). The difference in energy or wavelength is called Stokes shift. The Stokes shift is fundamental to the sensitivity of fluorescence technique because it allows the emission photons to be detected against a background isolated from excitation photons. The fluorescence quantum yield is measured as a ratio between the number of fluorescence photons emitted from relaxed excited state (S_1) to the number of photons absorbed during the transition from S_0 to S_{1*} (Fig. 5.1).

5.2 Fluorescence resonance energy transfer (FRET)

Electronic excitation energy can be efficiently transferred non-radiatively between a fluorescent energy donor and a suitable energy acceptor over a distance as large as 10nm. In 1948, Förster proposed a theory for this dipole-dipole energy transfer process which postulated that the rate of energy transfer (k_T) depends on the inverse sixth power of the distance between the donor and acceptor [196]. Later, Stryer and Haugland suggested that the energy transfer could be used as a spectroscopic ruler in the 1-6nm range to reveal proximity relationships in biological macromolecules [197]. According to Förster's theory, the rate of energy transfer (k_T) and the efficiency E are given by following equation:

$$k_T = (r^{-6} K^2 J n^{-4} k_F) \, x \, 8.71 \, x \, 10^{23} \; s^{-1}$$

$$E = [r^{-6}/(r^{-6} + R_0^{-6})]$$

$$R_0 = (JK^2 Q_0 n^{-4})^{1/6} \, x \, 9.7 \, x \, 10^3 \; \text{Å}$$

The geometric variables in the above expressions are: R_0, the distance at which the transfer efficiency is 50%; r, the distance between the centers of the donor and acceptor fluorophores; K^2, the orientation factor for dipole-dipole interactions. The spectroscopic variables in the above expressions are: J, the spectral overlap integral; n, the refractive index of the medium

between donor and acceptor; k_F, the rate constant for fluorescence emission by the energy donor; and Q_0, the quantum yield of fluorescence of the energy donor in the absence of acceptor. Efficient transfer requires that the energy donor and acceptor must be in resonance, which means that the fluorescence emission spectrum of the donor must overlap the absorption spectrum of the acceptor, as measured by the spectral overlap integral J ($cm^3\ M^{-1}$) in the following equation:

$$J = \frac{\int F(\lambda)\,\varepsilon(\lambda)\,\lambda^4\,d\lambda}{\int F(\lambda)\,d\lambda}$$

In the above expression, $F(\lambda)$ is the fluorescence intensity (a.u.) of the energy donor at wavelength λ (cm), and $\varepsilon(\lambda)$ is the extinction coefficient ($cm^{-1}\ M^{-1}$) of the energy acceptor. The medium between energy donor and acceptor has a relatively small effect on the energy transfer process (n^{-4}) provided that it is transparent over the range of wavelengths at which the donor emits [198].

From the above equations, it is clear that the rate of transfer depends on three important parameters: (1) the overlap of the donor emission and acceptor absorption spectra (parameter: J); (2) the relative orientation of the donor absorption and acceptor transition moments (parameter: K2, range 0 to 4); (3) the refractive index (parameter: n^{-4}, range ~1/3-1/5) [199].

5.3 Structural information about P2X receptors

Mutagenesis experiments have given some insight into the structural details of P2X receptors. Since year 2000, many attempts have been made to determine the three-dimensional structure of P2X receptors. A low resolution structure of rP2X2 receptors based on electron microscopy of single particles indicated that P2X2 receptors would have a volume of ~1200nm^3 [73]. However, the orientation of the molecule was not assigned. Later using atomic force microscopy (AFM), Barrera et al. suggested a smaller molecular volume of 490nm^3 [72]. Only recently, Young et al. suggested a distance of 5.6nm between the C-terminal tails of subunits [200] using FRET between yellow (YFP) or cyan (CFP) fluorescent protein tags at the C-terminal tails of P2X4 receptors. Furthermore, using single particle analysis and domain specific labeling they determined the three-dimensional structure of P2X4 receptors at a resolution of 21Å and its orientation with respect to the lipid bilayer. They found that P2X4 receptors are globular torpedo like molecules with a volume of ~270nm^3. P2X4 ectodomain

has a compact propeller-shaped structure (Fig. 5.2). In a similar study based on single particle analysis using cryo-electron microscopy of P2X2 receptors, Mio et al. have proposed a refined structure of P2X2 receptors at the resolution of 15Å [201]. Their study revealed a closed state of P2X2 receptors in an elongated vase-shaped structure of 202Å in height and 160Å in major diameter (Fig. 5.2).

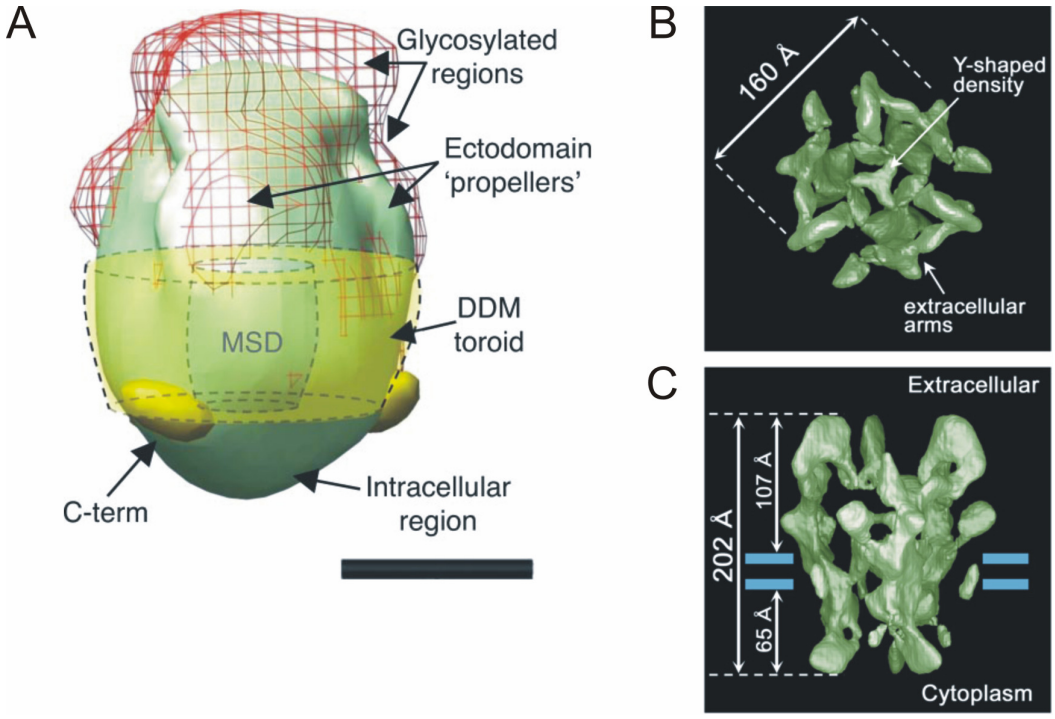

Fig. 5.2 Three-dimensional structures of P2X receptors as revealed by cryo-electron microscopy: (A) Side view of human P2X4 receptors in upright position (Ectodomain at top and C-terminal tail region at bottom). Yellow ball like structures at the C-terminal region are the gold particles. The distance between them was found to be 5.6nm. MSD denotes "membrane spanning domain". Scale bar represents 50Å. Structure of P2X4 receptors appears to be a shape of "torpedo" [200]. **(B)-(C)** Top and side view of rat P2X2 receptors respectively determined at the resolution of 15Å. The diameter and the height of P2X2 receptors were estimated to be ~160Å and ~202Å respectively. Structure of P2X2 receptors appears to be a shape of "elongated vase" [201].

When compared to acetylcholine receptors (AChR), whose structure was also determined using cryo-electron microscopy [202], both AChR and P2X2 receptors showed many structural similarities. Both of them have tall, fin shaped extracellular walls, wider at the outside and narrower at the transmembrane regions, forming a low density funnel like structure. However, AChR was found to be 160Å in height and P2X2 receptors was found to be taller (202Å in height).

P2X receptors show no obvious sequence similarities to known crystallized proteins; this reduced the possibilities to produce homology based models. However, acid-sensing ion channel subtype-1 (ASIC-1) whose structure was recently determined at 1.9Å resolution [26], showed striking similarities with P2X receptors i.e. trimeric subunit topology, central pore lined primarily by TM2 [26,203], large extracellular loop with cysteine-rich domains (CRDs). High resolution structure of ASIC-1 revealed that the "thumb" domain, which lies at the interface between subunits, shows extensive interactions with the "palm" domain of the neighboring subunit [26]. The "thumb" domain of ASIC1, which is a part of CRD-1 region, is structurally comparable to the CRD-1 region of P2X receptors (Fig. 5.3). This led us to speculate that the CRD-1 region of P2X1 receptors might lie at the interface between subunits and is therefore likely to be involved in subunit-subunit interactions.

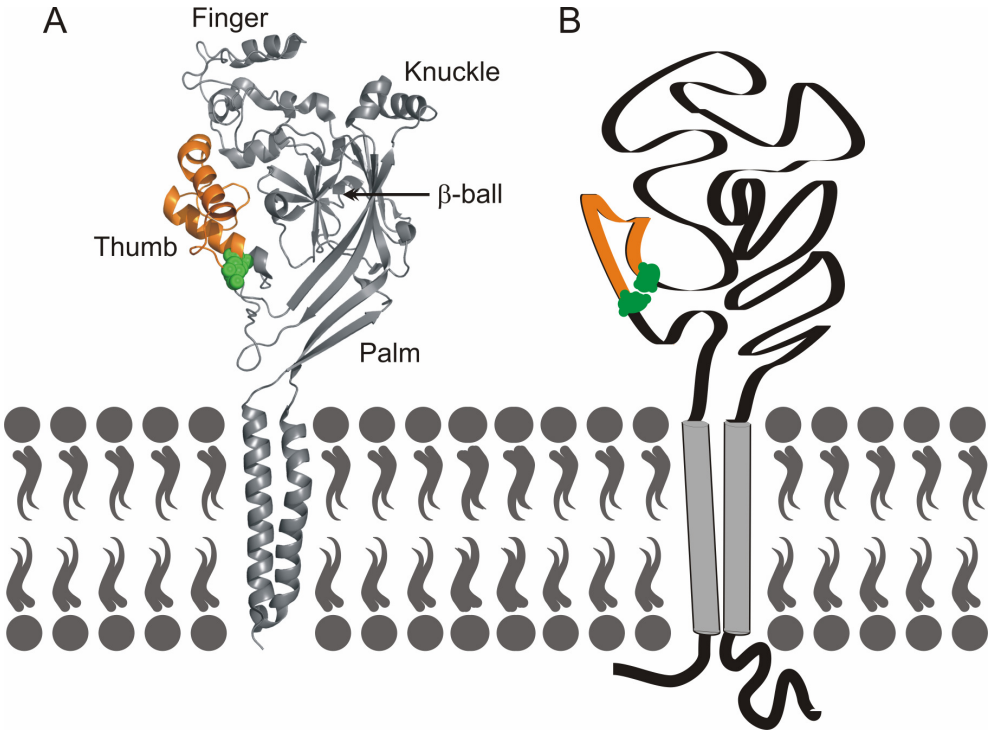

Fig. 5.3 Structural representation of ASIC-1 and P2X receptors: (A) Experimentally determined membrane topology for ASIC-1 [26]. **(B)** Schematic representation of P2X receptors based on the current understanding. Thumb region (orange color) in ASIC-1 structure (CRD-1 domain) is structurally comparable to the CRD-1 region of P2X receptors. In ASIC-1 thumb region, green color represents the C309 and C362. In P2X receptors it represents C117 and C165 (P2X1 numbering).

Therefore, in the following section, spatial proximity of C117 with respect to the binding pocket of P2X1 was determined using FRET between TMRM attached to C117 (in the mutant C165S) and Alexa-ATP bound to the ATP binding pocket.

5.4 FRET between TMRM and Alexa-ATP in C165S mutant of P2X1 receptors

Alexa-647 ATP (a fluorescent ATP analog) has agonist potency on wild type P2X1 receptors (Fig. 3.11). Spectral properties of TMRM and Alexa-ATP allowed their use as a FRET pair, in which TMRM acts as a donor fluorophore and Alexa-ATP acts as the acceptor fluorophore (Fig. 2.4) (Table 5.1).

Table 5.1: R_0 values for Alexa Fluor dyes*

Donor	Acceptor					
	Alexa Fluor 488	Alexa Fluor 546	Alexa Fluor 555	Alexa Fluor 568	Alexa Fluor 594	Alexa Fluor 647
Alexa Fluor 350	50					
Alexa Fluor 488	NA	64	70	62	60	56
Alexa Fluor 546		NA		70	71	74
Alexa Fluor 555			NA		47	51
Alexa Fluor 568				NA		82
Alexa Fluor 594					NA	85
Alexa Fluor 647						NA

* R_0 values in Å represent the distance at which fluorescence resonance energy transfer (FRET) from the donor to the acceptor dye is 50% efficient. The table is reproduced from Molecular Probes Handbook. The emission maximum of TMRM is 580nm, thus indicating the R_0 of 82-85nm during FRET between TMRM and Alexa-647.

We used FRET signal between TMRM attached to an engineered cysteine residue and the Alexa-ATP bound to the binding site of the receptor, to map the spatial location of the engineered cysteine residue with respect to the binding site. Interestingly, the CRD-1 region of P2X1 has six endogenous cysteine residues that form a unique pattern of disulfide bridges as follows: C117 (C1) pairs with C165 (C6), C126 (C2) pairs with C149 (C4) and C132 (C3) pairs with C159 (C5) (Fig. 1.1). Published observations from other groups suggest that the

individual deletion of these endogenous cysteine residues in CRD-1 region does not affect the functionality of receptors, but renders one corresponding free accessible cysteine residue which can be specifically labeled by cysteine reactive probes [46]. In the present study, one of the mutant i.e. C165S (which renders the C117 residue as free cysteine), was used. As a preliminary experiment, spatial proximity of C117 residue to the agonist binding site was determined with the help of FRET between TMRM bound at C117 residue and Alexa-ATP bound at the binding site of the mutant (Fig. 5.4).

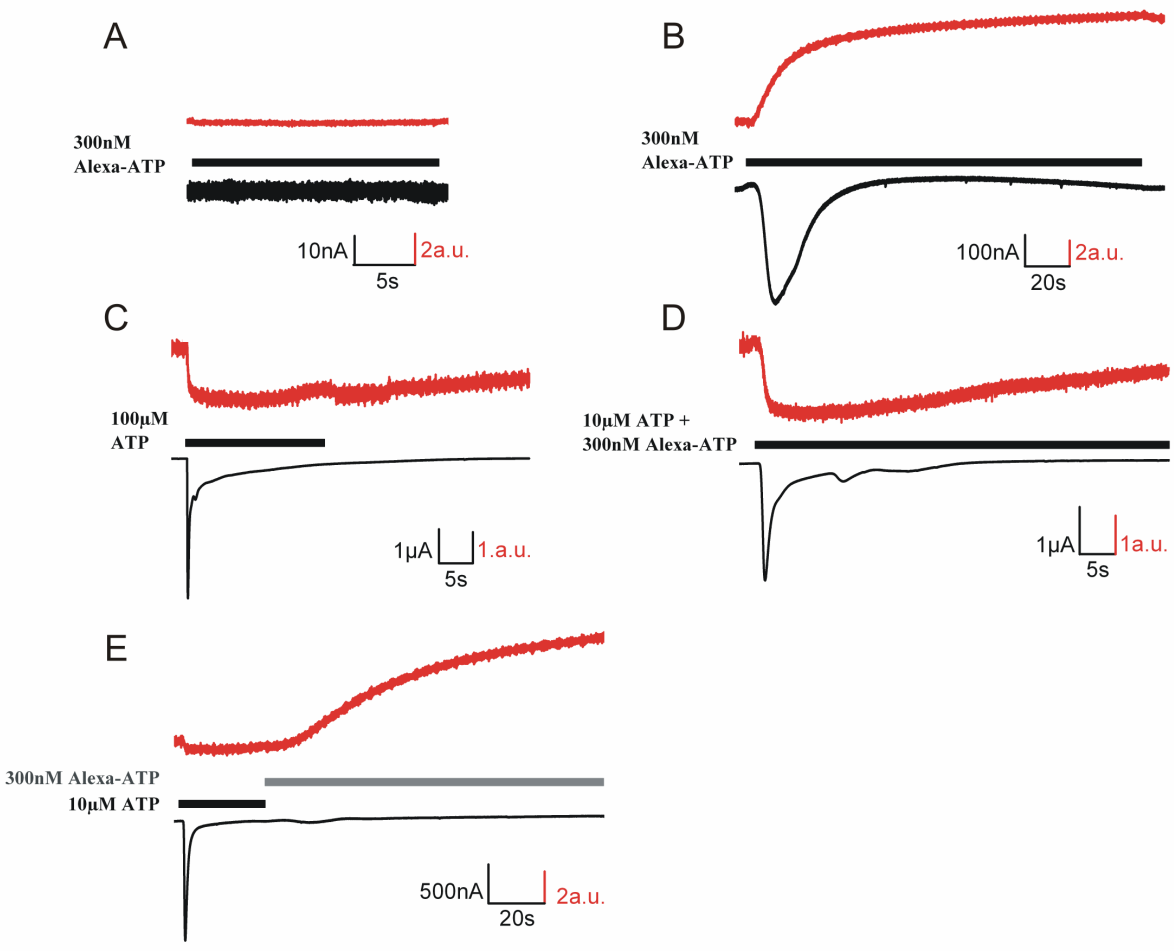

Fig. 5.4 FRET between TMRM and Alexa-ATP: Concurrent recording of current and change in TMRM fluorescence during different agonist application **(A)** 300nM Alexa-ATP applied to the control cell. This represents a control experiment for the FRET filter sets used in the present study. Mere presence of Alexa-ATP in the solution/medium showed no change in the fluorescence signal indicating FRET filter sets of appropriate cutoff. **(B)** C117 mutant activated with 300nM Alexa-ATP only. Specific FRET (as decreased TMRM fluorescence) signal suggests that TMRM is accessible to C117 position and lies in close proximity to the binding site of P2X1 receptors. **(C)** C117 mutant activated with 100µM ATP only. Application of high concentrations of ATP to TMRM labeled C117 showed an increase in TMRM fluorescence during receptor activation. Level of increased fluorescence remained constant over a long period indicating that binding of ATP

initiates some structural rearrangements in or around C117 position and their slow reversibility as sensed by TMRM alone. **(D)** C117 mutant activated with co-application of 10µM ATP + 300nM Alexa-ATP. Only increase in TMRM fluorescence was observed suggesting saturation of all the binding sites with ATP, therefore Alexa-ATP could not bind. This also suggests that FRET between TMRM and Alexa-ATP is highly specific and cannot occur by the mere presence of Alexa-ATP in solution. **(E)** C117 mutant first activated with 10µM ATP followed by 300nM Alexa-ATP. This suggests that all the binding sites were first occupied by ATP. When ATP was washed in the presence of Alexa-ATP, a slow decrease in TMRM fluorescence was observed due to FRET, because of the slow dissociation of ATP and replacement of the vacant binding sites by Alexa-ATP. In all the above experiments, TMRM was excited by incident light and change in TMRM fluorescence (up as decrease, down as increase) was measured during different agonist application using FRET filter sets (Fig. 2.4). TMRM fluorescence is expected to decrease as a result of FRET when TMRM and Alexa-ATP are in spatial proximity of 1-10nm.

In these experiments, TMRM treatment to control oocytes (No RNA injected) or oocytes expressing C117 cysteine mutant was done by incubating the oocytes in CaSORI buffer containing 3µM TMRM for 15 min on ice in dark. The labeling was brought about by the ability of the maleimide moiety in TMRM to form spontaneous covalent bond with the free cysteine. The excess dye was removed by extensive washing of the oocytes in dye free CaSORI buffer. Labeled oocytes were then stored in dark at room temperature until beginning of measurements. 300nM Alexa-ATP was used to elicit concurrent current response and the FRET. TMRM was excited in the presence of Alexa-ATP and change in the emitted fluorescence of TMRM due to transfer of energy to the Alexa-ATP was used as a parameter for FRET. Above results indicate that the endogenously occurring cysteine residue (C117) is accessible to TMRM labeling which contradicts earlier observations by Ennion et al. [46]. In their study they used MTSEA-biotinylation and found that positions C117 and C165 positions were not accessible for covalent modification. However, we speculate that the position C117 is only accessible to small molecules like TMRM for covalent modification which could explain the difference between their and our findings. Fig. 5.4 shows that FRET between TMRM and Alexa-ATP is highly specific and occurs only when Alexa-ATP binds to the binding site and not just in the solution.

After inducing FRET by Alexa-ATP application, the reversibility of the FRET signal was found to be very slow and incomplete when the C117 mutant was washed in the presence of ligand free buffer in order to dissociate Alexa-ATP,. It was too slow to account for receptor's recovery from desensitization (Fig. 5.5). As P2X1 receptors undergo agonist mediated internalization (see section 3.2.2), a possible explanation for this slow reversibility could be

internalization of Alexa-ATP bound receptors. The decrease in TMRM fluorescence could be associated with the FRET between Alexa-ATP bound to the desensitized receptors and TMRM attached to the C117 residue and (or) the quenching of TMRM fluorescence by the acidic environment of the endosomes (receptor bound internalized vesicles). Also, washout of Alexa-ATP could be hampered in the population of receptors which were internalized after Alexa-ATP activation. Therefore, we thought that the slow trafficking of these internalized receptors back to the surface of the oocyte membrane is responsible for the slow or incomplete recovery of TMRM fluorescence during ligand free washout, qualitatively similar to observations described in chapter 3.2 (section 3.2.2.2). In order to probe this possibility, FRET was measured on phenyl arsine oxide (PAO) treated oocytes. Fig. 5.5 shows the FRET effect and its recovery from PAO treated and non-treated oocytes expressing C117 cysteine mutant.

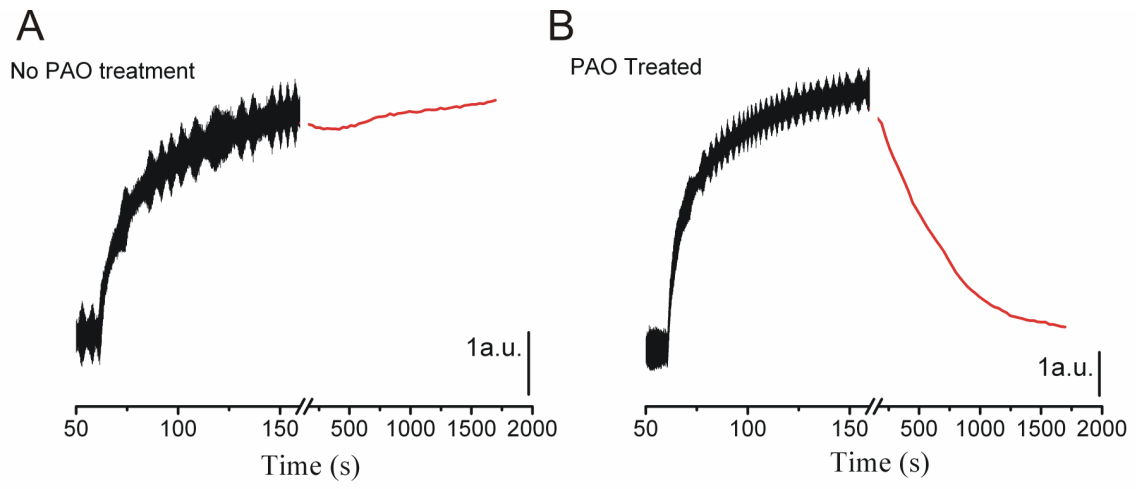

Fig. 5.5 FRET between TMRM bound to C117 residue and Alexa-ATP bound to the agonist binding pocket of this mutant receptor: Representative traces of FRET signal and its reversibility after Alexa-ATP washout from **(A)** Non-PAO treated oocyte; **(B)** PAO treated oocyte. FRET was observed as a decrease in the fluorescence of TMRM (black) upon Alexa-ATP binding to the receptor. Decay of FRET signal after Alexa-ATP washout (red) is slow and incomplete in non-PAO treated oocytes indicating possible internalization of receptors and their slow trafficking back to the surface. Pretreatment of oocytes with PAO (a non-specific internalization blocker) inhibited the agonist mediated receptor internalization, which is evident as the complete reversibility of FRET signal upon Alexa-ATP washout. Fluorescence during Alexa-ATP washout was measured with the light irradiation protocol in which light was applied for 2s every 30s.

It is interesting to note that the recently published 15Å resolution structure of P2X2 receptors [201] suggests that although the diameter of P2X2 receptors is ~160Å, the major portion of the extracellular region of P2X subunits lies in the range of less than 100Å with respect to the interface between subunits where binding of agonist (Alexa-ATP) occurs. Therefore, in the light of the currently available P2X structure, it is highly probable that FRET would occur between bound Alexa-ATP and any engineered cysteine residue in the extracellular region accessible to TMRM. Therefore, due to this limitation further experiments related to FRET studies were not pursued. However, an obvious advantage of the FRET technique in P2X research is to use it as a tool to study association and dissociation kinetics of different ligands. Washing of receptors (bound with non-fluorescent ligands) in the presence of Alexa-ATP will lead to the dissociation of already bound ligands (agonist or antagonist molecules) and thus resulting in the occupancy of Alexa-ATP in the vacant binding sites, which can be observed as an increase in the FRET signal between TMRM and Alexa-ATP. Thus, the rate of occurrence of FRET signal can be used to assess cooperative interactions between subunits or rate of association or dissociation of different ligands.

Summary

P2X receptors are ligand gated ion channels with ATP as their natural ligand. P2X receptors are non-selective cation channels, which upon activation, mediate membrane depolarization and Ca^{2+} influx and have physiological roles ranging from fast excitatory synaptic transmission, modulation of pain-sensation, LTP to apoptosis etc. Currently seven subtypes of P2X receptors are known in mammals designated from P2X1 to P2X7. These receptors express in a variety of cells/tissues which include smooth muscles, dorsal root ganglions and cells of immune origin. Because of their wide expression and diverse roles they may represent an attractive drug target. However, their potential as a drug target is limited by the lack of structural information available. Neither their high resolution structure is available, nor do they show any sequence homology with any known ATP binding proteins, and therefore, most of the structural understanding of P2X receptors comes from their biochemical and biophysical analysis. Based on collective evidences, it is proposed that P2X receptors by themselves constitute the third super-family of ligand gated ion channels, the other two being pentameric Cys-loop receptors and tetrameric ionotropic glutamate receptors. P2X receptors have been proposed to have trimeric subunit topology with cytoplasmic N and C terminal domains. Two putative transmembrane domains in P2X receptors are connected by a large extracellular loop which incorporates the ATP binding domain. Our previous work has proposed that ATP binding domain is located at the interface between receptor subunits. In spite of the structural details available from mutagenesis studies, basic understanding about the structure-function relationship of these receptors is still unclear. In order to better understand how their structure relates to their function and the specific domains involved, I have asked three questions in my thesis:

1) If P2X receptor subunits function independently or interact with each other after ATP (ligand) binding?
2) If interacting, what is the nature of these interactions?
3) Precisely, what are the molecular motions involved in these ligand-receptor interactions?

To determine the behavior of individual subunits in P2X receptors, I have taken advantage of *Xenopus laevis* oocytes heterologous expression system where I expressed recombinant rat P2X1, P2X2 and P2X2/1 receptor chimera (referred as chimera) and activated them using either their natural ligand ATP or other commercially available analogs of ATP. I have used

photo labeling or fluorescence labeling coupled to electrophysiological measurements in order to address the questions stated above. It was a prerequisite for my studies that the number of receptors remains constant, in other words concurrent labeling and current measurement from the same set of receptors in real time was required. I have designed a custom made oocyte chamber which allowed us to do concurrent photolabeling or fluorescence labeling along with the electrophysiological measurements.

Photolabeling causes the irreversible binding of the ligand to the ligand binding site of P2X receptors which overcomes the limitation of ligand unbinding events. After covalently attaching one or more photo-affinity ligands in the binding sites of P2X receptors, one can determine the contribution of the remaining binding sites to the gating process with the help of electrophysiology. Among various photo-affinity ATP analogs available, Benzophenone based ATP analog (BzATP) was found to be best suited for our studies as it can be photolyze at wavelength greater than 300nm, which minimizes the photo induced damage to the cell. In the absence of UV-light BzATP maintained agonist profile on all the three P2X receptors investigated in the present study. Prolonged application of 1µM BzATP on the P2X1 receptors in the absence of light had no effect on the subsequent recovery of receptors from desensitization which indicates that it behaves like the natural ligand ATP in the absence of light. Covalent attachment of BzATP to the ligand binding site of P2X1 receptors occurred only in the presence of UV-light, which was evident by the low recovery of receptors from desensitization in my experiments. This clearly demonstrates that the dissociation of bound agonist constitutes the recovery of P2X1 receptors from desensitization.

On the non-desensitizing P2X2 receptors, BzATP was found to have partial agonist profile. Again, after covalent labeling, the response generated by full agonist (ATP) from the same set of receptors was found to be decreased in P2X2 receptors. These results suggest that if one or two binding sites in P2X2 receptors were covalently occupied by a partial agonist then the efficacy of full agonist decreases. One can infer from these results that all the receptor subunits are contributing towards the gating. On the chimera, BzATP maintained the agonist profile, although it was less potent compared to ATP as was revealed by the complete dose response curve of BzATP and ATP on chimera. Progressive photolabeling of the chimera by saturated concentration of BzATP (1µM) showed an increase in the persistent current which could be specifically blocked by the external application of an open channel blocker i.e. 3mM Neomycin. We speculate that the persistent current from the chimera originated from the receptors in which all the binding sites were covalently attached by BzATP, therefore,

limiting the dissociation of bound ligands. In order to support our conclusion that all the subunits of the P2X receptors are contributing equally to the gating process, we generated complete dose response curves of full and partial agonists on the chimera before and after different levels of photolabeling. The levels of photolabeling were controlled by the amount of exposure of UV-light. We found that after progressive photolabeling, sub-saturating concentration of another full agonist (αβ-MetATP) became more potent as suggested by a leftward shift in the dose response curve. We propose that after photolabeling, the probability that these channels will be fully liganded at any given αβ-MetATP concentration would be higher. In contrary to P2X2 receptors where covalent attachment of a partial agonist (BzATP) decreased the response of full agonist (ATP), we expect on the chimera that covalent attachment of a full agonist (BzATP) should increase the response of a partial agonist. However, none of the ATP analogs have been tested for partial agonist profile on the chimera. As the chimera has high sensitivity towards different ligands, we found that saturating concentrations of TNP-ATP (300nM), which is a known potent antagonist of P2X1 receptors, elicited a weak inward current on the chimera suggesting a partial agonist profile. Upon progressive photolabeling, the efficacy of TNP-ATP on chimera was increased although we found no change in the apparent affinity of TNP-ATP on the chimera. We further estimated that at least two covalently attached BzATP were required to increase the efficacy of TNP-ATP to a maximum. Together, these results suggest that every subunit in P2X receptors contributes to the gating and that the contribution of each subunit towards the gating process is an additive one i.e. as the number of partial agonist in binding sites would increase, receptor response generated by full agonist would decrease and vise versa.

As described above, with the help of photolabeling technique coupled to electrophysiology we investigated the contribution of each receptor subunit to the gating process. Next, with the help of fluorescence labeling of the binding site coupled to electrophysiology, we provide further evidences that P2X receptor subunits are not independent but interacting with each other. It is known that the desensitized state of P2X1 receptors has a high affinity for the bound agonist, which is often associated with the slow dissociation and thereby slow recovery of receptors from desensitization. Moreover, the desensitized state of P2X1 receptors is an electrophysiologically silent state. Therefore, a fluorescent ATP analog was required which could activate and induce desensitization in the P2X1 receptors, so that we could measure the rate of dissociation of bound agonist from the desensitized state. Unfortunately, none of the fluorescent ATP analogs were analyzed for agonist potency on the P2X receptors. To the best

of our knowledge, our study for the first time describes the agonist potency of Alexa-ATP (a fluorescent ATP analog) on the P2X1 receptors and the chimera.

In order to determine the behavior of P2X1 receptor subunits, we used an approach similar to what is commonly used in classical radio-ligand binding experiments i.e. increased dissociation of radio-ligand bound to the receptors in the presence of high concentrations of unlabeled ligand suggest negative cooperativity, whereas reduced dissociation of radio-ligand indicates positive cooperativity. When we measured the dissociation of bound Alexa-ATP (as decay of fluorescence) in the presence and absence of various allosteric (Mg^{+2} and Ca^{+2}) and competing ligands (ATP, TNP-ATP and NF449), we found that the rate of decay of fluorescence was dependent on both, the concentration and the type of competing ligands. However, in all conditions the time course of decay of Alexa-ATP could be described by a mono-exponential function. High concentrations of competing ligands accelerated the rate of dissociation of bound Alexa-ATP suggesting negative cooperativity. On the other hand, in the presence of Ca^{+2} or NF449 (IC_{50} concentration) decreased rate of dissociation of bound Alexa-ATP was found suggesting positive cooperative interaction between subunits. When the recovery of P2X1 receptors from desensitization was functionally monitored in the presence of Ca^{+2} or NF449 (IC_{50} concentration), less receptors recovered from desensitization which again indicates positive cooperative interactions and thus, complement our fluorescence measurements.

In order to understand the negative cooperative interactions between subunits, we propose a simple allosteric model for ligand-receptor interactions. In this model, we speculate that negative cooperativity only occurs in fully occupied receptors and this leads to the fast dissociation of one of the bound Alexa-ATP from the receptors. Our model predicts mono-exponential decay of Alexa-ATP in the presence of high concentrations of competing ligands as the receptors would be fully liganded at all times. Further it predicts biphasic decay of Alexa-ATP in the absence of competing ligands as first Alexa-ATP would dissociate fast under negative cooperativity, whereas, the remaining two bound Alexa-ATP will dissociate slowly without the influence of negative cooperativity. However, our experimentally determined time courses could be described by mono-exponential function in both conditions i.e. presence and absence of competing ligands. In order to understand this ambiguity, the model was simulated using Gepasi 3.0 (MS windows based software) under the framework of our hypothesis proposed for the model. Interestingly, the simulated results exactly replicated our experimental results where, the dissociation of bound Alexa-ATP could be fitted with

mono-exponential function for both the conditions (presence and absence of competing ligands). The fact that the two rate constants (fast and slow) differ only by a factor of two and the difficulty in resolving the first tens of seconds (time taken for wash of nonspecific binding) in the experimentally determined fluorescence decay, could be the reason for this apparent mono-exponential behavior.

Desensitizing P2X receptors immediately undergo desensitization upon activation. However, the number of agonist molecules required to desensitize the P2X1 receptors is still a matter of debate. Therefore as a next study, we have tried to answer this intriguing question. To this end, we tested three hypotheses that binding of one, two or three agonist molecules is required to desensitize P2X1 receptors. First, the occupancy of receptors at different Alexa-ATP concentrations was determined using binding curve and then fractional distributions of 0, 1, 2 and 3 Alexa-ATP bound receptors were calculated for each Alexa-ATP concentration using the binomial equation. In order to use the binomial equation, we considered that the ligand binding in P2X1 receptors is a random process and occur without the influence of cooperativity because the binding rate between the first two ligands and the last ligand is not much different (only factor of two). After pre-equilibrating the binding sites with different Alexa-ATP concentrations, functional activation of P2X1 receptors was determined by near saturating concentrations of ATP (30μM) under voltage clamp conditions. These experiments showed a direct relationship between fractional population of closed-states (0, 1 and 2 bound Alexa-ATP) and the percentage of current generated from these receptors by near saturating concentration of ATP, suggesting that binding of three agonist molecules is required to desensitize P2X1 receptors.

With the use of fluorescent ATP analog and electrophysiology, we found that subunits in P2X1 receptors are not independent but interacting in a cooperative manner. The type of cooperativity however depends on the type of ligands used and their concentrations.

Finally, in order to get some insights into the structure-function relationship of P2X1 receptors, I have investigated the role of different domains/structures in P2X1 receptors during gating and desensitization. To this end, I used TMRM fluorophore as its fluorescence intensity is sensitive towards changes in hydrophobicity. The maleimide group in TMRM can form spontaneous covalent bond with any accessible cysteine residue available in the ionized form. Using site directed mutagenesis; one can engineer a free cysteine in nearly any part of the protein and label it with TMRM. However, the pre-requisite of this technique is to have a free and accessible cysteine on the functionally expressed mutants in the region which could

physically move in such a way that there would be a change in hydrophobicity in or around the engineered cysteine residue. Any change in the hydrophobicity would then be sensed by the attached TMRM during different states of the receptor. The lack of high solution structure of P2X receptors and also the absence of any sequence homology with any known ATP binding protein imposed a limitation for site directed mutagenesis. Luckily, recently solved high resolution structure of ASIC-1 channel is structurally quite correlated with the putative structure of P2X receptors. We intuitively hypothesized that the cysteine-rich-domain (CRD-1) of ASIC-1 is structurally comparable to the CRD-1 domain of P2X1 receptors, in which CRD-1 region acts like a loop, which moves around the ligand binding pocket in order to close it after ligand binding. We mutated eight individual amino acids (position 118 to 125) in the CRD-1 region of P2X1 receptors and their accessibility to TMRM labeling and change in TMRM fluorescence upon activation was determined. Quite surprisingly, all these mutants were fully functional before and after TMRM labeling suggesting that cysteine mutation in this conserved CRD-1 region can be tolerated without compromising receptor function. However, only six positions (120-125) were accessible for TMRM labeling. Upon activation with an agonist, kinetics of decrease in fluorescence was significantly correlated with the receptor activation at positions N120, G123 and I125C, whereas at positions P121C and E122C the increase in fluorescence was significantly correlated with the desensitization of P2X1 receptors, suggesting that different positions in the receptor sense different structural rearrangements. Not only the agonist, but also binding of competitive antagonist (NF449) induced some structural rearrangements in P2X1 receptors. Interestingly, no change in fluorescence at position N120C was seen when NF449 (antagonist) was applied, although binding of NF449 induced similar increase in TMRM fluorescence at positions P121C and E122C as induced by agonist suggesting that binding of antagonist also induced desensitization in P2X1 receptors. Taken together, our results suggest that not only agonists but also competitive antagonists like NF449 could induce structural rearrangements in or around CRD-1 region of P2X1 receptors.

We have been successful in answering some of the interesting questions in the field of P2X research which opens our avenues to many other questions that may be interesting to many of us like the physiological relevance of subunit-subunit interactions. Could it modulate synaptic responses or mediate synaptic plasticity? Other intriguing questions like single channel conductance of 1 or 2 covalently attached BzATP might shed more light in the field. We

strongly believe that our results would serve as a milestone in the P2X research to understand its structure-function relationship and take the P2X research to a next level.

Zusammenfassung

P2X-Rezeptoren sind ligandenaktivierte Ionenkanäle, deren natürlicher Agonist ATP ist. Sie sind nichtselektive Kationenkanäle, die nach Aktivierung Membrandepolarisation und Kalziumeinstrom vermitteln. Sie sind an einer Vielzahl physiologischer Prozesse wie z.B. excitatorische synaptische Übertragung, Modulation des Schmerzempfindens, Langzeit-Potenzierung und Apoptose beteiligt. Bislang sind sieben verschiedene Suptypen bekannt, die als P2X1 bis P2X7 bezeichnet werden. P2X-Rezeptoren werden in einer Vielzahl von Geweben bzw. Zelltypen exprimiert, wie zum Beispiel in der glatten Muskulatur, den dorsalen Wurzelganglien und verschiedenen Immunzellen. Wegen ihrer diversen Expression und der Beteiligung an einer Vielzahl physiologischer Prozessen repräsentieren sie ein viel versprechendes Target für die Medikamentenentwicklung. Eine zielgerichtete Wirkstoffentwickung wird jedoch durch fehlende Strukturdaten erschwert, da weder eine hoch aufgelöste Struktur verfügbar ist, noch Sequenzhomologien zu bekannten ATP-bindenden Proteinen vorliegen. Demzufolge müssen strukturelle Informationen aus biochemischen und biophysikalischen Untersuchungen abgeleitet werden. Die P2X-Rezeporfamilie bildet, neben der Cys-Loop-Rezeptorfamilie und der Glutamatrezeptor-Familie, die dritte Superfamile der ligandenaktivierten Ionenkanäle. Ein funktioneller Rezeptor wird aus drei homologen Proteinuntereinheiten gebildet. C- und N-Termini einer Untereinheit liegen intrazellulär, die zwei transmembranären Domänen sind durch eine große extrazelluläre Schleife verbunden. Erst kürzlich konnte gezeigt werden, dass die ATP-Bindungsstelle an der Grenzfläche zwischen zwei Untereinheiten gebildet wird. Trotz der strukturellen Informationen, die aus Mutagenese-Studien abgeleitet wurden ist die Kenntnis über Struktur-Funktionsbeziehungen nach wie vor sehr begrenzt.

Um ein besseres Verständnis darüber zu gewinnen, wie Struktur und Funktion ineinander greifen und welche spezifischen Strukturen an der Aktivierung und Desensibilisierung beteiligt sind, habe ich meiner Dissertation drei Fragen zu Grunde gelegt:

1) Funktionieren die drei Untereinheiten unabhängig voneinander oder interagieren sie nach der Bindung von ATP oder anderen Liganden?
2) Was ist die Natur einer eventuellen Interaktion?
3) Was sind die molekularen Umlagerungen, die an der Rezeptor-Ligand Interaktion beteiligt sind?

Um das Verhalten einzelner Untereinheiten zu untersuchen, habe ich das *Xenopus laevis* Expressionssystem benutzt und P2X1, P2X2 und eine P2X2/P2X1-Rezeptorchimäre heterolog in *Xenopus* Oozyten exprimiert und diese dann mit ATP und anderen kommerziell verfügbaren Liganden aktiviert. Für meine Untersuchungen habe ich die Methode der Zweielektroden-Spannungsklemme unter gleichzeitiger Anwendung von Photoaffinitäts-markierung und Fluoreszenzmarkierung benutzt. Eine Vorbedingung für diese Untersuchungen war, dass die Markierung und der gemessene Rezeptorstrom von dem gleichen Rezeptorpool stammten. Um dies zu gewährleisten, wurde eine spezielle Messkammer entwickelt. Das hier angewandte Prinzip der Photoaffinitätsmarkierung beruht auf einer irreversiblen Bindung von Liganden an oder nahe der P2X-Rezeptor-Bindungsstelle, was letztlich die Dissoziation des Liganden verhindert. Nach irreversibler Bindung eines oder mehrerer Liganden an den Rezeptor kann dann der Beitrag der noch freien Bindungsstellen bzw. unbesetzten Untereinheiten elektrophysiologisch untersucht werden.

Aus den potentiell verfügbaren Kandidaten wurde BzATP ausgewählt, da es bei Wellenlängen >300 nM aktiviert wird, und dadurch lichtunduzierte Schäden minimiert werden konnten. Im Weiteren konnte gezeigt werden, dass BzATP ein Agonist an allen drei untersuchten Rezeptortypen ist. Eine verlängerte Applikation von BzATP (ohne Belichtung) hatte keinen Effekt auf die Reversibilität der P2X1-Rezeptor Desensibilisierung im Vergleich zu Kontrollmessungen mit ATP. Eine kovalente Bindung von BzATP erfolgte nur während der Belichtung mit UV-Licht, was durch die verminderte Reversibilität der Desensibilisierung nachgewiesen wurde. Dies zeigte, dass die Reversibilität der Desensibilisierung nur nach Dissoziation des Agonisten erfolgen kann.

Am nicht-desensibilisierenden P2X2-Rezeptor wirkt BzATP als partieller Agonist. Es konnte gezeigt werden, dass der ATP-vermittelte Rezeptorstrom nach kovalenter Bindung von BzATP zunehmend vermindert wird. Dieser Befund legt nahe, dass die „efficacy“ von ATP abnimmt, wenn eine oder mehrere (zwei) Bindungsstellen bereits mit BzATP besetzt sind.

An der P2X2/P2X1-Rezeptorchimäre wirkt BzATP als voller Agonist mit einer im Vergleich zu ATP leicht verminderten Wirkstärke. Photoaffinitätsmarkierung mit BzATP führte zu permanenter Aktivierung der Chimäre, wobei der persistierende Rezeptorstrom zur Quantifizierung spezifisch durch den „open-pore“ Blocker Neomycin gehemmt werden konnte. Wir interpretieren dieses Ergebnis dahin gehend, dass der persistierende Rezeptorstrom von der Rezeptorpopulation stammt, in der alle Bindungsstellen kovalent von BzATP besetzt sind.

Um die Hypothese des individuellen Beitrags einzelner Untereinheiten weiter zu untersuchen, wurden Dosiswirkungskurven vor und nach Photoaffinitätsmarkierung aufgenommen. Um das Ausmaß der Markierung zu kontrollieren, wurden die Rezeptoren dem UV-Licht für verschiedene Zeitdauern ausgesetzt. Dadurch konnte gezeigt werden, dass mit zunehmendem Ausmaß der Markierung der volle Agonist αβ-MetATP in seiner Wirkstärke scheinbar zunahm, was sich in einer Linksverschiebung der Dosiswirkungskurve manifestierte. Wir erklären diesen Befund dadurch, dass eine Markierung einer oder mehrerer Bindungsstellen die Wahrscheinlichkeit der Bindung von freiem αβ-MetATP an die verbleibenden freien Bindungsstellen erhöht.

Da die Markierung mit dem am P2X2-Rezepor partiellen Agonisten BzATP die Wirkung von ATP (voller Agonist an P2X2) vermindert, sollte untersucht werden, ob ein partieller Agonist an der Rezeptorchimäre vergleichbare Effekte hervorruft. Allerdings waren bis zum Zeitpunkt meiner Untersuchungen keine partiellen Agonisten an der Rezeptorchimäre untersucht. Daher wurde TNP-ATP, ein hochpotenter P2X1-Antagonist, auf partiellen Agonismus an der Chimäre hin untersucht. Wir konnten zeigen, dass TNP-ATP in einer Konzentration von 300 nM tatsächlich ein sehr schwacher Agonist der Chimäre ist. Nach Photoaffinitätsmarkierung mit BzATP wurde die „efficacy“ von TNP-ATP erhöht, wobei es zu keiner Änderung der Dosiswirkungskurve von TNP-ATP kam. Durch eine statistische Analyse konnte abgeschätzt werden, dass erst die kovalente Markierung von zwei Bindungsstellen mit BzATP die „efficacy“-Erhöhung von TNP-ATP bedingt. Zusammenfassend zeigen diese Ergebnisse, dass jede einzelne Untereinheit des Rezeptors nach Ligandenbindung einen Beitrag zu den Konformationsänderungen liefert, die letztlich zum Öffnen des Kanals führen.

In den oben angeführten Experimenten wurde die Methode der Photoaffinitätsmarkierung und gleichzeitiger Analyse des Rezeptorstroms genutzt, um den Beitrag einzelner Untereinheiten zur Rezeptoraktivierung nach Bindung verschiedener Liganden zu untersuchen. Im folgenden Abschnitt wird unter Zuhilfenahme von Fluoreszenzmarkierung der Bindungsstellen gezeigt, dass die Rezeptoruntereinheiten abhängig von der Ligandenbindung miteinander interagieren, d.h. Kooperativität zeigen.

Es ist bekannt, dass der desensibilisierte Zustand des P2X1-Rezeptors eine hohe, nanomolare Affinität für ATP besitzt, was sich in einer sehr langsamen Reversibilität des desensibilisierten Zustands niederschlägt. Da der desensibilisierte Zustand nicht direkt durch elektrophysiologische Methoden abgebildet werden kann, sollte dieser Zustand durch Nutzung eines fluoreszierenden ATP-Analogon, das sich in Bezug auf Aktivierung und

Desensibilisierung möglichst ähnlich wie ATP verhält, untersucht werden. Zum Zeitpunkt des Beginns dieser Arbeit war keines der kommerziell erhältlichen fluoreszierenden ATP-Analoge an P2X-Rezeptoren getestet, so dass die in dieser Arbeit beschriebenen Experimente erstmals den Einsatz von fluoreszenzmarkiertes ATP als Agonist am P2X1-Rezeptor und der Chimäre beschreiben. Um das Verhalten der Rezeptoruntereinheiten zu untersuchen, wurde ein Ansatz gewählt, der dem bei klassischen Radioligand-Bindungsexperimente ähnelt: eine beschleunigte Dissoziation des Radioliganden in Anwesenheit einer hohen Konzentration eines unmarkierten Liganden bedeutete negative Kooperativität, eine verlangsamte Dissoziation deutet auf eine negative Kooperativität hin. Durch die Messung der Dissoziation von Alexa-ATP (durch Messung der Fluoreszenzintensität) in An- und Abwesenheit verschiedener allosterischer Modulatoren (Mg^{2+} und Ca^{2+}) und kompetitiver Liganden (ATP, TNP-ATP und NF449), konnten wir zeigen, dass die zeitliche Abnahme der Fluoreszenz von der Konzentration und der Art des anwesenden Liganden oder Modulators abhing. Der zeitliche Verlauf der Abnahme konnte dabei in allen Fällen durch eine monoexponentielle Funktion beschrieben werden. Hohe Konzentrationen der kompetitiven Liganden beschleunigten die Dissoziation von Alexa-ATP, gleichbedeutend mit negativer Kooperativität. Im Gegensatz dazu wurde die Dissoziation in Anwesenheit von 2 mM Ca^{2+} und der IC_{50} Konzentration von NF449 (0.3 nM) verlangsamt, was positive Kooperativität bedeutet. Die funktionelle Untersuchung der Reversibilität der Desensibilisierung des P2X1 Rezeptors ergab eine starke Verlangsamung in Anwesenheit von Ca^{2+} und konnte damit die Befunde aus den Flureszenzmessungen bestätigen. Zur Beschreibung der vorgenannten Befunde wurde ein einfaches Reaktionsmodell für die Rezeptor-Liganden-Interaktion heran gezogen. Dieses Modell beinhaltet, dass die negative Kooperativität nur im vollständig mit Ligand besetzten Zustand des Rezeptors vorliegt, was zu einer beschleunigten Dissoziation des jeweils ersten von den insgesamt drei gebundenen Liganden führt. Das Modell sagt in Anwesenheit sättigender freier Ligandenkonzentrationen einen monoexponentiellen Verlauf der Alexa-ATP Dissoziation voraus, was sich mit unseren experimentellen Befunden deckt. In Abwesenheit von freien Liganden sollte hingegen ein biphasischer Verlauf auftreten, da unter diesen Bedingungen der erste Ligand mit einer schnelleren Reaktionsrate als die beiden folgenden dissoziiert. Letztere Vorhersage steht in scheinbarem Widerspruch zu den experimentellen Ergebnissen, die einen monoexponentiellen Verlauf unter allen Versuchsbedingungen – wenn auch mit unterschiedlichen Zeitkonstanten - ergab.

Um diesen Widerspruch aufzulösen wurde der Zeitverlauf unter verschiedenen Bedingungen auf Basis des kinetischen Reaktionsmodells durch Einsatz der Simulationssoftware Gepasi 3.0 numerisch simuliert. Mit einem geeigneten Satz von Ratenkonstanten konnten die simulierten Zeitverläufe mit den experimentellen in Einklang gebracht werden; die simulierten Datensätze konnten für An- und Abwesenheit kompetitiver Liganden hinreichend genau mit einer Exponentialfunktion beschrieben werden. Gründe für das apparente monoexponentielle Verhalten sind zum einen, dass sich die schnelle und langsame Ratenkonstante nur um den Faktor zwei unterscheiden und zum anderen, dass im Experiment die ersten Sekunden nach Beginn des Lösungswechsels wegen der großen Hintergrundfluoreszenz des in Lösung befindlichen Fluorophors nicht dargestellt werden können.

P2X1-Rezeptoren desensibilisieren vollständig unmittelbar nach Aktivierung mit ATP, wobei die Frage wie viele der wahrscheinlich drei Bindungsstellen zur vollständigen Desensibilisierung mit ATP besetzt werden müssen, ungeklärt ist. Um diese Frage aufzuklären, wurden die experimentellen Ergebnisse darauf hin getestet, ob sie mit einer bestimmten zur Desensibilisierung notwendigen Anzahl von gebundenen Liganden kompatibel sind. Aus der Konzentrationsabhängigkeit der Alexa-ATP-Bindung wurden die relativen Rezeptorpopulationen berechnet, die 0, 1, 2, oder 3 Alexa-ATP-Moleküle gebunden hatten. Diese Verteilung wurde mit funktionellen Daten, der Alexa-ATP-Konzentrationsabhängigkeit der Gleichgewichtsdesensibilisierung, verglichen. Die beste Übereinstimmung beider Datensätze konnte unter der Annahme erzielt werden, dass erst die Bindung von drei ATP-Molekülen den Rezeptor öffnet und nachfolgend desensibilisiert.

Durch die sich ergänzende Nutzung von Fluoreszenzmessungen und Elektrophysiologie konnte gezeigt werden, dass eine Kooperativität zwischen den Untereinheiten des P2X1-Rezeptors existiert. Art und Ausmaß dieser Kooperativität hängen dabei von der Art der jeweiligen Liganden ab.

Als letztes ergänzendes Teilprojekt dieser Arbeit wurde die Methode der Voltage-Clamp-Fluorometrie eingesetzt, um Einblicke in die strukturelle Dynamik des P2X1-Rezeptors währen der Aktivierung und Desensibilisierung zu gewinnen. Dazu wurde als Fluorophor Rhodamin-Malemid (TMRM) eingesetzt, das eine kovalente Bindung mit freien Cystein-Resten eingeht und dessen Fluoreszenzintensität von der Hydrophobizität seiner nächsten Umgebung abhängt. Durch ortsgerichtete Mutagenese von einzelnen Aminosäuren zu Cystein kann das Fluoreszenzlabel TMRM dann an definierten Stellen der Rezeptoruntereinheiten angeheftet werden. Allerdings ist die Voraussetzung für eine effektive Markierung die

Zugänglichkeit des Cysteins für TMRM und der Erhalt der Rezeptorfunktionalität nach Mutagenese und Markierung. Nach erfolgreicher Markierung erfolgt eine Fluoreszenzänderung, wenn durch die Konformationsänderung des Rezeptors eine Änderung der Hydrophobizität in unmittelbarer Umgebung des Rhodamins erfolgt. Die Auswahl geeigneter Residuen zur Mutagenese wurde durch das Fehlen jeglicher detaillierter Strukturinformationen und Sequenzähnlichkeiten zu anderen Proteinen für den P2X1-Rezeptor erschwert. Daher wurde die kürzlich publizierte Kristallstruktur des ASIC-1 (acid sensing ion channel 1) aufgegriffen, da ASIC-1 ebenfalls wie der P2X1-Rezeptor eine Cystein-reiche Domäne aufweist, von der beim ASIC-1 angenommen wird, dass sie als Schleife fungiert, die nach Ligandenbindung eine Konformationsänderung erfährt. Durch diese Analogie angeregt, wurden die ersten acht Residuen (Aminosäuren 118-125 zwischen dem ersten und zweiten endogenen Cystein) der ersten Cystein-reichen Domäne (CRD-1) des Rezeptors einzeln zu Cystein mutiert. Die elektrophysiologische Analyse der Mutanten ergab überraschenderweise, dass alle Mutanten funktionell waren und sich nur marginal vom Wildtyp-Rezeptor unterschieden. Eine effektive Markierung mit TMRM konnte für die Mutanten 120C-125C nicht aber für die beiden Mutanten 118C und 119C nachgewiesen werden. Eine Fluoreszenzänderung nach Rezeptoraktivierung mit ATP konnte bei allen markierbaren Mutanten detektiert werden. Bei den Mutanten N120C, G123C und I125C war die Fluoreszenzabnahme zeitlich mit der Rezeptoraktivierung korreliert, bei den Mutanten P121C und E122C bestand eine zeitliche Korrelation zwischen einer Fluoreszenzzunahme und der Rezeptordesensibilisierung. Diese Befunde zeigen, dass die verschiedenen mutierten Residuen unterschiedliche spezifische Konformationsänderung während Aktivierung und Desensibilisierung des Rezeptors erfahren. Darüber hinaus zeigte sich, dass der kompetitiv wirkende P2X1 Antagonist NF449 an den Mutanten P121C und E122C ebenfalls eine Fluoreszenzänderung ähnlich der bei Gabe von ATP hervorrief, was vermuten lässt, dass die antagonistische Wirkung von NF449 auf einer Rezeptordesensibilisierung ohne vorhergehende Aktivierung beruhen könnte. Somit kann am P2X1-Rezeptor nicht nur die Bindung von Agonisten, sondern auch die von Antagonisten eine Konformationsänderung bewirken.

In der vorliegenden Arbeit konnten einige ungeklärte Fragen der P2X-Rezeptorforschung erfolgreich behandelt werden. Aus den vorliegenden Befunden ergeben sich weitere, interessante Fragestellungen wie zum Beispiel die physiologische Bedeutung der Kooperativität bei der Reversibilität der Rezeptor-Desensibilisierung. Eine mögliche

Bedeutung könnte diese Kooperativität zum Beispiel bei der Modulation synaptischer Signaltransduktion oder in der synaptischen Plastizität haben.

References

1. Conley EC: *The ion channel, Factsbook*, vol 1. San Diego: Academic Press; 1996.
2. Le Novere N, Changeux JP: **The Ligand Gated Ion Channel Database**. *Nucleic Acids Res* 1999, **27**:340-342.
3. Clark AJ: **The mode of action of drugs on cells**. Edited by: Edward Arnold & Co.; 1933:1-298.
4. Del Castillo J, Katz B: **Interaction at end-plate receptors between different choline derivatives**. *Proc R Soc Lond B Biol Sci* 1957, **146**:369-381.
5. Colquhoun D: **Binding, gating, affinity and efficacy: the interpretation of structure-activity relationships for agonists and of the effects of mutating receptors**. *Br J Pharmacol* 1998, **125**:924-947.
6. Pallotta BS: **Single ion channel's view of classical receptor theory**. *Faseb J* 1991, **5**:2035-2043.
7. Drury AN, Szent-Gyorgyi A: **The physiological activity of adenine compounds with especial reference to their action upon the mammalian heart**. *J Physiol* 1929, **68**:213-237.
8. Gillespie JH: **The biological significance of the linkages in adenosine triphosphoric acid**. *J Physiol* 1934, **80**:345-359.
9. Holton P: **The liberation of adenosine triphosphate on antidromic stimulation of sensory nerves**. *J Physiol* 1959, **145**:494-504.
10. Berne RM: **Cardiac nucleotides in hypoxia: possible role in regulation of coronary blood flow**. *Am J Physiol* 1963, **204**:317-322.
11. Burnstock G: **Purinergic nerves**. *Pharmacol Rev* 1972, **24**:509-581.
12. Burnstock G, Campbell G, Satchell D, Smythe A: **Evidence that adenosine triphosphate or a related nucleotide is the transmitter substance released by non-adrenergic inhibitory nerves in the gut**. *Br J Pharmacol* 1970, **40**:668-688.
13. Ferguson DR, Kennedy I, Burton TJ: **ATP is released from rabbit urinary bladder epithelial cells by hydrostatic pressure changes--a possible sensory mechanism?** *J Physiol* 1997, **505 (Pt 2)**:503-511.
14. Forrester T: **Release of ATP from heart. Presentation of a release model using human erythrocyte**. *Ann N Y Acad Sci* 1990, **603**:335-351; discussion 351-332.
15. Gordon JL: **Extracellular ATP: effects, sources and fate**. *Biochem J* 1986, **233**:309-319.
16. Osipchuk Y, Cahalan M: **Cell-to-cell spread of calcium signals mediated by ATP receptors in mast cells**. *Nature* 1992, **359**:241-244.
17. Burnstock G: **A basis for distinguishing two types of purinergic receptor** In *Cell Membrane Receptors for Drugs and Hormones*. Edited by Bolis L, Straub RW: Raven Press; 1978:107–118.
18. Burnstock G, Kennedy C: **Is there a basis for distinguishing two types of P2-purinoceptor?** *Gen Pharmacol* 1985, **16**:433-440.
19. O'Connor SE, Dainty IA, Leff P: **Further subclassification of ATP receptors based on agonist studies**. *Trends Pharmacol Sci* 1991, **12**:137-141.
20. Pintor J, Miras-Portugal MT: **Diadenosine polyphosphate (ApxA) as new neurotransmitters**. *Drug Development Research* 1993, **28**:259-262.
21. Fredholm BB, Abbracchio MP, Burnstock G, Daly JW, Harden TK, Jacobson KA, Leff P, Williams M: **Nomenclature and classification of purinoceptors**. *Pharmacol Rev* 1994, **46**:143-156.
22. Abbracchio MP, Burnstock G: **Purinoceptors: are there families of P2X and P2Y purinoceptors?** *Pharmacol Ther* 1994, **64**:445-475.

23. Fredholm BB, Burnstock G, Harden TK, Spedding M: **Receptor nomenclature**. *Drug Development Research* 1996, **39**:461-466.
24. Jarvis MF, Khakh BS: **ATP-gated P2X cation-channels**. *Neuropharmacology* **In Press, Corrected Proof**.
25. Dunn PM, Zhong Y, Burnstock G: **P2X receptors in peripheral neurons**. *Prog Neurobiol* 2001, **65**:107-134.
26. Jasti J, Furukawa H, Gonzales EB, Gouaux E: **Structure of acid-sensing ion channel 1 at 1.9 A resolution and low pH**. *Nature* 2007, **449**:316-323.
27. Khakh BS: **Molecular physiology of P2X receptors and ATP signalling at synapses**. *Nat Rev Neurosci* 2001, **2**:165-174.
28. Vial C, Roberts JA, Evans RJ: **Molecular properties of ATP-gated P2X receptor ion channels**. *Trends Pharmacol Sci* 2004, **25**:487-493.
29. Newbolt A, Stoop R, Virginio C, Surprenant A, North RA, Buell G, Rassendren F: **Membrane topology of an ATP-gated ion channel (P2X receptor)**. *J Biol Chem* 1998, **273**:15177-15182.
30. Torres GE, Egan TM, Voigt MM: **N-Linked glycosylation is essential for the functional expression of the recombinant P2X2 receptor**. *Biochemistry* 1998, **37**:14845-14851.
31. Priel A, Silberberg SD: **Mechanism of ivermectin facilitation of human P2X4 receptor channels**. *J Gen Physiol* 2004, **123**:281-293.
32. Boue-Grabot E, Archambault V, Seguela P: **A protein kinase C site highly conserved in P2X subunits controls the desensitization kinetics of P2X(2) ATP-gated channels**. *J Biol Chem* 2000, **275**:10190-10195.
33. Ennion SJ, Evans RJ: **P2X(1) receptor subunit contribution to gating revealed by a dominant negative PKC mutant**. *Biochem Biophys Res Commun* 2002, **291**:611-616.
34. Liu GJ, Brockhausen J, Bennett MR: **P2X1 receptor currents after disruption of the PKC site and its surroundings by dominant negative mutations in HEK293 cells**. *Auton Neurosci* 2003, **108**:12-16.
35. Kim M, Yoo OJ, Choe S: **Molecular assembly of the extracellular domain of P2X2, an ATP-gated ion channel**. *Biochem Biophys Res Commun* 1997, **240**:618-622.
36. Ennion SJ, Ritson J, Evans RJ: **Conserved negatively charged residues are not required for ATP action at P2X(1) receptors**. *Biochem Biophys Res Commun* 2001, **289**:700-704.
37. Jiang LH, Rassendren F, Surprenant A, North RA: **Identification of amino acid residues contributing to the ATP-binding site of a purinergic P2X receptor**. *J Biol Chem* 2000, **275**:34190-34196.
38. Tanner NK, Cordin O, Banroques J, Doere M, Linder P: **The Q motif: a newly identified motif in DEAD box helicases may regulate ATP binding and hydrolysis**. *Mol Cell* 2003, **11**:127-138.
39. Roberts JA, Evans RJ: **ATP binding at human P2X1 receptors. Contribution of aromatic and basic amino acids revealed using mutagenesis and partial agonists**. *J Biol Chem* 2004, **279**:9043-9055.
40. Brautigam CA, Chelliah Y, Deisenhofer J: **Tetramerization and ATP binding by a protein comprising the A, B, and C domains of rat synapsin I**. *J Biol Chem* 2004, **279**:11948-11956.
41. Ennion S, Hagan S, Evans RJ: **The role of positively charged amino acids in ATP recognition by human P2X(1) receptors**. *J Biol Chem* 2000, **275**:29361-29367.
42. Marquez-Klaka B, Rettinger J, Bhargava Y, Eisele T, Nicke A: **Identification of an intersubunit cross-link between substituted cysteine residues located in the putative ATP binding site of the P2X1 receptor**. *J Neurosci* 2007, **27**:1456-1466.

43. Freist W, Verhey JF, Stuhmer W, Gauss DH: **ATP binding site of P2X channel proteins: structural similarities with class II aminoacyl-tRNA synthetases**. *FEBS Lett* 1998, **434**:61-65.
44. Cusack S, Berthet-Colominas C, Hartlein M, Nassar N, Leberman R: **A second class of synthetase structure revealed by X-ray analysis of Escherichia coli seryl-tRNA synthetase at 2.5 A**. *Nature* 1990, **347**:249-255.
45. Clyne JD, Wang LF, Hume RI: **Mutational analysis of the conserved cysteines of the rat P2X2 purinoceptor**. *J Neurosci* 2002, **22**:3873-3880.
46. Ennion SJ, Evans RJ: **Conserved cysteine residues in the extracellular loop of the human P2X(1) receptor form disulfide bonds and are involved in receptor trafficking to the cell surface**. *Mol Pharmacol* 2002, **61**:303-311.
47. Nakazawa K, Ohno Y: **Neighboring glycine residues are essential for P2X2 receptor/channel function**. *Eur J Pharmacol* 1999, **370**:R5-6.
48. Nakazawa K, Ojima H, Ishii-Nozawa R, Takeuchi K, Ohno Y: **Amino acid substitutions from an indispensable disulfide bond affect P2X2 receptor activation**. *Eur J Pharmacol* 2004, **483**:29-35.
49. Nicke A, Baumert HG, Rettinger J, Eichele A, Lambrecht G, Mutschler E, Schmalzing G: **P2X1 and P2X3 receptors form stable trimers: a novel structural motif of ligand-gated ion channels**. *Embo J* 1998, **17**:3016-3028.
50. Rettinger J, Aschrafi A, Schmalzing G: **Roles of individual N-glycans for ATP potency and expression of the rat P2X1 receptor**. *J Biol Chem* 2000, **275**:33542-33547.
51. Brown SG, Townsend-Nicholson A, Jacobson KA, Burnstock G, King BF: **Heteromultimeric P2X(1/2) receptors show a novel sensitivity to extracellular pH**. *J Pharmacol Exp Ther* 2002, **300**:673-680.
52. Clarke CE, Benham CD, Bridges A, George AR, Meadows HJ: **Mutation of histidine 286 of the human P2X4 purinoceptor removes extracellular pH sensitivity**. *J Physiol* 2000, **523 Pt 3**:697-703.
53. Clyne JD, LaPointe LD, Hume RI: **The role of histidine residues in modulation of the rat P2X(2) purinoceptor by zinc and pH**. *J Physiol* 2002, **539**:347-359.
54. Coddou C, Morales B, Gonzalez J, Grauso M, Gordillo F, Bull P, Rassendren F, Huidobro-Toro JP: **Histidine 140 plays a key role in the inhibitory modulation of the P2X4 nucleotide receptor by copper but not zinc**. *J Biol Chem* 2003, **278**:36777-36785.
55. Egan TM, Khakh BS: **Contribution of calcium ions to P2X channel responses**. *J Neurosci* 2004, **24**:3413-3420.
56. Egan TM, Haines WR, Voigt MM: **A domain contributing to the ion channel of ATP-gated P2X2 receptors identified by the substituted cysteine accessibility method**. *J Neurosci* 1998, **18**:2350-2359.
57. Rassendren F, Buell G, Newbolt A, North RA, Surprenant A: **Identification of amino acid residues contributing to the pore of a P2X receptor**. *Embo J* 1997, **16**:3446-3454.
58. Surprenant A, Rassendren F, Kawashima E, North RA, Buell G: **The cytolytic P2Z receptor for extracellular ATP identified as a P2X receptor (P2X7)**. *Science* 1996, **272**:735-738.
59. Chaumont S, Jiang LH, Penna A, North RA, Rassendren F: **Identification of a trafficking motif involved in the stabilization and polarization of P2X receptors**. *J Biol Chem* 2004, **279**:29628-29638.
60. Bobanovic LK, Royle SJ, Murrell-Lagnado RD: **P2X receptor trafficking in neurons is subunit specific**. *J Neurosci* 2002, **22**:4814-4824.

61. Denlinger LC, Sommer JA, Parker K, Gudipaty L, Fisette PL, Watters JW, Proctor RA, Dubyak GR, Bertics PJ: **Mutation of a dibasic amino acid motif within the C terminus of the P2X7 nucleotide receptor results in trafficking defects and impaired function**. *J Immunol* 2003, **171**:1304-1311.
62. Royle SJ, Bobanovic LK, Murrell-Lagnado RD: **Identification of a non-canonical tyrosine-based endocytic motif in an ionotropic receptor**. *J Biol Chem* 2002, **277**:35378-35385.
63. Eickhorst AN, Berson A, Cockayne D, Lester HA, Khakh BS: **Control of P2X(2) channel permeability by the cytosolic domain**. *J Gen Physiol* 2002, **120**:119-131.
64. Smart ML, Gu B, Panchal RG, Wiley J, Cromer B, Williams DA, Petrou S: **P2X7 receptor cell surface expression and cytolytic pore formation are regulated by a distal C-terminal region**. *J Biol Chem* 2003, **278**:8853-8860.
65. Khakh BS, Zhou X, Sydes J, Galligan JJ, Lester HA: **State-dependent cross-inhibition between transmitter-gated cation channels**. *Nature* 2000, **406**:405-410.
66. Boue-Grabot E, Barajas-Lopez C, Chakfe Y, Blais D, Belanger D, Emerit MB, Seguela P: **Intracellular cross talk and physical interaction between two classes of neurotransmitter-gated channels**. *J Neurosci* 2003, **23**:1246-1253.
67. Boue-Grabot E, Emerit MB, Toulme E, Seguela P, Garret M: **Cross-talk and co-trafficking between rho1/GABA receptors and ATP-gated channels**. *J Biol Chem* 2004, **279**:6967-6975.
68. Khakh BS, Gittermann D, Cockayne DA, Jones A: **ATP modulation of excitatory synapses onto interneurons**. *J Neurosci* 2003, **23**:7426-7437.
69. Torres GE, Egan TM, Voigt MM: **Identification of a domain involved in ATP-gated ionotropic receptor subunit assembly**. *J Biol Chem* 1999, **274**:22359-22365.
70. Jiang LH, Kim M, Spelta V, Bo X, Surprenant A, North RA: **Subunit arrangement in P2X receptors**. *J Neurosci* 2003, **23**:8903-8910.
71. Aschrafi A, Sadtler S, Niculescu C, Rettinger J, Schmalzing G: **Trimeric architecture of homomeric P2X2 and heteromeric P2X1+2 receptor subtypes**. *J Mol Biol* 2004, **342**:333-343.
72. Barrera NP, Ormond SJ, Henderson RM, Murrell-Lagnado RD, Edwardson JM: **Atomic force microscopy imaging demonstrates that P2X2 receptors are trimers but that P2X6 receptor subunits do not oligomerize**. *J Biol Chem* 2005, **280**:10759-10765.
73. Mio K, Kubo Y, Ogura T, Yamamoto T, Sato C: **Visualization of the trimeric P2X2 receptor with a crown-capped extracellular domain**. *Biochem Biophys Res Commun* 2005, **337**:998-1005.
74. Evans RJ, Lewis C, Buell G, Valera S, North RA, Surprenant A: **Pharmacological characterization of heterologously expressed ATP-gated cation channels (P2x purinoceptors)**. *Mol Pharmacol* 1995, **48**:178-183.
75. Valera S, Hussy N, Evans RJ, Adami N, North RA, Surprenant A, Buell G: **A new class of ligand-gated ion channel defined by P2x receptor for extracellular ATP**. *Nature* 1994, **371**:516-519.
76. Werner P, Seward EP, Buell GN, North RA: **Domains of P2X receptors involved in desensitization**. *Proc Natl Acad Sci U S A* 1996, **93**:15485-15490.
77. Evans RJ, Lewis C, Virginio C, Lundstrom K, Buell G, Surprenant A, North RA: **Ionic permeability of, and divalent cation effects on, two ATP-gated cation channels (P2X receptors) expressed in mammalian cells**. *J Physiol* 1996, **497 (Pt 2)**:413-422.
78. Buell G, Lewis C, Collo G, North RA, Surprenant A: **An antagonist-insensitive P2X receptor expressed in epithelia and brain**. *Embo J* 1996, **15**:55-62.

79. Garcia-Guzman M, Soto F, Laube B, Stuhmer W: **Molecular cloning and functional expression of a novel rat heart P2X purinoceptor**. *FEBS Lett* 1996, **388**:123-127.
80. Garcia-Guzman M, Stuhmer W, Soto F: **Molecular characterization and pharmacological properties of the human P2X3 purinoceptor**. *Brain Res Mol Brain Res* 1997, **47**:59-66.
81. King BF, Wildman SS, Ziganshina LE, Pintor J, Burnstock G: **Effects of extracellular pH on agonism and antagonism at a recombinant P2X2 receptor**. *Br J Pharmacol* 1997, **121**:1445-1453.
82. Knight GE, Burnstock G: **The effect of pregnancy and the oestrus cycle on purinergic and cholinergic responses of the rat urinary bladder**. *Neuropharmacology* 2004, **46**:1049-1056.
83. Mok MH, Knight GE, Andrews PL, Hoyle CH, Burnstock G: **The effects of cyclophosphamide on neurotransmission in the urinary bladder of Suncus murinus, the house musk shrew**. *J Auton Nerv Syst* 2000, **80**:130-136.
84. Mulryan K, Gitterman DP, Lewis CJ, Vial C, Leckie BJ, Cobb AL, Brown JE, Conley EC, Buell G, Pritchard CA, et al.: **Reduced vas deferens contraction and male infertility in mice lacking P2X1 receptors**. *Nature* 2000, **403**:86-89.
85. O'Connor SE, Wood BE, Leff P: **Characterization of P2x-receptors in rabbit isolated ear artery**. *Br J Pharmacol* 1990, **101**:640-644.
86. Bianchi BR, Lynch KJ, Touma E, Niforatos W, Burgard EC, Alexander KM, Park HS, Yu H, Metzger R, Kowaluk E, et al.: **Pharmacological characterization of recombinant human and rat P2X receptor subtypes**. *Eur J Pharmacol* 1999, **376**:127-138.
87. Mahaut-Smith MP, Ennion SJ, Rolf MG, Evans RJ: **ADP is not an agonist at P2X(1) receptors: evidence for separate receptors stimulated by ATP and ADP on human platelets**. *Br J Pharmacol* 2000, **131**:108-114.
88. Rettinger J, Schmalzing G: **Desensitization masks nanomolar potency of ATP for the P2X1 receptor**. *J Biol Chem* 2004, **279**:6426-6433.
89. Wildman SS, Brown SG, King BF, Burnstock G: **Selectivity of diadenosine polyphosphates for rat P2X receptor subunits**. *Eur J Pharmacol* 1999, **367**:119-123.
90. Dunn PM, Blakeley AG: **Suramin: a reversible P2-purinoceptor antagonist in the mouse vas deferens**. *Br J Pharmacol* 1988, **93**:243-245.
91. Lambrecht G, Friebe T, Grimm U, Windscheif U, Bungardt E, Hildebrandt C, Baumert HG, Spatz-Kumbel G, Mutschler E: **PPADS, a novel functionally selective antagonist of P2 purinoceptor-mediated responses**. *Eur J Pharmacol* 1992, **217**:217-219.
92. Urbanek E, Nickel P, Schlicker E: **Antagonistic properties of four suramin-related compounds at vascular purine P2X receptors in the pithed rat**. *Eur J Pharmacol* 1990, **175**:207-210.
93. Soto F, Lambrecht G, Nickel P, Stuhmer W, Busch AE: **Antagonistic properties of the suramin analogue NF023 at heterologously expressed P2X receptors**. *Neuropharmacology* 1999, **38**:141-149.
94. Rettinger J, Schmalzing G, Damer S, Muller G, Nickel P, Lambrecht G: **The suramin analogue NF279 is a novel and potent antagonist selective for the P2X(1) receptor**. *Neuropharmacology* 2000, **39**:2044-2053.
95. Braun K, Rettinger J, Ganso M, Kassack M, Hildebrandt C, Ullmann H, Nickel P, Schmalzing G, Lambrecht G: **NF449: a subnanomolar potency antagonist at recombinant rat P2X1 receptors**. *Naunyn Schmiedebergs Arch Pharmacol* 2001, **364**:285-290.

96. Jacobson KA, Kim YC, Wildman SS, Mohanram A, Harden TK, Boyer JL, King BF, Burnstock G: **A pyridoxine cyclic phosphate and its 6-azoaryl derivative selectively potentiate and antagonize activation of P2X1 receptors**. *J Med Chem* 1998, **41**:2201-2206.
97. Lambrecht G, Rettinger J, Baumert HG, Czeche S, Damer S, Ganso M, Hildebrandt C, Niebel B, Spatz-Kumbel G, Schmalzing G, et al.: **The novel pyridoxal-5'-phosphate derivative PPNDS potently antagonizes activation of P2X(1) receptors**. *Eur J Pharmacol* 2000, **387**:R19-21.
98. Virginio C, Robertson G, Surprenant A, North RA: **Trinitrophenyl-substituted nucleotides are potent antagonists selective for P2X1, P2X3, and heteromeric P2X2/3 receptors**. *Mol Pharmacol* 1998, **53**:969-973.
99. North RA, Surprenant A: **Pharmacology of cloned P2X receptors**. *Annu Rev Pharmacol Toxicol* 2000, **40**:563-580.
100. King BF, Liu M, Pintor J, Gualix J, Miras-Portugal MT, Burnstock G: **Diinosine pentaphosphate (IP5I) is a potent antagonist at recombinant rat P2X1 receptors**. *Br J Pharmacol* 1999, **128**:981-988.
101. Haines WR, Torres GE, Voigt MM, Egan TM: **Properties of the novel ATP-gated ionotropic receptor composed of the P2X(1) and P2X(5) isoforms**. *Mol Pharmacol* 1999, **56**:720-727.
102. Buell G, Michel AD, Lewis C, Collo G, Humphrey PP, Surprenant A: **P2X1 receptor activation in HL60 cells**. *Blood* 1996, **87**:2659-2664.
103. Cook SP, McCleskey EW: **Desensitization, recovery and Ca(2+)-dependent modulation of ATP-gated P2X receptors in nociceptors**. *Neuropharmacology* 1997, **36**:1303-1308.
104. Rettinger J, Schmalzing G: **Activation and desensitization of the recombinant P2X1 receptor at nanomolar ATP concentrations**. *J Gen Physiol* 2003, **121**:451-461.
105. Dutton JL, Poronnik P, Li GH, Holding CA, Worthington RA, Vandenberg RJ, Cook DI, Barden JA, Bennett MR: **P2X(1) receptor membrane redistribution and down-regulation visualized by using receptor-coupled green fluorescent protein chimeras**. *Neuropharmacology* 2000, **39**:2054-2066.
106. Li GH, Lee EM, Blair D, Holding C, Poronnik P, Cook DI, Barden JA, Bennett MR: **The distribution of P2X receptor clusters on individual neurons in sympathetic ganglia and their redistribution on agonist activation**. *J Biol Chem* 2000, **275**:29107-29112.
107. Ennion SJ, Evans RJ: **Agonist-stimulated internalisation of the ligand-gated ion channel P2X(1) in rat vas deferens**. *FEBS Lett* 2001, **489**:154-158.
108. Brunner J: **New photolabeling and crosslinking methods**. *Annu Rev Biochem* 1993, **62**:483-514.
109. Cusack NJ, Hourani SMO: **Photoaffinity labelling of purinergic receptors**. In *Purinergic Receptors: Receptors and Recognition*. Edited by Burnstock G: Chapman and Hall; 1981:327-345. Receptors and Recognition, vol 12.]
110. Karpen JW, Brown RL: **Covalent activation of retinal rod cGMP-gated channels reveals a functional heterogeneity in the ligand binding sites**. *J Gen Physiol* 1996, **107**:169-181.
111. Ruiz ML, Karpen JW: **Single cyclic nucleotide-gated channels locked in different ligand-bound states**. *Nature* 1997, **389**:389-392.
112. Dorman G, Prestwich GD: **Benzophenone photophores in biochemistry**. *Biochemistry* 1994, **33**:5661-5673.
113. Fleming SA: **Chemical reagents in photoaffinity labeling**. *Tetrahedron* 1995, **51**:12479-12520.

114. Hatanaka Y, Hashimoto M, Hidari KI, Sanai Y, Tezuka Y, Nagai Y, Kanaoka Y: **Synthesis and characterization of a carbene-generating biotinylated lactosylceramide analog as a novel chromogenic photoprobe for GM3 synthase**. *Chem Pharm Bull (Tokyo)* 1996, **44**:1111-1114.
115. Singh A, Thornton ER, Westheimer FH: **The photolysis of diazoacetylchymotrypsin**. *J Biol Chem* 1962, **237**:3006-3008.
116. Fleet GWJ, Porter RR, Knowles JR: **Affinity Labelling of Antibodies with Aryl Nitrene as Reactive Group**. *Nature* 1969, **224**:511-512.
117. Kudlow JE, Leung Y: **Photoaffinity labelling of the ATP-binding site of the epidermal growth factor-dependent protein kinase**. *Biochem J* 1984, **220**:677-683.
118. Agboh KC, Powell AJ, Evans RJ: **Characterisation of ATP analogues to cross-link and label P2X receptors**. *Neuropharmacology* 2008.
119. Brunswick DJ, Cooperman BS: **Photo-affinity labels for adenosine 3':5'-cyclic monophosphate**. *Proc Natl Acad Sci U S A* 1971, **68**:1801-1804.
120. Cooperman BS, Brunswick DJ: **On the photoaffinity labeling of rabbit muscle phosphofructokinase with O2'-(ethyl-2-diazomalonyl)adenosine 3':5'-cyclic monophosphate**. *Biochemistry* 1973, **12**:4079-4084.
121. Guthrow CE, Rasmussen H, Brunswick DJ, Cooperman BS: **Specific photoaffinity labeling of the adenosine 3':5'-cyclic monophosphate receptor in intact ghosts from human erythrocytes**. *Proc Natl Acad Sci U S A* 1973, **70**:3344-3346.
122. Haley BE, Hoffman JF: **Interactions of a photo-affinity ATP analog with cation-stimulated adenosine triphosphatases of human red cell membranes**. *Proc Natl Acad Sci U S A* 1974, **71**:3367-3371.
123. Erb L, Lustig KD, Ahmed AH, Gonzalez FA, Weisman GA: **Covalent incorporation of 3'-O-(4-benzoyl)benzoyl-ATP into a P2 purinoceptor in transformed mouse fibroblasts**. *J Biol Chem* 1990, **265**:7424-7431.
124. Erb L, Lustig KD, Sullivan DM, Turner JT, Weisman GA: **Functional expression and photoaffinity labeling of a cloned P2U purinergic receptor**. *Proc Natl Acad Sci U S A* 1993, **90**:10449-10453.
125. Gonzalez FA, Wang DJ, Huang NN, Heppel LA: **Activation of early events of the mitogenic response by a P2Y purinoceptor with covalently bound 3'-O-(4-benzoyl)-benzoyladenosine 5'-triphosphate**. *Proc Natl Acad Sci U S A* 1990, **87**:9717-9721.
126. Wohland T, Friedrich K, Hovius R, Vogel H: **Study of ligand-receptor interactions by fluorescence correlation spectroscopy with different fluorophores: evidence that the homopentameric 5-hydroxytryptamine type 3As receptor binds only one ligand**. *Biochemistry* 1999, **38**:8671-8681.
127. Tsien RY: **The green fluorescent protein**. *Annu Rev Biochem* 1998, **67**:509-544.
128. Cha A, Bezanilla F: **Characterizing voltage-dependent conformational changes in the Shaker K+ channel with fluorescence**. *Neuron* 1997, **19**:1127-1140.
129. Parola AL, Lin S, Kobilka BK: **Site-specific fluorescence labeling of the beta2 adrenergic receptor amino terminus**. *Anal Biochem* 1997, **254**:88-95.
130. Schreiter C, Gjoni M, Hovius R, Martinez KL, Segura JM, Vogel H: **Reversible sequential-binding probe receptor-ligand interactions in single cells**. *Chembiochem* 2005, **6**:2187-2194.
131. Jameson DM, Eccleston JF: **Fluorescent nucleotide analogs: synthesis and applications**. *Methods Enzymol* 1997, **278**:363-390.
132. Yount RG: **ATP analogs**. *Adv Enzymol Relat Areas Mol Biol* 1975, **43**:1-56.
133. Bagshaw C: **ATP analogues at a glance**. *J Cell Sci* 2001, **114**:459-460.

134. Hiratsuka T, Uchida K: **Preparation and properties of 2'(or 3')-O-(2,4,6-trinitrophenyl) adenosine 5'-triphosphate, an analog of adenosine triphosphate**. *Biochim Biophys Acta* 1973, **320**:635-647.
135. Mockett BG, Housley GD, Thorne PR: **Fluorescence imaging of extracellular purinergic receptor sites and putative ecto-ATPase sites on isolated cochlear hair cells**. *J Neurosci* 1994, **14**:6992-7007.
136. Mannuzzu LM, Moronne MM, Isacoff EY: **Direct physical measure of conformational rearrangement underlying potassium channel gating**. *Science* 1996, **271**:213-216.
137. Smith PL, Yellen G: **Fast and slow voltage sensor movements in HERG potassium channels**. *J Gen Physiol* 2002, **119**:275-293.
138. Meinild AK, Hirayama BA, Wright EM, Loo DD: **Fluorescence studies of ligand-induced conformational changes of the Na(+)/glucose cotransporter**. *Biochemistry* 2002, **41**:1250-1258.
139. Li M, Lester HA: **Early fluorescence signals detect transitions at mammalian serotonin transporters**. *Biophys J* 2002, **83**:206-218.
140. Chang Y, Weiss DS: **Site-specific fluorescence reveals distinct structural changes with GABA receptor activation and antagonism**. *Nat Neurosci* 2002, **5**:1163-1168.
141. Li M, Farley RA, Lester HA: **An intermediate state of the gamma-aminobutyric acid transporter GAT1 revealed by simultaneous voltage clamp and fluorescence**. *J Gen Physiol* 2000, **115**:491-508.
142. Larsson HP, Tzingounis AV, Koch HP, Kavanaugh MP: **Fluorometric measurements of conformational changes in glutamate transporters**. *Proc Natl Acad Sci U S A* 2004, **101**:3951-3956.
143. Dahan DS, Dibas MI, Petersson EJ, Auyeung VC, Chanda B, Bezanilla F, Dougherty DA, Lester HA: **A fluorophore attached to nicotinic acetylcholine receptor beta M2 detects productive binding of agonist to the alpha delta site**. *Proc Natl Acad Sci U S A* 2004, **101**:10195-10200.
144. Geibel S, Kaplan JH, Bamberg E, Friedrich T: **Conformational dynamics of the Na+/K+-ATPase probed by voltage clamp fluorometry**. *Proc Natl Acad Sci U S A* 2003, **100**:964-969.
145. Pless SA, Dibas MI, Lester HA, Lynch JW: **Conformational variability of the glycine receptor M2 domain in response to activation by different agonists**. *J Biol Chem* 2007, **282**:36057-36067.
146. Nernst W: **Die elektromotorische Wirksamkeit der Ionen.** *Zeitschrift für Physikalische Chemie* 1889, **4**:129-181.
147. Cole KS: **Dynamic electrical characteristics of squid axon membrane**. *Arch. Sci. Physiol* 1949, **3**:253-258.
148. Axon-Instruments: *The Axon Guide for Electrophysiology and Biophysics.* Edited by Sherman-Gold R. California: Axon Instruments Inc.; 1993.
149. Schwarz W, Rettinger J: *Foundations of Electrophysiology* edn Second. Aachen: Shaker Verlag; 2003.
150. Miyazawa A, Fujiyoshi Y, Unwin N: **Structure and gating mechanism of the acetylcholine receptor pore**. *Nature* 2003, **423**:949-955.
151. Armstrong N, Gouaux E: **Mechanisms for activation and antagonism of an AMPA-sensitive glutamate receptor: crystal structures of the GluR2 ligand binding core**. *Neuron* 2000, **28**:165-181.
152. Armstrong N, Sun Y, Chen GQ, Gouaux E: **Structure of a glutamate-receptor ligand-binding core in complex with kainate**. *Nature* 1998, **395**:913-917.

153. Lin X, Hume RI, Nuttall AL: **Voltage-dependent block by neomycin of the ATP-induced whole cell current of guinea-pig outer hair cells**. *J Neurophysiol* 1993, **70**:1593-1605.
154. Quick MW, Lester RA: **Desensitization of neuronal nicotinic receptors**. *J Neurobiol* 2002, **53**:457-478.
155. Paradiso KG, Steinbach JH: **Nicotine is highly effective at producing desensitization of rat alpha4beta2 neuronal nicotinic receptors**. *J Physiol* 2003, **553**:857-871.
156. Reitstetter R, Lukas RJ, Gruener R: **Dependence of nicotinic acetylcholine receptor recovery from desensitization on the duration of agonist exposure**. *J Pharmacol Exp Ther* 1999, **289**:656-660.
157. Sun Y, Olson R, Horning M, Armstrong N, Mayer M, Gouaux E: **Mechanism of glutamate receptor desensitization**. *Nature* 2002, **417**:245-253.
158. Robert A, Armstrong N, Gouaux JE, Howe JR: **AMPA receptor binding cleft mutations that alter affinity, efficacy, and recovery from desensitization**. *J Neurosci* 2005, **25**:3752-3762.
159. Pizard A, Marchetti J, Allegrini J, Alhenc-Gelas F, Rajerison RM: **Negative cooperativity in the human bradykinin B2 receptor**. *J Biol Chem* 1998, **273**:1309-1315.
160. Carraway KL, 3rd, Cerione RA: **Fluorescent-labeled growth factor molecules serve as probes for receptor binding and endocytosis**. *Biochemistry* 1993, **32**:12039-12045.
161. Krieger F, Mourot A, Araoz R, Kotzyba-Hibert F, Molgo J, Bamberg E, Goeldner M: **Fluorescent agonists for the Torpedo nicotinic acetylcholine receptor**. *Chembiochem* 2008, **9**:1146-1153.
162. Wallace RA, Ho T: **Protein incorporation by isolated amphibian oocytes. II. A survey of inhibitors**. *J Exp Zool* 1972, **181**:303-317.
163. Lewis CJ, Surprenant A, Evans RJ: **2',3'-O-(2,4,6- trinitrophenyl) adenosine 5'-triphosphate (TNP-ATP)--a nanomolar affinity antagonist at rat mesenteric artery P2X receptor ion channels**. *Br J Pharmacol* 1998, **124**:1463-1466.
164. Cook SP, Rodland KD, McCleskey EW: **A memory for extracellular Ca2+ by speeding recovery of P2X receptors from desensitization**. *J Neurosci* 1998, **18**:9238-9244.
165. Mourot A, Bamberg E, Rettinger J: **Agonist- and competitive antagonist-induced movement of loop 5 on the alpha subunit of the neuronal alpha4beta4 nicotinic acetylcholine receptor**. *J Neurochem* 2008, **105**:413-424.
166. He Y, Karpen JW: **Probing the interactions between cAMP and cGMP in cyclic nucleotide-gated channels using covalently tethered ligands**. *Biochemistry* 2001, **40**:286-295.
167. Forman SA, Zhou QL, Stewart DS: **Photoactivated 3-azioctanol irreversibly desensitizes muscle nicotinic ACh receptors via interactions at alphaE262**. *Biochemistry* 2007, **46**:11911-11918.
168. Stoop R, Thomas S, Rassendren F, Kawashima E, Buell G, Surprenant A, North RA: **Contribution of individual subunits to the multimeric P2X(2) receptor: estimates based on methanethiosulfonate block at T336C**. *Mol Pharmacol* 1999, **56**:973-981.
169. Bean BP: **ATP-activated channels in rat and bullfrog sensory neurons: concentration dependence and kinetics**. *J Neurosci* 1990, **10**:1-10.
170. Mead F, Williams AJ: **Block of the Ryanodine Receptor Channel by Neomycin Is Relieved at High Holding Potentials**. *Biophys. J.* 2002, **82**:1953-1963.
171. Ding S, Sachs F: **Single channel properties of P2X2 purinoceptors**. *J Gen Physiol* 1999, **113**:695-720.

172. Cao L, Young MT, Broomhead HE, Fountain SJ, North RA: **Thr339-to-Serine Substitution in Rat P2X2 Receptor Second Transmembrane Domain Causes Constitutive Opening and Indicates a Gating Role for Lys308**. *J. Neurosci.* 2007, **27**:12916-12923.
173. Lape R, Colquhoun D, Sivilotti LG: **On the nature of partial agonism in the nicotinic receptor superfamily**. *Nature* 2008, **454**:722-727.
174. Low DA, Baker JB, Koonce WC, Cunningham DD: **Released protease-nexin regulates cellular binding, internalization, and degradation of serine proteases**. *Proc Natl Acad Sci U S A* 1981, **78**:2340-2344.
175. Wiley HS, Cunningham DD: **The endocytotic rate constant. A cellular parameter for quantitating receptor-mediated endocytosis**. *J Biol Chem* 1982, **257**:4222-4229.
176. Knutson VP, Ronnett GV, Lane MD: **Rapid, reversible internalization of cell surface insulin receptors. Correlation with insulin-induced down-regulation**. *J Biol Chem* 1983, **258**:12139-12142.
177. Hertel C, Coulter SJ, Perkins JP: **A comparison of catecholamine-induced internalization of beta-adrenergic receptors and receptor-mediated endocytosis of epidermal growth factor in human astrocytoma cells. Inhibition by phenylarsine oxide**. *J Biol Chem* 1985, **260**:12547-12553.
178. Lazareno S, Gharagozloo P, Kuonen D, Popham A, Birdsall NJ: **Subtype-selective positive cooperative interactions between brucine analogues and acetylcholine at muscarinic receptors: radioligand binding studies**. *Mol Pharmacol* 1998, **53**:573-589.
179. Michel AD, Chambers LJ, Walter DS: **Negative and positive allosteric modulators of the P2X(7) receptor**. *Br J Pharmacol* 2008, **153**:737-750.
180. Michel AD, Miller KJ, Lundstrom K, Buell GN, Humphrey PP: **Radiolabeling of the rat P2X4 purinoceptor: evidence for allosteric interactions of purinoceptor antagonists and monovalent cations with P2X purinoceptors**. *Mol Pharmacol* 1997, **51**:524-532.
181. Michel AD, Lundstrom K, Buell GN, Surprenant A, Valera S, Humphrey PP: **A comparison of the binding characteristics of recombinant P2X1 and P2X2 purinoceptors**. *Br J Pharmacol* 1996, **118**:1806-1812.
182. De Lean A, Munson PJ, Rodbard D: **Multi-subsite receptors for multivalent ligands. Application to drugs, hormones, and neurotransmitters**. *Mol Pharmacol* 1979, **15**:60-70.
183. Saltiel AR, Powell-Jones CH, Thomas CG, Jr., Nayfeh SN: **Apparent "negative cooperativity" kinetics in the absence of a nonlinear Scatchard plot of thyrotropin-receptor interaction in a human thyroid adenoma**. *Biochem Biophys Res Commun* 1980, **95**:395-403.
184. Macdonald JL, Pike LJ: **Heterogeneity in EGF-binding affinities arises from negative cooperativity in an aggregating system**. *Proc Natl Acad Sci U S A* 2008, **105**:112-117.
185. Prinz H, Striessnig J: **Ligand-induced accelerated dissociation of (+)-cis-diltiazem from L-type Ca2+ channels is simply explained by competition for individual attachment points**. *J Biol Chem* 1993, **268**:18580-18585.
186. Mendes P: **GEPASI: a software package for modelling the dynamics, steady states and control of biochemical and other systems**. *Comput Appl Biosci* 1993, **9**:563-571.
187. Mendes P: **Biochemistry by numbers: simulation of biochemical pathways with Gepasi 3**. *Trends Biochem Sci* 1997, **22**:361-363.

188. Yan Z, Liang Z, Tomic M, Obsil T, Stojilkovic SS: **Molecular determinants of the agonist binding domain of a P2X receptor channel**. *Mol Pharmacol* 2005, **67**:1078-1088.
189. Haines WR, Voigt MM, Migita K, Torres GE, Egan TM: **On the contribution of the first transmembrane domain to whole-cell current through an ATP-gated ionotropic P2X receptor**. *J Neurosci* 2001, **21**:5885-5892.
190. Khakh BS, Egan TM: **Contribution of transmembrane regions to ATP-gated P2X2 channel permeability dynamics**. *J Biol Chem* 2005, **280**:6118-6129.
191. Akabas MH, Stauffer DA, Xu M, Karlin A: **Acetylcholine receptor channel structure probed in cysteine-substitution mutants**. *Science* 1992, **258**:307-310.
192. Roberts DD, Lewis SD, Ballou DP, Olson ST, Shafer JA: **Reactivity of small thiolate anions and cysteine-25 in papain toward methyl methanethiosulfonate**. *Biochemistry* 1986, **25**:5595-5601.
193. Karlin A, Akabas MH: **Substituted-cysteine accessibility method**. *Methods Enzymol* 1998, **293**:123-145.
194. Pratt EB, Brink TS, Bergson P, Voigt MM, Cook SP: **Use-dependent inhibition of P2X3 receptors by nanomolar agonist**. *J Neurosci* 2005, **25**:7359-7365.
195. Hovius R, Vallotton P, Wohland T, Vogel H: **Fluorescence techniques: shedding light on ligand-receptor interactions**. *Trends Pharmacol Sci* 2000, **21**:266-273.
196. Förster T: **Zwischenmolekulare Energiewanderung und Fluoreszenz**. *Ann. Physik* 1948, **6**:55.
197. Stryer L, Haugland RP: **Energy transfer: a spectroscopic ruler**. *Proc Natl Acad Sci U S A* 1967, **58**:719-726.
198. Stryer L: **Fluorescence energy transfer as a spectroscopic ruler**. *Annu Rev Biochem* 1978, **47**:819-846.
199. Jares-Erijman EA, Jovin TM: **FRET imaging**. *Nat Biotechnol* 2003, **21**:1387-1395.
200. Young MT, Fisher JA, Fountain SJ, Ford RC, North RA, Khakh BS: **Molecular shape, architecture, and size of P2X4 receptors determined using fluorescence resonance energy transfer and electron microscopy**. *J Biol Chem* 2008, **283**:26241-26251.
201. Mio K, Ogura T, Yamamoto T, Hiroaki Y, Fujiyoshi Y, Kubo Y, Sato C: **Reconstruction of the P2X(2) receptor reveals a vase-shaped structure with lateral tunnels above the membrane**. *Structure* 2009, **17**:266-275.
202. Unwin N: **Refined structure of the nicotinic acetylcholine receptor at 4A resolution**. *J Mol Biol* 2005, **346**:967-989.
203. Li M, Chang TH, Silberberg SD, Swartz KJ: **Gating the pore of P2X receptor channels**. *Nat Neurosci* 2008, **11**:883-887.

Acknowledgements

This thesis is a result of years of research that has been done since I came to Prof Bamberg's department. Since then, I have worked with great number of people and whose contribution to my research and making of the thesis deserve special mention. It is my pleasure to convey my gratitude to all of them in my humble acknowledgement.

I would like to express my sincere appreciation and gratitude to Prof. Ernst Bamberg for his support and unflinching encouragement throughout my thesis. He has provided an optimum working environment at the Department of Biophysical Chemistry at the institute, where a lack of resources is something unimaginable due to his managerial skills and foresight.

I am thankful to Dr. Jürgen Rettinger for his constant and excellent supervision throughout my PhD studies. I express my profound gratitude to him for training me in electrophysiology and introducing me to the exciting field of P2X research. His intellectual support and constructive arguments has shaped my thesis in a form that I can be proud on. Through my association with him, I have gained invaluable experience on how to identify, approach, and tackle the problems in the scientific field.

I am happy to acknowledge Dr. Annette Nicke from Max Planck Institute for Brain Research, Frankfurt, for a very fruitful collaboration. I would like to pay my sincere thanks to her PhD student and my friend Benjamin Marquez-Klaka for generating several cysteine mutants of P2X receptors and happily sharing them with me.

I thank Dr. Alexander Mourot for helping me to design and build setups for concurrent photolabeling/fluorescence and electrophysiological measurements. I would also like to thank Eva Bongartz for providing me with open channel blockers of P2X receptors and Eva Harte (summer student) for voltage-clamp fluorometry experiments.

I would like to thank all the members of our department especially Heidi Bergemann for helping me with all the administrative works, Helga Volk for helping me with the poster related works, Anja Becker for helping me in getting started in the lab, Dr. Robert Dempski for his cooperation in building two-electrode voltage clamp fluorometry setup, Dr. Klaus Hartung for his help in German translation of summary, Janna Lustig for her help in molecular biology and Stefan Geys for being my good office mate.

Special thanks to my friends Anamika and Ravi for just being the best and enjoying Europe with me. I thank Chenguang, Sachin, Ajeeta, Vivekananda, Jagdeep, Juan, Preeti, Panchali,

Devrishi, Shweta, Mouli, Vikrant, Abhishek for the great times I had with them and more importantly for our delicious dinners together.

I express my regards to all the staff members of the workshop of Max Planck Institute of Biophysics for providing technical help and assistance during the course of my PhD projects.

Anamika deserves special thanks for being always available for going through each line of my thesis and critically correcting and commenting on the thesis and often proving help in scientific writing. I thank her for the love and encouragement during all tough times especially during the writing phase.

I must say the unforgettable role of my brother Pranesh who came all the way from pacific coast to correct my thesis. I thank him for his constant support and encouragement during all tough times especially during the writing phase.

During this research, there have been times when I was down and out. Who else, but my parents stood there to help me pull myself together. I thank my father for playing deftly the role of a friend, philosopher and guide when I needed the most. He always pulled me out of the blues that are familiar to graduate students all around the globe. Thanks to my mother, whose rock-solid support, smiling face and silent consent did most of what thousand words wouldn't do.

And finally, it's the divine intervention that shaped my life during this time and I hope the *due ex machina continues* to be with me forever.

Yogesh Bhargava

Curriculum Vitae

Personal details

Name	: Yogesh Bhargava
Date of Birth	: 24th Oct 1977
Nationality	: Indian
Gender	: Male
Marital status	: Single
Languages known	: English, Hindi, German (beginner level)
Education medium	: English

Educational qualifications

- **Master of Philosophy (M. Phil)**, Biotechnology, 2005.
  Supervisor: Prof D. Panda and late Prof A. Lala.
  Indian Institute of Technology (IIT) Bombay, India.

- **Master of Science (MSc)**, Microbiology, 2000.
  R. D. University, Jabalpur, India.

- **Bachelor of Science (BSc),** Biology, 1998.
  Govt. Science College, R. D. University, Jabalpur, India.

Research experience and Skills

- **Date:** 2005 - till date
  Title: "Structural rearrangements and subunit interactions in P2X receptors".
  Place: Max Planck Institute of Biophysics, Frankfurt am Main, Germany.
  Techniques: Two electrode voltage clamp coupled to photolabeling or fluorescence measurement, outside out patch clamp, *Xenopus laevis* oocyte expression system, cRNA preparation and injections.

- **Date:** 2000 – 2005
  Title: "Apoptosis: Proteins that form channels in the mitochondrial membrane".
  Place: Indian Institute of Technology (IIT), Bombay, India.
  Techniques: Molecular biology, recombinant Bcl-2 protein and Diphtheria toxin expression (bacterial expression system), chromatographic purification (affinity, gel, HPLC), electrophoresis (SDS, 2D PAGE), proteomic analysis (MALDI-TOF), radioactive hydrophobic photolabeling, isolation of liver mitochondria and marker enzyme assays.

- **Date:** 2000
  Title: "In-vitro and In-vivo investigation of cytoprotective roles of natural metabolites (plant and tea-fungus) during Lead and Chromium toxicity".
  Place: Defence Institute of Physiology and Allied Science (DIPAS), New Delhi, India.
  Techniques: Marker enzyme assays, macrophage and lymphocyte culture, animal experimentation (rat).

Scholarships and Awards

2005 International Max Planck Research School (IMPReS) Fellowship of Max Planck Society.
2003 Eureka First prize in poster presentation at IIT Kanpur, India.
2000 Research Assistantship of Indian Institute of Technology, Bombay.
2000 Graduate Aptitude Test in Engineering (GATE-2000) with a score of 90.99 and placed in top 7% among students of life science appeared nationwide.
2000 Gold medalist in MSc in Microbiology.
1993 Governor Award for scouting services.

Supervisory experience

- Teaching assistantship at Frankfurt University (practical courses for the diploma students during the years 2008, 2006, 2005).
- Supervised three summer students in the years 2008, 2006 and 2003.

Other courses and certificates

- MALDI MS training course from Manchester (UK) at Kratos Analytical Ltd (2004).
- Certificate in Management Development Program from IIT Bombay (2004).
- Certificate in Entrepreneurship Development Program from IIT Bombay (2003).
- Yoga teachers training course from Bihar School of Yoga, Munger (1994).

Presentations at International and National meetings

Oral presentations

Bhargava Y, Rettinger J. Use of fluorescent ATP analogs to study ligand binding properties of P2X receptors in real time. "Workshop on the molecular basis of membrane transport", Ringberg, Germany, June 2008.

Bhargava Y, Rettinger J. Use of fluorescent ATP analogs to study ligand binding properties of P2X receptors in real time. FG-748 meeting on "Neuronal and glial P2 receptors; molecular basis and functional significance", Frankfurt am Main, Germany, March 2008.

Bhargava Y, Rettinger J. Allosteric effect of covalently tethered BzATP on the efficacy of TNP-ATP in P2X receptors "Workshop on the molecular basis of membrane transport", Ringberg, Germany, May 2007.

Bhargava Y, Apoptosis: Proteins that form channels in the mitochondrial membrane. "Workshop on the molecular basis of membrane transport", Ringberg, Germany, May 2005.

Poster presentations

Bhargava Y, Rettinger J. Allosteric effect of covalently tethered BzATP on the efficacy of TNP-ATP in the P2X2/P2X1 receptor chimera. "Second joint Italian-German purine club meeting", Leipzig, Germany, Sept 2007.

Marquez-Klaka B, **Bhargava Y**, Rettinger J, Nicke A. Identification of an inter-subunit cross-link between substituted cysteine residues located in the putative ATP binding site. "8th International Symposium on Adenosine and Adenine Nucleotides", Ferrara, Italy, May 2006.

Bhargava Y. Evaluation of antioxidant and immunomodulatory activity of Tea-fungus metabolites during Lead induced sub-chronic toxicity. "EUREKA (Genesis) program", Kanpur, India, March 2003.

Publications

Bhargava Y, Mourot A, Bamberg E, Rettinger J. "Gating is individually contributed by each receptor subunit in homomeric P2X receptors". (In preparation).

Bhargava Y, Bamberg E, Rettinger J. "Fluorescent ATP unravels negative intersubunit cooperativity in the desensitized state of P2X1 receptor". (In preparation).

Marquez-Klaka B, Rettinger J, **Bhargava Y**, Eisele T, Nicke A. "Identification of an intersubunit cross-link between substituted cysteine residues located in the putative ATP binding site of the P2X1 receptor". J Neurosci., 2007, 27, 1456-66.

Mathur A, Sethi A, Jogini V, **Bhargava Y**, Tembe BL and Lala AK. "Energetics of insertion of soluble proteins into membrane". Curr. Sci. (India), 2004, 87, 181-189.

Dipti P, **Bhargava Y**, Kain AK, Pauline T, Anju B, Sairam M, Singh B, Mongia SS, Kumar GI and Selvamurthy W. "Lead induced oxidative stress: beneficial effects of Kombucha tea". Biomed Environ Sci., 2003, 16, 276-82.

Sairam M, Dutt N, **Bhargava Y**, Anju B, Dipti P, Pauline T, Sharma SK, Sarada SK, Ilavazhagan G, Kumar D and Selvamurthy W. "Cyto-protective and immunomodulating properties of Amla (Emblica officinalis) on lymphocytes: an in-vitro study". J Ethnopharmacol., 2002, 81, 5-10.